DOCTORAL THESIS FOR THE DEGREE OF PHILOSOPHIAE DOCTOR

A NOVEL METHOD FOR THE ESTIMATION OF THERMOPHYSICAL PROPERTIES OF WALLS FROM SHORT AND SEASONALLY INDEPENDENT IN-SITU SURVEYS

VIRGINIA GORI

UCL Energy Institute
University College London

12th April 2017
(Corrections submitted and approved July 2017)

Virginia Gori: *A novel method for the estimation of thermophysical properties of walls from short and seasonally independent in-situ surveys,* © 12th April 2017
(Corrections submitted and approved July 2017)

DECLARATION

I, Virginia Gori, confirm that the work presented in this thesis is my own. Where information has been derived from other sources, I confirm that this has been indicated in the thesis.

London, 12th April 2017
(Corrections submitted and approved July 2017)

Virginia Gori

ABSTRACT

This work presents a novel grey-box dynamic method — building on and significantly expanding that presented in Biddulph *et al.*[1] — to estimate the thermophysical properties of building elements from short monitoring campaigns undertaken at all times of the year. The estimation of thermophysical characteristics of building elements from *in-situ* measurements accounts for the state of conservation (*e.g.*, moisture) and conditions the structure is exposed to, potentially reducing the performance gap.

A family of lumped-thermal-mass models was devised to describe the dynamic heat transfer across building elements. Bayesian-based optimisation techniques (either using maximum a posteriori estimates or a Markov Chain Monte Carlo sampling) were adopted for the identification of the best-fit parameters, their distributions and correlations, and the associated uncertainties. Model-comparison and cross-validation techniques were applied to objectively select the best model at describing the measured data, and to test its ability to generalise to out-of-sample observations.

Five walls of different construction and orientation (one housed in a thermal chamber and four *in-situ*) were monitored to test the ability of the method to shorten the monitoring period and to extend the data collection to non-winter seasons. A two-thermal-mass model (2TM) was selected as best by model comparison in all cases. It was able to account for direct solar radiation on the walls and provided a robust characterisation of the elements surveyed and their thermal structure, while reducing the length of the monitoring period. The systematic errors of the 2TM model were within acceptable ranges throughout the year and its estimates were within the margin of error of the other lumped-thermal-mass models, the average method and literature values. The method developed improves the understanding of the thermal comfort and energy performance in buildings, helping closing the performance gap, and informing tailored retrofitting solutions and space conditioning strategies aiming to reduce energy consumption while improving thermal comfort.

1 Biddulph, P., Gori, V., Elwell, C.A., Scott, C., Rye, C., Lowe, R., & Oreszczyn, T. 2014. Inferring the thermal resistance and effective thermal mass of a wall using frequent temperature and heat flux measurements. Energy and Buildings. DOI: 10.1016/j.enbuild.2014.04.004.

ACKNOWLEDGEMENTS

I would like to thank all those who made this research possible and supported me during this PhD.

I owe gratitude to my supervisors, Dr Cliff Elwell and Prof. Mike Davies, for their encouragement, guidance, and enthusiasm for this research. I deeply appreciated the trust and freedom they offered me to lead and explore my research, while being always there checking on me and helping me to get back on track when needed. I never felt they did not have time for me despite their busy diaries. I am also sincerely grateful to Dr Phill Biddulph for his enthusiasm, guidance and stimulating discussion, as well as his significant contribution to the original development of the method and software.

I would also like to express my gratitude to all those that provided inspirational discussion, encouragement, feedback, occasions for personal and professional growth, or simply friendly time during the past four years: Prof. Bob Lowe, Andrew Smith, Valentina Marincioni, Dr Jez Wingfield, Dr Sam Stamp, Prof. Tadj Oreszczyn, Lisa Izsatt, Madalina Hanc, Dr Hector Altamirano-Medina, Dr Alaa Alfakara, Dr Selin Yilmaz, Dr Sofie Pelsmakers, Emily Nix, Jonathan Chambers, Prof. Paul Ruyssevelt, Yekatherina Bobrova, Dr Melissa Lott, Lucy Campbell, Dr Sadaf Sultan Khan, Prof. Dejan Mumovic, Dr Jenny Love, Elsa Barazza, Pamela Fennell (I hope I haven't missed anyone!).

Finally, I would like to acknowledge the EPSRC Centre for Doctoral Training in Energy Demand (LoLo), grant numbers EP/L01517X/1 and EP/H009612/1, and the UCL BEAMS Overseas Doctoral Award for awarding me my scholarship, without which all this would not have been possible. I am thankful both for the financial support and the opportunity offered me to be part of such an inspiring and stimulating Centre and Institute. Thanks to Alison Parker, Mae Oroszlany and Rosanna Seels for admin support.

I am indebted to the owners of the CLWall and HSWall, those who made the OWall study possible and those who have been sitting close to it, and to Valentina Marincioni and colleagues for the TCWall data. Thank you also to Cameron Scott and Caroline Rye of Archimetrics Ltd for helping during the initial equipment installation on the OWall.

Finally, my sincere thanks go to my extended family and friends for always being there. A special thank you to Luca for always believing in me, offering encouragement and love.

PUBLICATIONS

Part of this work has been published in peer-reviewed journals and presented at conferences.

Journals

- Gori, V., Marincioni, V., Biddulph, P., Elwell, C. 2017. Inferring the thermal resistance and effective thermal mass distribution of a wall from in situ measurements to characterise heat transfer at both the interior and exterior surfaces. *Energy and Buildings*, 135, pp. 398–409.
- Li, F.G.N., Smith, A.Z.P., Biddulph, P., Hamilton, I.G., Lowe, R., Mavrogianni, A., Oikonomou, E., Raslan, R., Stamp, S., Stone, A., Summerfield, A.J., Veitch, D., Gori, V., Oreszczyn, T. 2015. Solid-wall U-values: heat flux measurements compared with standard assumptions. *Building Research & Information*, 43(2), pp. 238-252.
- Biddulph, P., Gori, V., Elwell, C.A., Scott, C., Rye, C., Lowe, R., Oreszczyn, T. 2014. Inferring the thermal resistance and effective thermal mass of a wall using frequent temperature and heat flux measurements. *Energy and Buildings*, 49, pp.443– 453.

Conferences

- Gori, V., Elwell, C. 2017. Characterisation of the thermal structure of different building constructions using in-situ measurements and a Bayesian analysis. Paper presented at the Nordic Symposium on Building Physics (NSB 2017) conference and to be published on Energy Procedia.
- Chambers, J., Gori, V., Biddulph, P., Hamilton, I., Oreszczyn, T., Elwell, C. 2015. How solid is our knowledge of solid walls? Comparing energy savings through three different methods. Proceedings of the International Conference Future Buildings & Districts Sustainability from Nano to Urban Scale (CISBAT 2015). Oral Presentation.
- Gori, V., Biddulph, P., Elwell, C., Scott, C., Rye, C., Lowe, R., Oreszczyn, T. 2014. Seasonal factors influencing the estimation of the U-value of a wall. Proceedings of the Building Simulation and Optimization (BSO14) conference. Oral presentation.

CONTENTS

LIST OF FIGURES

LIST OF TABLES

NOMENCLATURE

Symbol	*Description*	*Units*
Q	Heat flux density	$[\mathrm{Wm^{-2}}]$
$\mathcal{Q}$	Heat flow rate	$[\mathrm{W}]$
$\mathcal{A}$	Area of a building element	$[\mathrm{m^2}]$
T	Temperature	[°C or K]
ΔT	Temperature difference	[°C or K]
Λ	Thermal conductance	$[\mathrm{Wm^{-2}K^{-1}}]$
U	U-value (or thermal transmittance)	$[\mathrm{Wm^{-2}K^{-1}}]$
R	R-value (or thermal resistance)	$[\mathrm{m^2KW^{-1}}]$
h_c	Convection heat transfer coefficient	$[\mathrm{Wm^{-2}K^{-1}}]$
h_r	Radiation heat transfer coefficient	$[\mathrm{Wm^{-2}K^{-1}}]$
d	Thickness of a building material	$[\mathrm{m}]$
v	Wind speed adjacent to the surface of a building element	$[\mathrm{ms^{-1}}]$
λ	Thermal conductivity of a building material	$[\mathrm{Wm^{-1}K^{-1}}]$
ρ	Density of a building material	$[\mathrm{kgm^{-3}}]$
c	Specific heat capacity of a building material	$[\mathrm{Jkg^{-1}K^{-1}}]$
κ	Thermal mass per unit area of a building material	$[\mathrm{Jm^{-2}K^{-1}}]$
t	Time	[s]
τ	Length of the sampling interval (*i.e.* the interval between measurements)	[s]
S	Laplace variable	
Z	Time-shift operator	
R_n	n-th lumped thermal resistance (starting from the internal side)	$[\mathrm{m^2KW^{-1}}]$
C_n	n-th effective lumped thermal mass (starting from the internal side)	$[\mathrm{Jm^{-2}K^{-1}}]$

Symbol	*Description*	*Units*
T_{C_n}	Estimated temperature of the n-th effective lumped thermal mass	$[°C]$
$T^0_{C_n}$	Initial temperature of the n-th lumped effective thermal mass	$[°C]$
T_{int},T_{ext}	Measured internal and external temperature	$[°C]$
$Q_{m,in}$,$Q_{m,out}$	Measured heat flux into and out of the internal and external surfaces	$[Wm^{-2}]$
Q_{sun}	Incoming solar radiation	$[Wm^{-2}]$
$Q_{e,in}$, $Q_{e,out}$	Estimated heat flux into and out of the internal and external surfaces	$[Wm^{-2}]$
Φ_m,Φ_e	Observation and estimation of the model	
g	Absorbance of the building element	$[-]$
y	Vector of the observations	
θ	Vector of the unknown parameters of the model	
H	Model	
$\mathcal{L}(\theta; y, H)$	Likelihood function in the maximum likelihood framework	
$P(\theta \mid y, H)$	Posterior probability distribution	
$P(y \mid \theta, H)$	Likelihood function in the Bayesian framework	
$P(\theta \mid H)$	Prior probability distribution	
$P(y \mid H)$	Evidence (or marginal likelihood)	
ΔL_j	Width of the uniform prior distribution on the j-th parameter of the model	
L_{θ_j},U_{pk}	Measure of location of the log-normal prior distribution of respectively the j-th parameter and the U-value, based on previous knowledge	
D_{θ_j},D_{pk}	Measure of dispersion of the log-normal prior distribution of respectively the j-th parameter and the U-value, based on previous knowledge	
μ	Mean of a normal distribution	
v	Variance of a normal distribution	

Symbol	*Description*	*Units*
A	Inverse of the Hessian of the negative logarithm of the posterior probability distribution around its global optimum	
r	Vector of the residuals	
σ_ε	Systematic measurement error on each data stream	
σ_Φ^2	Variance of an additive noise term affecting the residuals of the model	
$\delta^{\mathrm{r}}_{\Phi,\varepsilon}$	Total relative uncertainty for each data stream	
$\delta^{\mathrm{a}}_{\Phi,\varepsilon}$	Total absolute uncertainty for each data stream	

	Superscripts
p, $p-1$	Current and previous time step

	Subscripts
ε	Identifier of the data stream (*e.g.*, internal heat flux)

	Acronyms and abbreviations
HFP	Heat flux plate
AM	Average method
1TM	One thermal mass model
2TM	Two thermal mass model
3TM	Three thermal mass model
4TM	Four thermal mass model
(1 HF)	One heat flux data stream used for model fitting
(2 HF)	Two heat flux data streams used for model fitting
MLE	Maximum likelihood estimation
MAP	Maximum a posteriori
MCMC	Markov Chain Monte Carlo
iid	Independent and identically distributed
TCWall	Solid wall in a thermal chamber

Symbol	*Description*	*Units*
OWall	Solid wall in an office building (north-west facing)	
CLWall	Cavity wall in an occupied house (north facing)	
HSWall_E	Cavity wall in an unoccupied house (east facing)	
HSWall_N	Cavity wall in an unoccupied house (north facing)	

Part I

INTRODUCTION AND LITERATURE REVIEW

1

INTRODUCTION

Climate change has been acknowledged as a global concern affecting every country around the world (United Nations, 2015). The 5th assessment report by the Intergovernmental Panel on Climate Change (IPCC, 2013) recognised anthropogenic activities as central to global warming and climate change since the mid-20th century. The rapidly growing global energy use and carbon dioxide (CO_2) emissions were identified among its causes (Pérez-Lombard et al., 2008).

Acting on the energy demand side of buildings has been deemed as essential and cost-effective to attain climate-change mitigation and carbon-emission targets (DECC, 2009) as the sector still offers significant margins for improvement (International Energy Agency, 2013). The building sector accounts for over a third of global final energy demand (half of which is used for space conditioning and hot water production) and a third of global carbon emissions, being the largest energy-consuming sector in the world (International Energy Agency, 2013). These figures are expected to increase in the future due to improvements in living standards, economic development and ageing of the building stock (International Energy Agency, 2013).

It is estimated that between 50% (globally) and 75% (in the member countries of the Organisation for Economic Co-operation and Development, OECD) of current buildings will still be standing in 2050 (International Energy Agency, 2013), highlighting the potential extent of the demand for decarbonisation or retrofit measures over the next decades. Research suggests that a 77% reduction in the total CO_2 emissions from buildings (compared to today's levels) would be required by 2050 to meet the goal of limiting the global temperature rise below 2 °C (International Energy Agency, 2013), as negotiated in the Paris agreement (United Nations, 2015). Further studies by the International Energy Agency (2011b) showed that 47% of the energy need for space conditioning could potentially be reduced in the future by implementing aggressive policy actions.

It is recognised (International Energy Agency, 2013) that coordinated actions by policy makers and governments around the globe are essential to exploit the energy demand

reduction potential, as simply implementing current energy-efficiency measures and using already available technologies would not suffice to address the problem. In the UK, the Climate Change Act (2008) has been issued to commit to the climate change mitigation targets negotiated with the European Community (European Community, 2009, 2010), aiming for an 80% reduction in greenhouse gas emissions by 2050 compared to 1990 levels.

1.0.1 *Forecasting the energy demand of the building stock*

Forecasts of the energy demand of buildings are used at the large scale to support the policy-making process and inform long-term programmes (Swan and Ugursal, 2009). At the building level, simulation tools are used to support the decision-making during retrofitting or new construction processes, to size energy-efficient interventions and evaluate their cost-effectiveness (Hopfe and Hensen, 2011), to perform quality assurance tests, and to evaluate the energy performance of buildings when issuing energy performance certificates (Castillo et al., 2014). Several calculation methods and software tools have been developed to forecast the energy performance of buildings (Crawley et al., 2008).

A number of studies have shown a gap (in either direction) in the energy performance of real buildings compared to the estimates from simulations (Norford et al., 1994; Stein and Meier, 2000; de Wit, 2004; Baker, 2011; van Dronkelaar et al., 2016), with evident implication for the cost-effectiveness of energy-saving measures (Byrne et al., 2013), the evaluation of heating and cooling loads, or policy prioritisation. This discrepancy is often referred to as "performance gap" (Zero Carbon Hub, 2014). Several factors may contribute to the performance gap, including occupant behaviour and use of technology (Norford et al., 1994); thermophysical performance of the building envelope (Johnston et al., 2015); lack of knowledge, skills and understanding of the energy performance across the building industry (*e.g.*, poor workmanship, installation or design (Zero Carbon Hub, 2014)), and lack of understanding of the benefits of closing the performance gap by the stakeholders (Zero Carbon Hub, 2014).

A number of sensitivity analysis studies have shown that one of the most important parameters in the estimation of the energy performance of buildings is the thermophysical properties of the building envelope (*e.g.*, thermal resistance and U-value) (Feuermann, 1989; de Wit, 2004; Hopfe and Hensen, 2011; Hughes et al., 2015). Collecting accurate information is usually challenging, especially for existing buildings, for a number of reasons. Little documentation about construction materials and building techniques is generally available. Therefore, the thermophysical properties of the ele-

ment under study are selected from look-up tables or software libraries (de Wit, 2004) after visual inspection or from the knowledge of the period of construction of the building (Biddulph et al., 2014), potentially introducing significant uncertainties in the simulation outputs (de Wit, 2004). Building material categories may present broad ranges of tabulated properties and similarly looking materials may have very different thermophysical performance (CIBSE, 2007). Additionally, the thermophysical properties of building materials provided by manufactures or literature references are usually characterised in controlled environments, which may not be representative of their actual performance *in situ* as they do not account for environmental factors (*e.g.*, moisture migration and air movement), defects and situational inhomogeneities of the structure (*e.g.*, thermal bridges, delamination of materials), and quality of installation (Anderson, 1984; Siviour, 1994; Cesaratto and De Carli, 2013). Studies have shown significant discrepancies between the thermophysical properties of the building fabric tabulated in the literature and those estimated from data collected *in situ* (Cesaratto and De Carli, 2013; Li et al., 2014; Johnston et al., 2015).

1.0.2 *In-situ monitoring for the characterisation of the energy performance of buildings*

In-situ monitoring has been widely explored in industry and academia to estimate the thermophysical properties of building elements (Wouters et al., 1993; Baker and van Dijk, 2008; International Energy Agency, 2011a; Rye, 2012; Stevens and Bradford, 2013; Roels et al., 2015a). This reduces the uncertainties that would be otherwise introduced by assuming the building structure and the properties of its constituent materials from visual inspection, year of construction and tabulated values (Biddulph et al., 2014). It also allows the characterisation of the building element in its environment and state of conservation (Cesaratto and De Carli, 2013). However, the cost, time and expertise required to undertake high-quality data collection and analysis is still a barrier to the wider adoption of this method (Energy Saving Trust, 2005).

Usually, steady-state methods (*e.g.*, the average method and linear regression models (Jiménez and Madsen, 2008; BS ISO 9869-1, 2014), discussed in Section 2.3) are adopted for the estimation of the R-value and U-value of building elements (Deconinck and Roels, 2016). However, these methods are seasonally bounded and may need long surveys as, by definition, they aim at averaging out the effects of the thermal mass over a sufficiently long period (BS ISO 9869-1, 2014) instead of modelling it. These requirements may play an important role in the slow uptake of the use of *in-situ* measurements for diagnostic purposes and tailored energy demand forecasts. Consequently, dynamic

methods have been increasingly developed (Kristensen et al., 2004; Baker and van Dijk, 2008; Jiménez et al., 2009; Kramer et al., 2012; Deconinck and Roels, 2016) as they require shorter surveys and may provide more information about the element studied by simultaneously characterising its thermal resistance and effective thermal mass.

This thesis presents a novel combination of lumped-thermal-mass models and Bayesian analysis for the estimation of the thermophysical properties of building elements from *in-situ* measurements. Applications of the Bayesian framework in building physics applications have increasingly gained interest recently (Dubois et al., 2014; Berger et al., 2016; Rouchier et al., 2017), although their use in building physics applications is still limited. In this work the performance of the dynamic grey-box method devised was tested on walls, however its applicability is not restricted to this element. Although the use of lumped-thermal-mass models is not new in the field (Paschkis and Baker, 1942; Madsen and Holst, 1995; Gutschker, 2008a; Jiménez et al., 2009; Kramer et al., 2012; Naveros et al., 2014), their combination with Bayesian-based optimisation technique provides several advantages to the grey-box method previously proposed. These include the combination of the information contained in the observed data with our previous knowledge, the estimation of both the parameters of the model and the associated statistical errors accounting for the parameters' correlation, and the use of statistical evidence to objectively select the model that is more likely to describe the measured data (Biddulph et al., 2014; Gori et al., 2017).

1.1 RESEARCH AIM AND OBJECTIVES

The aim of this research was to develop a novel dynamic grey-box method that may decrease the length of monitoring campaigns for the estimation of the thermophysical properties of *in-situ* building elements, while ensuring robust estimates and providing useful physical insights into their thermal structure. The method may be used to encourage a wider use of *in-situ*-monitored data to assess the thermophysical performance of buildings in their environment and state of conservation, for example to assess the impact of retrofitting interventions, the quality of the building process, or their energy performance.

The dynamic method devised builds on and significantly expands that proposed by Biddulph et al. (2014). It consists of a combination of lumped-thermal-mass models and the Bayesian framework to solve the inverse heat transfer problem and estimate the thermophysical properties (*e.g.*, R-value and thermal mass) of *in-situ* building elements from monitored data. The choice of a dynamic method was dictated by the aim of

overcoming the main limitations of current standard methods (*e.g.*, BS ISO 9869-1 (2014) Standard) for the characterisation of the thermophysical performance of *in-situ* elements, such as the length and seasonality of the monitoring period. The statistical framework was selected to provide robust estimates while keeping error and uncertainties within acceptable ranges.

To attain this aim, the following objectives were identified and achieved:

- the method proposed by Biddulph et al. (2014) was extended to multi-thermal mass models using more robust and computationally efficient techniques to discretise and solve the linear differential equations describing the dynamic heat transfer through the building element under study;
- a Markov Chain Monte Carlo (MCMC) method was added to the original maximum a posteriori (MAP) approach to investigate whether the additional information on the distribution of the thermophysical estimates it provides may be used to gather additional information on the case studies;
- non-uniform prior probability distributions were introduced to investigate their potential ability to shorten the length of the monitoring campaigns and the robustness of the estimates, also in comparison to those obtained using uniform prior;
- a method for the estimation of the systematic error on the U-value from the dynamic method was developed.

Secondary data collected on a wall housed in a thermal chamber and primary data collected from long-term monitoring campaigns undertaken by the candidate on four walls of distinct construction and different orientation were used as applications to test the performance of the proposed method in terms of:

- its ability to shorten the monitoring period and extend it to all times of the year;
- investigating the robustness of the estimates and the associated errors obtained both from the MAP and MCMC approaches, using uniform and non-uniform prior probability distributions. The estimates were compared to standard methods of estimating the thermal performance of *in-situ* building elements and tabulated thermophysical properties;
- investigating to what extent the potential influence of environmental factors (*e.g.*, air movement and solar radiation) may influence the estimates of the model and whether these can be accounted for in the proposed method.

1.2 THESIS OUTLINE

This thesis comprises eight chapters. Chapter 2 will expand the introduction above presenting a literature review of heat transfer theory and the main contributions to the performance gap in the context of the application of this work to the building fabric. Steady-state and dynamic methods to model the heat transfer through building elements and estimate their thermal performance are reviewed.

Chapter 3 identifies the desirable features that a novel dynamic grey-box method should have in the light of the literature review. Subsequently, it presents the theoretical background of the method developed, the family of lumped thermal mass models devised, the model-fitting and parameter-optimisation phases, and the validation phase consisting of model selection and cross-validation techniques. Both the MAP and the MCMC approaches are presented.

Chapter 4 describes the case studies surveyed in this work and the monitoring methods. It illustrates the experimental analysis by contextualising the theoretical background described in Chapter 3 to the specific application of this research and describing the software implementation. Finally it introduces the methods adopted for error analysis, both for the average and dynamic method.

Chapters 5, 6 and 7 present the main results of this work. Specifically, Chapter 5 tests the performance of the proposed method using thermal chamber data and *in-situ* measurements collected according to best-practice recommendations (*i.e.* north-facing walls and winter period). Both the MAP and MCMC frameworks using uniform and non-uniform prior probability distributions were adopted to estimate the thermophysical properties of the walls investigated by means of the family of lumped-thermal-mass models devised. Model validation was undertaken to select the best model. Chapter 6 extends the investigation undertaken in Chapter 5 to data collected on north-facing walls under non-conventional conditions (*i.e.* at all times of the year). The analysis aims at exploring the monitoring length required by the dynamic method compared to standard methods, and the ability of the method developed to provide robust estimates throughout the year while keeping the systematic error within acceptable ranges. Chapter 7 investigates the potential effects of air movement and direct solar radiation on the thermophysical estimates and whether these can be accounted for in the framework proposed.

Chapter 8 summarises the key findings of this research, relating them to policy implications, potential applications of the method proposed and future work.

2

THE ENERGY PERFORMANCE OF THE BUILDING STOCK AND THE ASSESSMENT OF THE PERFORMANCE GAP

Understanding the thermophysical performance of buildings is essential to inform policy decisions on large-scale long-term strategies aiming at cutting energy consumption in the built environment (Swan and Ugursal, 2009). Similarly, it enables professionals to evaluate different energy-efficient solutions and their cost-effectiveness at the building design or retrofitting stages (Hopfe and Hensen, 2011), to ensure compliance with quality assessment procedures (Deconinck and Roels, 2016) and test the performance of new building materials (Samardzioska and Apostolska, 2016), and to issue energy performance certificates (EPC) (Castillo et al., 2014; Chambers et al., 2015). Consequently, numerous models and software tools have been developed to quantify the energy performance of the building stock (Crawley et al., 2008), although discrepancies between the simulation outputs and the as-built performance has been observed (Sanders and Phillipson, 2006). This mismatch is usually referred to as "performance gap" (Zero Carbon Hub, 2014).

A number of sensitivity analysis studies have identified the thermophysical properties of the building envelope (*e.g.*, the U-value) among the most important causes of uncertainties in the characterisation of the thermophysical behaviour of buildings (Feuermann, 1989; de Wit, 2004; Hopfe and Hensen, 2011; Hughes et al., 2015). Studies have shown significant discrepancies between the thermophysical properties of building elements inferred from tabulated values in the literature and those estimated from *in-situ* measurements (Bankvall, 1978; Cesaratto et al., 2011; Byrne et al., 2013; Li et al., 2014; Johnston et al., 2015), with obvious implications. Although *in-situ* measurements have been widely used in industry and academia to understand the thermophysical properties of building elements (Wouters et al., 1993; Baker and van Dijk, 2008; Baker, 2011; Cesaratto and De Carli, 2013; Stevens and Bradford, 2013; Roels et al., 2015a), the cost, time and expertise required to undertake high-quality *in-situ* measurement and analysis are still a barrier to the wider adoption of this method to characterise the building stock

(Energy Saving Trust, 2005). Several steady-state (Jiménez and Madsen, 2008; BS ISO 9869-1, 2014) and dynamic (Roulet et al., 1987; Rabl, 1988; Norlén, 1994; Madsen and Holst, 1995; Jiménez et al., 2009; Naveros et al., 2014; Rouchier et al., 2016; Deconinck and Roels, 2016) methods have been developed and applied to estimate the thermophysical properties of buildings from monitoring campaigns, depending on the final purpose of the analysis, the available data, the experience and expertise of the team. None of these methods can be considered the best in absolute terms and their usefulness rather depends on the application. The choice of the most appropriate approach is a non-trivial task that involves multidisciplinary knowledge (Rabl, 1988; Jiménez and Madsen, 2008).

This chapter presents the main heat transfer mechanisms of building elements (Section 2.1), followed by a review of the main causes of the performance gap of the building envelope (Section 2.2). The use of *in-situ* measurements as a means to close the performance gap is introduced before exploring the modelling techniques (Section 2.3 and Section 2.4) that have been developed to describe the heat transfer in building-related applications and to estimate the thermophysical performance of building elements from monitored data. Finally, the rationale for the development of a novel grey-box dynamic method is discussed (Section 3.1).

2.1 HEAT TRANSFER THROUGH BUILDING ELEMENTS

Heat transfer refers to the transit of energy over time occurring between two systems at different temperatures (Cengel, 2002). The three basic mechanisms for heat transfer are conduction, convection and radiation, which are also used to define useful thermophysical properties to describe the thermal behaviour of building elements. These are briefly discussed in the following.

CONDUCTION At the microscopic level, the energy transfer for conduction is induced by the interaction of particles at higher temperature (*i.e.* higher energy) with the adjacent particles at lower temperature (*i.e.* lower energy) (Cengel, 2002). At the macroscopic level conduction occurs within a substance (either solid, liquid or gas) and/or between two substances in direct contact in the presence of a temperature gradient.

The heat conduction is described by the general Fourier's Law, postulated in 1822 (Cengel, 2002). It states that the conductive heat flow rate (*i.e.* the amount of energy per unit time) at any point in an isotropic material is proportional to the temperature gradient at that point (Hens, 2012) and a coefficient of proportionality called thermal conductivity (usually indicated as λ $\left[\mathrm{Wm^{-1}K^{-1}}\right]$):

$$\mathbf{Q} = -\lambda \nabla \mathbf{T} \tag{2.1}$$

where $\mathbf{Q}$ is the vector of the heat flux density $\left[\mathrm{Wm}^{-2}\right]$ (*i.e.* heat flow rate, $\mathcal{Q}$ [W], per unit area, $\mathcal{A}$ $\left[\mathrm{m}^2\right]$); $\mathbf{T}$ is the vector of the temperatures [K or °C]. Thermal conductivity is an intrinsic property of the material, and for simplicity it is assumed to be constant and scalar (though this is not the case in reality) (Hens, 2012). In engineering applications, it is often assumed that the temperature gradient occurs mainly along one direction (x) while the others are negligible. This is referred to as one-dimensional heat flow. Under this assumption, Equation 2.1 becomes:

$$Q_x = \frac{\mathcal{Q}_x}{\mathcal{A}} = -\lambda \frac{\partial T}{\partial x}. \tag{2.2}$$

Given the property of real materials to both exert a resistance to the heat flow and store part of the transferring energy to be released at a shifted time interval (*i.e.* thermal mass effect), the dynamic one-dimensional heat flux within the material is described by imposing the conservation of energy between the heat stored and the heat transferred at any time interval. Assuming that no mass transfer occurs and that the thermophysical properties of the material are constant (Hens, 2012):

$$\rho c \frac{\partial T}{\partial t} + \frac{\partial Q_x}{\partial x} = 0 \Rightarrow \rho c \frac{\partial T}{\partial t} = \frac{\partial}{\partial x}\left(\lambda \frac{\partial T}{\partial x}\right) \tag{2.3}$$

where ρ, c are the density $\left[\mathrm{kgm}^{-3}\right]$ and specific heat capacity $\left[\mathrm{Jkg}^{-1}\mathrm{K}^{-1}\right]$ of the material; t is time [s]. In many applications, the further assumption of steady-state heat flux is introduced. It assumes that the heat flow rate and the temperatures are independent of time (*i.e.* temperatures are constant). Owing to this condition, Equation 2.3 can be simplified into:

$$Q_x = \frac{\mathcal{Q}_x}{\mathcal{A}} = -\lambda \frac{\mathrm{d}T(x)}{\mathrm{d}x} = \lambda \frac{T_2 - T_1}{d} \tag{2.4}$$

where T_1, T_2 are the temperatures of two points on the material [K or °C]; d is the thickness of the material along the direction where the one-dimensional heat flow occurs.

CONVECTION Convection describes the heat transfer between a solid surface and an adjacent liquid (or gas) in motion, from a warm region to a cold one (Cengel, 2002). It involves both conduction and fluid motion. Convection heat transfer is described by the Newton's law of cooling, which states that the heat flux density is proportional

to a coefficient, called convection heat transfer h_c $\left[\mathrm{Wm^{-2}K^{-1}}\right]$, and the temperature difference:

$$Q = \frac{\mathcal{Q}}{\mathcal{A}} = h_c \left(T_s - T_\infty\right) \tag{2.5}$$

where T_s is the temperature of the surface (which coincides with the temperature of the fluid at the surface) [K or °C]; T_∞ is the temperature of the undisturbed fluid [K or °C]. The convection heat transfer coefficient is not a property of the fluid and it has to be determined experimentally. It is a function of the geometry of the surface, the nature and properties of the fluid in motion, and the bulk fluid velocity (Cengel, 2002).

RADIATION In general, radiation is related to the changes in the electronic configuration of atoms and it represents the energy emitted by matter in the form of electromagnetic waves (Cengel, 2002). Unlike conduction and convection, radiation occurs also in a vacuum, in the absence of an intervening medium. Heat transfer by radiation only accounts for the radiation emitted by the surfaces of a body due to their temperatures (*i.e.* thermal radiation) (Cengel, 2002). The radiation heat transfer is described as:

$$Q = \varepsilon\sigma \left(T_s^4 - T_{surr}^4\right) \tag{2.6}$$

where ε is the hemispherical emissivity of the surface and σ the Stephan-Boltzmann constant ($5.67{\cdot}10^8\,\mathrm{Wm^{-2}K^{-4}}$); T_s is the temperature of the emitting surface [K]; T_{surr} is the temperature of the surrounding [K].

For analogy to the Newton's Law, the radiation heat transfer can be rewritten as the product of a coefficient, called the radiation heat transfer coefficient h_r $\left[\mathrm{Wm^{-2}K^{-1}}\right]$, and the temperature difference:

$$Q = h_r \left(T_s - T_{surr}\right) \tag{2.7}$$

where:

$$h_r = \varepsilon\sigma \left(T_s + T_{surr}\right)\left(T_s^2 + T_{surr}^2\right) \sim 4\varepsilon\sigma T_m^3 \tag{2.8}$$

being T_m the mean thermodynamic temperature of the surface and of its surroundings [K] (BS EN ISO 6946, 2007; Hens, 2012, Ch.1.4.5). Typical values for the radiation heat transfer coefficient for building physics applications are provided by the BS EN ISO 6946 (2007, Appendix A) Standard.

THERMOPHYSICAL PROPERTIES OF BUILDING ELEMENTS A number of useful thermophysical properties for building physics applications can be defined from the basic principles. In these applications, the assumption of one-dimensional steady-state heat flow is frequently adopted. The thermal gradient, and consequently the heat flow, within a building material is assumed to occur along the direction perpendicular to the surfaces (*i.e.* along the thickness) of the layer investigated. The ratio of the thickness of a material and its thermal conductivity (from Equation 2.4) is usually referred to as thermal resistance of the material $\left[\mathrm{m^2KW^{-1}}\right]$ (BS EN ISO 7345, 1996):

$$R_i = \frac{d}{\lambda}. \tag{2.9}$$

For multi-layer elements of n slabs, the thermal resistance of the whole element (defined as R-value, according to the BS ISO 9869-1 (2014) Standard) is represented by the sum of the thermal resistance (Equation 2.9) of each layer constituting the structure:

$$R = \sum_{i=1}^{n} R_i. \tag{2.10}$$

The heat transfer between two surfaces of a building element is generally assumed to occur only by conduction (usually calculated from Equation 2.4, where T_1 and T_2 are the temperatures of the surfaces). The convective and radiative effects occurring at the internal and external surfaces are accounted for in the calculation through the definition of the surface (or air film) resistance (BS EN ISO 6946, 2007), which provide an extra thermal resistance to that of the material(s):

$$R_\mathrm{s} = \frac{1}{h_\mathrm{c} + h_\mathrm{r}}. \tag{2.11}$$

Empirical values for the convection and radiation heat transfer coefficient for building physics applications are provided by the BS EN ISO 6946 (2007, Appendix A) Standard. For planar elements the convection heat transfer at the external surface (h_ce) is a function of the wind speed adjacent to the surface v $\left[\mathrm{ms^{-1}}\right]$:

$$h_\mathrm{ce} = 4 + 4v. \tag{2.12}$$

For vertical elements (which are the application of this work), the conventional value for h_ce is $20\,\mathrm{Wm^{-2}K^{-1}}$ (calculated assuming $v = 4\,\mathrm{Wm^{-2}K^{-1}}$), while that for h_ci is assumed to be $2.5\,\mathrm{Wm^{-2}K^{-1}}$. Similarly, the value suggested in the standard for the radiation heat transfer is evaluated from Equation 2.8 assuming an emissivity of 0.9, and a mean thermodynamic temperature of 20 °C for the internal and 10 °C for the external surfaces.

These values lead to an air film resistances of $0.13\,\mathrm{m^2KW^{-1}}$ for the internal surface and $0.04\,\mathrm{m^2KW^{-1}}$ for the external, which are the conventional surface resistances generally used in applications (BS EN ISO 6946, 2007, Table 1).

The sum of the R-value (Equation 2.10) and the thermal resistance of the air film (Equation 2.11) on the two sides of the element is referred to as total R-value (BS ISO 9869-1, 2014) and its inverse is the thermal transmittance (or U-value) $\left[\mathrm{Wm^{-2}K^{-1}}\right]$ (BS EN ISO 7345, 1996):

$$U = \frac{1}{R_{\mathrm{tot}}} = \frac{1}{R_{\mathrm{si}} + R + R_{\mathrm{se}}}. \tag{2.13}$$

Note that the air film resistances have to be added to calculate the U-value only in case surface temperatures are considered for the calculation of the R-value of the material (as illustrated above). Conversely, if air temperatures are used, these already account for convective and radiative effects. The inverse of the R-value represents the thermal conductance (Λ) $\left[\mathrm{Wm^{-2}K^{-1}}\right]$ (BS EN ISO 7345, 1996):

$$\Lambda = \frac{1}{R}. \tag{2.14}$$

2.2 THE PERFORMANCE GAP OF THE BUILDING ENVELOPE

This section reviews the main causes of the performance gap (Sanders and Phillipson, 2006; Zero Carbon Hub, 2014), defined as the mismatch between the outputs of building simulations and the as-built thermal performance. Uncertainties affecting the as-built thermophysical performance of the building envelope potentially contribute to the observed performance gap. They arise from incremental assumptions and approximations made to describe real constructions when modelling the thermophysical performance of building elements. The sources of uncertainties can be broadly grouped into four categories: environmental factors, structural and situational inhomogeneities and defects of the building envelope, modelling- and monitoring-related uncertainties (Gori, 2013). The following sections will explore each category and illustrate how *in-situ* measurements may be used to close the performance gap.

2.2.0.1 *Environmental factors*

Environmental factors potentially affecting the thermophysical performance of the building envelope include short- and long-term variability of the boundary and in-wall conditions of the structure induced by weather and seasonal patterns (*e.g.*, wind, solar radiation, rain), and the usage of the indoor ambient (*e.g.*, cooking, showering). These

aspects have a direct effect on the heat and moisture transfer mechanisms (Section 2.1) as well as on the thermophysical properties of the building materials (Anderson, 1984), which may be difficult or practically impossible to account for in models at the design or retrofitting stage.

At the interior and exterior surfaces, wind, air movement, window opening patterns, and indoor space conditioning affect the convective heat transfer coefficient (BS EN ISO 6946, 2007) and the resistance of the air film (Arens and Williams, 1977; BS EN ISO 6946, 2007), consequently impacting on the overall heat exchange and the convective heat losses of the element (Janssen et al., 2007). Pressure differences may be induced on the structure by the wind and result in air infiltration (or leakage) especially through porous materials (Arens and Williams, 1977; Lecompte, 1987).

Liquid water and water vapour can be introduced within the element by the usage of indoor spaces, building defects, raising dump, or by the combined effects of wind and rain (*i.e.* wind-driven rain) effectively pumping water inside the structure (Lecompte, 1987; Janssen et al., 2007). The temporary increase in the building materials of water content in liquid and vapour phase may affect their thermal conductivity and increase the conductive heat losses (Siviour, 1974). The transient variation may be magnified on the external side by the evaporation process induced by subsequent solar radiation or wind (Siviour, 1974).

Temperature swings and radiative effects may introduce non-negligible drifts and uneven distributions of air and surface temperatures both on the internal and external surfaces (Anderson, 1984; McIntyre, 1985), which affect the radiative heat transfer coefficient and the resistance of the air film. Internally these effects can be introduced by heating, ventilation and air conditioning (HVAC) units or radiators (Cesaratto et al., 2011). Surrounding buildings and vegetation absorb and re-irradiate thermal radiation from and to the external facade and possibly contribute to uneven shadow on it (Siviour, 1974).

2.2.0.2 *Structural and situational inhomogeneities and defects*

Similarly to the environmental factors, structural and situational inhomogeneities and defects cause a deviation between the real building element and its abstract representation used to build the model. Layers are usually assumed as uniform, but this is often not the case in reality because of inhomogeneities or defects that are difficult or practically impossible to foresee and account for at the modelling stage.

Structural inhomogeneities include delamination, cracks and gaps (Siviour and McIntyre, 1982; Anderson, 1984), as well as the variable proportion or porosity of constituent ma-

terials (*e.g.*, in concrete or masonry structures) (Byrne et al., 2013), imperfect adherence or discontinuity of adjacent materials due to the ageing process, the adjustments of the structure and/or the relative thermal expansion (or shrinking) of building materials (Kalthod and Knickle, 1982). Defects may also occur in elements where portions of the material(s) (*e.g.*, insulation layer) are missing or the thickness varies, for example due to an inadequate management of the building process, a lack of integration of different aspects of the building process, or limited or missing information on the installation procedure of particularly complex elements (Zero Carbon Hub, 2014; Deconinck and Roels, 2016). Air movement in encapsulated pipes and embedded cavities (Harrje et al., 1979; Siviour, 1994; Lowe et al., 2007) may also introduce uncertainties in the estimations.

Situational inhomogeneities include furniture layout within the room or against the walls, water infiltrations from leaking pipes or gutters, creepers and plants on the external walls. The main difference between a situational and a structural inhomogeneity is represented by the temporary nature of the former issues.

2.2.0.3 *Modelling uncertainties*

Besides the uncertainties listed above, which describe the deviation between the real building element and its abstract representation in the model, additional uncertainties may be introduced by the modelling process itself. These uncertainties arise from additional simplifications (*e.g.*, one-dimensional heat flow) that the modeller may introduce when describing the underlying physical process of interest by means of mathematical descriptions (Zhao et al., 2015), and discretising the processes on digital computers (*e.g.*, due to its finite precision).

Modelling simplifications generally aim to ensure that the simulation is computationally efficient and its complexity is adequate for the purpose of the analysis. Thermal bridges occurring at the intersection between vertical and horizontal elements, or between different materials alternating along the element (*e.g.*, structural members separated by panels (Anderson, 2006), mortar joints (Byrne et al., 2013), or plaster dabs (in the void between the wall and the plasterboard) (McIntyre, 1985)) are often not represented in models. Although simplified calculations such as the standard assessment procedure (SAP) and the reduced data SAP (rdSAP) (Building Research Establishment, 2011) provide guidance for the characterisation of thermal bridges, the methodology may not capture all aspects of the heat transfer and include significant assumptions that may not be representative (Marincioni et al., 2016). Similarly, three-dimensional effects introduced by the variable proportion or porosity of constituent materials (*e.g.*, concrete or masonry structures) (Byrne et al., 2013), or embedded water pipes (*e.g.*, the supply and

return pipes for heating services (Guattari et al., 2017)) are also often neglected from simulations.

2.2.0.4 *Monitoring uncertainties*

By definition, the performance gap represents the discrepancies between thermophysical modelling simulation of building elements and their measured thermal performance. As such, it can be subdivided into two components: the difference between the modelled and the real behaviour, and the mismatch between the real behaviour and the measurements. While the former has been investigated in the three sections above, this section investigates the latter.

Monitoring uncertainties are related to the intrusiveness of the equipment compared to the undisturbed scenario, its fixing and setting strategy, the equipment specifications, and its calibration and state of repair. Insufficient accuracy of sensors, which may not have been recently calibrated, as well as their placement in locations not representative of the general behaviour of the system investigated introduce a bias in the observations (Section 4.5). The latter can be mitigated by undertaking preliminary surveys to assess the placement of the sensors. Similarly, an inappropriate selection of the sampling interval (*i.e.* too frequent or too slow) compared to the time period over which the observed physical process can occur, either introduce artefacts in the recorded signal (*e.g.*, aliasing) or fail to capture useful information (Madsen et al., 2015). Some general guidelines on the mitigation of the potential uncertainties are presented in the Section 2.2.0.4.

A number of studies (mainly conducted in the 1980s) investigated the potential effects of, and the measurement errors introduced by, the presence, installation and fixing of the monitoring equipment, such as heat flux plates (HFP) and temperature sensors (Wright et al., 1983; Trethowen, 1986; Standaert, 1987; Cesaratto et al., 2011; Meng et al., 2015). These studies were generally conducted by means of numerical computer simulations (*e.g.*, finite difference approaches), usually assuming that the characteristics of the equipment used match the specifications of common commercial sensors available at the time of the study, and investigating specific building stratigraphies. Results showed that, although the presence of the HFP may impact on the quality of the measurements by distorting the isotherms, large errors can be avoided by using large HFPs (Trethowen, 1986; Standaert, 1987; Meng et al., 2015), increasing the size of the guard ring (Trethowen, 1986), keeping an adequate proportion between the guard zone (*i.e.* the portion of passive material surrounding the sensing area) and the overall size of the HFP to minimise edge effects (Standaert, 1987), and decreasing the contact resistance between the sensor and the surface (Wright et al., 1983; Trethowen, 1986).

The operational error was found to be a function both of the thermal resistance of the HFP (Trethowen, 1986; Standaert, 1987) and the thermal resistance of the measured structure and air film layer (Trethowen, 1986; Standaert, 1987). Building on Trethowen's (1986) research Cesaratto et al. (2011) used a number of post-processing methods to investigate how uncertainties on the input data (in this case, synthetic time series recreated from data measured *in-situ*) influence the steady-state estimates of thermophysical parameters. Specifically, the authors investigated the cases of significant variation of the external temperature over time, the use of temperatures recorded over the internal HFP, and differences in emissivity between the HFP and the wall surface. Results showed that the presence of the HFP reduces the mean specific heat flux exchanged by the element at the measured point compared to the undisturbed case, while the presence of significant variations in external temperature introduced a deviation (whose magnitude varied depending on the data analysis method adopted) in the estimated R-value. The authors also observed that the use of surface temperature recorded over the HFP seemed to generate a slight improvement on the estimates of the methods considered, while an emissivity of the HFP lower than that of the wall seemed to slightly worsen the outputs.

Wright et al. (1983) conducted laboratory experiments to investigate the effects of the thermal contact resistance and the roughness of the surface of the element. They concluded that surface roughness and poor adhesion of the sensor were the variables having major influence on the heat flux measurements. On the thermal contact, Siviour and McIntyre (1982) investigated the impact of different bonding strategies (*i.e.* dry contact, double-sided tape, silicone grease and rubber) on the measured heat flux. They concluded that the grease had the least influence on the measurements while the dry press against the wall was the less reliable mounting method. However, its advantage of causing no damage to the finishes compared to the grease was considered a good reason to accept its lower accuracy.

Although these studies investigated several useful aspects of the uncertainties related to monitoring equipment, it is difficult to use them to derive specific uncertainties for different monitoring campaigns. Since all these studies focussed on specific conditions and equipment, it is challenging to generalise such findings and thus provide contextual rather than specific information for those undertaking monitoring. Additionally these studies tended to investigate one aspect at a time, while more than one source of uncertainty may simultaneously affect *in-situ* measurements, and their interrelations may be very complex. Of the studies reviewed, only Meng et al. (2015) acknowledged this potential limitation. More studies would be valuable (especially if supported by *in-situ* and thermal lab experiments) to understand the sources of uncertainties potentially af-

fecting *in-situ* measurements and to improve guidelines for the placement of sensors, aiming at minimising their effects.

IN-SITU MEASUREMENTS AS A MEANS TO CLOSE THE PERFORMANCE GAP Although all methods for the characterisation of the thermophysical properties of building elements are affected by the uncertainties listed above, methods based on *in-situ* measurements are generally preferable to the use of literature values or laboratory tests for the reasons illustrated below. Whilst laboratory tests would in principle (but not necessarily (Roels et al., 2004)) allow a more accurate characterisation of the thermophysical properties of building materials than *in-situ* measurements, thanks to a better control of the environment and boundary conditions, the latter are more representative of the in-use behaviour of the structure at scale (Lindfors et al., 1995) and generally do not cause damage to the building element (*e.g.*, to collect specimens) (Flanders, 1980). Additionally, a large portion of the sources of uncertainties affecting *in-situ* measurements can be minimised by adopting best-practice techniques (Energy Saving Trust, 2005). For example, measurement uncertainties can be minimised by attentive selection and set up of the monitoring equipment, ensuring that it is well calibrated and the accuracy is adequate. Similarly, the use of a thermal camera to instruct the placement of sensors and avoid structural inhomogeneities and defects helps to ensure that the location surveyed is representative of the average behaviour of the element (Energy Saving Trust, 2005; C1155-95, 2011).

By collecting direct information on the case study investigated, *in-situ* measurements enable the characterisation of the conditions and state of conservation (*e.g.*, air infiltration, moisture content) of the structure (Cesaratto and De Carli, 2013), the local microclimate (*e.g.,* prevalent wind velocity and atmospheric excitations, local environment topography, geometry and orientation of the element/building), and the quality of the building construction and installation (Feuermann, 1989). All these aspects cannot be accounted for by thermophysical values (*e.g.*, U-value, thermal conductivity, specific heat capacity, density) provided by manufactures or literature references, as these are generally estimated by testing the building materials in controlled environments (*e.g.*, thermal chambers or test cells) (Rasooli et al., 2016) and subject to well characterised temperature profiles and moisture content, at least on the internal side. Additionally, each building material category may present broad ranges of tabulated properties and similarly looking materials may have very different thermophysical performance, with obvious implications on the energy performance estimations in the absence of case-specific informations on the value to use. For example, according to the Chartered Institution of

Building Services Engineers (CIBSE) (2007), the thermal conductivity of homogeneous "brick masonry" ranges between 0.36 and 1.51 $Wm^{-1}K^{-1}$ if protected from the external weather and between 0.50 and 2.06 $Wm^{-1}K^{-1}$ if exposed; similarly, the thermal conductivity of "plaster" ranges from 0.22 to 0.52 $Wm^{-1}K^{-1}$, "gypsum plaster" ranges between 0.51 and 0.81 $Wm^{-1}K^{-1}$, and "cement plaster" between 0.72 and 1.50 $Wm^{-1}K^{-1}$.

The following sections present a review of steady-state and dynamic methods to characterise the thermophysical performance of buildings (and building elements) from *in-situ* measurements.

2.3 STEADY-STATE METHODS TO ASSESS THE THERMOPHYSICAL PROPERTIES OF BUILDINGS

Steady-state methods represent the simplest approach to model heat transfer as they enable a simplification of the general Fourier's Law (Section 2.1). The first application of steady-state methods in building-related applications was proposed by Box in 1868 when he suggested a practical approach to determine the "*loss of heat by buildings artificially heated*" (Urbikain and Davies, 2008). Box (1868) described the three simultaneous equilibrium steps of the cooling process of a wall by considering uniform temperature in the element to "*calculate the quantity of heat transmitted by several formulae*":

- as "*the amount of heat which the wall will absorb*", "*knowing the temperature of the internal air [...] and of the internal surface of the wall in contact with it*";
- "*from the known temperature of the two surfaces of the wall [...] and the conducting power of the material [...] irrespective of the temperatures of the internal and external air*"
- "*from the known temperature of the external surface of the wall [...] and the temperature of external air and surrounding objects which absorb radiant heat*".

Within the notation of this thesis, the equivalence of the three formulae above can be expressed as:

$$\frac{T_{\text{int,a}} - T_{\text{int,s}}}{R_{\text{si}}} = \frac{\lambda}{d}\left(T_{\text{int,s}} - T_{\text{ext,s}}\right) = \frac{T_{\text{ext,s}} - T_{\text{ext,a}}}{R_{\text{se}}}$$

where $T_{\text{int,s}}$ and $T_{\text{ext,s}}$ are the temperatures of the internal and external surface of the element; $T_{\text{int,a}}$ and $T_{\text{ext,a}}$ are the temperatures of the internal and external air.

Steady-state methods are still the most commonly used approach to describe the heat transfer through building elements and characterise their as-built thermophysical properties (Deconinck and Roels, 2016). These include the average method (BS ISO 9869-1, 2014) — or summation method in C1155-95 (2011) — and regression models (Jiménez

and Madsen, 2008). Steady-state models assume constant boundary conditions, time-independent thermophysical properties of building materials, and neglect heat storage effects (Hens, 2012). These conditions are very unlikely to be achieved on site for real building elements, although reasonable estimates may be obtained in stable conditions (BS ISO 9869-1, 2014).

Given the theoretical simplifications, the use of steady-state methods for the characterisation of the thermal structure of building elements from *in-situ* measurements of heat flux and temperatures present a number of practical limitations. To ensure that thermal mass effects have been minimised, negligible changes in the net heat storage have to be observed between the start and the end of the monitoring period. This is achieved by collecting data over long monitoring periods and requiring that the temperature of the thermal mass at the beginning and at the end of the survey coincide. Additionally, large average temperature differences between the two sides of the element are also required to obtain robust estimates. Given the mathematical definition of U-value (*i.e.* the ratio of the mean integral heat flow rate density over the mean integral temperature difference, Equation 2.15) small temperature differences, and consequently small heat fluxes, would result in an undetermined form (0/0 type) of the ratio. Similarly, small temperature differences and heat fluxes would magnify the noise on the relative error on the U-value estimates (Equation 4.25).

To ensure that estimates obtained using steady-state methods are a good proxy for the on-site dynamic thermophysical behaviour of the element under study, good-practice recommendations have been developed to account for the theoretical requirements discussed above. These advise to avoid monitoring periods where the average temperature difference is small, as this may decrease the accuracy of the estimates and lengthen the survey (Roulet et al., 1987; Desogus et al., 2011). Measurements have to be undertaken during the winter season, preferably when the average temperature difference is above 10 °C (Siviour and McIntyre, 1982; Energy Saving Trust, 2005; Baker and van Dijk, 2008; Desogus et al., 2011), to avoid that small temperature gradients (and therefore heat flux) are observed or that the heat flux reverses during the survey (Lindfors et al., 1995). Additionally, measurements have to be collected on north-facing elements (in the northern hemisphere) to avoid direct solar radiation effects (Anderson, 1984), and away from sources of heat such as radiators, pipes, appliances and lights (Energy Saving Trust, 2005). Finally, it is advised that an integer number of full days is considered during the analysis, such that the differences between the initial and final conditions (*i.e.* temperature and net heat storage) of the thermal mass are minimised.

2.3.1 *The BS ISO 9869-1:2014 Standard*

Among steady-state approaches, the average method (AM) is one of the most commonly used to evaluate the thermophysical properties of building elements from *in-situ* measurements (Deconinck and Roels, 2016). In the UK this method is standardised in BS ISO 9869-1 (2014), which is the British implementation of the European BS ISO 9869-1 (2014). It defines the thermal transmittance (U-value) of a building element as the ratio of the mean integral heat flow rate density and the mean integral temperature difference collected over a sufficiently long period of time:

$$U = \frac{\frac{\tau}{n}\sum_{p=1}^{n} Q^p}{\frac{\tau}{n}\sum_{p=1}^{n}\left(T^p_{\text{int,a}} - T^p_{\text{ext,a}}\right)} = \frac{\sum_{p=1}^{n} Q^p}{\sum_{p=1}^{n}\left(T^p_{\text{int,a}} - T^p_{\text{ext,a}}\right)} \tag{2.15}$$

where Q^p is the density of heat flow rate measured at each time step p $\left[\text{Wm}^{-2}\right]$; τ is the duration of the step between successive observations (*i.e.* the recording interval for the measured quantities) and n is the number of observations; $T^p_{\text{int,a}}, T^p_{\text{ext,a}}$ are the interior and exterior environmental (ambient) temperature at each time step [°C or K].

To ensure the U-value estimates from *in-situ* measurements are representative, the minimum length of the time series to be analysed has to be determined. This is obtained by checking that the estimates have converged to an asymptotic value and that the steady-state assumptions hold. Section 7.1 of the BS ISO 9869-1 (2014) Standard lists the stabilisation criteria that have to be met to determine the minimum number of observations. A distinction is made between lightweight (*i.e.* specific heat capacity per unit area less than $20\,\text{kJm}^{-2}\text{K}^{-1}$) and heavyweight (*i.e.* specific heat capacity per unit area above $20\,\text{kJm}^{-2}\text{K}^{-1}$) building elements. In the former case, the Standard recommends the analysis of night-time data (*i.e.* "*from 1h after sunset until sunrise*") and requires that the test is stopped when the results do not differ by more than 5% after three subsequent nights. In the latter case, the following criteria have to be met simultaneously:

- the analysis period is an integer multiple of 24 hours;
- the test period exceeds 72 hours;
- the surface-to-surface R-value at the end of the test does not deviate by more than 5% from that obtained 24 hours before;
- the surface-to-surface R-value calculated for an initial period comprising a number of full days equal to two thirds (or its integer part) of the duration of the monitor-

> ing campaign should not differ by more than 5% from the value computed from an equally long period at the end of the campaign;

Additionally, if the change in the heat stored in the building element is more than the 5% of the heat passing through it over the test period, storage effects have to be accounted for according to one of the methods described in Section 7.2 or in Annex B.

To improve the performance of the AM, Section 7.2 and Annex F propose a procedure for the calculation of correction factors ("*thermal mass factors*") which account for storage effects. The Standard encourages the use of this procedure especially for heavyweight building elements in the cases where the stabilisation criteria are not fulfilled, as it should in principle shorten the time series to be analysed compared to the regular AM. However, the method suggested in the Standard contains the significant assumption that the thermal mass may be derived from the literature rather than *in-situ* measurements. The factors are in fact calculated assuming thermophysical properties from look-up tables, potentially introducing the uncertainties related to the use of tabulated properties of building materials (discussed in Section 2.2) and the practical limitations of performing boroscopic investigations or destructive analysis when the structure of the element investigated is unknown (Rasooli et al., 2016). Furthermore, the method suggested retains a semi-stationary approach, which does not model the dynamic effects and is still affected by the core assumptions of the steady-state approach described above (Deconinck and Roels, 2016).

The BS ISO 9869-1 (2014, p.12) Standard provides a list of the main uncertainties affecting the measurements and a quantification of their proportional effect on the final U-value estimation (summarised in Table 2.1 on page 60). Although these are useful references, the Standard does not state how the percentages (which in most cases are reported as fixed values) were calculated, nor does it provide a method to account for situations when alternative values may be more appropriate. For example, the Standard states that "*the accuracy of the measurement depends on errors caused by the variations over time of the temperatures and heat flow*" and that "*such errors can be very large but, if the criteria described in 7.1 and 7.2 or Annex C are fulfilled, they can be reduced to less than ± 10 % of the measured value*". However it does not report a procedure to reduce the error when the criteria are met — which in principle should represent the majority of cases if the Standard is applied correctly (Table 2.1 on page 60). Additionally, the Standard lists the "*accuracy of the calibration of the HFP and the temperature sensors, and the accuracy of the data logging system*" as sources of uncertainties. However, in the case of calibration errors it does not provide criteria to determine whether the use of the 5% uncertainty suggested is representative of the case study, nor an alternative method for the determination

Table 2.1: Sources of measurement uncertainties and their quantification, according to Section 9 of the BS ISO 9869-1 (2014, p.12) Standard. A summary of other sections of the Standard cross-referenced in Section 9 is also provided.

Uncertainty	Quantification	Cross-reference to other sections
Accuracy of the calibration of the HFP and the temperature sensor	5% (if the instruments are well calibrated)	-
Accuracy of the data logging system (see Annex E)	-	*Annex E*: Procedure for checking the accuracy of the measurement system of heat flow rate
Random variations due to slight differences in thermal contact between the sensors and the surface	5% of the mean value (if the sensors are carefully installed)	-
Operational error of the HFP due to modifications of the isotherms caused by the presence of the HFP	2-3% (if the operational error is estimated by a suitable method (*i.e.* finite-element analysis), and a correction is applied to the data)	-
Errors caused by the variations over time of the temperatures and heat flow	<10% if the criteria in 7.1 and 7.2 or Annex C are met. This contribution can be further reduced by: a) recording extended time series; b) minimising the variations of indoor temperatures; c) using the dynamic interpretation method (Annex C)	*Section 7.1*: Stabilisation criteria to ensure representative U-value estimates *Section 7.2*: Procedure for the calculation of the thermal mass factors *Annex C*: Examination of the structure of the element
For U-value measurements, temperature variations within the space and differences between air and radiant temperatures	-	-

of the relative uncertainty based on the specification of the sensors. Similarly, in the case of data logging system the Standard refers to Appendix E, where a procedure is provided to guide the surveyor on the selection of appropriate equipment. Specifically, the method calculates the ratio between the measurement minimum output value and the density of heat flow rate (E) and suggests that $E \leq 10\%$ is preferable:

$$E = \frac{Q_{\mathrm{Hm}}}{Q} \cdot 100 = \frac{e_{\mathrm{m}}}{1/f} \cdot \frac{1}{Q} \cdot 100 \tag{2.16}$$

where Q_{Hm} is the minimum output of the heat flow rate measurement system; Q is the density of heat flow rate, either calculated from the measurements (if the test is performed after the monitoring campaign) or using the indoor-to-outdoor temperature difference calculating the U-value from look-up tables (if the test is performed beforehand); $1/f$ is the calibration factor of the HFP; e_{m} is the minimum output of the data logger. However, the procedure suggested does not provide methods to quantify and account for the accuracy of the data logging system.

2.4 DYNAMIC METHODS TO ASSESS THE THERMOPHYSICAL PROPERTIES OF BUILDINGS

Dynamic methods have been developed to overcome some of the limitations of steady-state approaches (discussed in the previous sections) and to gain a more comprehensive understanding of the thermodynamic performance of the built environment by accounting for the dynamic fluctuations of the system rather then neglecting them (Deconinck and Roels, 2016). This section presents an historical overview of dynamic methods developed and adopted to evaluate the thermal performance of buildings.

2.4.1 *Historical overview*

One of the first attempts at describing the thermodynamic behaviour of buildings, based on the one-dimensional Fourier's Law (Section 2.1), was proposed by Esser and Krischer in 1930 (as cited in Urbikain and Davies, 2008). The model describes the thermodynamic response of the building element as the ratio of the heat stored (S) and the heat loss (L) in steady-state conditions, assuming that the introduction of an impulse excitation in the system results in an exponential heat loss decay after a time delay. Although the quantity S/L has the units of time, it was Bruckmayer in 1940 who first gave a physical interpretation to it as the "*flow through time*" (*i.e. "the time needed for the entire heat content*

to be lost if passing through at its initial rate") (Davies, 2004). This measure of the thermal stability of the building envelope has been later referred to as time constant, decay time, or response time. Further studies have shown that Esser and Krischer (1930) model is correct only for simple models, but not generalisable (Davies, 1984).

Depending on the approach used to simplify and solve the Fourier's equation, different dynamic methods have been subsequently proposed to estimate the thermophysical properties of buildings and building elements (Parnis, 2012). These can be solved either numerically or analytically and they can be mainly categorised as: lumped parameter methods, finite difference methods and response function methods. The latter can be formulated either in the time or the frequency domain (in which case it is sometimes referred to as the harmonic method) (Wang and Chen, 2003; Underwood and Yik, 2004).

The sections below explore the different approaches and present more recent advances.

2.4.1.1 *Electrical analogy and lumped thermophysical parameter method*

In the early 1940s, Paschkis and Baker (1942) firstly introduced the idea of electrical analogy to heat transfer to simulate the thermophysical performance of buildings. The method takes advantage of the mathematical equivalence of heat flow equations to electrical circuit theory to map the thermophysical problem (*e.g.*, the building structure or thermal zones, the building technologies, and the surrounding environmental conditions) in terms of equivalent electrical components (Paschkis and Heisler, 1944). The model construction implies the approximation of evenly distributed boundary conditions and thermophysical properties of materials into a number of thermally uniform lumped elements, where thermal resistances are represented by resistors, thermal capacitances (or thermal masses) by capacitors, the amount of heat stored in each thermal mass is analogous to the electrical charge in each capacitor, temperature differences are equivalent to the voltage, and heat flow to the current (see Section 3.3).

Given the direct analogy of the electrical and the thermal problem, each parameter of the equivalent electrical circuit has a clear thermophysical interpretation and the estimates can be easily converted back into the thermal context (Gouda et al., 2002) to gain useful information on the thermodynamic behaviour (*i.e.* heat transfer and storage) of the system under study. As the thermal mass effects introduce a time delay in the response of the measured heat flux to changes in external and internal temperatures, differential equations have to be introduced (Section 2.1). By imposing the conservation of heat (the thermal analogues to the Kirchhoff's current law (Parnis, 2012)) at each node, the resulting differential equations can be solved analytically by means of compu-

tationally efficient approaches (Gouda et al., 2002) as the lumping process reduces the problem complexity at the model construction level rather than at the computational phase (Parnis, 2012). However, the simplification introduced by the lumping process may impact on the accuracy of these models and the insights gained (Parnis, 2012). Accuracy can be improved by increasing the model order (*i.e.* adding lumped elements) (Gouda et al., 2002), although the model may use the extra complexity to describe the noise in the observations rather than the underlying physical process (a phenomenon known as "overfitting") (MacKay, 2007, Chs.39,44).

Originally, electric circuits were analysed either mathematically, by applying electrical circuit theory, or experimentally, by physically building the circuit and measuring the current (or voltage) at its nodes (Paschkis and Heisler, 1944; Burnand, 1952). The latter method proved to be particularly useful to solve those case studies that were too difficult to be solved mathematically (Paschkis and Heisler, 1944) or to allow its use for practical purposes also by those not mathematically inclined (Nottage and Parmelee, 1954; Parnis, 2012). Although the advent of digital computers and the ever-increasing computing power has enabled the development of more complex and computationally demanding dynamic methods, electric circuits and the electrical analogy are still extensively adopted nowadays (Kristensen et al., 2004; Wang and Xu, 2006; Gutschker, 2008a; Naveros et al., 2014), for example as a starting point to model buildings and building structures (Kramer et al., 2012) and to derive heat balance equations (Parnis, 2012).

2.4.1.2 *Response function methods*

In the early 1940s, Mackey and Wright (1944; 1946) (as cited in Urbikain and Davies, 2008) proposed a frequency-domain-based solution to the one-dimensional heat transfer equation. Although the idea of predicting the heat flow rate through multi-slab elements using *"fonction d'influence de flux"* had been already solved in principle in an extensive study by Nessi and Nisolle in 1925 (as cited in Oh, 2013), their approach was unpractical as the calculations had to be done by hand (Mitalas and Stephenson, 1967). Mackey and Wright (1944) solved the problem by using the same framework as Nessi and Nisolle (1925) but restricting their approach to the case of periodic external temperatures and constant internal temperatures. They introduced the idea of a complex U-value (u) — whose magnitude is smaller than the steady-state U-value — to account for the fact that after a peak in (sol-)air temperature has been reached, a building element attenuates and shifts by some hours the peak of heat entering the building (Urbikain and Davies, 2008). The quantity u was defined as the ratio of the "*amplitude of heat flow to the room index temperature over the amplitude of daily swing of outdoor sol-air temperature, with constant room*

index temperature" (Urbikain and Davies, 2008). The complex U-value was also tabulated to allow the calculation of the heat transfer through single- and double-slab walls, given the variation in outdoor air temperature. Limitations of Mackey and Wright (1944; 1946) formulation were represented by the assumption of sinusoidal external air temperature swings (Wang and Chen, 2003) and the introduction of non-negligible errors when the shape of the excitation and the response do not match (Ruivo and Vaz, 2015). Correction factors were developed to adjust for non-perfect sinusoidal behaviour (Urbikain and Davies, 2008). A further contribution to this branch of research was provided by Danter (1960), who defined an additional thermophysical parameter (y) representing the ratio of the "*amplitude of heat flow into the internal surface of a room over the amplitude of daily swing of the room index temperature*" (Urbikain and Davies, 2008). The work of Mackey and Wright (1944; 1946), Danter (1960) and the definition of steady-state U-value resulted in the formulation of the admittance procedure by Guide and Book (1970). The admittance method (still in use in the EN ISO 13786 (2008) Standard) provides a means to estimate the thermophysical response of a building element subject to sinusoidal heat flux or temperatures on its boundary(ies). The sinusoidal assumption represents a limitation for the application of this valuable method, as it is not able to properly model more-realistic non-sinusoidal daily variations (Urbikain and Davies, 2008). However, this limitation can be overcome in linear time-invariant problems by decomposing the signal(s) into a number of sinusoidal components, applying the admittance method to each component obtained and then recombining the outputs using the superposition principle (Balocco et al., 2012). Due to the use of the discrete Fourier transform to decompose the thermodynamic signals, this method is well suited for those cases where the time series is preceded and followed by a few days of similar thermal profiles. Conversely it cannot accurately model the cases where sudden changes had occurred just before or after the period analysed (Balocco et al., 2012).

In the 1950s new methods were implemented to overcome the limitations of the assumption of sinusoidal and linear inputs made by Mackey and Wright (1944; 1946) (as cited in Wang and Chen, 2003). In 1956 Brisken and Reque introduced for the first time the basis for response function methods by developing a numerical method that used a lumped parameter model to calculate what is termed "response factors" to estimate the heat flux profile through a multi-layer slab exposed to rectangular unitary air temperature pulses (Wang and Chen, 2003). A decade later, an important improvement to the response factor approach was proposed by Stephenson (1962) by replacing the unitary rectangular pulses with triangular ones (*i.e.* equivalent to trapezoidal integration rule), which allowed them to analytically solve the problem (Wang and Chen, 2003). Steph-

enson modelled the heat loss at any time step using a backward moving average (MA) model that estimates the heat flow as the convolution of the series of values of the driving temperature with the response function to a unitary triangular pulse (Stephenson, 1962). This method was later extended into the conduction transfer function method (Stephenson and Mitalas, 1971) by mapping the differential equations (*i.e.* response factors) using a Z-transform, effectively obtaining an auto-regressive moving average (ARMA) model. A limitation of this approach was represented by the method used to calculate the roots of the characteristic equations, which in some cases may lead to incorrect and inefficient calculation (Ouyang and Haghighat, 1991). Improvements to the calculation of the roots of the characteristic equations were provided by Gough (1982); Hittle and Bishop (1983) (as cited in Wang and Chen (2003)). Further formulation of the conduction transfer function method included the use of a state-space model representation either in continuous time, through the S-transform, or in discrete time, through the Z-transform. Using state-space models, the thermal response factors of multi-layer walls can be obtained without finding the roots of the characteristic equations (Ouyang and Haghighat, 1991).

2.4.1.3 *Finite difference method*

The finite difference method is an alternative approach to the response factor methods (Underwood and Yik, 2004). It solves Fourier's Law by approximating the partial differential equations with difference equations and uses numerical methods for their solution (Gouda et al., 2002). Whilst approximation of the derivative using finite differences was already known by Euler in 1768 (Euler, 1755), approaches based on the finite differences method become very popular only in the 1950s when the new high-speed computing machines proved their suitability to solve very complex numerical problems (Ames, 1992). The finite difference method consists of subdividing the spatial (*i.e.* the building structure) and the temporal domains into a finite number of control volumes and time steps, and it assumes that the state of each volume at each time step can be represented by the state at a fixed point of the volume (*e.g.*, a point in the mid-plane) (Underwood and Yik, 2004). Specifically, it assumes that the state of each volume is constant throughout it. An indexed sequence of the original continuous dynamic function is obtained by sampling it at discrete intervals. Therefore, high spatial resolution and short time intervals are fundamental for accurate estimates, which may result in high computational demand (Gouda et al., 2002) especially in those cases where the dynamics of the system vary on a short time scale.

Several methods are available to approximate the derivative (Underwood and Yik, 2004), and model stability criteria have to be considered to identify the most appropriate one (Gouda et al., 2002). The most commonly used are the forward, backward and central forms (further discussion is provided in Section 3.3). The forward form approximates the derivative at the current step with the slope of the cord between the next and current step, the backward form approximates the derivative at the current step with slope of the cord between the current and previous step, while the central form approximates the derivative at the current step with the slope of the chord between the previous and the next step (Smith, 1985, Ch.1). From the Taylor expansion of the function to be approximated, it can be observed that the leading error of the central-difference is smaller ($O\left(h^2\right)$) than the leading error for the forward- or the backward-difference ($O\left(h\right)$) (Smith, 1985, Ch.1) .

2.4.2 *Recent advances*

The recent increasing availability of computational power has eased the development of more complex dynamic models to simulate the thermophysical performance of buildings and building elements (Kramer et al., 2012). The thermophysical properties of a building element can be estimated either by inputting the measurements into models derived from first principles (*e.g.*, a set of governing laws, system properties and boundary conditions) or by matching our understanding of the system (model) to the measured data by means of optimisation algorithms (Rabl, 1988; Coakley et al., 2014). The former are generally referred to as forward, law-driven or white-box methods, and the latter as inverse or data-driven methods. The matching between observations and estimates is achieved by using optimisation algorithms minimising a specified objective function (Kramer et al., 2012). Inverse models are generally categorised as black-box or grey-box. Black-box models do not require any physical knowledge of the system as they use mathematical or statistical techniques to infer the relationship among the inputs and outputs of the problem (Kramer et al., 2012). Conversely, grey-box models combine the advantages of white- and black-models by including the knowledge of the underlying physical process in the statistical description of the system and its behaviour, representing the prior information of the relationships between its parameters (Kristensen et al., 2004).

Given their formulation, law-driven models require an understanding of the dominant relationships among the mechanisms governing a physical effect of interest (Mustafaraj et al., 2010). Therefore, as they assume the physical model to be known, a model

misspecification[1] results in incorrect estimates. Additionally, the approach may quickly require a larger number of inputs (given the large number of physical factors involved) than available measurements (Coakley et al., 2014). Conversely, due to the statistical approach, inverse problems can account for uncertainties in the model's inputs (Kristensen et al., 2004) and are able to infer the properties of a system from a restricted set of physical measurement of the phenomenon of interest.

Unlike white-box models, black-box models can evaluate the behaviour of the system for cases that have not been observed (Coakley et al., 2014), although the set of output variables estimated generally does not have a direct physical interpretation (Kramer et al., 2012). By incorporating both physical knowledge and prior information, grey-box models usually require a relatively small number of parameters that have a physical interpretation. Additionally the estimates are more robust and reproducible, and less affected by bias (*i.e.* the approximation error due to the assumption and simplifications introduced in the model) (Kristensen et al., 2004).

In the context of the estimation of the thermophysical properties of building components under real dynamic conditions (*i.e. in-situ* buildings or test cells), a number of black-box and grey-box methods have been developed and applied, for example through the PASSYS project and the PASLINK Network (Baker and van Dijk, 2008; Androutsopoulos et al., 2008). Among the black-box models, ARX and ARMAX models (Norlén, 1990; Jiménez et al., 2008; Naveros et al., 2015) are used to describe the heat transfer in the building element by means of discrete transfer functions and identify the parameters by using multiple linear regression to fit the parameters to the observations. Given the nature of the modelling approach, the estimates have no direct physical interpretation. However, both Norlén (1994) and Naveros et al. (2015) presented methods to associate a physical interpretation to the parameter estimated, partially overcoming the limitations of using a black-box model. The methods were successfully applied to *in-situ* measurements.

Two of the most widely adopted grey-box models are those proposed by Gutschker (2008b) and Kristensen et al. (2004). The method by Gutschker (2008b), also known as LORD (*i.e.* LOgical R-Determination), is a deterministic method modelling the thermal structure by means of equivalent electrical circuits and discretising the temperature field using a number of temperature nodes. The parameters are identified by minimising an objective function describing the root mean square of the differences (*i.e.* the residuals) between the measured and modelled temperatures. The accuracy and reliability of the

1 In statistics, model misspecification is the problem arising when some of the explanatory variables are missing, when the functional form relating the variables is incorrect, or some of the assumptions are not met in reality (Winship and Western, 2016).

estimates is quantified in the form of confidence intervals. The method has been used in a number of applications (Androutsopoulos et al., 2008; Baker, 2008; Jiménez et al., 2009). The method by Kristensen et al. (2004), also known as CTSM (*i.e.* continuous time stochastic modelling), uses equivalent electrical circuits to define a set of stochastic differential equations that, in combination with a set of discrete measurement equations, form a continuous-discrete stochastic state-space model (Janssens, 2016). The parameter estimation is generally based on extended Kalman filter and maximum likelihood estimation (Deconinck and Roels, 2016). The method provides statistical techniques for the model assessment and validation (Janssens, 2016). The method has been applied in several occasions, including those by Jiménez and Madsen (2008); Jiménez et al. (2009); Naveros et al. (2014); Roels et al. (2015b); Deconinck and Roels (2016).

Although black- and grey-box methods have been successfully devised in inverse heat-transfer problems (Wang and Zabaras, 2004; Kaipio and Fox, 2011), the definition and application of Bayesian-based methods in building physics has started to gain interest only very recently. In the context of the evaluation of the thermophysical properties of *in-situ* building components, applications have been first proposed by Biddulph et al. (2014); Dubois et al. (2014); Berger et al. (2016); Rouchier et al. (2017).

2.5 SUMMARY

This chapter reviewed potential sources of uncertainties contributing to the performance gap, a mismatch between the estimated and measured energy performance of buildings (and building elements). Several factors (*i.e.* environmental factors, inhomogeneities and inaccuracies during the modelling and monitoring processes) were identified among its causes. The use of *in-situ* measurements was identified as an important practice to evaluate the thermophysical behaviour of in-use buildings and overcome some of the limitations introduced by the use of tabulated thermophysical properties.

Current methods widely used for the analysis of *in-situ* measurements (*i.e.* steady-state methods) present a number of limitations because of their theoretical formulation. Specifically, these methods require the analysis of sufficiently long time series to minimise thermal mass effects (as these are not modelled by the method) and ensure that the temperature of the thermal mass at the beginning and at the end of the survey coincide. Additionally, large average temperature differences between the internal and external ambient are required to provide robust estimates both in terms of U-value and associated error. To obviate these limitations the analysis usually requires long and seasonally bounded monitoring campaigns, which present a number of limitations for a wider use

of steady-state methods in practical applications. The simultaneous modelling of the heat transfer and storage within a building element may allow dynamic methods to overcome the limitations above. A review of existing steady-state and dynamic methods for the evaluation of the thermal behaviour of buildings (and building elements) was undertaken in this chapter.

The next chapter describes the requirements and desirable features for the development of a novel dynamic grey-box method aiming at overcoming the main limitations of current standard methods (*e.g.,* BS ISO 9869-1 (2014)) for a robust characterisation of the thermophysical performance of *in-situ* elements at all times of the year. Subsequently, it presents the theoretical framework for the dynamic grey-box method developed in this research.

Part II

METHODOLOGY

3

A NOVEL DYNAMIC GREY-BOX METHOD FOR THE ESTIMATION OF THERMOPHYSICAL PROPERTIES OF BUILDING ELEMENTS

The previous chapter presented a review of the literature on the performance gap in buildings and identified the representativeness of the thermophysical properties of the building envelope as one of the most influential aspects contributing to it. A wider use of *in-situ* measurements for the estimation of the performance of buildings in general, and the fabric in particular, was deemed as key (Zero Carbon Hub, 2014) to tackle the problem. Subsequently the chapter revised the theory and methods available (both steady-state and dynamic) for the characterisation of the thermal performance of building elements from *in-situ* measurements.

This chapter identifies and presents the requirements and desirable features for the development of a novel dynamic grey-box method (Section 3.1), followed by a description of the theoretical framework for the method developed[1] in this research, which builds on and further develops the work by Biddulph et al. (2014). A dynamic grey-box method combining a Bayesian framework and lumped-thermal-mass models was identified as an appropriate approach that has not been already explored, and that provides an opportunity to make a distinct contribution and advance the field. The novel method uses the electrical analogy (Section 2.4.1.1) to devise lumped-thermal-mass models simulating the heat transfer through a building element and Bayesian analysis to estimate the set of parameters that best reproduce the monitored data. Section 3.2 provides an overview of Bayesian inference and data analysis, detailing the main steps required for the evaluation of the parameters of interest and contextualising them to the novel method presented in this chapter. Specifically, Section 3.3 presents the family of physically informed lumped-thermal-mass models formulated, Section 3.4 describes the Bayesian framework devised to evaluate the thermophysical parameters of interest, and Section

1 The material presented in this chapter has appeared in Biddulph et al. (2014) and Gori et al. (2017), and was used in Gori and Elwell (2017).

3.5 illustrates model selection and validation techniques used to identify the best model among the several available.

3.1 RATIONALE FOR THE DESIGN OF A NOVEL METHOD

The literature review on the performance gap of the building fabric (Section 2.2) identified the need for diagnostic tests, standardisation and development of analysis methods (or further development of existing methods) as one of the priorities to enhance the current limited understanding of the as-built energy performance across the whole construction sector (Zero Carbon Hub, 2014). Particular stress was placed on the robustness and consistency of the outcomes of the methods. This need for an improved knowledge of the as-built thermophysical performance of buildings and building elements, however, is not isolated nor new. The reliable characterisation of the energy performance of the built environment from measured data has been the topic of three energy in buildings and communities (EBC) Annexes promoted by the International Energy Agency: Annex 58 (International Energy Agency, 2011a), Annex 70 (International Energy Agency, 2016a) and Annex 71 (International Energy Agency, 2016b). In all cases, the aims include(d) the development of common procedures for quality data collection, storage and analysis methods.

From a review of the literature, a statistics-based dynamic grey-box method was deemed as an appropriate approach that had not been already explored (Section 2.4.2) to provide robust estimates while overcoming the main limitations (*i.e.* long and seasonally constrained monitoring campaigns) of the methods commonly adopted (Section 1.0.2 and Section 2.3) for the characterisation of the thermal performance of the building envelope from measured data. The following aspects were considered and selected for the development of the method proposed.

DYNAMIC GREY-BOX METHOD A dynamic grey-box method was chosen as it allows the combination of the advantages of white- and black-box models (Section 2.4.2), effectively coupling the information in the observed data with our previous knowledge about the underlying physical process(es). Being a data-driven approach, the model does not need fine-grained information of the stratigraphy of the building element (and consequently on the thermophysical parameters of the model), if these are not available. However, when this information is available, it can be incorporated to provide better insights (as mentioned in the "statistical framework" subsection below).

The dynamic approach was selected to allow the characterisation and understanding of both heat transfer and storage of building elements (Section 2.1). By modelling both the thermal resistance and the thermal mass(es), the applicability of the approach may be extended to periods where small temperature differences are observed between the two sides of the element, effectively extending the monitoring to non-winter periods (Section 2.3).

Lumped-thermal-mass models were chosen to describe the heat transfer across the building element, as they enabled the parsimonious definition of thermophysical parameters with clear physical interpretation. The physical interpretation of the parameters was considered a useful aspect as it allows the direct use and communication of the estimates for practical purposes, such as quality assurance, design and evaluation of retrofitting interventions, or improved understanding of the thermophysical behaviour of buildings.

STATISTICAL FRAMEWORK A Bayesian framework was selected (Section 2.4.2) for the several advantages provided, which are illustrated in the following. It is flexible, suitable for complex problems, and able to provide a direct quantification of the uncertainties on the parameters of the model accounting for parameters' correlation (Gelman et al., 2013). The method is also able to output the distribution of the parameters (*e.g.*, through Markov Chain Monte Carlo sampling) to explore the probability distribution of the parameters of the model given the observations, which provides further insights into the validity of the results obtained and the relationships between parameters. This framework allows for the inclusion of prior probabilities in the models to account for the potential correlation of the observations (*i.e.* the time series collected *in situ*) or our prior knowledge on the parameters of the model (*e.g.*, the stratigraphy of the building element). This may help reduce the number of observations required to provide robust estimates (which translates into shorter monitoring campaigns) while preserving their quality. Finally, the Bayesian framework allows the use of objective techniques based on statistical evidence to select the model that is more likely to describe the measured data.

NON-DESTRUCTIVE METHOD The use of *in-situ* measurements of temperatures and heat fluxes enables the investigation and characterisation of the thermal performance of building elements by means of non-destructive monitoring campaigns. This implies that the method is suitable for a large range of building elements, including historical ones. Additionally, the use of monitored data allows the investigation of the structure in

its environment and state of conservation, overcoming some of the potential limitations introduced by the use of literature values (Section 2.2).

SCALABILITY Scalability of the method was identified as a desirable feature to easily allow future implementation of new models should the knowledge about the case studies or the underlying physical process change. Lumped-thermal-mass models were selected to describe the heat transfer across the building element.

The remaining of this chapter introduces an overview of Bayesian inference and describes the theoretical framework of the novel dynamic grey-box developed based upon the above specifications.

3.2 BAYESIAN INFERENCE AND DATA ANALYSIS

Bayesian inference refers to "*the process of fitting a probability model to a set of data and summarising the result by a probability distribution on the parameters of the model and on unobserved quantities such as predictions for new observations*" (Gelman et al., 2013). It uses statistical methods based on the Bayes' theorem (Equation 3.41) to estimate the probability of a hypothesis as more information (*e.g.*, data and knowledge) on the process of interest become available. Unlike classic statistics approaches (*i.e.* the frequentist approach), probability in Bayesian terms is defined as an expression of the degree of belief that a hypothesis occurs rather than as long-run frequency (Glickman and Van Dyk, 2007).

Bayes' theorem is named after Thomas Bayes, who firstly proposed a special case of what is now known under this name in a work published (and possibly substantially edited) posthumously by Richard Price in 1763 (Bayes and Price, 1763). A generalised discrete version of the Bayes' theorem and a more articulated version of the inference problem was independently proposed in 1774 by Pierre-Simon Laplace (as cited by Fienberg, 2006). His studies extensively contributed to the development of the Bayesian interpretation of probability and applied it to a wide range of disciplines (Jaynes, 1986). Laplace's rationale was further investigated and refined by a number of researchers in the twentieth century (Jaynes, 1986; Fienberg, 2006). However, it was not until the 1980s that Bayesian research and applications saw a significant growth, when methods able to deal with complex computational problems were formulated (*e.g.*, Markov Chain Monte Carlo sampling).

Two distinct inference phases are usually performed when analysing observations within a Bayesian framework for the purpose of modelling an underlying process (MacKay, 2007, Ch.28): inference on the parameters of interest and model comparison. Bayesian inference on the parameters of the model is undertaken according to the following four main steps (Glickman and Van Dyk, 2007; Gelman et al., 2013, Ch.1.1):

1. Definition of the full probability model expected to describe the underlying process of interest (*i.e.* the distribution that the observations would have if the parameters were known and the model adopted was perfectly true).

2. Definition of the prior probability distribution(s) describing the uncertainty in the values of the unknown parameters of the model, based on the prior knowledge available for the parameters before observing the data.

3. Calculation of the posterior probability distribution except for a normalising constant (also referred to as unnormalised posterior probability distribution), quantifying the uncertainty in the value of the unknown parameters of the model after observing the data. The unnormalised posterior probability distribution is obtained combining the prior probability distribution(s) with the likelihood function. The latter is computed from the full probability model defined in step 1 and the observed data.

4. Calculation of the evidence (*i.e.* the normalising constant) to determine the full posterior probability distribution.

In case more than one probability model is plausible, their evidences (step 4) can be used to compare their relative performance and identify the one that is most likely to describe the underlying process in light of the data.

The rest of this chapter describes the application of the Bayesian framework illustrated above in the context of this research. The full probability model in step 1 was formulated in two phases: a physically informed lumped-thermal-mass model simulating the heat transfer across the building element (simulation phase, Section 3.3) and a model describing the error between the simulated and the observed time series of interest (Section 3.4.1). Section 3.4.2 introduces the prior probability distributions used while Section 3.4.3 presents the optimisation techniques adopted (*i.e.* maximum a posteriori and Markov Chain Monte Carlo). Figure 3.1 on page 78 visually summarises the parameter estimation process for the dynamic grey-box method when using maximum a posteriori estimates and calculating the evidence by means of the Laplace approximation (Section 3.5.1.1). The MCMC algorithm works in a similar fashion, except that rather

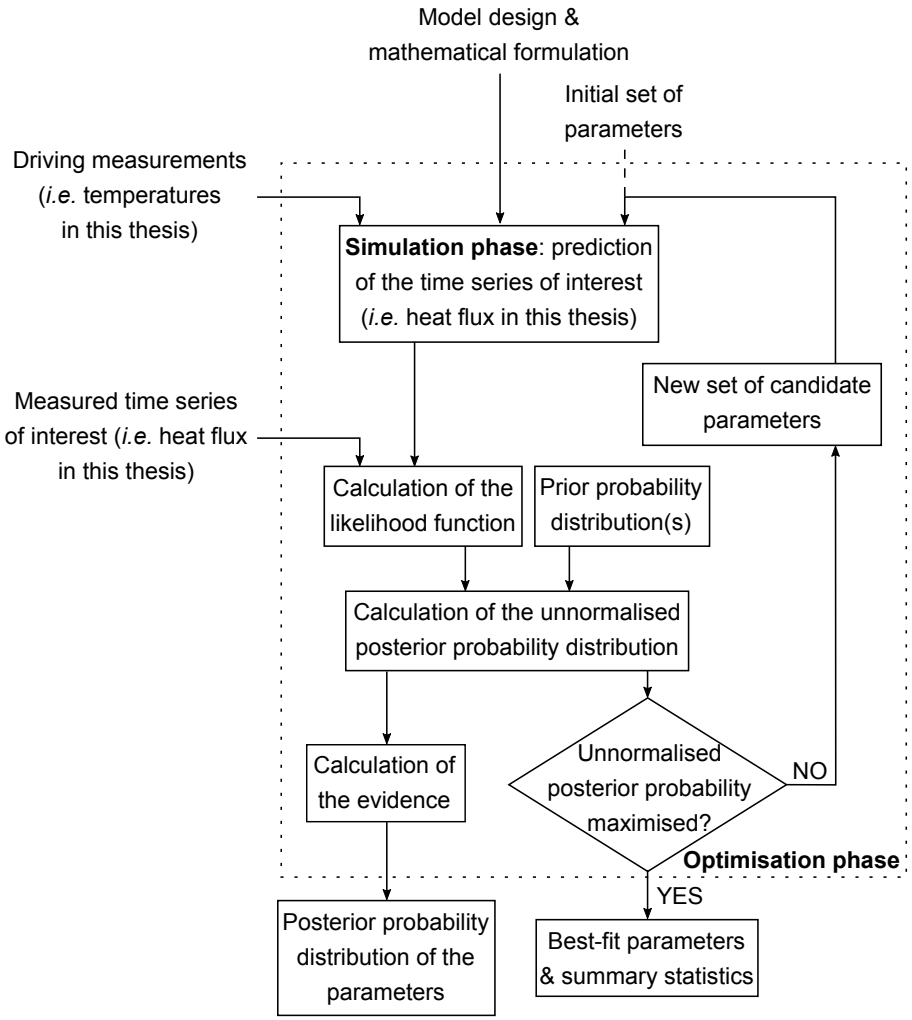

Figure 3.1: Flow chart of the simulation and optimisation phases (using maximum a posteriori estimates) for the dynamic grey-box method devised.

than maximising the posterior probability at each step it proposes a new set of candidate parameters based on the Metropolis-Hastings algorithms (Section 3.4.3.2) and calculates the evidence based on the reciprocal importance sampling method (Section 3.5.1.2). Model validation techniques such as Bayesian model comparison and cross-validation are applied to identify the most probable model among the several devised and ensure that it is able to generalise to new data sets (Section 3.5).

3.3 SIMULATION PHASE: MODELS OF A WALL

As introduced in Section 3.2, the full probability model describing the process of interest was defined in two phases: a physically informed model simulating the heat transfer through the building element of interest and a model describing the error between the simulated and the observed time series. This section describes the former phase (*i.e.*

Thermal quantity	Electrical quantity	Equivalent electrical component
Heat flow density: (Q) $[\mathrm{Wm}^{-2}]$	Electrical current: (I) [A]	Current source: (measured) Ammeter: (computed)
Temperature difference: (ΔT) [K or °C]	Voltage: (V) [V]	Voltage source: (measured) Voltmeter: (computed)
Heat transfer: $Q = \frac{Q}{A} = \lambda\frac{\Delta T}{d} = \frac{\Delta T}{R}$	Ohm's law: $I = \frac{V}{R}$	Resistor:
Heat storage: $Q(t) = C\frac{\mathrm{d}T(t)}{\mathrm{d}t}$	Capacitor charge: $I(t) = \frac{\mathrm{d}V(t)}{\mathrm{d}t}$	Capacitor:
Conservation of heat: $\sum Q_j(t) = 0$	Kirchhoff's junction rule: $\sum I_j(t) = 0$	Junction:

Table 3.1: Electrical analogy to the heat transfer. Correspondence between the thermal and electrical theory and relative electrical circuit components.

simulation phase), while the latter is addressed in Section 3.4.1. In general, simulation consists in representing the behaviour of a system by investigating the behaviour of another system modelled after it. This is achieved by devising abstract models of reality that capture all relevant features and dynamics, omitting secondary effects and minor details (Godfrey-Smith, 2006; Saitta and Zucker, 2013). Once the model is identified, a mathematical description of it in the form of equations has to be defined to simulate the model and compute the quantity of interest from the model's inputs (Nersessian, 1998).

In this work a family of physically informed mathematical models based on the electrical analogy (Section 2.4.1.1) was devised to predict[2] a quantity of interest (*e.g.*, the dynamic heat flow[3] through walls[4]) from physical measurements (*e.g.*, the indoor and external temperatures) and a fixed set of parameters assumed to be known. Adopting the electrical analogy, the models (illustrated in Section 3.3.1 to Section 3.3.3) consisted of a variable number of equivalent electrical components (Table 3.1 on page 79) to describe the thermophysical properties (*e.g.*, thermal resistance and thermal capacitance) of the building element under study. Note that for a multi-layer structure, an individual equivalent electrical component may not coincide with a layer of homogeneous material.

The heat flow through the structure can be determined by imposing the conservation of heat (*i.e.* electrical current) at each node (Table 3.1 on page 79) and solving the system of linear differential equations obtained. The Laplace transform can be used to replace

2 The term "predict" is used in this work in its statistical meaning of estimating the value of a random variable rather than as a synonym of forecast, which implies making a prediction of the value of the variable at a given time in the future.

3 Although heat fluxes were predicted in this thesis using temperature measurements, the theory illustrated in this chapter can be easily adapted to predict other physical quantities, for example temperatures from heat flux measurements.

4 In principle the approach and techniques devised in this research can be applied to different building elements than walls, however walls were the application for this thesis.

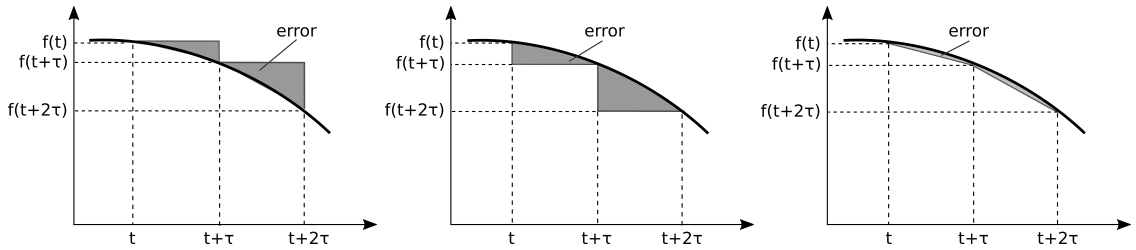

Figure 3.2: Approximation error of the integral operator $(1/S)$ using the forward Euler (left), the backward (middle) and the bilinear (right) transformation.

the linear differential equations with polynomial operations (Lathi and Green, 2014, Ch.8.1.2) in the complex variable S representing the derivative operator. As continuous-time systems cannot be directly simulated on a digital computer, the differential equations have to be sampled and approximated into a discrete-time system (Lathi and Green, 2014, Ch.8.1.2). This is achieved using a sampling transform, which maps a continuous-time system into an approximated discrete-time system (Lathi and Green, 2014, Ch.8.1.2) and the Laplace variable S into the time-shift operator Z. The time shift operator is used in discrete-time systems to represent the observation at the following $\left(Z^{+1}\right)$ or at the previous time step $\left(Z^{-1}\right)$ (Siebert, 1986). Several sampling transform methods are available, and the most common ones include: the forward Euler transformation, the backward transformation and the bilinear transformation.

FORWARD EULER TRANSFORMATION The forward Euler transformation is perhaps one of the simplest transformations. It approximates the continuous-time derivative as:

$$S = \frac{z-1}{\tau}$$

where z and $1\left(\equiv z^0\right)$ are the value of the signal respectively at the next and current time step; τ is the length of the sampling interval. A drawback of this transformation is that the approximation error for the integral operator $1/S$ can be large for a given sampling interval (Figure 3.2 on page 80) and the total accumulated error in the approximate solution tends to grow with time unless the sampling interval is sufficiently small. The forward transformation may also lead to numerically unstable discrete algorithms even when the continuous system is stable (Hauser, 2009, Ch.10).

BACKWARD TRANSFORMATION The backward transformation overcomes the instability problem affecting the forward method, although the sampling interval has still to be sufficiently small. It approximates the continuous signal as:

$$S = \frac{1 - z^{-1}}{\tau}$$

where z^{-1} is the value of the signal at the previous time step. The approximation error for the integral operator $1/S$ can still be large (Figure 3.2 on page 80) and the backward transformation may lead to stable discrete algorithms even when the continuous system is unstable (Hauser, 2009, Ch.10).

BILINEAR TRANSFORMATION The bilinear transformation approximates the continuous signal as:

$$S = \frac{2}{\tau}\frac{1 - z^{-1}}{1 + z^{-1}}.$$

The use of the bilinear transformation is recommended because the approximation error for the integral operator $1/S$ is substantially smaller (Figure 3.2 on page 80) than in the previous two cases (Smith, 1985, Ch.1) and because it leads to a stable discrete-time system if and only if the continuous time system is stable (Hauser, 2009, Ch.10).

The following sections contextualise the general theory illustrated above to the family of models devised and illustrate their mathematical formulation. Specifically, four models with an increasing number of thermal masses (namely the 1TM, 2TM, 3TM, and 4TM models) were implemented.

3.3.1 *Single thermal mass model*

One of the simplest representations of the dynamic heat transfer through a building element is the single thermal mass (1TM) model, a model describing all the heat storage ability of a structure by means of one lumped effective thermal mass[5]. A single thermal mass model incorporating solar radiation as separate source of heat is possible in case incoming solar radiation measurements are available. The two models are described below.

5 A pure resistive model consisting of only one thermal resistance (*i.e.* the zero thermal mass model) was also devised by the authors (Biddulph et al., 2014), however this model is not presented in this thesis as it cannot describe the dynamics of the system.

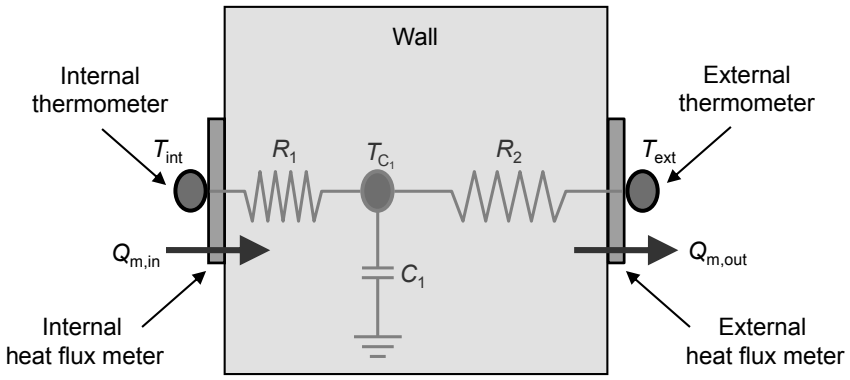

Figure 3.3: Schematic diagram of the single thermal mass model (1TM) showing the equivalent electrical circuit for the heat transfer through the wall and the measured quantities. Parameters of the model are the effective thermal mass (C_1), its initial temperature $\left(T^0_{C_1}\right)$ and two thermal resistances (R_1, R_2). The measured quantities are the internal (T_{int}) and external (T_{ext}) temperatures, and the heat fluxes entering the internal $(Q_{m,in})$ and leaving the external $(Q_{m,out})$ surfaces.

3.3.1.1 *Single thermal mass model without solar radiation input*

The single thermal mass (1TM) model in its simpler form uses the temperature of the internal and external surfaces of the wall (or that of the indoor and outside air[6]) as drivers for the heat flow through the element. The model incorporates four unknown lumped parameters $\theta_{1TM} = \left[R_1, R_2, C_1, T^0_{C_1}\right]^T$ namely: two thermal resistances, one thermal capacitance (or effective thermal mass) and its initial temperature (Figure 3.3 on page 82). The temperature of the effective thermal mass (T_{C_1}) is proportional to the heat stored in the effective thermal mass (C_1), which in turn is the integral of the net heat flux entering the thermal mass. According to the electrical analogy, the temperature of the thermal mass can be predicted by imposing the conservation of heat at the node (Table 3.1 on page 79) as:

$$C_1 \frac{\mathrm{d}}{\mathrm{d}t} T_{C_1}(t) = \frac{T_{int}(t) - T_{C_1}(t)}{R_1} + \frac{T_{ext}(t) - T_{C_1}(t)}{R_2}, \tag{3.1}$$

where T_{int} and T_{ext} are the internal and external temperatures; T_{C_1} is the temperature of the effective thermal mass; R_1 and R_2 are the two thermal resistances; C_1 is the effective thermal mass of the wall. Introducing the Laplace transform (Section 3.3) to replace the derivative operator of the linear differential equation (necessary to describe the heat flux released by the thermal mass) with polynomial operations, Equation 3.1 can be rewritten as:

$$SC_1 T_{C_1} = \frac{T_{int} - T_{C_1}}{R_1} + \frac{T_{ext} - T_{C_1}}{R_2}. \tag{3.2}$$

6 Note that the lumped-thermal-resistance parameters estimated using air temperature measurements as the driver for the heat transfer through the element will already account for the thermal resistance of the air film, as discussed in Section 2.1. For simplicity of notation, surface temperatures will be assumed in the rest of the chapter in the cases where either surface or air measurements could have been used.

The bilinear transform (Section 3.3) was adopted (Gori et al., 2017) instead of the backward difference transform previously used in Biddulph et al. (2014), as it is known to provide a better approximation to the derivative operation (Smith, 1985, Ch.1). Substituting the complex Laplace variable S with the time-shift operator Z and rearranging, the temperature of the thermal mass at each time step can be predicted as:

$$T_{C_1}^{p} = \frac{\frac{T_{int}^{p} - T_{int}^{p-1}}{R_1} + \frac{T_{ext}^{p} - T_{ext}^{p-1}}{R_2} + \left(\frac{2C_1}{\tau} - \frac{1}{R_1} - \frac{1}{R_2}\right) T_{C_1}^{p-1}}{\left(\frac{2C_1}{\tau} + \frac{1}{R_1} + \frac{1}{R_2}\right)} \tag{3.3}$$

where $T_{C_1}^{p}$ and $T_{C_1}^{p-1}$ are respectively the temperature of the effective thermal mass at the current (p) and previous $(p-1)$ time step; T_{int}^{p}, T_{ext}^{p} and T_{int}^{p-1}, T_{ext}^{p-1} are the internal and external temperature of the wall surface at the current and previous time step; τ is the duration of the step between successive observations (*i.e.* the recording interval for the measured quantities).

Assuming a reference system where the heat flowing towards the external ambient is positive[7], a time series of the estimated heat flow entering the internal surface of the wall $\left(Q_{e,in}^{p}\right)$ and leaving the external one $\left(Q_{e,out}^{p}\right)$ at each time step can be predicted knowing the heat per unit area stored in the thermal mass at each time step and the amount of heat that has entered or left it during that time interval. Consequently:

$$Q_{e,in}^{p} = \frac{T_{int}^{p} - T_{C_1}^{p}}{R_1}; \qquad Q_{e,out}^{p} = \frac{T_{C_1}^{p} - T_{ext}^{p}}{R_2}. \tag{3.4}$$

The time series of the estimated heat flow — either the internal or the external one, or both simultaneously — calculated according to the equations above is used to optimise the thermophysical parameters (θ_{1TM}) of the model (as illustrated in Section 3.4.3). Since model comparison tests (Section 3.5.1) require that the performance of different models is evaluated using the same amount of information in terms of monitoring period, number of data streams used for model fitting and observations, the 1TM model using both internal and external measured heat flux is particularly useful to compare this model to more complex ones (*e.g.*, the two thermal mass model) that use both the indoor and outside heat fluxes to fit the model.

3.3.1.2 *The single thermal mass model with solar radiation input*

A different version of the 1TM model can be devised when the incoming solar radiation measurements are available as additional driver for the heat flow through the

7 The same reference system is assumed for clarity for all models illustrated in the following. However, this is not a requirement of the method.

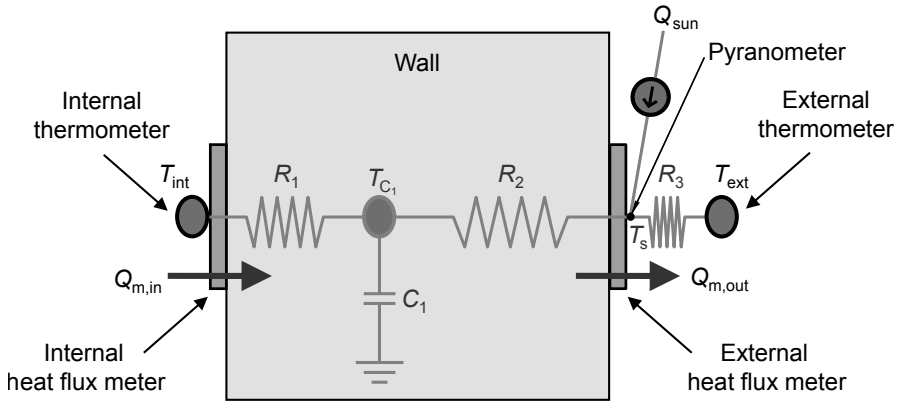

Figure 3.4: Schematic diagram of the single thermal mass model (1TM) when the incoming solar radiation is accounted for separately. The diagram shows the equivalent electrical circuit for the heat transfer through the wall and the measured quantities. Parameters of the model are the effective thermal mass (C_1), its initial temperature $\left(T^0_{C_1}\right)$, three thermal resistances (R_1, R_2, R_3) and the absorbance of the wall (g). The measured quantities are the internal (T_{int}) and external (T_{ext}) temperatures, the heat fluxes entering the internal $(Q_{m,in})$ and leaving the external $(Q_{m,out})$ surfaces, and the incoming solar radiation (Q_{sun}).

element (Figure 3.4 on page 84). In this case, the temperature of the external air has to be used (Section 2.1), while internally either surface or air temperatures can be adopted. The solar radiation input can be modelled as a current source in the equivalent electrical circuit (Figure 3.4 on page 84), which is constituted of six parameters $\theta_{1TM} = \left[R_1, R_2, R_3, C_1, T^0_{C_1}, g\right]^T$. Specifically, it consists of three thermal resistances, one effective thermal mass, its initial temperature, and the absorbance[8] of the wall surface.

A system of two equations is obtained by imposing the conservation of heat at each node:

$$\begin{cases} SC_1T_{C_1} = \dfrac{T_{int} - T_{C_1}}{R_1} + \dfrac{T_s - T_{C_1}}{R_2} \\ 0 = \dfrac{T_{C_1} - T_s}{R_2} + \dfrac{T_{ext} - T_s}{R_3} + g\,Q_{sun} \end{cases} \tag{3.5}$$

where T_s is the temperature of the external wall surface; T_{ext} is the temperature of the external air in this case; g is the absorbance of the wall; Q_{sun} is the incoming solar radiation. Note that the first equation is equivalent to Equation 3.2 when the surface temperature of the wall is used. Substituting T_s in the first equation, replacing the Laplace variable S with the bilinear transform and rearranging, Equation 3.5 becomes:

8 The absorbance of the wall accounts for the proportion of solar radiation entering the wall surface.

$$\begin{cases} \frac{2}{\tau}C_1\left(T^p_{C_1} - T^{p-1}_{C_1}\right) = \frac{T^p_{int} + T^{p-1}_{int} - T^p_{C_1} - T^{p-1}_{C_1}}{R_1} + \frac{T^p_{ext} + T^{p-1}_{ext} - T^p_{C_1} - T^{p-1}_{C_1}}{R_2 + R_3} \\ \qquad\qquad + \frac{gR_3\left(Q^p_{sun} + Q^{p-1}_{sun}\right)}{R_2 + R_3} \\ T_s = \frac{R_2 T_{ext} + R_3 T_{C_1} + gR_2R_3Q_{sun}}{R_2 + R_3} \end{cases} \tag{3.6}$$

where T^p_s, T^{p-1}_s are the temperature of the surface of the wall at the current (p) and previous $(p-1)$ time step; Q^p_{sun} and Q^{p-1}_{sun} are the incoming solar radiation at the current and previous time step. The temperature of the effective thermal mass at the current time step $T^p_{C_1}$ can be estimated as:

$$T^p_{C_1} = \frac{\frac{T^p_{int} - T^{p-1}_{int}}{R_1} + \left(\frac{2}{\tau}C_1 - \frac{1}{R_1} - \frac{1}{R_2+R_3}\right)T^{p-1}_{C_1} + \frac{T^p_{ext} + T^{p-1}_{ext}}{R_2+R_3} + g\frac{R_3}{R_2+R_3}\left(Q^p_{sun} + Q^{p-1}_{sun}\right)}{\frac{2}{\tau}C_1 + \frac{1}{R_1} + \frac{1}{R_2+R_3}} \tag{3.7}$$

The estimated heat flow entering the internal surface of the wall and leaving the external one at each time step can be predicted as:

$$Q^p_{e,in} = \frac{T^p_{in} - T^p_{C_1}}{R_1}; \quad Q^p_{e,out} = \frac{T^p_{C_1} - T^p_{ext} - gR_3Q^p_{sun}}{R_2 + R_3}. \tag{3.8}$$

Observing Equation 3.7 and Equation 3.8 it can be noticed that the thermal resistances R_2 and R_3 and the absorbance g only contribute through the terms gR_3 and $R_2 + R_3$. Therefore the system is underdetermined as three variables are used to determine two quantities that eventually affect the optimisation. Consequently it is impossible to find a unique optimal solution for the individual parameters as one of the three variables can be arbitrarily fixed just satisfying the positiveness constraint. For example, assuming that the combination $[1, 2, 2]$ is identified as optimal for the parameters $[g, R_2, R_3]$, then $[2, 3, 1]$ (and all the combinations yielding the same values of gR_3 and $R_2 + R_3$) is an equally probable solution because it will predict exactly the same time series. The indetermination issue can be overcome by fixing $g = 1$ in Equation 3.7 and Equation 3.8, and the optimal value obtained for R_3 will automatically account for the absorbance of the wall.

Comparing Figure 3.3 on page 82 and Figure 3.4 on page 84, it can be observed that the 1TM model without the incoming solar radiation input is a particular case of the model accounting for it as a separate heat source. Consequently, Equation 3.7 and Equation 3.8 can be reduced to Equation 3.3 and Equation 3.4 when R_3 is set to zero.

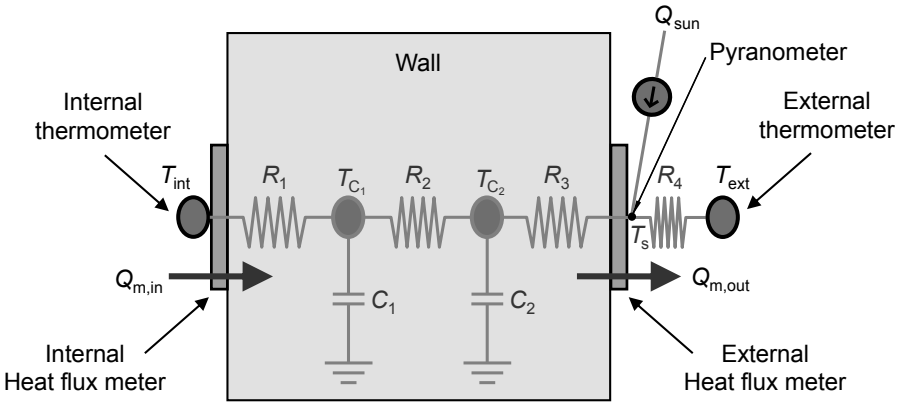

Figure 3.5: Schematic diagram of the two thermal mass model (2TM) when the incoming solar radiation is accounted for separately. The diagram shows the electrical equivalent circuit for the heat transfer through the wall and the measured quantities. Parameters of the model are two effective thermal masses (C_1, C_2), their initial temperature $\left(T^0_{C_1}, T^0_{C_2}\right)$, four thermal resistances $(R_1 \text{ to } R_4)$ and the absorbance of the wall (g). The measured quantities are the internal (T_{int}) and external (T_{ext}) temperatures, the heat fluxes entering the internal $(Q_{m,in})$ and leaving the external $(Q_{m,out})$ surfaces, and the solar radiation (Q_{sun}).

3.3.2 *Two thermal mass model*

A natural extension of the 1TM model is the two thermal mass (2TM) model, a model consisting of an additional thermal mass compared to the 1TM model. The increased complexity of the model may provide a better description of the thermal structure of the building element, particularly for more complex building elements like a cavity wall or an inhomogeneous stratigraphy. Similarly to the 1TM model, two versions of the 2TM model can be devised depending on the availability of measurements of the incoming solar radiation. The derivation of the relationships for the more general 2TM model with solar radiation input is presented below; the simplifications to be made to reduce this model to the one without solar radiation will be discussed at the end of the section.

Similarly to the 1TM model, the 2TM model with solar radiation input uses the measured internal and external temperatures and the incoming solar radiation as drivers for the heat transfer across the structure. The model is constituted of four thermal resistances and two lumped thermal masses (Figure 3.5 on page 86). It incorporates nine parameters (θ_{2TM}), namely four thermal resistances $(R_1 \text{ to } R_4)$, two effective thermal masses (C_1, C_2), their initial temperatures $\left(T^0_{C_1}, T^0_{C_2}\right)$ and the absorbance of the wall (g).

Following the same approach as described in Section 3.3.1, the temperature of the effective thermal masses at each time step can be predicted by imposing the conservation of heat at each node:

$$\begin{cases} SC_1 T_{C_1} = \dfrac{T_{int} - T_{C_1}}{R_1} + \dfrac{T_{C_2} - T_{C_1}}{R_2} \\ SC_2 T_{C_2} = \dfrac{T_{C_1} - T_{C_2}}{R_2} + \dfrac{T_s - T_{C_2}}{R_3} \\ 0 = \dfrac{T_{C_2} - T_s}{R_3} + \dfrac{T_{ext} - T_s}{R_4} + g\, Q_{sun} \end{cases} \tag{3.9}$$

Substituting T_s in the second equation, using the bilinear transform to substitute the Laplace variable and rearranging, the system in Equation 3.9 can be rewritten as:

$$\begin{cases} \dfrac{2}{\tau} C_1 \left(T^p_{C_1} - T^{p-1}_{C_1} \right) = \dfrac{T^p_{int} + T^{p-1}_{int} - T^p_{C_1} - T^{p-1}_{C_1}}{R_1} + \dfrac{T^p_{C_2} + T^{p-1}_{C_2} - T^p_{C_1} - T^{p-1}_{C_1}}{R_2} \\ \dfrac{2}{\tau} C_2 \left(T^p_{C_2} - T^{p-1}_{C_2} \right) = \dfrac{T^p_{C_1} + T^{p-1}_{C_1} - T^p_{C_2} - T^{p-1}_{C_2}}{R_2} + \dfrac{T^p_{ext} + T^{p-1}_{ext} - T^p_{C_2} - T^{p-1}_{C_2}}{R_3 + R_4} \\ \qquad\qquad + \dfrac{g R_4 \left(Q^p_{sun} + Q^{p-1}_{sun} \right)}{R_3 + R_4} \\ T_s = \dfrac{R_3 T_{ext} + R_4 T_{C_2} + g R_3 R_4 Q_{sun}}{R_3 + R_4} \end{cases} \tag{3.10}$$

where $T^p_{C_2}$ and $T^{p-1}_{C_2}$ are respectively the temperature of the most external effective thermal mass at the current and previous time step. Grouping all the variables at the current time step $\left(T^p_{C_1}, T^p_{C_2} \right)$ as first member and all the rest as constant terms (*i.e.* the value assumed at the previous time step is known at the current time step), the coefficients of the parameters and the constant terms can be renamed for simplicity:

$$a_{11} = \frac{2}{\tau} C_1 + \frac{1}{R_1} + \frac{1}{R_2} \tag{3.11a}$$

$$a_{12} = -\frac{1}{R_2} \tag{3.11b}$$

$$a_{13} = \left(\frac{2}{\tau} C_1 - \frac{1}{R_1} - \frac{1}{R_2} \right) T^{p-1}_{C_1} + \frac{T^{p-1}_{C_2}}{R_2} + \frac{T^p_{int} + T^{p-1}_{int}}{R_1} \tag{3.11c}$$

$$a_{21} = -\frac{1}{R_2} \tag{3.11d}$$

$$a_{22} = \frac{2}{\tau} C_2 + \frac{1}{R_2} + \frac{1}{R_3 + R_4} \tag{3.11e}$$

$$a_{23} = \frac{T^{p-1}_{C_1}}{R_2} + \left(\frac{2}{\tau} C_2 - \frac{1}{R_2} - \frac{1}{R_3 + R_4} \right) T^{p-1}_{C_2} + \frac{T^p_{ext} + T^{p-1}_{ext}}{R_3 + R_4} + \frac{g R_4 \left(Q^p_{sun} + Q^{p-1}_{sun} \right)}{R_3 + R_4} \tag{3.11f}$$

and the linear system can be rewritten as:

$$\begin{cases} a_{11}T^p_{C_1} + a_{12}T^p_{C_2} = a_{13} \\ a_{21}T^p_{C_1} + a_{22}T^p_{C_2} = a_{23} \end{cases}. \tag{3.12}$$

The linear system in Equation 3.12 can be solved by applying the Gaussian elimination method[9] (Howard, 2010), and the initial temperature of the two effective thermal masses at each time step can be predicted as:

$$T^p_{C_1} = \frac{a_{13} - a_{12}T^p_{C_2}}{a_{11}}; \quad T^p_{C_2} = \frac{a_{11}a_{23} - a_{21}a_{13}}{a_{11}a_{22} - a_{12}a_{21}}. \tag{3.13}$$

The estimated heat flow from the indoor ambient into the internal wall surface $\left(Q^p_{e,in}\right)$ and the estimated heat flow leaving the external surface of the wall $\left(Q^p_{e,out}\right)$ at each time step can be predicted as:

$$Q^p_{e,in} = \frac{T^p_{in} - T^p_{C_1}}{R_1}; \quad Q^p_{e,out} = \frac{T^p_{C_2} - T^p_{ext} - gR_4Q^p_{m,sol}}{R_3 + R_4}. \tag{3.14}$$

Both the internal and external heat fluxes are used during the optimisation phase, enabling the model to account for thermal mass effects and to characterise the thermal structure of building elements both at the interior and exterior surfaces simultaneously (Gori et al., 2017). Similarly to the 1TM model, it can be observed that the quantities gR_4 and $R_3 + R_4$ in Equation 3.11f and Equation 3.14 only contribute through the terms gR_4 and $R_3 + R_4$. The same considerations discussed for the 1TM model with solar radiation input can be applied for the 2TM model and the underdetermination issue can be solved by assuming $g = 1$. For the 2TM model, both the internal and external estimated heat flows are simultaneously used for the optimisation of the thermophysical parameters (θ_{2TM}) of the model, as described in Section 3.4.3.

It is easy to show that, like in the 1TM model, the 2TM model without the solar radiation input is a particular case of the model accounting for it as separate heat source (Figure 3.5 on page 86). Therefore, the estimated heat flows entering the indoor surface and leaving the external one in case of the 2TM model without separate incoming solar radiation input can be obtained by setting R_4 to zero in Equation 3.11f and Equation 3.14.

9 The Gaussian elimination method (also known as row reduction) is used in linear algebra to solve a system of equations in the matrix form of $Ax = B$.

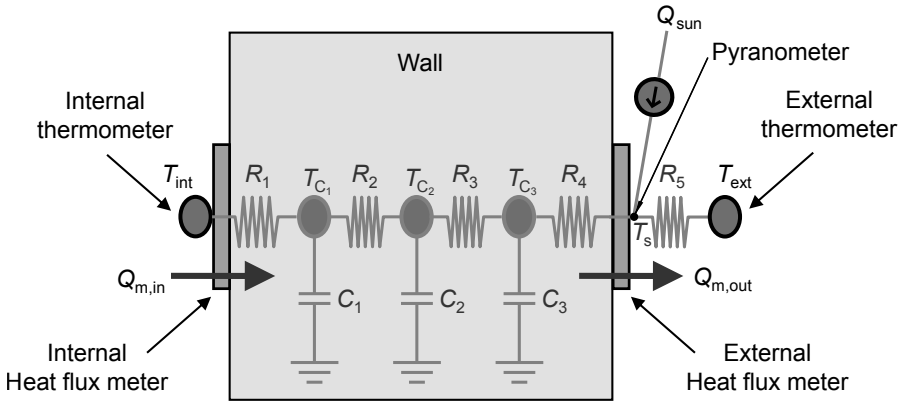

Figure 3.6: Schematic diagram of the three thermal mass model (3TM) when solar radiation is accounted for separately. The diagram shows the electrical equivalent circuit for the heat transfer through the wall and the measured quantities. Parameters of the model are three effective thermal masses $(C_1 \text{ to } C_3)$, their initial temperature $\left(T^0_{C_1} \text{ to } T^0_{C_3}\right)$, five thermal resistances $(R_1 \text{ to } R_5)$. The measured quantities are the internal (T_{int}) and external (T_{ext}) temperatures, the heat fluxes entering the internal $(Q_{m,in})$ and leaving the external $(Q_{m,out})$ surfaces, and the incident solar radiation (Q_{sun}).

3.3.3 *Other models*

The approach illustrated in the previous sections for the 1TM and 2TM models can be easily scaled up to devise increasingly more complex models, either incorporating the incoming solar radiation as separate source of heat or not. Two models respectively consisting of three and four thermal masses (*i.e.* the 3TM and 4TM models) were also developed as part of this research.

The 3TM model (Figure 3.6 on page 89) includes eleven parameters namely five thermal resistances $(R_1 \text{ to } R_5)$, three effective thermal masses $(C_1 \text{ to } C_3)$, their initial temperature $\left(T^0_{C_1} \textit{ to } T^0_{C_3}\right)$, and the absorbance[10] (g) of the wall[11]. Similarly, the 4TM model (Figure 3.7 on page 90) comprises fourteen parameters. The same rationale illustrated for the 1TM model (Section 3.3.1) can be applied to reduce these models to the case without solar radiation.

The models presented above were not used for data analysis in this thesis. While stepping up from the AM to the 1TM and 2TM models represents a significant improvement in the characterisation of the thermal structure of a building element and specifically of the thermal mass effects both at the interior and exterior surfaces (Chapter 5), the further increase of complexity of the 3TM and 4TM models introduces more incremental and

10 Likewise the 2TM model, the absorbance of the wall can be fixed during the optimisation phase of the 3TM and 4TM models.

11 In the interests of space, only the schematic diagrams for the 3TM and 4TM models are shown. Their mathematical formulation (both with and without incoming solar radiation input) can be easily derived scaling up the approach used for the 1TM and 2TM models.

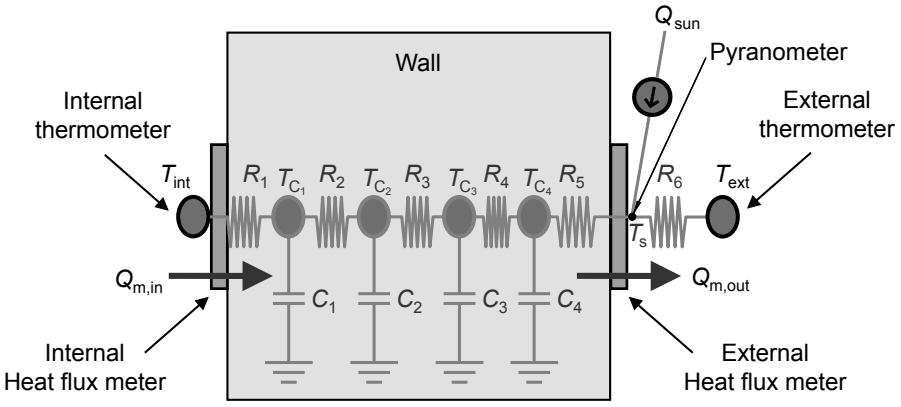

Figure 3.7: Schematic diagram of the four thermal mass model (4TM) when solar radiation is accounted for separately. The diagram shows the electrical equivalent circuit for the heat transfer through the wall and the measured quantities. Parameters of the model are four effective thermal masses (C_1 to C_4), their initial temperature ($T^0_{C_1}$ to $T^0_{C_4}$), six thermal resistances (R_1 to R_6). The measured quantities are the internal (T_{int}) and external (T_{ext}) temperatures, the heat fluxes entering the internal ($Q_{m,in}$) and leaving the external ($Q_{m,out}$) surfaces, and the incident solar radiation (Q_{sun}).

less radical improvements. These models have been used in complementary research where in-wall measurements were available and heat flow was used as driver for the heat transfer across the element to predict measured temperatures.

3.4 OPTIMISATION PHASE: MODEL FITTING AND PARAMETER ESTIMATION

As illustrated in Section 3.3 and Figure 3.1 on page 78, during the simulation phase computational models with given values of the parameters are used to predict the heat transfer across a building element. The optimisation phase (or model fitting) iteratively changes these parameters and runs the simulation in order to identify the set of parameters that best explain the observations while possibly accounting for our prior knowledge. This requires defining a measure of how well a given set of model parameters fits the data. In a probabilistic setting, natural choices are the likelihood function or the posterior probability of the parameters given the data.

In the frequentist framework, the maximum likelihood estimation (MLE) (Madsen, 2007) identifies the best-fit parameters of a model (θ_{opt}) by maximising the likelihood function of the parameters, a data-dependent term describing the probability of obtaining the observations (*i.e.* the measured data) given the parameters and the model used to describe the heat transfer:

$$\theta_{opt} \equiv \theta_{MLE} = \arg\max_{\theta} \mathcal{L}(\theta; y, H) \tag{3.15}$$

where $\mathcal{L}(\theta; y, H) = \mathrm{P}(y|\theta, H)$ is the likelihood function; y are the observations; θ are the parameters of the model; H is the model. Conversely, in the Bayesian framework maximum a posteriori (MAP) and Markov Chain Monte Carlo (MCMC) sampling estimate the best set of the parameters by studying the posterior probability distribution, $\mathrm{P}(\theta|y, H)$, which represents the probability of the parameters given the data and the model. Specifically, the MAP approach only estimates the best-fit value (*i.e.* the mode of the distribution):

$$\theta_{\mathrm{opt}} = \arg\max_{\theta} \mathrm{P}(\theta|y, H), \tag{3.16}$$

while the MCMC framework can be used to estimate the full probability distribution of the parameters. The investigation of the full distribution of the parameters of the model, instead of just their most probable values, is valuable to gain further insights into the problem investigated. For example, it may indicate potential dependencies among the parameters and how quickly the fit of the model decreases moving away from the optimal set of parameters identified (as illustrated in Section 6.4 and in Gori and Elwell (2017)). In this research, both the MAP and MCMC approaches were used (Section 3.4.3).

According to Bayes' theorem (Gregory, 2005), the posterior probability distribution (representing the probability of the parameters given the model and the observations) is expressed as:

$$\mathrm{P}(\theta|y, H) = \frac{\mathrm{P}(y|\theta, H)\,\mathrm{P}(\theta|H)}{\mathrm{P}(y|H)} \tag{3.17}$$

where $\mathrm{P}(y|\theta, H)$ is the likelihood function (or likelihood[12]); $\mathrm{P}(\theta|H)$ is the prior probability distribution (often simply referred to as prior[13]); $\mathrm{P}(y|H)$ is the evidence (or marginal likelihood). Specifically, the prior represents the initial estimated probability distribution of each parameter based on expert knowledge before observing any data, the likelihood describes the ability of the model at predicting the observations, and the evidence is a normalisation factor.

The following sections illustrate the rationale for the formulation of the likelihood and the choice of uniform and non-uniform priors adopted. An overview of the methods used (*i.e.* MAP and MCMC) for the estimation of the parameters is also provided.

12 The likelihood function will be referred to as "likelihood" in the following.
13 Prior probability distributions will be referred to as "priors" in the following.

3.4.1 *The likelihood function*

As introduced in Section 3.2, the full probability model (*i.e.* the likelihood function) describing the process of interest was defined in two phases: a physically informed model simulating the heat transfer through the building element of interest and a model describing the error between the simulated and the observed time series. While the family of lumped-thermal-mass models devised was described in Section 3.3, this section introduces the three error models explored in this research.

A simple and widely used approach to formulate the likelihood function is to assume that the residuals of the model are independent and identically distributed (iid) (Madsen, 2007, Ch.5.3). Since the assumption of iid residuals is a strong one, the structure of the residuals has to be checked at the end of the optimisation analysis to ensure that the iid assumption effectively holds and the residuals are white noise (Madsen, 2007, Ch.6.6). Section 3.5 will discuss techniques for the validation of this assumption.

In this thesis the Bayesian framework was used to obviate the iid assumption by introducing a prior distribution on the residuals that accounts for their potential autocorrelation. The formulation of the likelihood function for iid residuals is presented below, followed by the description of an inverse Wishart distribution and a discrete cosine transform adopted to account for the potential autocorrelation of the residuals in the likelihood.

3.4.1.1 *Independent and identically distributed residuals*

A common assumption for the definition of the likelihood function is that the residuals (*i.e.* the discrepancies between the estimates of the model and the observations) of each data stream involved in the optimisation can be modelled as additive white (*i.e.* iid (Madsen, 2007, Ch.5.3)) Gaussian noise. This yields:

$$\mathrm{P}\left(y\,|\theta, H\right) = \prod_{\varepsilon\in E}\prod_{p=1}^{n}\frac{1}{\sigma_{\Phi,\varepsilon}\sqrt{2\pi}}\exp\left[-\frac{\left(\Phi^{p}_{\mathrm{e},\varepsilon}-\Phi^{p}_{\mathrm{m},\varepsilon}\right)^{2}}{2\,\sigma^{2}_{\Phi,\varepsilon}}\right] \tag{3.18}$$

where E is the set of data streams involved in the fit (*i.e.* the measured internal or external heat flux in this work); p is the index of the time step and n the number of observations analysed per data stream; $\Phi^{p}_{\mathrm{m},\varepsilon}$ and $\Phi^{p}_{\mathrm{e},\varepsilon}$ are respectively the observation and the estimation of the model for each data stream at each time step (*i.e.* the measured $\left\{Q^{p}_{\mathrm{m,in}}, Q^{p}_{\mathrm{m,out}}\right\}$ and estimated $\left\{Q^{p}_{\mathrm{e,in}}, Q^{p}_{\mathrm{e,out}}\right\}$ heat flux in this work); $\sigma^{2}_{\Phi,\varepsilon}$ is the variance of an additive noise term affecting the residuals of each data stream (*i.e.* the heat flux in this work). The additive noise term is derived according to the common assumption

that the independent variables of the model (model inputs) have been observed without error while the dependent variables (model outputs) are affected by an additive noise term accounting for all the sources of uncertainties occurring in reality (*e.g.*, errors on the observations both in the minimisation and parameter estimation processes, fitting errors and errors on the outputs). It has to be defined a priori, accounting for all the known and quantifiable sources of uncertainties (Section 4.2.1 illustrates the calculation of the noise term for the applications analysed in this thesis).

Renaming the residuals of each data stream as the vector r_ε with elements $r_\varepsilon^p = \left(\Phi_{\mathrm{e},\varepsilon}^p - \Phi_{\mathrm{m},\varepsilon}^p\right)$, the probability density function of the residuals is a multivariate Gaussian distribution $(\mathcal{N})$ with zero mean and diagonal covariance matrix $\Sigma_\varepsilon = \sigma_{\Phi,\varepsilon}^2 I_n$ (where I_n is an identity matrix of dimension n):

$$r_\varepsilon \sim \mathcal{N}\left(0_n, \sigma_{\Phi,\varepsilon}^2 I_n\right). \tag{3.19}$$

Consequently, the likelihood in Equation 3.18 can be also expressed as:

$$\mathrm{P}\left(r\,|\theta, H\right) = \prod_{\varepsilon\in E} \frac{1}{\left[\sqrt{2\pi\sigma_{\Phi,\varepsilon}^2}\right]^n} \exp\left[-\frac{1}{2}\sum_i \frac{r_{\varepsilon,i}^2}{\sigma_{\Phi,\varepsilon}^2}\right] = \prod_{\varepsilon\in E} (2\pi)^{-\frac{n}{2}} \left|\Sigma_\varepsilon\right|^{-\frac{1}{2}} \exp\left(-\frac{1}{2} r_\varepsilon^{\mathrm{T}} \Sigma_\varepsilon^{-1} r_\varepsilon\right) \tag{3.20}$$

Taking the natural logarithm of the likelihood (also referred to as log-likelihood) of Equation 3.20:

$$\ln \mathrm{P}\left(r\,|\theta, H\right) = \sum_{\varepsilon\in E} -\frac{n}{2}\ln\left(2\pi\right) - \frac{1}{2}\ln\left|\Sigma_\varepsilon\right| - \frac{1}{2} r_\varepsilon^{\mathrm{T}} \Sigma_\varepsilon^{-1} r_\varepsilon. \tag{3.21}$$

3.4.1.2 *Inverse Wishart distribution*

The Bayesian framework allows the assumption of iid residuals to be relaxed by assuming that the probability density function of the residuals of each data stream follows a multivariate Gaussian distribution with zero mean and unknown covariance matrix (Σ_ε). A common choice for the probability distribution of covariance matrices is the inverse Wishart distribution[14] $\left(\mathcal{W}^{-1}\right)$ (Congdon, 2006, Ch.3):

$$r_\varepsilon \sim \mathcal{N}\left(0_n, \Sigma_\varepsilon\right) \tag{3.22}$$

$$\Sigma_\varepsilon \sim \mathcal{W}^{-1}\left(\psi_\varepsilon, v\right) \tag{3.23}$$

14 The inverse Wishart distribution is a distribution over matrices, *i.e.* each random sample is a matrix rather than a scalar value.

where ψ_ε is the scale matrix of the inverse Wishart distribution; v are the degrees of freedom of the distribution (*i.e.* a quantity indicating how informative the prior should be).

In this work, the scale matrix of the prior is chosen so that the expected value (*i.e.* the mean of the inverse Wishart distribution) of the covariance matrix coincides with our prior knowledge of the variance of the noise term:

$$\overline{\Sigma}_\varepsilon = \mathbb{E}\left[\Sigma_\varepsilon\right] = \frac{\psi_\varepsilon}{v-n-1} = \sigma^2_{\Phi,\varepsilon} I_n. \tag{3.24}$$

Marginalising over the covariance matrix, the likelihood can be expressed as:

$$\mathrm{P}\left(r_\varepsilon \left|\theta, \psi_\varepsilon\right.\right) = \int \mathrm{P}\left(r_\varepsilon \left|\Sigma_\varepsilon, \theta\right.\right) \mathrm{P}\left(\Sigma_\varepsilon \left|\psi_\varepsilon\right.\right) \mathrm{d}\Sigma_\varepsilon = \frac{\left|\psi_\varepsilon\right|^{\frac{v}{2}} \Gamma_n\left(\frac{v+1}{2}\right)}{\pi^{\frac{n}{2}} \left|\psi_\varepsilon + r_\varepsilon r_\varepsilon^{\mathrm{T}}\right|^{\frac{v+1}{2}} \Gamma_n\left(\frac{v}{2}\right)} \tag{3.25}$$

where $\mathrm{P}\left(r_\varepsilon \left|\Sigma_\varepsilon, \theta\right.\right)$ is the Gaussian distribution of the residuals given the covariance matrix and the parameters; $\mathrm{P}\left(\Sigma_\varepsilon \left|\psi_\varepsilon\right.\right)$ is the prior on the covariance matrix; $\Gamma_n\left(\cdot\right)$ is the multivariate gamma function (MacKay, 2007, Appendix A). Using the matrix determinant lemma[15]:

$$\left|\psi_\varepsilon + r_\varepsilon r_\varepsilon^{\mathrm{T}}\right| = \left(1 + r_\varepsilon^{\mathrm{T}} \psi_\varepsilon^{-1} r_\varepsilon\right) \left|\psi_\varepsilon\right|, \tag{3.26}$$

the log-likelihood can be calculated from Equation 3.25 as:

$$\ln\left(\mathrm{P}\left(r_\varepsilon \left|\theta, \psi_\varepsilon\right.\right)\right) = \ln\Gamma_n\left(\frac{v+1}{2}\right) - \frac{n}{2}\ln\pi - \frac{v+1}{2}\ln\left(1 + r_\varepsilon^{\mathrm{T}}\psi_\varepsilon^{-1} r_\varepsilon\right) - \frac{1}{2}\ln\left|\psi_\varepsilon\right| - \ln\Gamma_n\left(\frac{v}{2}\right). \tag{3.27}$$

Substituting ψ_ε from Equation 3.24 in Equation 3.27, the log-likelihood of the residuals given the parameters and the estimated covariance matrix becomes:

$$\begin{aligned}
&\ln\left(\mathrm{P}\left(r_\varepsilon \left|\theta, \overline{\Sigma}_\varepsilon\right.\right)\right) = \\
&= \ln\Gamma_n\left(\frac{v+1}{2}\right) - \frac{n}{2}\ln\pi - \frac{v+1}{2}\ln\left(1 + \frac{r_\varepsilon^{\mathrm{T}}\overline{\Sigma}_\varepsilon^{-1} r_\varepsilon}{v-n-1}\right) - \frac{1}{2}\ln\left|\left(v-n-1\right)\overline{\Sigma}_\varepsilon\right| - \ln\Gamma_n\left(\frac{v}{2}\right) \\
&= \ln\Gamma_n\left(\frac{v+1}{2}\right) - \frac{n}{2}\ln\pi - \frac{v+1}{2}\ln\left(1 + \frac{r_\varepsilon^{\mathrm{T}}\overline{\Sigma}_\varepsilon^{-1} r_\varepsilon}{v-n-1}\right) - \frac{n}{2}\ln\left(v-n-1\right) - \frac{1}{2}\ln\left|\overline{\Sigma}_\varepsilon\right| \\
&\quad - \ln\Gamma_n\left(\frac{v}{2}\right).
\end{aligned} \tag{3.28}$$

15 Given an invertible square matrix A and column vectors u and v, the matrix determinant lemma states that $\left|A + uv^{\mathrm{T}}\right| = \left(1 + v^{\mathrm{T}}A^{-1}u\right)\left|A\right|$.

3.4.1.3 *Discrete cosine transform*

Using the inverse Wishart prior on the covariance matrix of the residuals presents two main limitations. Firstly, Equation 3.28 is a non-convex function with very fat tails and as such it may render the problem of local optima significantly worse. Secondly, the inverse Wishart distribution was devised as prior for the covariance of generic multivariate random vectors, making no assumptions about the ordering of the elements within the vector or any specific structure. In the following, an alternative prior is introduced to account for the peculiar structure of the covariance matrix of the residuals while also mitigating the problem of local optima[16].

In our case, the index of each residual within the vector r_ε represents time and it is reasonable to assume that the random process generating r_ε has a temporal structure. Specifically, it can be assumed that it is weakly stationary, *i.e.* that the covariance between any two residuals, r_ε^p and r_ε^q, only depends on the time elapsed between the two samples: $\mathbb{E}\left[(r_\varepsilon^p - 0)(r_\varepsilon^q - 0)\right] = \gamma_{r_\varepsilon r_\varepsilon}(p-q)$ for all p and q, where $\gamma_{r_\varepsilon r_\varepsilon}(\tau)$ is the autocovariance function at lag τ (Madsen, 2007, Ch.5). This is a common assumption which is implicitly made when the validity of the iid assumption is investigated by means of the autocorrelation function. It is easy to show that covariance matrices of weakly stationary discrete-time random processes are symmetric Toeplitz matrices, *i.e.* matrices where all elements along a diagonal have the same value. A prior imposed on the unknown covariance matrix Σ_ε can thus be used to account for this structure, as explained below.

Interestingly, the covariance matrix of weakly stationary discrete-time random processes can be asymptotically diagonalised by the application of a transformation called discrete cosine transform (DCT) (Rao and Yip, 1990; Sánchez et al., 1995), which represents a finite signal as a sum of cosine functions at different frequencies. Stated otherwise, this important property of the DCT states that, as the length of a signal increases, the coefficients resulting from the application of the DCT tend to be decorrelated, *i.e.* to have a diagonal covariance matrix. Since the application of the DCT can be conveniently expressed as a matrix multiplication with the ortho-normal DCT basis matrix D (*i.e.* $\mathrm{DCT}[r_\varepsilon] = D\, r_\varepsilon$), the decorrelation property of the DCT can be mathematically stated in this case as follows:

$$D\, r_\varepsilon \sim \mathcal{N}\left(0_n, \Xi_\varepsilon\right), \tag{3.29}$$

with Ξ_ε diagonal, or equivalently as:

16 The theory described in this section was formulated under the guidance of Dr Luca Citi.

$$r_\varepsilon \sim \mathcal{N}(0_n, \Sigma_\varepsilon) \text{ with } \Sigma_\varepsilon = D^{\mathrm{T}} \Xi_\varepsilon D, \tag{3.30}$$

in the limit as the length of r_ε grows to infinity. In practice, the decorrelation properties of the DCT transform are successfully used in a wide range of applications for finite-length signals (Rao and Yip, 1990). Replacing Σ_ε from Equation 3.30 in Equation 3.20, the likelihood of the residuals for each data stream can be written[17] in terms of the matrix Ξ_ε and its diagonal elements $\xi_{i,i}$:

$$\begin{aligned} \mathrm{P}(r_\varepsilon | \Xi_\varepsilon, \theta, H) &= (2\pi)^{-\frac{n}{2}} \left| D^{\mathrm{T}} \Xi_\varepsilon D \right|^{-\frac{1}{2}} \exp\left[-\frac{1}{2} r_\varepsilon^{\mathrm{T}} \left(D^{\mathrm{T}} \Xi_\varepsilon D \right)^{-1} r_\varepsilon \right] \\ &= (2\pi)^{-\frac{n}{2}} |\Xi_\varepsilon|^{-\frac{1}{2}} \exp\left[-\frac{1}{2} (D r_\varepsilon)^{\mathrm{T}} \Xi_\varepsilon^{-1} (D r_\varepsilon) \right] \\ &= (2\pi)^{-\frac{n}{2}} \left(\prod_i \xi_{i,i}^{-\frac{1}{2}} \right) \exp\left[-\frac{1}{2} \sum_i \frac{(D_i r_\varepsilon)^2}{\xi_{i,i}} \right], \end{aligned} \tag{3.31}$$

where D_i is the i-th row of the DCT matrix D. As a result, it is now possible to place a simple prior on the diagonal elements of Ξ_ε to indirectly obtain covariance matrices Σ_ε with the desired Toeplitz structure which is typical of stationary signals. Since the elements $\xi_{i,i}$ of the diagonal matrix Ξ_ε represent the variance of the different oscillatory components, a natural choice would be to place an inverse Gamma prior on each $\xi_{i,i}$ element or, equivalently, a Gamma prior on $\xi_{i,i}^{-1}$ (Congdon, 2006, Ch.3):

$$\xi_{i,i}^{-1} \sim \Gamma(\alpha, \beta). \tag{3.32}$$

The Gamma distribution has probability density function:

$$\mathrm{P}(x | \alpha, \beta) = \frac{\beta^\alpha}{\Gamma(\alpha)} x^{\alpha-1} e^{-\beta x}, \tag{3.33}$$

where α is a shape parameter; β is an inverse scale parameter.

Similarly to the inverse Wishart distribution, the Gamma distribution yields a likelihood with fat tails and consequently it may facilitate the presence of local optima in the probability function to be optimised. To overcome this potential issue, a shifted and tapered version of the Gamma distribution was introduced:

$$\xi_{i,i}^{-1} \sim \Gamma_\delta(\alpha, \beta) \tag{3.34}$$

17 The following properties of ortho-normal matrices are used in Equation 3.31: $|D| = 1$, $D^{\mathrm{T}} = D^{-1}$, as well as the general properties of square invertible matrices: $(AB)^{-1} = B^{-1}A^{-1}$ and $(AB)^{\mathrm{T}} = B^{\mathrm{T}}A^{\mathrm{T}}$.

with probability density function:

$$\mathrm{P}\left(x\,|\alpha,\beta,\delta\right) = \frac{\beta^{\alpha}}{\Gamma(\alpha,\beta\delta) - \beta\delta\Gamma(\alpha-1,\beta\delta)}\, x^{\alpha-1}e^{-\beta x}\left(1-\frac{\delta}{x}\right)\, u(x-\delta), \tag{3.35}$$

where $u(\cdot)$ is the unitary step function, which assumes value one for a positive argument and zero otherwise. The probability density in Equation 3.35 is zero when the argument is smaller than δ, effectively setting an upper limit on the variance $\xi_{i,i}$ and having the effect of reducing the occurrence of local optima. The parameter α determines the strength of the prior and can be set to a small value to impose a weak prior. The parameter β was chosen so that the expected value of $\xi_{i,i}^{-1}$ according to Equation 3.34 coincides with the reciprocal of the variance of the noise term $\sigma^2_{\Phi,\varepsilon}$ that can be computed from the uncertainties on the measurement (described in Section 4.2.1).

Likewise the case of the inverse Wishart distribution, it is possible to marginalise out the prior on the unknown covariance to obtain a likelihood that can be incorporated into any calculations requiring a likelihood term. For the value $\alpha = 1.5$ (which satisfies the requirement of a weak prior) the marginal likelihood of each data stream has a relatively simple form:

$$\begin{aligned}\mathrm{P}\left(r_\varepsilon\,|\alpha,\beta,\delta,\theta,H\right) &= \int \mathrm{P}\left(r_\varepsilon\,|\Xi_\varepsilon,\theta,H\right)\mathrm{P}\left(\Xi_\varepsilon\,|\alpha,\beta,\delta\right)\mathrm{d}\Xi_\varepsilon \\ &= \prod_i \left(\frac{\beta^{\frac{3}{2}}\exp\left\{-\delta\left[\beta+\frac{1}{2}\left(D_i\, r_\varepsilon\right)^2\right]\right\}}{\sqrt{2\pi}\,\left[\Gamma\left(\frac{3}{2},\beta\delta\right)-\beta\delta\Gamma\left(\frac{1}{2},\beta\delta\right)\right]\,\left[\beta+\frac{1}{2}\left(D_i\, r_\varepsilon\right)^2\right]^2}\right).\end{aligned} \tag{3.36}$$

If more than one data stream is used, the probability of the residuals of all data streams is simply the product of terms like that in Equation 3.36 calculated for each data stream.

After preliminary testing of the likelihood formulation using the inverse Wishart distribution on the covariance matrix and the DCT transform approach, it was decided to adopt the latter (Equation 3.36) for the data analysis presented in this thesis. The decision was taken both on the basis of its theoretical advantages in accounting for stationarity and its robustness to local optima.

3.4.2 *Prior probability distributions on the parameters of the model*

As introduced in Section 3.2 and Section 3.4, the use of prior probability distributions on the parameters of the model during data fitting is a feature of the Bayesian framework. Priors enable the coupling of previous knowledge (*e.g.*, from the literature) with the

data, effectively combining the two sources of information. Specifically, priors allow the inclusion of our knowledge of the physical phenomena under investigation in the statistical description of the system and its behaviour. The combination of different sources of information in the analysis may help decrease the number of observations needed to obtain the desired accuracy compared with methods that do not facilitate the use of prior information, such as the MLE approach. The choice of priors represents an important aspect of Bayesian analysis (Congdon, 2006). In general, both uniform and non-uniform priors can be defined. The former assign an equal probability to observations falling within the chosen range and null probability elsewhere, while the latter overcome this limitation by enabling the assignment of low probabilities to unlikely observations.

In the following, both uniform and log-normal priors are presented. In all cases, the priors on the parameters of the model were assumed independent to avoid imposing a specific correlation structure of the parameters, which is unknown a priori. This choice, however, will not prevent the model from identifying correlations in the estimates of the parameters should the data support this behaviour (as found in Section 5.2.2). Consequently, the prior probability of the vector of parameters θ can be calculated as the product of the prior distribution of each parameter:

$$\mathrm{P}\left(\theta \,|H\right) = \prod_j \mathrm{P}\left(\theta_j \,|H\right). \tag{3.37}$$

Section 4.2.2 will discuss the use of priors in the context of this work and provide details of the uniform and non-uniform priors adopted for model fitting.

3.4.2.1 *Uniform priors on the parameters of the model*

Uniform prior distributions are generally used when the initial knowledge about the parameters of the problem is limited. Uniform priors (Figure 3.8 on page 99) on the parameters of the model assign equal probability to any value of the parameter within the prior limits and null probability elsewhere:

$$\mathrm{P}\left(\theta_j \,|H\right) = \left(\Delta L_j\right)^{-1} \tag{3.38}$$

where ΔL_j is the width of the uniform prior distribution on the j-th parameter of the model. Therefore, the definition of the prior limits is crucial because choosing a range that is too broad will over-represent the probability of rare events, while a range that is too small will imply that rare but possible events are considered statistically impossible and could therefore prevent the method from identifying the parameters of the model.

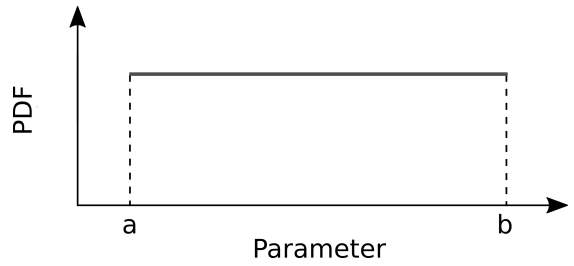

Figure 3.8: Uniform prior probability distribution.

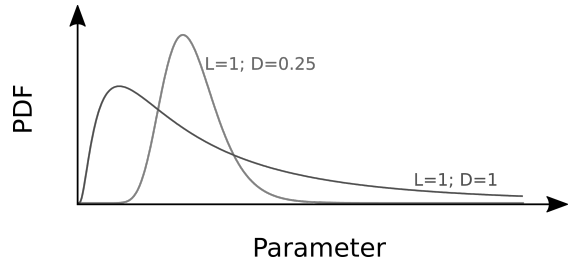

Figure 3.9: Log-normal prior probability distribution, where L and D are a measure of location and dispersion.

Consequently, the prior limits have to be chosen large enough to ensure that any reasonable value the parameter may assume is encompassed, although this may penalise the performance of the model during model selection (Section 3.5.1). Section 4.2.2 provides details on the choice of uniform priors for the analysis presented in this thesis.

3.4.2.2 *Log-normal priors on the parameters of the model*

Non-uniform prior distributions are usually adopted when more information is available about the parameters of the model investigated. The adoption of continuous and smooth non-uniform priors may overcome the issues introduced by uniform priors by enabling the assignment of low probabilities to unlikely but possible events. As a consequence, a poor choice of a non-uniform prior can be overturned by the information contained in the data, if enough observations are available.

Due to the physical constraints of the problem investigated in this thesis, distributions over the positive reals (*e.g.*, log-normal, gamma, inverse Gaussian (MacKay, 2007, Ch.23)) were considered to reflect the fact that the thermophysical parameters of the models (*i.e.* thermal resistances and effective thermal masses) are strictly positive; this requirement can also be imposed for the initial temperature of the effective thermal mass by transforming the temperature observations from degree Celsius to Kelvin. Log-normal priors (Figure 3.9 on page 99) were selected for the following two reasons. Firstly, the log-normal scale represents a more realistic description of our knowledge on the degree of magnitude of the random variable (*i.e.* the parameter) compared to a linear scale (Limpert et al., 2001). For example, it assigns equal probability to values smaller than

half the median and to those larger than twice the median. Secondly, since building elements may be modelled either in terms of thermal resistance or thermal conductance, this distribution has the distinctive property that imposing a log-normal prior on one of the two parameters implicitly implies a log-normal prior on the other (this is not generally true for other families of distributions). In fact, if the thermal resistance is distributed according to a log-normal distribution, its logarithm is a Gaussian distribution. Since the thermal conductance is the reciprocal of the thermal resistance, its logarithm is the negative of that of the thermal resistance and its distribution is also Gaussian, hence the thermal conductance is also log-normal.

For each parameter θ_j of the model, the associated log-normal prior distribution $\mathrm{P}\left(\theta_j \,|H\right)$ can be calculated as:

$$\mathrm{P}\left(\theta_j \,|H\right) = \frac{1}{\theta_j \, D_{\theta_j} \sqrt{2\pi}} \exp\left[-\frac{\ln^2\left(\theta_j / L_{\theta_j}\right)}{2\, D_{\theta_j}^2}\right] \tag{3.39}$$

where L_{θ_j} and D_{θ_j} represent respectively a measure of location and dispersion of the log-normal prior distribution of the j-th parameter based on prior knowledge. Note that a non-canonical parametrisation of the location parameter has been used in Equation 3.39. Specifically, the median of the distribution of each parameter $\left(L_{\theta_j}\right)$ has been used as the location parameter instead of the often used μ_{θ_j} (*i.e.* the mean of the natural logarithm of the parameters); the two are simply related by $\mu_{\theta_j} = \ln L_{\theta_j}$. This parametrisation, also used by MacKay (2007, Ch.23), is advantageous as each parameter of the model and the corresponding location parameter have the same units, which may ease the interpretation. Additionally, the median is a more robust measure of location (*e.g.*, to outliers) than the mean in case the distribution of the parameters has to be estimated from observations. The calculation of the location and dispersion parameters for log-normal priors on the parameters of the model in the context of this thesis is discussed in Section 4.2.2.2.

3.4.2.3 *Log-normal priors on estimates of the model*

Besides the parameters of the model, priors can also be imposed on intermediate or final estimates of the model. This possibility may be used when there is no information available on the parameters but there is still information available about some of the outputs.

In the context of this thesis, the assumption of non-uniform priors on the U-value of the wall can be used when the stratigraphy is unknown, but it is possible to gather in-

formation on the overall thermophysical performance of the element (*e.g.*, from the age of construction of the building or from visual inspection of similar constructions). For the same reasons mentioned above when discussing log-normal priors on the parameters of the model, a log-normal prior distribution on the U-value was chosen. Conversely, uniform priors were kept on the individual parameters of the model due to the lack of information on them. The prior probability distribution of the U-value can be expressed as:

$$\mathrm{P}\left(\theta_U \,|H\right) = \frac{1}{U_\mathrm{e}\, D_{\mathrm{U_{pk}}} \sqrt{2\pi}} \exp\left[-\frac{\ln^2\left(U_\mathrm{e}/U_\mathrm{pk}\right)}{2\, D^2_{\mathrm{U_{pk}}}}\right] \tag{3.40}$$

where U_e is the U-value estimated by the model; U_pk and D_pk are respectively a measure of location and dispersion of the log-normal prior distribution of the U-value based on previous knowledge (pk). Similarly to the case discussed above, the choice of a log-normal prior on the U-value has the advantage that implicitly imposes a log-normal prior on the total R-value (with same dispersion and reciprocal location $R_\mathrm{e} = 1/U_\mathrm{e}$). The calculation of the location and dispersion parameters for a log-normal prior on the U-value in the context of this thesis is discussed in Section 4.2.2.3.

3.4.3 *Optimal parameter estimation*

As introduced in Section 3.4, different methods are available for parameter estimation depending on whether the most probable value of the parameters or their full probability distribution is to be estimated. In this thesis, the former has been achieved using a maximum a posteriori approach (MAP), while a Metropolis-Hastings sampler within a Markov Chain Monte Carlo (MCMC) method has been adopted for the latter (Section 4.3.1 describes the MAP and MCMC optimisation software adopted in this work).

3.4.3.1 *Maximum a posteriori*

Maximum a posteriori estimates were chosen as best-fit parameters (θ_MAP). These are obtained by maximising the posterior probability (*i.e.* investigating the posterior probability distribution around its global maximum):

$$\theta_\mathrm{MAP} = \arg\max_\theta \mathrm{P}\left(\theta \,|y, H\right) = \arg\max_\theta \frac{\mathrm{P}\left(y \,|\theta, H\right) \mathrm{P}\left(\theta \,|H\right)}{\mathrm{P}\left(y \,|H\right)}. \tag{3.41}$$

The evidence is generally omitted in the model-fitting phase (MacKay, 2007, Ch.28), reducing Equation 3.41 to the maximisation of the unnormalised posterior (*i.e.* the product of the likelihood and the prior, Equation 3.16). It is notable that MAP and MLE (intro-

duced in Section 3.4) optimisation coincide[18] when no prior or a uniform prior is adopted as, in general, constant terms do not contribute towards the maximisation process (Kristensen et al., 2004). Taking the natural logarithm of the unnormalised posterior and including only the non-constant terms from the logarithm of the likelihood in Equation 3.36) and the log-prior (*i.e.* the natural logarithm of the chosen prior probability distribution, Section 3.4.2), the best-fit parameters can be estimated as:

$$\theta_{\mathrm{MAP}} = \arg\max_{\theta} \ln \mathrm{P}\left(y \,|\theta, H\right) + \ln \mathrm{P}\left(\theta \,|H\right) \tag{3.42}$$

Numerical simulation software (introduced in Section 4.3.1) was used to investigate the unnormalised posterior probability distribution surface and estimate the best-fit parameters at its global maximum as well as the systematic and statistical error associated with the estimates (Section 4.5).

3.4.3.2 *Markov Chain Monte Carlo sampling*

Markov Chain Monte Carlo sampling is a method used in Bayesian inference to approximate a multi-dimensional posterior probability distribution (Congdon, 2006, Ch.1) and, for example, evaluate its expected value. MCMC sampling has proven particularly useful within the Bayesian framework, where the numerical integration of complex and often mathematically intractable posterior probability distributions is frequently required for parameter estimation (Robert and Casella, 2011).

In MCMC sampling, the parameter space is randomly explored by a number of "walkers". The sequence $\left\{\theta^{(p)} : p = 0, 1, \ldots, P\right\}$ of dependent random points visited by each walker is called a "Markov chain" because it is iteratively created according to the Markov property — *i.e.* at each step the transition to the current state solely depends on the previous one $\mathrm{P}\left(\theta^{(p)} \middle| \theta^{(0)}, \theta^{(1)}, \theta^{(2)}, \ldots, \theta^{(p-1)}\right) = \mathrm{P}\left(\theta^{(p)} \middle| \theta^{(p-1)}\right)$ (Congdon, 2006, Ch.1.3). Provided that the sequence drawn is irreducible, positive recurrent, and aperiodic[19] the Markov chain converges to a unique stationary distribution (Gelman et al., 2013, Ch.11.2), which in the limit $(P \to \infty)$ is called equilibrium distribution and coincides with the target distribution (*i.e.* the posterior probability of interest). Among the most common MCMC sampling algorithms there are the Metropolis-Hastings (M-H) and the Gibbs sampling, the latter being a special case of the former. In the following

18 Although MLE and MAP estimates coincide when using uniform priors, the use of the Bayesian framework is still advantageous for model comparison especially as it does not require that the models tested are nested (Section 3.5.1).

19 A Markov chain is irreducible if the probability of transitioning from any set of states to any other is non-zero; it is positive recurrent if the expected number of steps to return to a given set of states is finite; it is aperiodic if it is possible to return to a given set of states at irregular times. These conditions are generally met within Bayesian frameworks (Gelman et al., 2013, Ch.11.2).

only the M-H sampling algorithm is illustrated as this is at the basis at the software used in this work for MCMC optimisation (illustrated in Section 4.3.1.2).

In the M-H algorithm each walker is originally initialised with an arbitrary position $\theta^{(0)}$; then, a new point $\theta^{(p+1)}$ is generated from the current point $\theta^{(p)}$ according to the following steps (Congdon, 2006, Ch.1.4). At each iteration, a new point θ^* is proposed from a proposal (or jumping) density f. An acceptance ratio ζ of the proposed point in respect to the previous one is calculated as:

$$\zeta\left(\theta^* \middle| \theta^{(p)}\right) = \min\left(1, \frac{\mathrm{P}\left(\theta^* \middle| y\right) f\left(\theta^{(p)} \middle| \theta^*\right)}{\mathrm{P}\left(\theta^{(p)} \middle| y\right) f\left(\theta^* \middle| \theta^{(p)}\right)}\right) \tag{3.43}$$

where $f\left(\theta^* \middle| \theta^{(p)}\right)$ is the probability of moving to θ^* from $\theta^{(p)}$; $f\left(\theta^{(p)} \middle| \theta^*\right)$ is the probability of returning to the current point from θ^*; $\mathrm{P}\left(\theta^{(p)} \middle| y\right)$ and $\mathrm{P}\left(\theta^* \middle| y\right)$ are respectively the values of the posterior in the current and the proposed points. Since only the ratio of the posteriors is required, the unnormalised posteriors can be used to calculate ζ as the normalisation factor (*i.e.* the evidence) cancels out in the ratio. If the acceptance ratio is one, the new point is accepted and $\theta^{(p+1)} = \theta^*$. Conversely, if ζ is in the range zero to one, a random number is drawn from a standard uniform distribution; the proposed point θ^* is accepted if the outcome is less than ζ and rejected $\left(\theta^{(p+1)} = \theta^{(p)}\right)$ otherwise.

Asymptotically the Markov chains converge to the stationary distribution, which by definition does not depend on their initialisation value (Congdon, 2006, Ch.1). However, since the samples of a chain are dependent, an initial set of samples may still be affected by the choice of the starting values before the chains reach the "region of the posterior" (Congdon, 2006, Ch.1.5). This initial set of samples is usually referred to as burn-in, and it might be desirable to discard it from the analysis since the choice of the initial values is usually arbitrary. Nevertheless, the debate is still open on the criteria for the assessment of the convergence of MCMC sampling algorithms (Congdon, 2006, Ch.1.5). Several methods have been proposed, among which the use of several parallel chains independently initialised. This approach has the advantage of reducing the chances that a walker gets trapped in a local optima or it explores a small portion of the parameter space, and can also be used for diagnosis purposes (*e.g.*, poor identifiability of a model) (Congdon, 2006, Ch.1.5). According to Gelman and Rubin (1992), each chain has to be independently initialised drawing the values (θ_0) from an over-disperse distribution around the mode (or modes) of the target probability, previously identified using an optimiser. This approach ensures that important regions of the target distribution are not entirely missed by the iterative process (Gelman and Rubin, 1992).

In this work, the multi-chain method was adopted. Each chain was initialised by sampling the starting values from a multivariate distribution centred at the MAP with variance three times larger than the inverse of the Hessian (*i.e.* the covariance matrix).

3.5 MODEL SELECTION AND VALIDATION

Once potential models explaining the phenomenon of interest have been formulated and their parameters have been estimated in the light of the observation available, they have to be tested for selection and validation purposes. This is an important phase of model building to ensure that the model devised is suitable and robust, and thus its performance is generalisable, trustable and replicable (Hastie et al., 2008, Ch.7). According to Norlén (1994) (as cited in Jiménez et al., 2009) six criteria for model selection and validation have to be considered:

1. *Fit to the data*. This criteria is investigated by looking at the raw and estimated time series, and checking for patterns in the residuals that have not been accounted for by the model. In case the likelihood function was formulated assuming iid residuals (introduced in Section 3.4.1), it is required to ensure that this strong assumption is in fact justified after the model-fitting process (Jiménez et al., 2009). Specifically, it has to be ensured that the residuals are small and not significantly different from white noise[20] (Madsen, 2007, Ch.6.6). This is tested by investigating the autocorrelation function (ACF) of the residuals in the time-domain and their cumulated periodogram (CP) in the frequency-domain (Madsen, 2007, Ch.6.6) and verifying that no more than 5-10% of the lags of the ACF (or 5-10% of the time of the CP) exceed a 95% confidence band (Madsen et al., 2016).
   The introduction of a DCT transform in the likelihood formulation (described in Section 3.4.1) allowed the model to account for the potential autocorrelation of the residuals without having to make the iid assumption. Consequently the autocorrelation function and cumulated periodogram were not checked in this work. Plots of the measured and predicted heat flux are shown in Section 5.2 and Section 5.3, as recommended by Madsen et al. (2016).

2. *Simplicity*. This criteria is based on the idea that the simplest theory explaining a phenomenon should be preferred (MacKay, 2007, Ch.28). Although increasingly complex models result in a better fit to the observations, which is in principle de-

20 A sequence $\{r_t : t = 1, \ldots, n\}$ is white noise if its expected value is zero, its variance is finite and the elements are uncorrelated. In many applications, the further assumption of independence is made. If the sequence is Gaussian distributed, then $r_t \sim \mathcal{N}(0, \sigma^2)$ is called white Gaussian noise.

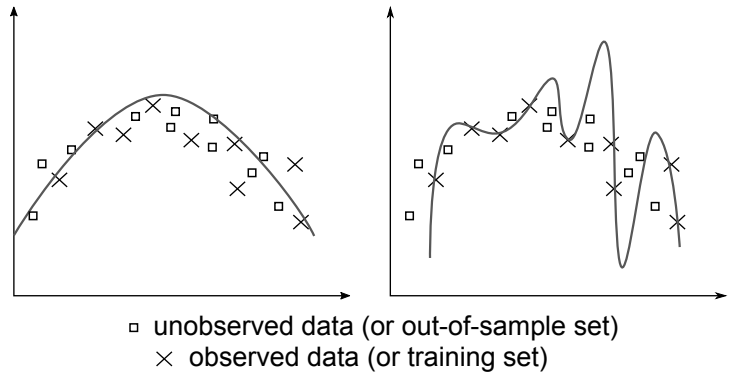

Figure 3.10: Model order and overfitting. The increased complexity of the higher order model (on the right) improved the fitting performance to the observed data, to the detriment of its ability to describe the behaviour of the underlying physical process and generalise to unobserved data.

sirable, over-complex models may start to describe the noise in the data instead of the underlying process (Figure 3.10 on page 105). This phenomenon is known as overfitting (MacKay, 2007, Chs.39,44). Simplicity is at the basis of model comparison techniques, which aim at selecting the best model describing the observations using the smallest number of parameters (Jiménez et al., 2009). The model comparison method adopted in this research is illustrated in 3.5.1.

3. *Internal validity*. This criteria refers to the ability of a model to ensure robust parameter estimates across different data sets (other than the one used for model fitting). Stated otherwise, the model has to be able to generalise to new observations (*i.e.* out-of-sample data set) (Madsen et al., 2016). As illustrated in Figure 3.10 on page 105, the higher order model (on the right) matches very accurately the data used for model fitting (*i.e.* training set) but it would provide poor prediction of the unobserved data. Internal validity is generally assessed using cross-validation techniques. The cross-validation method applied in this research is illustrated in Section 3.5.2.

4. *External validity*. This criteria is met by ensuring that the estimates of the model are in agreement with previous knowledge or past experience, unless a strong justification can be identified to explain the disagreement (Jiménez et al., 2009). The use of prior probability distributions (introduced in Section 3.4.2) in the Bayesian framework aim at addressing this requirement. Additionally, external validity can be encouraged by devising models complying with the theoretical background of the phenomenon investigated (*e.g.*, physically informed models in the context of this research).

5. *Dynamic stability.* The model should ensure that the effects of a temporary perturbation gradually fade out. This is particularly important for steady-stated models, where transient effects are not described (Jiménez et al., 2009).

6. *Identifiability*. This criteria aims at ensuring that the model is able to return unique estimates of the parameters from the data, and consequently that the outputs are reproducible. This requirement can be achieved by using a number of precautions including good quality experimental design and data collection (Madsen et al., 2016) and informed modelling choices, for example adopting an appropriate parametrisation of the problem also in relation to the measurements available or to be collected. In optimisation problems, this requirement may also be achieved by adopting precautions against local minima. In the context of this research, identifiability was addressed by undertaking careful primary data collection (described in Section 4.1), and selecting both a likelihood function (Section 3.4.1) and minimisation algorithms less prone to local optima (Section 4.3.1).

The following sections illustrate the model comparison and cross-validation methods applied in this research.

3.5.1 *Model comparison*

In case more than one model of different complexity is plausible to describe the system under study (*i.e.* the heat transfer across a building element in this research), it may be valuable to identify the one that provides the best description of the data observed and the underlying physical process. In general terms model comparison techniques are based on the Occam's razor principle (or principle of parsimony), which affirms a preference to accept the simplest theory that explains the observations (MacKay, 2007, Ch.28). Bayesian model comparison incorporates the Occam's razor principle by requiring that the extra-complexity of a model (*e.g.* an increase of the number of parameters used) is justified only in case it produces an increase in the goodness of the model fitting. Increasing the number of parameters enlarges the prior probability space of the parameters, effectively penalising more complicated models (Good, 1968; Jefferys and Berger, 1992; Jeffreys, 1998).

In this thesis the plausibility of two models (*e.g.*, the 1TM and 2TM models, $H_{1\text{TM}}$, $H_{2\text{TM}}$, described in Section 3.3.1 and Section 3.3.2) fitted to their most probable parameters

$(\theta_{\text{MAP}1}, \theta_{\text{MAP}2})$ have been inferred using the Odds ratio, *i.e.* the ratio of their posterior probability distributions of a model given the data (MacKay, 2007, Ch.28):

$$\frac{\mathrm{P}\left(H_{1\text{TM}}\,|y\right)}{\mathrm{P}\left(H_{2\text{TM}}\,|y\right)} = \frac{\mathrm{P}\left(y\,|H_{1\text{TM}}\right)\mathrm{P}\left(H_{1\text{TM}}\right)}{\mathrm{P}\left(y\,|H_{2\text{TM}}\right)\mathrm{P}\left(H_{2\text{TM}}\right)} \tag{3.44}$$

where $\mathrm{P}\left(H_{1\text{TM}}\,|y\right)$ and $\mathrm{P}\left(H_{2\text{TM}}\,|y\right)$ are the posterior probability distribution of each model; $\mathrm{P}\left(y\,|H_{1\text{TM}}\right)$ and $\mathrm{P}\left(y\,|H_{2TM}\right)$ are the evidence of each model (their ratio can be referred to as Bayes factor); $\mathrm{P}\left(H_{1\text{TM}}\right)$ and $\mathrm{P}\left(H_{2\text{TM}}\right)$ are the prior probability of each model (if available). Prior probabilities on the proposed models may be introduced in the calculation in case one of the two models is believed to be more likely than the other, based on previous knowledge. Depending on the approach adopted for model fitting (*i.e.* MAP or MCMC), different methods are available to calculate the evidence (or marginal likelihood) by marginalising over the parameters as discussed below.

Unlike classical approaches, the Bayesian framework does not require that the models tested are nested, effectively extending the applicability of this useful technique (Congdon, 2006, Ch.1). It requires that the performance of each model is evaluated using the same amount of information in terms of monitoring period, number of data streams used for model fitting, and number of observations. In the context of this research, this has been possible by comparing the performance of the 1TM model fitted using both the internal and external heat flux measurements and the 2TM model. Whilst the use of both the internal and external heat flux data streams for the 1TM model is essential for model comparison, this model does not always performs well in describing the data (as discussed in Section 6.5).

3.5.1.1 *Maximum a posteriori*

The Odds ratio method requires the calculation of the evidence $\mathrm{P}\left(y\,|H\right)$ for each model H compared (Equation 3.44). When using the MAP approach, the evidence (or marginal likelihood) can be calculated by marginalising over the parameters θ of each model as:

$$\mathrm{P}\left(y\,|H\right) = \int \mathrm{P}\left(y, \theta\,|H\right)\mathrm{d}\theta = \int \mathrm{P}\left(y\,|\theta, H\right)\mathrm{P}\left(\theta\,|H\right)\mathrm{d}\theta \tag{3.45}$$

where $\mathrm{P}\left(y, \theta\,|H\right)$ is the joint probability of the data and the parameters given the model; $\left(y\,|\theta, H\right)$ is the likelihood; $\mathrm{P}\left(\theta\,|H\right)$ is the prior probability of the parameters. Assuming that the posterior distribution can be approximated with a Gaussian distribution centred

in the MAP, the Laplace's method[21] (MacKay, 2007, Ch.27) can be used to approximate Equation 3.45 as (MacKay, 2007, Ch.28.1):

$$\mathrm{P}\left(y\,|H\right) \approx \mathrm{P}\left(y\,|\theta_{\mathrm{MAP}}, H\right) \mathrm{P}\left(\theta_{\mathrm{MAP}}\,|H\right) \left[\det\left(2\pi A\right)\right]^{1/2} \tag{3.46}$$

where $\mathrm{P}\left(y\,|\theta_{\mathrm{MAP}}, H\right)$ is the best-fit likelihood (*i.e.* the likelihood calculated for $\theta = \theta_{\mathrm{MAP}}$); $\mathrm{P}\left(\theta_{\mathrm{MAP}}\,|H\right)\left[\det\left(2\pi A\right)\right]^{1/2}$ is the Occam's factor; $\mathrm{P}\left(\theta_{\mathrm{MAP}}\,|H\right), \left[\det\left(2\pi A\right)\right]^{1/2}$ are respectively the prior probability and a coefficient that depends on the curvature of the posterior distribution around the MAP; A is the inverse of the Hessian of the negative logarithm of the posterior probability distribution around its global optimum. As discussed in Section 3.4.2, the priors on the parameters of the model were assumed independent. Consequently, the prior probability distribution of the best-set of parameters of the model $\left(\mathrm{P}\left(\theta_{\mathrm{MAP}}\,|H\right)\right)$ can be calculated according to Equation 3.37.

3.5.1.2 *Markov Chain Monte Carlo*

When using an MCMC approach, the evidence $\mathrm{P}\left(y\,|H\right)$ for each model H being compared (Equation 3.44) can be calculated from the posterior density function at each step of a chain. According to Bayes' theorem, the posterior density function at each step can be computed as:

$$\mathrm{P}\left(\theta\,|y\right) = \frac{h\left(\theta\,|y\right)}{\mathrm{P}\left(y\right)} \tag{3.47}$$

where $h\left(\theta|y\right)$ is the unnormalised posterior (*i.e.* the likelihood times the prior) of the parameters θ at each step of the chain; $\mathrm{P}\left(y\right)$ is the evidence. Renaming the evidence as $\frac{1}{\mathcal{Z}}$, it can be calculated from Equation 3.47 as:

$$\mathcal{Z} = \left\{\frac{\mathrm{P}\left(\theta|y\right)}{h\left(\theta|y\right)}\right\}^{-1}. \tag{3.48}$$

An estimator $\widehat{\mathcal{Z}}$ of the evidence can be defined according to the reciprocal importance sampling (rIS) method (Diciccio et al., 1997), which uses samples of the unnormalised posterior generated by the MCMC analysis during model fitting:

$$\widehat{\mathcal{Z}} = \left\{\frac{1}{m}\sum_{i}\frac{s\left(\theta_i\right)}{h\left(\theta_i\right)}\right\}^{-1} \tag{3.49}$$

21 The Laplace's method is used for the approximation of integrals of the form $I\left(n\right) = \int \mathrm{e}^{-nh(x)}\mathrm{d}x$, where $I\left(n\right)$ is the value of interest as n approaches a limit (*e.g.*, infinity); $h\left(x\right)$ is a unimodal function with strictly positive second derivative at its modal value x_{MAP}. The approximation is achieved by applying a Taylor series expansion both to $h\left(x\right)$ and the exponential function. In statistics it provides a general approach for marginalisation problems, and consequently for the calculation of the evidence.

where m is the number of samples included to define the estimator; $s(\cdot)$ is an arbitrary probability density function used to approximate the evidence; $h(\cdot)$ is the unnormalised posterior. Given the mathematical formulation of Equation 3.49, the analysis has to be restricted to a small region around the mode to avoid infinite variance in the estimator when its tails are thicker than the tails of the unnormalised posterior distribution $[h(\theta_i) \ll s(\theta_i)]$. This was achieved in Diciccio et al. (1997) by restricting the calculation to an ellipsoid B to avoid that the ratio s/h is large.

To accomplish the requirements above, in this application $s(\cdot)$ was assumed to be a uniform probability within the ellipsoid B (centred in the MAP) having a shape factor according to the covariance matrix (*i.e.* the Hessian around the MAP) and a radius such to contain only the points with unnormalised posterior greater than half the value at the mode. Therefore, the estimator of the evidence was calculated as:

$$\widehat{\mathcal{Z}} = \left\{ \frac{1}{m} \sum_{\theta \in B} \frac{\frac{1}{v}}{h(\theta|y)} \right\}^{-1} \tag{3.50}$$

where v is the volume of the ellipsoid containing the samples of interest from the unnormalised posterior.

3.5.2 *Cross-validation*

Cross-validation is an important model-validation technique to measure the quality of the best model selected (Hastie et al., 2008, Ch.7). As introduced in Section 3.5, it measures the predictive performance of a statistical model by analysing the out-of-sample prediction (Madsen, 2007, Ch.6.6) and testing the ability of the model to generalise to new observations (*i.e.* an independent data set not used for model fitting).

In general, cross-validation should be performed by randomly splitting the observations in two independent datasets (*i.e.* the training set and the test set). The training set is used to fit the model, while the other is used to test its predictive performance (Hastie et al., 2008, Ch.7) by means of the expected extra-sample error (Hastie et al., 2008, Chs.7.2,7.10):

$$\mathrm{Err} = \mathbb{E}\left[L\left(Y, \widehat{f}(X)\right) \right] \tag{3.51}$$

where $L\left(Y, \widehat{f}(X)\right)$ is the generalisation error (*i.e.* a loss function between the vector of the observations Y and the predictions from the model $\widehat{f}(X)$ given a vector of inputs X). Common choices for the generalisation error are either the squared error $\left(Y - \widehat{f}(X)\right)^2$

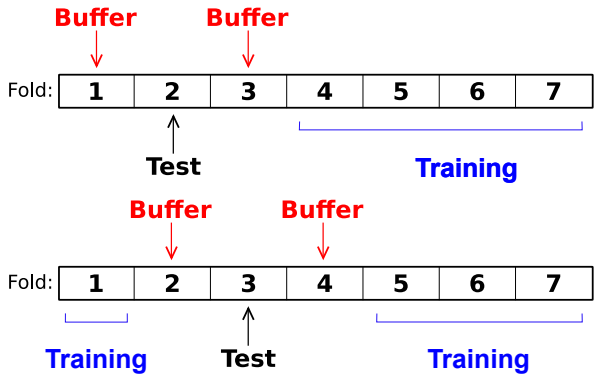

Figure 3.11: Schematic of the revised *K*-fold cross-validation method proposed. The time series was subdivided into 24-hour-long folds and two of them (one before and one after the test set) were left out from the analysis as a buffer to mitigate the requirement of independence of the test and training sets during cross-validation.

or the absolute error $\left|Y - \hat{f}(X)\right|$. This approach to cross-validation, however, is often not possible due to the unavailability of large enough datasets. In these cases the *K*-fold cross-validation method can be adopted (Hastie et al., 2008, Ch.7.10).

K-fold cross-validation consists of randomly subdividing the dataset available into *K* equal-sized independent subsets (or "folds"), and in rotation use one of these to fit the model and the others (*K*-1) to test it. The prediction errors obtained from each fold is then combined to evaluate the cross-validation prediction error, as the expected value of the loss functions obtained from each k-fold. Due to the requirement of independence for the test and training sets, cross-validation is usually difficult to perform in time series analysis (and, more in general, on intrinsically ordered data). An additional difficulty in the context of this work arises from the fact that the initial temperature of the thermal mass is one of the parameters of the model (Section 3.3). Therefore the initial part of the time series cannot be used for testing purposes. To account for these limitations, a revised *K*-fold cross-validation was proposed in this work.

The time series analysed was subdivided into 24-hour-long folds assuming that a full-day period is sufficient to make the autocorrelation negligible. The condition of independence for the training and test sets was mitigated by leaving out one folder before and one after the test set as buffer (Figure 3.11 on page 110). To obviate the issue of the estimation of the initial temperature of the effective thermal mass, all folds were used to predict the time series of interest (*i.e.* the heat flux in this work) during the simulation phase, however only the data belonging to the training fold were used for the optimisation of the parameters. Expressed differently, the parameters were fitted maximising the posterior probability only on the training set (Section 3.4.3). From the time series predicted with the optimal parameters, only the window belonging to the

test set was used to compute the cross-validation prediction error as the mean square root error of the residuals. The first fold was never used for test purposes to enable the estimation of the initial temperature of the effective thermal mass. For visualisation purposes the cross-validated time series can be reconstructed by joining the cross-validated time series obtained for each test fold.

3.6 SUMMARY

This chapter discussed the novel dynamic grey-box method proposed in this research to estimate the thermophysical properties of building elements using *in-situ* measurements. The method proposed consisted of lumped-thermal-mass models to simulate the heat transfer through walls and Bayesian analysis to optimise the parameters of the models.

The chapter presented the family of models developed in this research and the Bayesian framework used to calculate the posterior probability distribution of the parameters. Four lumped-thermal-mass models were devised, which are able to account for solar radiation input as separate source of information if this is available. Both uniform and log-normal priors on the parameter and the estimates (*e.g.,* the U-value) of the model were used to incorporate available knowledge. A likelihood accounting for the potential correlation of the residuals of the model was defined owing to the Bayesian approach to replace the common strong assumption of independent and identically distributed residuals. Maximum a posteriori and Markov Chain Monte Carlo sampling were adopted to explore the posterior probability distribution of the parameters of the model and estimate their optimal set of values. Model selection, based on the odds' ratio, was used to evaluate the best model (*i.e.* the one more likely to describe the phenomenon of interest), and a model validation method was presented to test its ability to generalise to out-of-sample observations.

The next chapter illustrates the case studies and monitoring campaigns used in this thesis to test the performance of the method proposed. Subsequently it describes the experimental analysis, the optimisation software adopted to explore the posterior probability distribution, and the error analysis techniques undertaken depending on the method (*i.e.* dynamic or steady state) adopted for parameter estimation.

4

EXPERIMENTAL METHOD, CASE STUDIES AND ANALYSIS

Chapter 3 described the theory behind the grey-box dynamic method developed in this research for the estimation of the thermophysical properties of building elements using *in-situ* measured data. This chapter presents the experimental method and the implementation of the theory used to test the method developed under best-practice conditions (*i.e.* north-facing walls and winter season) first (Chapter 5), and extending it to all times of the year and different wall orientations later (Chapter 6 and Chapter 7). Specifically, this chapter describes the five case studies, one located in a thermal chamber and four *in-situ* (Section 4.1), used to assess the performance of the method. Subsequently, it details the preliminary evaluations and calculations necessary to initialise the analysis (Section 4.2), followed by an overview of the software selected for the implementation of the novel method (Section 4.3.1) and the checks on the time series investigated (Section 4.4). Finally, it describes the different error analysis approaches used (Section 4.5) depending on the data analysis method (*i.e.* dynamic or steady state) undertaken.

4.1 EXPERIMENTAL EQUIPMENT AND CASE STUDIES

Of the four case studies presented in this thesis, three long-term monitoring campaigns were set up and maintained by the candidate[1] while the fourth was undertaken by Marincioni et al. (2014). Primary data were preferred wherever possible to gain a close control of the experiment design and monitoring method, which enables a more insightful understanding of the results and greater appreciation of the limitations in the accuracy of the equipment or its placement.

1 Further two short-term surveys, which have not been included in this thesis, were undertaken as part of side projects and consultancy work.

Type	Make	Model	Accuracy
Heat flux plates	Hukseflux (2016)	HFP01	±5% reading
Thermistors	n/a	n/a	±0.1 °C
Thermocouple	Labfacility (2016)	type -T	±0.5 °C
Pyranometer	Kipp and Zonen (2016)	CMP3	Zero offset: a) thermal radiation (at 200 Wm^{-2}): < 15 Wm^{-2} b) temperature change (5 Kh^{-1}): < 5 Wm^{-2}
Air velocity	Sontay (2010)	AV-DSP	±5% of range (range: [0; 8] ms^{-1})

Table 4.1: List of monitoring equipment and specifications.

Make	Model	Accuracy	Precision	Operating settings
Campbell Scientific (2015)	CR1000	±(8.0 µV+0.12% read)	±1.0 µV	T = [-25, +50] °C Volt. range: ±7.5 mV
Eltek (2015)	451/L 851/L	±0.1% read ±0.1% range span		
Rotronic (2014)	Higrolog NT with standard climate probe	±0.2 K ±1.5% RH		T = [-50, +100] °C RH = [0, 100]%

Table 4.2: List of data loggers and their specifications.

4.1.1 *Experimental equipment*

The minimum experimental equipment for each monitoring campaign comprised a variable number of heat flux plates (HFP) and temperature sensors. Additional pieces of equipment were installed on a case-by-case basis, taking into account the limitations of the site and the individual purpose of the study (*e.g.*, investigation of the performance of the model over seasons when boundary conditions may change over time). All sensors and data loggers make, model and specifications are reported in Table 4.1 on page 114 and Table 4.2 on page 114. The equipment mounting and set up for each case study is discussed in Section 4.1.2.

4.1.2 *Case studies*

Five walls of different construction and exposed to different environmental conditions were monitored[2] to test different aspects of the performance of the novel dynamic method proposed. A well-characterised insulated solid wall constituted of aerated clay blocks and wood fibre insulation (TCWall) housed in a thermal chamber was monitored to test the performance of the dynamic method under controlled conditions, and to compare the estimates of its thermophysical properties using the dynamic method to those from the AM and calculated values from manufacturer's specifications. Four differently oriented *in-situ* elements — two north-facing (CLWall, HSWall_N) and one east-facing (HSWall_E) insulated cavity walls, and one north-west-facing traditional solid wall (OWall) — were monitored long-term to investigate the performance of the method when the building elements are exposed to changing environmental conditions, such as different insolation levels and temperature differences. In all cases, site inspection and a thermal camera were used to assist the placement of the equipment on representative locations on the wall surface, away from artefacts and unusual thermal patterns (Energy Saving Trust, 2005; C1155-95, 2011).

4.1.2.1 *Aerated clay block wall in a thermal chamber (TCWall)*

A wall constituted of eight sections (1865 mm by 500 mm each) was built in the centre of a Design Environmental thermal chamber and monitored by Marincioni et al. (2014) to test different wall-construction technologies. The thermal chamber was constituted of two adjacent thermal zones (type WIR11/28-10H) 2840 mm wide (max) by 3800 mm deep and 2600 mm high each, individually controllable in terms of temperature and relative humidity. The central position of the wall was chosen to minimise possible edge effects introduced by the structure of the chamber itself.

Section 2 was investigated in this thesis (Figure 4.1 on page 116). It was a (303 ± 3) mm thick heavy-weight solid-wall constituted of seven layers. This specific section was chosen as its heavy-weight construction, similar to the OWall (described in Section 4.1.2.2) but significantly different in terms of structure and expected thermal mass distribution, provides a useful contrast to the OWall. From the cold side it comprised: (175 ± 2) mm of aerated clay blocks, (10 ± 2) mm of gypsum plaster, (5 ± 1) mm of lime plaster, (20 ± 1) mm of woodfibre insulation board, (0.10 ± 0.05) mm functional layer

2 The specifications of all pieces of equipment and data loggers mentioned in the following sections are summarised in Table 4.1 on page 114 and Table 4.2 on page 114.

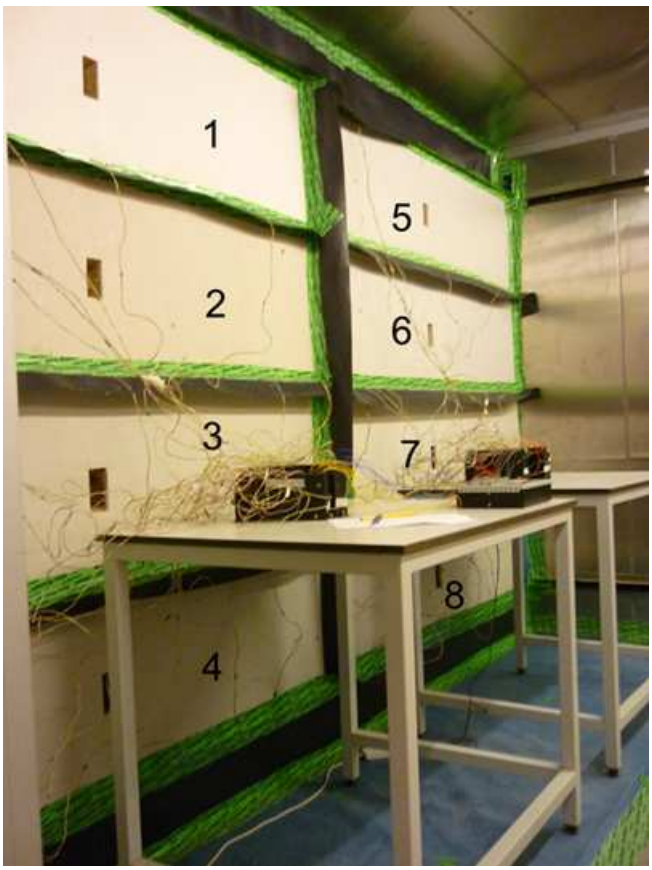

Figure 4.1: Thermal chamber wall, warm side view (courtesy of Valentina Marincioni).

glued to a (80 ± 1) mm of woodfibre insulation board and (12.5 ± 0.5) mm of gypsum fibreboard.

The external ambient temperature profile in the thermal chamber was set to repeat the hourly temperatures of a typical day derived from the UK Test Reference Year (TRY) for Manchester (Levermore and Parkinson, 2006). The indoor daily profile was set to replicate a typical UK indoor heating pattern derived from the Warm Front dataset, a project where air temperature and relative humidity were monitored for up to four weeks in the main living spaces of more than 1600 dwellings in five urban areas across the UK (Oreszczyn et al., 2006).

The wall was instrumented with two HFPs and two Rotronic standard climate probes (Table 4.1 on page 114), placed in-line with each other on opposite sides[3]; the temperature sensors were mounted on the wall surface close to each HFP (Figure 4.2 on page 117). Duct tape was used to fix the HFP and thermistors to the wall; a layer of thermal compound was applied under the sensors to ensure good thermal contact. A Campbell Scientific CR3000 data logger was used to record the heat flux entering and leaving the

3 For conciseness this configuration of HFPs and temperature sensors will be referred to as "pair" in the following.

Figure 4.2: Monitoring equipment on the TCWall, warm and cold side view respectively (courtesy of Valentina Marincioni).

wall, while a Rotronic Higrolog NT (Table 4.2 on page 114) was used to record surface temperatures. Data were averaged and recorded over 5-minute intervals.

4.1.2.2 *Solid brick wall in an office building (OWall)*

The OWall case study was a solid brick north-west-oriented (327° between the normal to wall and north) wall, located on the first floor above ground of a detached office building in central London (UK) (Gori et al., 2014, 2017). The office was occupied throughout the monitoring period (except public holidays and closure days) and the heating pattern was dictated by occupancy; no control on the thermostat settings was imposed as part of the experiment. The data presented in this thesis were collected over the period between the beginning of November 2013 and the beginning of December 2014. From the exterior, the wall consists of (350 ± 5) mm of exposed solid brick masonry and (20 ± 5) mm of plaster (expected to be lime) for a total thickness of (370 ± 7) mm. The wall depth is expected to comprise one and a half bricks, potentially with air pockets at the interface between adjacent bricks.

Pairs of HFP and type-T thermocouples were mounted on the wall (Figure 4.3 on page 118). The internal HFP was fixed by covering the wall-facing side of the sensor with a layer of low-tack tape followed by a layer of double-sided tape. The additional thermal mass and resistance of the thin fixing layers were assumed to be negligible in

Figure 4.3: Internal and external monitoring set up for the OWall.

comparison to the thermophysical properties of the wall (Rye, 2012). The external HFP was secured using a water-resistant elastomeric polymer on the edge of the plate and thermal paste on the measuring area. The temperature sensors were taped on top of each HFP (on the guard ring, outside the measuring area), using thermal paste to ensure good thermal contact (Rye, 2012). As the thermal resistance of the HFP $\left(6.25{\cdot}10^{-3}\,\mathrm{m^2KW^{-1}}\right)$ (Hukseflux, 2016) is about 1% of the typical resistance of a solid-brick wall similar to the OWall, the difference between the wall and HFP surface temperatures is considered negligible. Data were recorded by a Campbell Scientific CR1000 (Table 4.2 on page 114) datalogger averaging 5 second samples over 5-minute intervals.

4.1.2.3 *Cavity wall in an occupied house (CLWall)*

The CLWall case study was a 1970s north-oriented cavity wall, located at the ground floor of an occupied residential building in Cambridgeshire (UK). Similarly to the OWall, no heating-control strategy of the indoor ambient was part of the experiment and the heating pattern of the room surveyed was determined by the occupants' preferences and space usage. The survey was undertaken between the beginning of February and the end of August 2016. The total wall depth is (275 ± 10) mm and it consists of four layers; from the exterior, (100 ± 5) mm of exposed bricks are followed by a (65 ± 5) mm cavity filled with urea formaldehyde foam, (100 ± 5) mm aerated concrete blocks and (10 ± 5) mm plaster, likely to be gypsum-based. Visual inspection through a disused opening for a flue suggested that the original full fill of insulation layer has severely shrunk through the years (Figure 4.4 on page 119); such shrinkage is expected to happen throughout the wall, introducing potential by-pass loops and air movement in the cavity. Evidence of shrinkage of urea formaldehyde foam was reported by Kalthod and Knickle (1982); Thun et al. (1982) and this issue may have represented one of the reasons for its dismissal as insulating material in the building sector.

Two pairs of HFPs and thermistors were installed approximately 500 mm apart and vertically aligned (Figure 4.5 on page 119). For each pair, the HFPs and thermometers

Figure 4.4: Stratigraphy of the wall as inspected through a disused opening for a flue (external layer on the left). Notably, the urea formaldehyde foam has shrunk, leaving potential paths for air movement in the cavity.

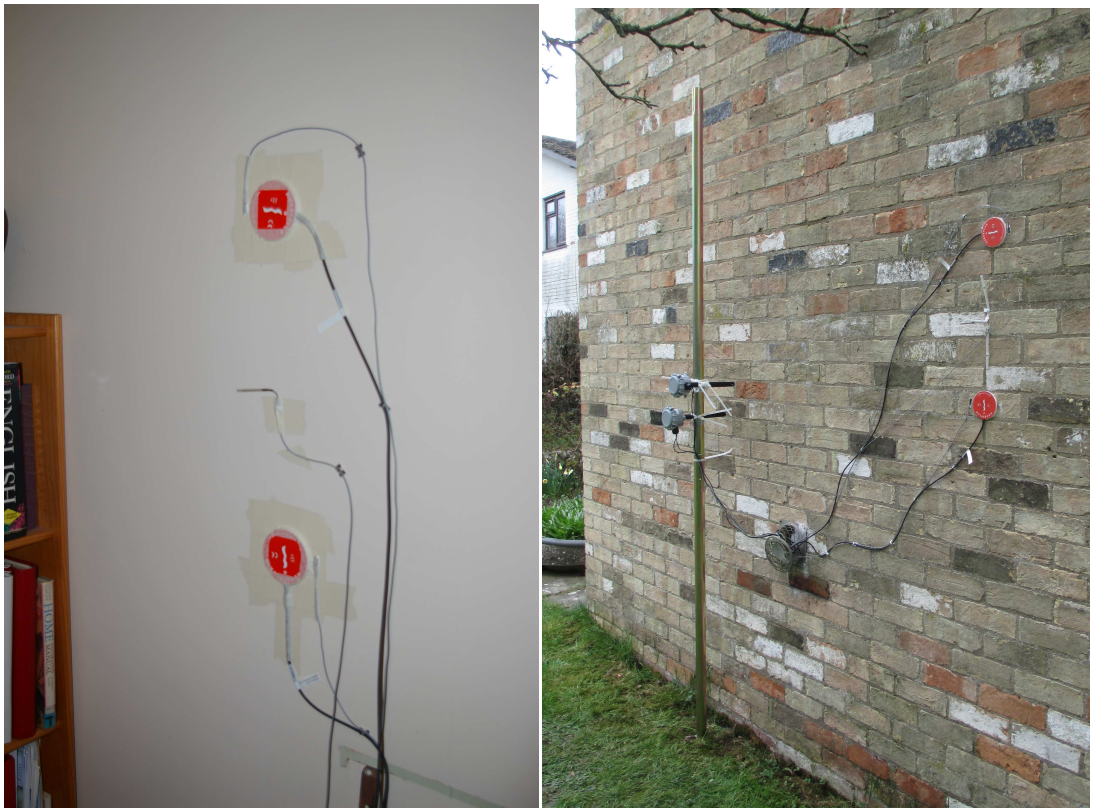

Figure 4.5: Internal and external monitoring set up for the CLWall.

were placed in-line with each other on opposite sides of the wall; the thermistors were placed on the wall next to the plate. A layer of Servisol silicon-free heat sink compound was used under each sensor to ensure good thermal contact. Duct tape was used to fix the indoor HFPs (measuring part excluded) and thermistors to the wall surface; the external sensors were secured using a thin layer of silicone sealant on the edges. Two Sontay air velocity sensors, one vertically and one horizontally oriented, were also installed close to the external surface of the wall (Figure 4.5 on page 119) to investigate the air movement in proximity of its surface. The measuring part was about (25 ± 10) mm from the vertical plane. Data were collected using three Eltek 451/L Squirrel data loggers (Table 4.2 on page 114) set up to sample every 5 seconds and average over 5 minutes.

4.1.2.4 *Cavity wall in an unoccupied house (HSWall)*

The HSWall case study was a 1970s unoccupied detached house in Cambridgeshire (UK). The monitoring period spanned between mid March and end of August 2015. For accessibility and security reasons only two ground floor cavity walls were surveyed: one north- (HSWall_N) and one east-oriented (HSWall_E). The indoor ambient was constantly heated to 20 °C. The total thickness of the wall was (275 ± 10) mm on the north and (283 ± 10) mm on the east side. Although limited information was available about the thickness of the layers, detailed physical inspection showed that the wall is constituted of exposed bricks followed by a cavity that was originally fully filled with insulation (according to the owner), a layer of aerated concrete blocks and a layer of plaster. An original certificate shows that the insulation material is Propotec Warmfoam installed during a post-built intervention in 1979. Given the year of installation and the visual aspect, the insulation is assumed to be urea formaldehyde foam. Additionally, given the comparable age band to that of the CLWall and assuming that the thicknesses of masonry blocks and bricks are standard, the cavity is expected to be 65 mm deep for the north-facing and 73 mm for the east-facing wall.

The two walls were instrumented using pairs of HFPs and thermistors (Table 4.2 on page 114), placed and secured following the same procedure illustrated in Section 4.1.2.3 (Figure 4.6 on page 121). A pyranometer (Table 4.2 on page 114) was mounted on the east wall to record the incoming vertical solar radiation.

Eltek 451/L and 851/L data loggers (Table 4.2 on page 114) were used to record the HFP and thermistor data. The signal was sampled every 5 seconds and averaged over 5-minute intervals. The pyranometer data were recorded using an Eltek wireless data logger. Solar radiation was sampled every 30 seconds and averaged over 5-minute intervals.

Figure 4.6: Internal (left) and external (HSWall_E in the centre picture and HSWall_N on the right) monitoring equipment for the HSWall. Internally, the three sensors on the left were on the north-facing wall and the rest on the east-facing one.

4.2 EXPERIMENTAL ANALYSIS

A number of quantities have to be pre-computed to initialise the data analysis. These include the calculation of an additive noise term on the observations (Section 4.2.1) and the definition of the prior probability distributions needed to inform the Bayesian framework (Section 4.2.2).

4.2.1 *Calculation of the additive noise term on the observations*

The calculation of the likelihood (Section 3.4.1), both used in the optimisation (Section 3.4.1) and model comparison (Section 3.5.1) phases, requires the definition a priori of an additive noise term $\left(\sigma^2_{\Phi,\varepsilon}\right)$ to account for all the quantifiable sources of uncertainties affecting the observations (*i.e.* the data streams used in the analysis). Depending on the uncertainty considered, this can be classified as relative (if it is proportional to the magnitude of the observation), or absolute (if it is a constant bias). In cases when the uncertainties within the two categories can be assumed independent (*i.e.* the occurrence of one type of uncertainty in the measurements does not imply an increase or decrease in other uncertainties), a total relative and absolute uncertainty affecting the observations can be calculated as the quadrature sum of the individual uncertainties. The additive noise term is calculated combining the absolute uncertainty and the relative uncertainty times the observations it refers to. Consequently, the variance of the additive noise term for each data stream can be calculated as:

$$\sigma^2_{\Phi,\varepsilon} = \left(\delta^{\mathrm{a}}_{\Phi,\varepsilon}\right)^2 + \left(\frac{\sum_{p=1}^{n} \left|\Phi^p_{\mathrm{m},\varepsilon}\right|}{n}\, \delta^{\mathrm{r}}_{\Phi,\varepsilon}\right)^2 \tag{4.1}$$

where $\delta^{\mathrm{a}}_{\Phi,\varepsilon}$ is the total absolute uncertainty for each data stream ε; $\delta^{\mathrm{r}}_{\Phi,\varepsilon}$ is the total relative uncertainty for each data stream; $\Phi^p_{\mathrm{m},\varepsilon}$ are the observations for each data stream at each time step p; n is the number of observations analysed.

In this work the noise term accounted for the uncertainties affecting the heat flux measurements, being the data streams used in the optimisation phase to calculate the residuals (Section 3.4.1); therefore, $\sigma^2_{\Phi,\varepsilon} \equiv \sigma^2_{Q,\varepsilon}$ and $\Phi^p_{\mathrm{m},\varepsilon} \equiv Q^p_{\mathrm{m},\varepsilon}$. In principle, both the uncertainties on heat flux and temperature observations should be considered in the optimisation phase. However our assumption is not uncommon (Roulet et al., 1987; Jiménez et al., 2009; Naveros et al., 2014) and also supported by the BS ISO 9869-1 (2014) Standard, where the uncertainties on the heat flux measurements have been identified as

the main source of error on the estimates. For each data stream analysed, the following uncertainties were considered to calculate the noise term:

- the accuracy of the equipment (*i.e.* HFP and data logging system(s) involved in the analysis, according to Table 4.1 on page 114 and Table 4.2 on page 114 in our case);
- the effect of random variations caused by imperfect thermal contact between the sensor and the wall (5% according to BS ISO 9869-1 (2014), Table 2.1 on page 60);
- an uncertainty due to the modification of the isotherms caused by the presence of the HFP (3% according to BS ISO 9869-1 (2014), Table 2.1 on page 60).

The uncertainties listed above were also used in this work for the calculation of the systematic measurement error on the heat flux observations for each data stream ($\sigma_{Q,\varepsilon}$) in the estimation of the systematic error on the U-value (Section 4.5).

4.2.2 *Definition of priors*

Estimates of the thermophysical properties of building materials can be inferred from look-up tables in the literature. However, the use of literature values for the characterisation of the thermophysical behaviour of *in-situ* elements may not be representative of their actual performance as materials with similar appearance may have quite different thermophysical characteristics and tabulated properties for materials with similar descriptions may present quite large ranges (Section 2.2). Additionally, literature values do not account for the actual conditions (*e.g.*, moisture content and boundary conditions) of the building element under study. Conversely, the sole use of measured data may require a higher number of observations (which may result in more expensive and time-consuming monitoring campaigns), and be more prone to unrepresentative results of the overall thermal performance of the element in relation to the actual location surveyed, being *in-situ* monitoring based on spot measurements. The use of prior probability distributions enables the coupling of information extracted from measurements with tabulated values, which enhances the quality and robustness of the estimates and potentially reduces the monitoring time and costs.

As introduced in Section 3.4.2, both uniform and log-normal priors were used in this work. The former assign an equal probability to observations falling within the chosen range and null probability elsewhere. Therefore, the definition of ranges that are too broad will over-represent the probability of rare events (*e.g.*, high interstitial temperat-

ure), while ranges that are too small will exclude the possibility of correctly identifying rare but possible events. Conversely, non-uniform priors overcome this limitation by enabling the assignment of low probabilities to unlikely observations. The following sections illustrate the priors on the parameters of the model adopted in this analysis.

4.2.2.1 *Uniform priors on the parameters of the model*

Large uniform priors on the parameters of the model were used in the cases where limited information about the wall structure was available (Section 4.1.2). Specifically, for all case studies all thermal resistances ranged in $[0.01,\ 4.00]\ \mathrm{m^2KW^{-1}}$, all thermal masses between $\left[0.1,\ 2\cdot 10^6\right]\ \mathrm{Jm^{-2}K^{-1}}$, and their initial temperature ranged in $[-5,\ 40]\ ^\circ\mathrm{C}$. These ranges encompass all expected values, with significant safety margin.

4.2.2.2 *Log-normal priors on the parameters of the model*

In this thesis log-normal priors on the parameters of the model were defined only for the OWall site as an illustrative example, since the distribution of the thermophysical properties of some of the materials constituting the other case studies were not readily available in the literature. Given the increasing interest in the probabilistic assessment of the hydrothermal behaviour of building components, Zhao et al. (2015) have recently started the development of a stochastic database from measurements sampled on common building materials. At present, the database includes normal distributions of the thermal conductivity, density and specific heat capacity of a number of common building material categories including brick, stone, plaster and mortar, and insulation. The authors are working on enlarging the database to include concrete and aerated blocks, however the sample is not large enough yet for statistical analysis (Zhao, 2016). It is hoped that this useful resource will be available shortly.

In principle, it would be possible to build the missing distributions from data sets created from tabulated thermophysical properties. However this approach presents some theoretical issues. Since the source of tabulated values is generally omitted, the merged data set may be redundant (*i.e.* accounting as independent pieces of information that actually come from the same source) and affected by higher uncertainties (Zhao et al., 2015). For this reason the thermophysical property distributions in Macdonald (2002) were not used in this work, as the data set (Clarke et al., 1990) used to extrapolate them did not investigate the redundancy, and consequently the reliability, of the sources (Zhao, 2016).

The mean and standard deviation of Gaussian distributions of the thermophysical properties of the building materials in the paper by Zhao et al. (2015) were used to define

the location and dispersion of log-normal-distributed priors on the lumped thermal resistances and thermal capacitances of the models. For a multi-layer element like the OWall, the R-value and effective thermal mass is a function of two (or more) measured quantities. Therefore, the mean and variance of the resulting Gaussian distribution can be determined according to the linear propagation of errors theory (Bohm and Zech, 2010, Ch.4.3), which is based on a first-order Taylor expansion. Assuming that as a first approximation the measured quantities x_i are independent, the mean (μ_y) and the variance (v_y) of the output function of interest $(y = f(x_1, \ldots, x_n))$ can be calculated as:

$$\mu_y = \mathbb{E}\left[y\left(x_1, \ldots, x_n\right)\right] \approx y\left(\mu_{x_1}, \ldots, \mu_{x_n}\right) \tag{4.2}$$

$$v_y = \mathbb{E}\left[\left(y - \mu_y\right)^2\right] \approx \sum_{i=1}^{n} \left(\frac{\partial y}{\partial x_i}\right)^2 v_{x_i} \tag{4.3}$$

where μ_{x_i} is the mean of the distribution of each measured quantity x_i, and v_{x_i} its variance. The location $(\ln L_Y)$ and dispersion (D_Y) of a log-normal distribution (to be substituted in Equation 3.39) describing the thermophysical quantity of interest can be calculated from the mean (μ_y) and variance (v_y) of the normal distribution as:

$$D_Y = \sqrt{\ln\left(1 + \frac{v_y}{\mu_y^2}\right)} \tag{4.4}$$

$$\ln L_Y = \ln \mu_y - \frac{1}{2} D_y^2. \tag{4.5}$$

The R-value of a multi-layer element is a function of the thickness of each layer (d_i) and its thermal conductivity (λ_i) (BS EN ISO 7345, 1996):

$$R = \sum_{i=1}^{n} \frac{d_i}{\lambda_i}; \tag{4.6}$$

according to Equation 4.2 and Equation 4.3 the mean (μ_R) and the variance (v_R) of its normal distribution are:

$$\mu_R = \sum_{i=1}^{n} \frac{\mu_{d_i}}{\mu_{\lambda_i}} \tag{4.7}$$

$$v_R = \sum_{i=1}^{n} \left(\frac{1}{\mu_{\lambda_i}^2} v_{d_i} + \frac{\mu_{d_i}^2}{\mu_{\lambda_i}^4} v_{\lambda_i}\right) \tag{4.8}$$

where μ_{d_i} and μ_{λ_i} are respectively the mean of the distribution of the thickness and the thermal conductivity of each layer; v_{d_i} and v_{λ_i} their variances. Similarly, the thermal mass per unit area (*i.e.* the heat capacity) (EN ISO 13786, 2008) can be calculated as:

$$\kappa = \sum_{i=1}^{n} (d_i \rho_i c_i) \tag{4.9}$$

where ρ_i is the density of each layer and c_i its specific heat capacity. The mean (μ_C) of the normal distribution of the lumped effective thermal mass and its variance (v_C) can be determined from Equation 4.2 and Equation 4.3 as:

$$\mu_C = \sum_{i=1}^{n} \left(\mu_{d_i} \mu_{\rho_i} \mu_{c_i}\right) \tag{4.10}$$

$$v_C = \sum_{i=1}^{n} \left(\mu_{\rho_i} \mu_{c_i}\right)^2 v_{d_i} + \sum_{i=1}^{n} \left(\mu_{d_i} \mu_{c_i}\right)^2 v_{\rho_i} + \sum_{i=1}^{n} \left(\mu_{d_i} \mu_{\rho_i}\right)^2 v_{c_i}. \tag{4.11}$$

In this work, the estimators of the log-normal distribution of the lumped thermophysical parameters were identified by fixing the position of the effective thermal mass(es) according to the effective thickness method described in EN ISO 13786 (2008, Appendix A). This method defines the effective thermal mass contributing to a thermal zone as in Equation 4.9, considering only the materials included within the effective thickness of the component. The effective thickness is determined as the minimum value from the following three criteria:

- half of the total thickness of the component;
- the thickness of the materials comprised between the wall surface and the first insulating layer;
- a maximum effective thickness as a function of the period of variation, which for a period of 24 hours is 100 mm.

The effective thermal mass is calculated as the sum of the thermal mass (*i.e.* the product of the density, specific heat capacity and thickness) of the materials included in the effective thickness. Upon fixing the thermal mass(es), the Gaussian mean and variance of each lumped parameter was calculated from Equation 4.7 (or Equation 4.10) and Equation 4.8 (or Equation 4.11) by accounting for the thermophysical properties of the material(s) contributing to it.

The location and dispersion of the log-normal distribution for each parameter were calculated from Equation 4.5 and Equation 4.4. The location of the log-normal prior on the initial temperature of the thermal mass(es) for each month of the year was defined

from the test reference year (TRY) for London (Eames et al., 2016), by aggregating the corresponding hourly air temperatures. The dispersion of the distribution was chosen to cover a range of values reasonable for this application. The values for the location and dispersion of the log-normal distributions for each month are shown in Table 4.3 on page 128. The location and dispersion of the log-normal distributions for the thermal resistances and effective thermal mass(es) used with the 1TM and 2TM models are respectively shown in Table 4.4 on page 129 and Table 4.5 on page 129.

4.2.2.3 *Log-normal prior on the U-value*

As discussed in Section 3.4.2, a log-normal prior on the U-value of the element (instead of on the thermophysical properties of the materials, as above) can be adopted when the actual stratigraphy of the element is not known but enough information (*e.g.*, from visual inspection, age of construction, *etc.*) are still available to identify the type of structure under study (*e.g.*, cavity wall, solid wall). In this case the distribution of the U-value is required.

For the OWall, the location and dispersion of a log-normal distribution describing the U-value of solid brick walls were calculated substituting in Equation 4.4 and Equation 4.5 the mean ($1.29\,\mathrm{Wm^{-2}K^{-1}}$) and standard deviation ($0.35\,\mathrm{Wm^{-2}K^{-1}}$) of the distribution reported in Li et al. (2014), where *in-situ* measurements from forty solid-walled dwellings (Stevens and Bradford, 2013) were analysed. The location and dispersion calculated were respectively $1.245\,\mathrm{Wm^{-2}K^{-1}}$ and $0.267\,\mathrm{Wm^{-2}K^{-1}}$. Note the analysis using the aforementioned prior on the U-value was mainly conducted for illustrative purposes, as the OWall may be thicker (*i.e.* one and a half brick) than the traditional residential solid walls monitored in Stevens and Bradford (2013) field trial. Should similar studies to those by Stevens and Bradford (2013) or Baker (2011) be carried out focussing on cavity walls or non-domestic solid walls, these would provide useful information to extend the use of priors on the U-value to the CLWall, HSWall_N and HSWall_E case studies or to retest the performance of non-uniform priors on the OWall.

	Jan	Feb	Mar	Apr	May	Jun	Jul	Aug	Sept	Oct	Nov	Dec	Units
Location (L_Y)	4.9072	5.5296	6.5760	8.6470	13.2212	16.0922	17.9930	0.0515	0.0520	0.0525	0.0534	0.0537	°C
Dispersion (D_Y)	0.0539	0.0537	0.0535	0.0531	0.0523	0.0518	0.0514	17.8643	15.0601	12.1177	7.2075	5.9127	°C

Table 4.3: Measure of location and dispersion of the initial temperature of the thermal mass(es) of the 1TM and 2TM model for the OWall case study.

Parameter	Location (L_Y)	Dispersion (D_Y)	Units
R_1	0.1501	0.3707	m^2KW^{-1}
R_2	0.3755	0.3158	m^2KW^{-1}
C_1	146450	0.2199	$Jm^{-2}W^{-1}$

Table 4.4: Measure of location and dispersion of the parameters of the 1TM model for the OWall case study.

Parameter	Location (L_Y)	Dispersion (D_Y)	Units
R_1	0.1501	0.3707	m^2KW^{-1}
R_2	0.2365	0.3158	m^2KW^{-1}
R_3	0.1391	0.3158	m^2KW^{-1}
C_1	146450	0.2199	$Jm^{-2}W^{-1}$
C_2	153542	0.1525	$Jm^{-2}W^{-1}$

Table 4.5: Measure of location and dispersion of the parameters of the 2TM model for the OWall case study.

4.3 SOFTWARE IMPLEMENTATION

The methodology and the theory described in Chapter 3 was implemented in Python 3.0 (Python Software Foundation, 2017). Whilst the framework and a number of algorithms had been already implemented prior the start of this project (Biddulph et al., 2014), the work undertaken towards this doctoral research has included a significant reorganisation of existing functions and the implementation of a number of new software algorithms and functionalities. Figure 4.7 on page 130 shows the dependencies in the software, where the functions at the tip of the arrow are called by those at the tail receiving some input parameters and returning some outputs. An overview on the optimisation software adopted for MAP and MCMC analysis is provided in the following.

4.3.1 *Optimisation software*

As introduced in Section 3.4.3, both MAP and MCMC approaches were adopted in this work to optimise multi-parameter posterior probability distributions. While the former approach only estimates the best-fit parameters, the latter provides the estimation of the full probability distribution of the parameters and enables a more insightful interpretation of the results obtained (as discussed in Chapter 5 and Section 6.4). The Python SciPy "Basinhopping" function was used for MAP optimisation and the Python library "EMCEE" for MCMC sampling, as discussed below.

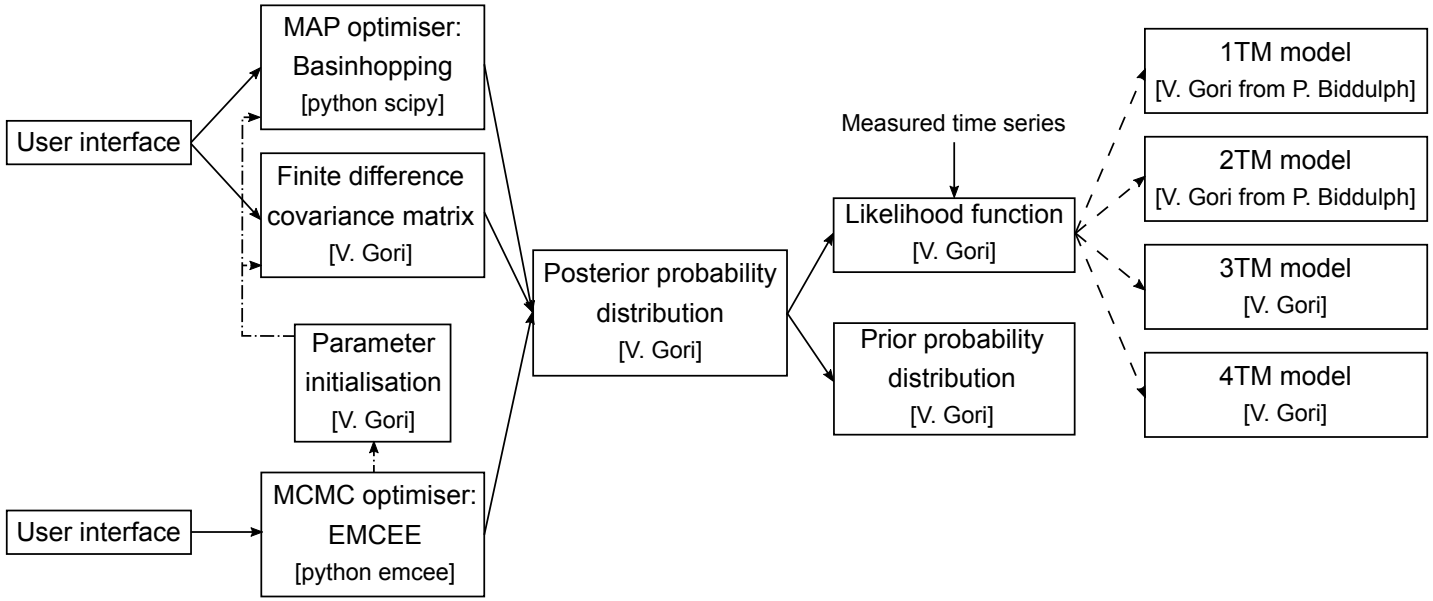

Figure 4.7: Diagram of the dependencies in the software implemented. The function at the tail of the arrow calls the one at the tip passing some parameters and receiving the outcomes. The dash-dotted lines indicate the functions called only once, while the dashed line show alternative options.

4.3.1.1 *Maximum a posteriori optimiser: the basin-hopping algorithm*

The original implementation of the software used in this research (Biddulph et al., 2014) only allowed MAP estimates, using the CERN Minuit package (James and Winkler, 2004). This package is designed to investigate multi-parameter functions to identify their minimum value and analyse the shape of the function around it. Minuit can estimate the best-fit parameters and the associated uncertainties, also accounting for the correlation between parameters. Since the Minuit Python binding used by Biddulph et al. (2014) is no longer maintained, the Python SciPy implementation of the basin-hopping algorithm (Wales and Doye, 1997) was introduced in the proposed framework as part of the software reorganisation undertaken in this work.

The basin-hopping algorithm has been proved to be robust to local minima (ScyPy community, 2016), especially in the cases where many minima were separated by large barriers, and has been applied to solve several scientific problems (see for example the Cambridge Cluster Database (Wales et al., 2017)). Basin-hopping is a stochastic algorithm to find the global minimum of a multi-parameter objective function (ScyPy community, 2016). It is an iterative algorithm consisting of the application of a random perturbation to the coordinates of the starting value followed by a local minimisation; the new coordinates obtained are either accepted (or rejected) according to the acceptance criterion used in Metropolis-Hastings algorithms (described in Section 3.4.3.2). In this work, the Powell method was chosen as minimiser among the options suggested in the Basinhopping function in SciPy. The Powell method in SciPy (ScyPy community, 2016) implements a modification of Powell's method (1964) for the optimisation of multi-dimensional functions without requiring the calculation of derivatives.

4.3.1.2 *Markov Chain Monte Carlo optimiser: EMCEE*

As discussed in Section 3.4, the MCMC framework provides additional information on the full distribution of the posterior probability and the parameters compared to MAP approaches (where only the best-set of parameters and the shape of the peak is investigated). An MCMC-based optimiser, the Python library EMCEE (Foreman-Mackey et al., 2013), was added to the original software implementation. It implements the MCMC sampler presented in Goodman and Weare (2010).

In this research the posterior probability distribution was sampled using 500 walkers[4], each one initialised according to the method described in Section 3.4.3.2. Each Markov chain consisted of 1000 samples, of which 50 were discarded as burn-in. Trace plots

4 For terminology related to MCMC sampling, refer to Section 3.5.1.

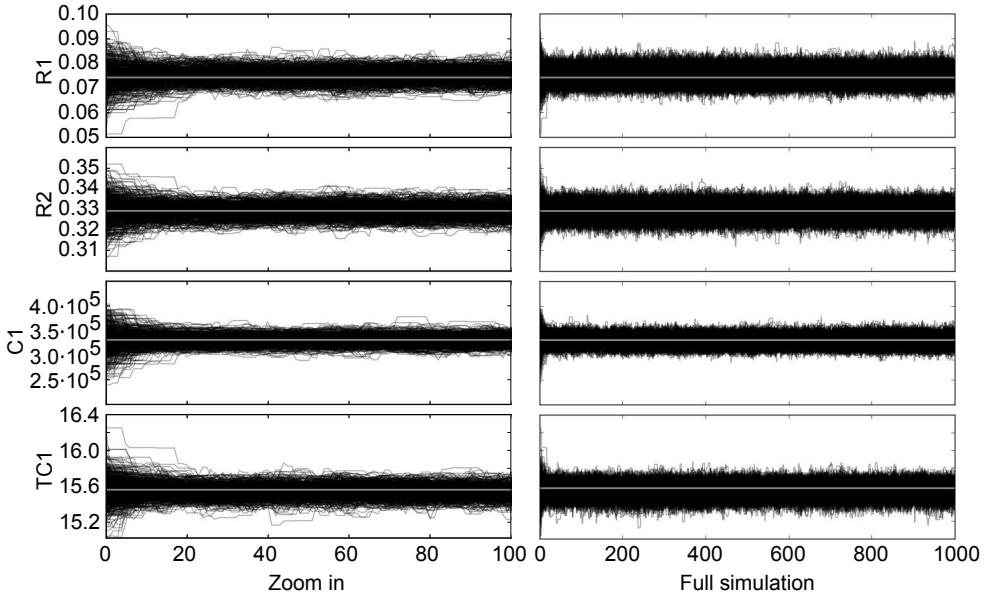

Figure 4.8: Plot of the Markov chains for each parameter, for an illustrative example using a 1TM model. On the left, a zoom in of the first 100 iterations shows the burn-in samples.

like the one in Figure 4.8 on page 132 were produced and visually inspected to check whether the chains had stabilised and the burn-in was sufficient. Trace plots show the values sampled by the walker over time for each parameter and are valuable for convergence assessment and diagnostics. During the burn-in period the trace plot shows a narrowing (Figure 4.8 on page 132) or clear monotonic trend of the chains (Congdon, 2006, Ch.1.5). The latter is also observed in case convergence has not been achieved. Convergence issues are often related to problems in model identifiability, such as redundant parameters or overfitting (Congdon, 2006, Ch.1.5).

Corner plots were also produced to summarise the probability distribution of the parameters of the model and provide insights into their potential dependencies; an example of corner a plot is shown in Figure 4.9 on page 133. In the plot, the histograms along the diagonal show the marginalized distribution for each parameter, while the remaining panels represent the marginalized 2D distributions for each pair of parameters. This type of graph provides useful information about the correlation between the parameters. When a pair of parameters is uncorrelated (*e.g.*, C_1 and T_{C_1} in Figure 4.9 on page 133), the posterior probability is often circular or elliptical with axes parallel to the Cartesian axes. Conversely, when a pair of parameters is correlated (*e.g.*, R_1 and R_2 in Figure 4.9 on page 133), the posterior probability distribution is rotated and the orientation of the major axis of the ellipsis indicates the nature of the relationship (positive or negative). This information was used in Section 6.4, Chapter 5 and Gori and Elwell (2017) to gain insights into the thermal structure of the building elements.

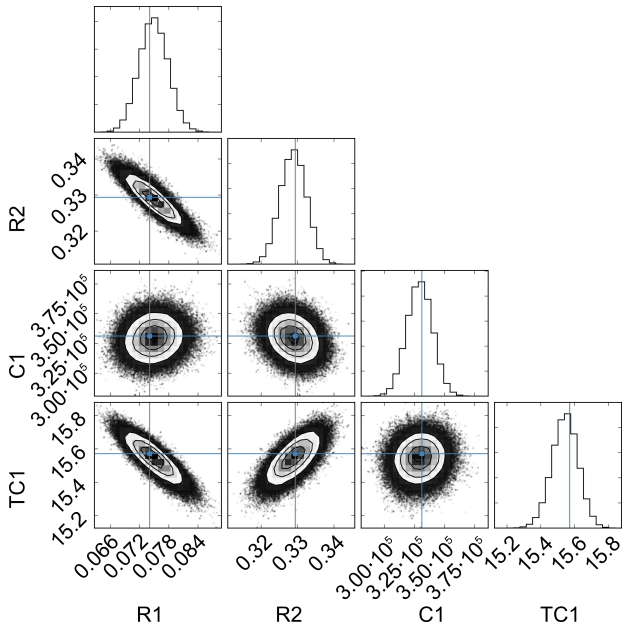

Figure 4.9: Corner plot of the estimates of the probability distribution of the parameters, for an illustrative example using a 1TM model. The blue cross identifies the MAP value.

To facilitate the comparison of the estimates obtained with MAP outputs, the mean of the parameter distributions were calculated and their statistical uncertainties (discussed in Section 4.5) were determined by computing the covariance matrix of the samples in the chains.

4.4 STABILISATION CRITERIA

During the experimental analysis, it is good practice to ensure that the length of the time series used for the estimation of the thermophysical properties of the element is appropriate, and consequently the estimates obtained are representative of the actual performance of the building element surveyed. This requirement arises from the contrasting need for a time series that is sufficiently long to ensure that the estimates are accurate and have small variability, but that is not too long to ensure that the assumption of a unique model to explain the data over the monitoring period (*e.g.*, constant parameters) holds. Short monitoring campaigns are also preferable for practical reasons, such as containing the costs and minimising the inconvenience to the occupants. Therefore, it is important to determine the minimum number of observations that return robust estimations of the thermophysical parameters of the building element investigated. Initially, the estimates are noisy and prone to overfitting as the time series analysed are too short. The supplement of new observations significantly improves the estimates until the addition of new data does not enhance the prediction of the parameters anymore

and the values stabilise around a final value. This concept is referred to as "stabilisation" in the following chapters.

As introduced in Section 2.3.1, the BS ISO 9869-1 (2014) Standard lists a number of stabilisation criteria to ensure that the assumptions underlying steady-state approaches (Section 2.3) hold for the period investigated. Conversely, no standardised criteria are available (to the candidate's knowledge) for dynamic methods. Therefore, the criteria to determine the length of the time series listed in the BS ISO 9869-1 (2014) Standard were also imposed in this work for dynamic analysis, although the test may be too conservative for the dynamic method (as illustrated in Chapter 5). Besides assuring good-quality estimates, the enforcement of stabilisation criteria was used in this research to test different aspects of the performance of the dynamic method proposed, also in comparison with the AM. Specifically, two scenarios were considered[5]:

- The first scenario consisted of fixing the length of the time series according to the minimum number of days needed for the AM to stabilise. The time series obtained were adopted for data analysis, both using the AM and the dynamic method (with different lumped-thermal-mass models). This scenario enabled the comparison of the performance of the different approaches in terms of estimation of the best-fit parameters and their associated systematic errors, and Bayesian model comparison.

- The second scenario consisted of testing the different approaches (*i.e.* AM and dynamic method with different lumped-thermal-mass models) using time series whose minimum length was independently determined by imposing the stabilisation criteria on each analysis. This scenario investigated the relative ability of the AM and dynamic method (with different models) to describe the underlying physical process and their relative ability to return robust estimates using a different number of observations, effectively exploring the potential ability of different lumped thermal mass models within the dynamic method to shorten the monitoring period.

In this thesis the two scenarios were applied to the long-term monitoring campaigns to extract shorter time series. Each time series started one week apart and lasted until the stabilisation criteria were met. This approach, referred to as "hypothetical monitoring campaigns", effectively replicated the case where surveys were undertaken at different periods of the year to test the aims of this research (Figure 4.10 on page 135 shows the

5 Note that given the definition of the stabilisation criteria in the BS ISO 9869-1 (2014) Standard (summarised in Section 2.3.1), the time series analysed have a minimum length of three days.

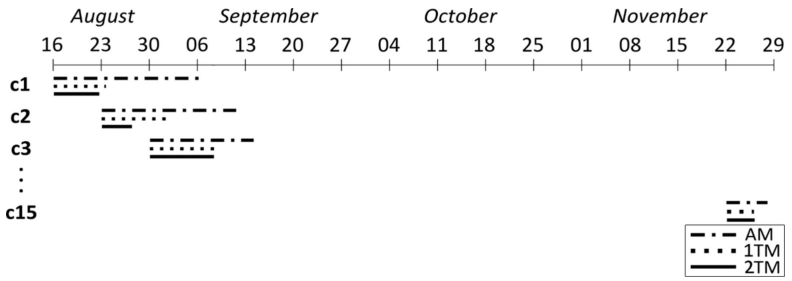

Figure 4.10: Schematic of the concept of hypothetical monitoring campaign applied to the second data analysis scenario. Each line represents the number of days required by each hypothetical monitoring campaign to stabilise with different analysis methods (*i.e.* the AM and the dynamic method with 1TM and 2TM models).

concept of hypothetical monitoring campaign applied to the second scenario described).

The hypothetical-monitoring-campaign approach described above may present potential limitations, which can be minimised by adopting good-practice precautions. Firstly, it does not take into account the time needed for the equipment and the wall to reach thermal equilibrium between hypothetical monitoring campaigns, as after the first one the system is already in thermal equilibrium. However, this is not an actual limitation as also when analysing individual time series, it is good practice to investigate the row data before starting the analysis and discard the initial observations until the traces show to have reached thermal equilibrium. Secondly, environmental conditions (such as variations in the indoor and external temperatures) may not be the only aspects introducing variations in the estimates of thermophysical properties. Other issues may also play a role including the drying process of the thermal paste over time, moisture content in the element, and weather patterns. Given that the thermal paste layer is very thin, this contribution is expected to be negligible compared to other signals; however, specific lab-based experiments investigating the effects that different fixing methods may have on the estimation of thermophysical parameters would be useful.

Future work will investigate and propose new criteria to determine the minimum length of the time series to be analysed when using dynamic methods (*e.g.*, based on cross-validation methods).

4.5 ERROR ANALYSIS

When performing a probabilistic analysis of *in-situ* measurements it is necessary to identify and quantify the different types of uncertainties affecting the observed data (*i.e.* the model's input). These are subsequently combined and propagated to estimate the error affecting the model estimates (Section 3.4.3). These uncertainties can be

broadly grouped as modelling and measurement errors, either of which can be random or systematic.

- MODELLING VS MEASUREMENT ERRORS — Modelling errors are generated by discrepancies between the mathematical description of the underlying physical process and the actual phenomenon being modelled (Zhao et al., 2015; Winship and Western, 2016), while measurement errors represent the difference between the magnitude of the signal measured by a sensor and its true value (Trethowen, 1986).

- SYSTEMATIC VS RANDOM ERRORS — Systematic errors are attributed to a bias in the system that affects all the observations in a consistent manner, following a constant or a fixed pattern (Macdonald, 2002). Typical systematic uncertainties are miscalibration and non-linearity in the relationship of the actual physical quantity and the sensor's reading. These errors can only be minimised by using calibrated instrumentation and attentive experimental procedure (*e.g.*, minimising potential reading bias; using more sophisticated instrumentation or appropriate experimental techniques); or improving the model used to describe the data (*e.g.*, adding parameters to account for extra effects or introducing additional data streams) (Bohm and Zech, 2010; Zhao et al., 2015). Random errors are fluctuations of any specific measurement around the value that would be obtained by averaging the outcome of an infinite number of repeated measurements (Bohm and Zech, 2010). Random uncertainties are generally represented by noise in the system (*e.g.*, thermal noise) or dependency of the reading on other randomly varying factors in addition to the physical quantity measured. In cases that these uncertainties can be considered independent of each other, the precision of the combined result can be improved by averaging an increasing number of observations.

Potential sources of uncertainties contributing to the different type of errors in the context of this thesis are discussed below.

- SYSTEMATIC MODELLING ERRORS — Systematic modelling uncertainties may be introduced by adopting an unrepresentative model of the wall or an incomplete one, for example due: to the use of a limited number of parameters or data streams; the assumptions and simplifications made during its design (such as one-dimensional heat transfer across the wall).

- RANDOM MODELLING ERRORS — Random modelling uncertainties may be a consequence of the use of digital computers including: the discretisation of continuous-time differential equations for simulation purposes; rounding effects; tolerance in the termination criteria of iterative optimisation algorithms.

- SYSTEMATIC MEASUREMENT ERRORS — Systematic measurement uncertainties may be generated by offsets in the measurement system, for example due to: the use of non-calibrated equipment; an improper fixing or poor thermal contact of the sensors; an erroneous set up of the equipment.

- RANDOM MEASUREMENT ERRORS — Random measurement uncertainties include thermal and electromagnetic noise in the equipment (*e.g.*, grounding and shielding).

Different approaches for the propagation of the systematic error on the estimates of the average and dynamic method were implemented in this thesis to reflect the different mathematical modelling and data analysis of the two frameworks. Specifically, in the AM the average of the temperature differences is the denominator of the formula to calculate the U-value (Equation 2.15), while this is not the case for the dynamic method. Therefore, the mathematical formulation of the AM introduces a fundamental limitation to the applicability of this method when the average of the temperature differences is close to zero (*e.g.*, when the heat flux reverts over the monitoring period), which affects both the U-value estimate and its associated error. Conversely, this is not an issue for the the dynamic method. Additionally, the time window for the applicability of the AM may be more restricted compared to the dynamic method as, in general, the average of the temperature differences over the monitoring period is lower than the temperature difference at each time step, and this may be particularly emphasised in periods where the temperature readings present considerable diurnal swings (see Figure 4.11 on page 138 as an example).

The following sections present the methods adopted (and implemented in the Python software) for the propagation of the systematic error on the estimates of the average and dynamic method, and the method for the calculation of the random uncertainties on the thermophysical parameters of the lumped-thermal-mass model.

4.5.1 *Random error on the thermophysical properties estimated with the dynamic method*

The statistical framework of the dynamic method returns the random error (also referred to as "statistical errors[6]" (Bohm and Zech, 2010, Ch.4.2)) on the best-fit parameters as an output of the analysis (as discussed in Section 3.1). These are determined from the inverse of the Hessian of the unnormalised posterior probability distribution around its global optimum (*i.e.* the covariance matrix under the Laplace approximation, A)

6 In the following chapters these random errors will be referred to as "statistical errors".

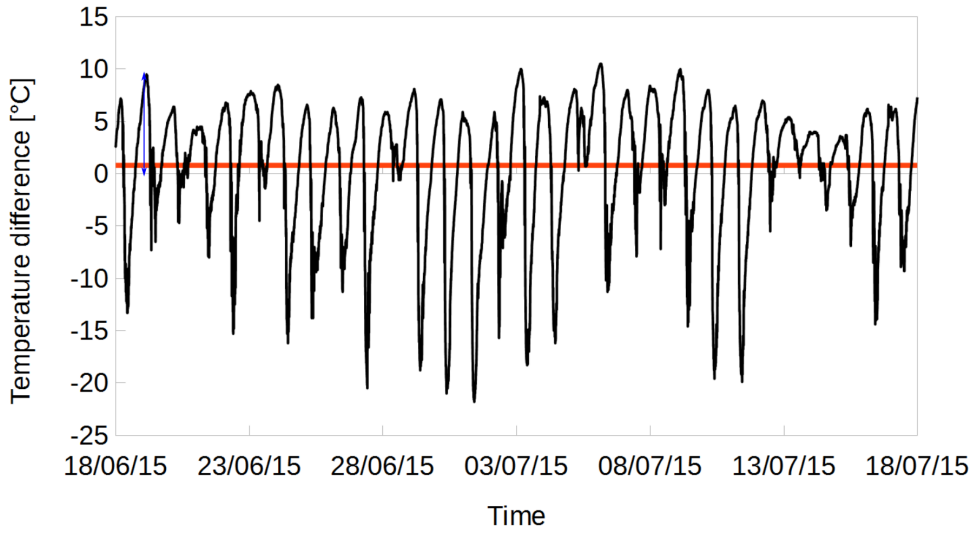

Figure 4.11: Measured temperature difference at each sampling interval (black line) and average of the temperature differences over the monitoring period (red line). The blue arrow shows the amplitude of the temperature difference at a given sampling interval.

(MacKay, 2007, Ch.27). Specifically, the random error on each parameter of the model can be calculated from the covariance matrix as the square root of the corresponding diagonal element:

$$\sigma_{j,j} = \sqrt{A_{j,j}}. \tag{4.12}$$

The random error on the total R-value and U-value can be calculated from the random error on the thermal resistance estimates using error propagation methods. As the total R-value (R_{tot}) is a function of the sum of the individual R_i estimates (plus the air film resistances R_{si} and R_{se}):

$$R_{\text{tot}} = f(R_1, R_2, \ldots, R_m) = R_{\text{si}} + \sum_{i=1}^{m} R_i + R_{\text{se}}, \tag{4.13}$$

its variance $\left(\sigma^2_{R_{\text{tot}}}\right)$ can be calculated as the error of a function of several observations (Bohm and Zech, 2010):

$$\sigma^2_{R_{\text{tot}}} = \nabla_f^{\text{T}} A \nabla_f \tag{4.14}$$

where ∇_f is the gradient of the sum function R_{tot} with respect to all parameters (and ∇_f^{T} it its transpose); A is the covariance matrix of the parameters. In the case of Equa-

tion 4.13, the gradient is a vector having ones in correspondence to the thermal resistances contributing to R_{tot} and zeros otherwise:

$$\nabla_f = \begin{bmatrix} \frac{\partial R_{\text{tot}}}{R_1} \\ \frac{\partial R_{\text{tot}}}{C_1} \\ \vdots \\ \frac{\partial R_{\text{tot}}}{R_m} \end{bmatrix} = \begin{bmatrix} 1 \\ 0 \\ \vdots \\ 1 \end{bmatrix}. \tag{4.15}$$

Consequently, the absolute random error on the total R-value can be rewritten as:

$$\sigma_{R_{\text{tot}}} = \sqrt{\sum_{i=1}^{m}\sum_{j=1}^{m} A_{i,j}}. \tag{4.16}$$

Similarly, the absolute random error on the U-value can be propagated as a first-order Taylor expansion of its definition, under the assumption that the error is small compared to the R-value estimates:

$$\sigma_U = \frac{\mathrm{d}U}{\mathrm{d}R_{\text{tot}}}\sigma_{R_{\text{tot}}} = \frac{\mathrm{d}\left(R_{\text{tot}}^{-1}\right)}{\mathrm{d}R_{\text{tot}}}\sigma_{R_{\text{tot}}} = \frac{\sigma_{R_{\text{tot}}}}{R_{\text{tot}}^2}. \tag{4.17}$$

4.5.2 *Systematic error on the thermophysical parameters and properties estimated with the dynamic method*

The systematic error affecting the thermophysical parameters of the dynamic method can be calculated analysing the global optimum of the unnormalised posterior distribution. Defining $\ell(y,\theta)$ as the log-posterior of the parameters (θ) given all observations (y) (both heat flux(es) and temperature measurements), its gradient with respect to the parameters has to be zero at the MAP where the maximum of the function is achieved:

$$\left.\frac{\mathrm{d}\,\ell(y,\theta)}{\mathrm{d}\theta}\right|_{y,\theta_{\text{MAP}}(y)} = 0. \tag{4.18}$$

Since θ_{MAP} depends on the observations, using the chain rule[7] the derivative of Equation 4.18 with respect to the data can be broken down as:

$$\left.\frac{\partial^2\ell(y,\theta)}{\partial\theta\,\partial y}\right|_{y,\theta_{\text{MAP}}(y)} + \left.\frac{\partial^2\ell(y,\theta)}{\partial\theta^2}\right|_{y,\theta_{\text{MAP}}(y)}\frac{\mathrm{d}\theta_{\text{MAP}}}{\mathrm{d}y} = 0. \tag{4.19}$$

7 The chain rule for a composition of functions $f(x, g(x))$ states that:
$\frac{\mathrm{d}f(x,g(x))}{\mathrm{d}x} = \left.\frac{\partial f(x,w)}{\partial x}\right|_{x,g(x)} + \frac{\partial f(x,w)}{\partial w}g'(x)$.

The dependency of the MAP from the observations can be calculated from Equation 4.19 as:

$$\frac{\mathrm{d}\theta_{\mathrm{MAP}}}{\mathrm{d}y} = \left(- \left. \frac{\partial^2 \ell\left(y,\theta\right)}{\partial \theta^2} \right|_{y,\theta_{\mathrm{MAP}}(y)} \right)^{-1} \left. \frac{\partial^2 \ell\left(y,\theta\right)}{\partial \theta \, \partial y} \right|_{y,\theta_{\mathrm{MAP}}(y)} \tag{4.20}$$

where $-\left. \frac{\partial^2 \ell(y,\theta)}{\partial \theta^2} \right|_{y,\theta_{\mathrm{MAP}}(y)}$ is the Hessian of the minus logarithm of the posterior probability distribution and its inverse coincides with the covariance matrix A under the Laplace approximation; $\frac{\mathrm{d}\theta_{\mathrm{MAP}}}{\mathrm{d}y}$ is a matrix whose elements i, j contain the derivative of the i-th parameter with respect to perturbations of the j-th data stream. The variations of the total R-value are simply the sum of the variations of the R parameters contributing to R_{tot}. Formally, this can be expressed as:

$$\frac{\mathrm{d}R_{\mathrm{tot,MAP}}}{\mathrm{d}y} = \nabla_f^{\mathrm{T}} \frac{\mathrm{d}\theta_{\mathrm{MAP}}}{\mathrm{d}y}. \tag{4.21}$$

Consequently, as the U-value is the inverse of the total R-value, its variations can be calculated according to the formulas for the error propagation of a ratio (Bohm and Zech, 2010, Ch.4.3):

$$\frac{\mathrm{d}U_{\mathrm{MAP}}}{\mathrm{d}y} = -\frac{1}{R_{\mathrm{tot,MAP}}^2} \frac{\mathrm{d}R_{\mathrm{tot,MAP}}}{\mathrm{d}y} \tag{4.22}$$

The absolute systematic error on the U-value is represented by the quadrature sum of the uncertainties on each data stream, assuming that these are independent:

$$\sigma_U = \sqrt{\sum_{\varepsilon} \left(\frac{\mathrm{d}U_{\mathrm{MAP}}}{\mathrm{d}y_\varepsilon} \sigma_\varepsilon \right)^2} \tag{4.23}$$

where σ_ε is the systematic measurement error on each data stream, which comprises both the error on the heat flux $(\sigma_{Q,\varepsilon})$ and temperature $(\sigma_{T,\varepsilon})$ measurements. For heat flux observations, $\sigma_{Q,\varepsilon}$ was calculated according to Section 4.2.1, accounting for the accuracy of the equipment (both sensor and data logging system), its potentially imperfect thermal contact, and modifications of the isotherms by the HFP. For temperature observations, the system systematic measurement error $\sigma_{\mathrm{T},\varepsilon}$ was calculated according to Equation 4.1 and included the accuracy of the temperature sensor and the data logging system.

4.5.3 *Systematic error on the U-value estimated with the average method*

The systematic error affecting the U-value calculated using the AM was determined by propagating the error linearly, using a first-order Taylor expansion (Bohm and Zech, 2010, Ch.4.3) of its definition (Equation 2.15):

$$\begin{aligned} \mathrm{d}U = \mathrm{d}\left(\frac{Q_\mathrm{m}}{\Delta T}\right) &= \frac{\partial U}{\partial Q_\mathrm{m}}\mathrm{d}Q_\mathrm{m} + \frac{\partial U}{\partial \Delta T}\mathrm{d}\Delta T \\ &= \frac{1}{\Delta T}\mathrm{d}Q_\mathrm{m} - \frac{Q_\mathrm{m}}{\Delta T^2}\mathrm{d}\Delta T \end{aligned} \tag{4.24}$$

where Q_m and ΔT are respectively the measured heat flux and the temperature difference between the indoor and external ambient; $\mathrm{d}Q_\mathrm{m}$ and $\mathrm{d}\Delta T$ are their differential. Assuming that the differentials coincide with the systematic measurement errors on the heat flux observations (σ_{Q_m}) and each temperature data streams $(\sigma_{T,\varepsilon})$, the relative systematic error on the U-value can be propagated from Equation 4.24 as:

$$\frac{\sigma_U}{U} = \sqrt{\frac{\sigma^2_{\mathrm{Q_m}}}{Q^2_\mathrm{m}} + \frac{\sigma^2_{\mathrm{T},\varepsilon}}{\Delta T^2}} = \sqrt{\frac{\sigma^2_{\mathrm{Q_m}}}{Q^2_\mathrm{m}} + \frac{\sigma^2_{\mathrm{T},\varepsilon}}{\left(T_\mathrm{int} - T_\mathrm{ext}\right)^2}}. \tag{4.25}$$

In this work, the systematic error affecting both temperature data streams was calculated according to Equation 4.1 and included the accuracy of the temperature sensor and the data logging system combined in quadrature sum. Similarly, the systematic error affecting the heat flux observations included the same uncertainties described in Section 4.2.1 (*i.e.* accuracy of the equipment, imperfect thermal contact, and modifications of the isotherms by the HFP) plus an extra 10% uncertainty added in quadrature sum to account for errors caused by the variations over time of the temperatures and heat flow, as suggested in BS ISO 9869-1 (2014) (listed in Section 2.3.1). Although the BS ISO 9869-1 (2014) Standard suggests that this percentage can be reduced to less than 10% if the criteria for analysis stabilisation are fulfilled as in this thesis, it does not provide indications on how to do so in practice (as discussed in Section 2.3.1). Consequently, in the absence of a clear alternative method, it was decided to use the value reported in the Standard. Owing to the use of surface temperatures, the calculation omitted the 5% uncertainty suggested in BS ISO 9869-1 (2014) to accounts for temperature variations within the space and the differences between air and radiant temperatures.

4.6 SUMMARY OF THE CHAPTER

This chapter described the experimental monitoring and case studies, and the data analysis undertaken in this research. The error analysis method was also presented. Five walls of different construction were monitored and used to test the grey-box dynamic method proposed. One of these was of solid construction and housed in a thermal chamber, while the others (one solid and two cavity walls) were *in-situ.* The experimental data analysis consisted of the calculation of a number of quantities necessary to initialise the software developed. Specifically, these include the calculation of an additive noise term on the observations to account for the uncertainties affecting them, and the definition of the prior probability distributions from previous knowledge (*e.g.*, literature). Subsequently, the software implementation of the theoretical models and methods implemented in Chapter 3 was presented, as well as the optimisers selected for parameters' estimation. The stabilisation criteria to ensure that the length of the time series used for the estimation of the thermophysical properties of the element is appropriate were presented, followed by a description of the different error analysis methods implemented in this research to reflect the different mathematical modelling and data analysis of the average and dynamic methods.

The next chapter adopts the experimental method and analysis described in this chapter and in the previous one to investigate the performance of the dynamic grey-box method under best-practice conditions for the estimation of the thermophysical properties of building elements from *in-situ* measurements. Specifically, the solid wall in the thermal chamber and the *in-situ* north-facing walls (both cavity and solid) were analysed during the winter season. Both MAP and MCMC approaches, also using non-uniform priors where possible, were tested with the family of models presented in Section 3.3. The analysis included the estimation of the parameters of the models and the associated statistical and systematic error, model comparison and cross-validation.

Part III

RESULTS AND CONCLUSIONS

5

PERFORMANCE OF THE DYNAMIC GREY-BOX METHOD TESTED UNDER CONVENTIONAL MONITORING CONDITIONS

Chapter 3 and Chapter 4 illustrated the theoretical framework for the dynamic grey-box method proposed and the experimental monitoring and analysis used to test it under different environmental conditions. A family of lumped-thermal-mass models and a Bayesian framework were developed to provide potential descriptions of the heat transfer through the walls surveyed and estimate the thermophysical properties of building elements from *in-situ* measurements (Chapter 3). After a description of the case studies surveyed, Chapter 4 illustrated the implementation of the novel method proposed. Subsequently it introduced the error analysis method and the approaches used to evaluate the systematic errors on the U-value to reflect the differences in the mathematical modelling of the heat transfer across the building element with the average and dynamic method.

The present chapter[1] tests the performance and robustness of the method proposed using data collected in a thermal chamber (TCWall) and *in-situ* on north-facing walls (OWall, CLWall and HSWall_N). The time series analysed for the *in-situ* walls were chosen such that the average temperature difference between the inside and external surfaces of the wall[2] were comparable to the average temperature difference set up in the thermal chamber (*i.e.* 4.8 °C) (indicated as "lower temperature difference" case in the following). This choice allowed the investigation of the performance of the proposed method on walls exposed to a similar temperature differences but different boundary conditions: a controlled temperature regime in the thermal chamber and real non-stationary excitations *in-situ*. Since the temperature difference in the thermal cham-

1 This chapter builds on and expands the material presented in Gori, V., Marincioni, V., Biddulph, P., Elwell, C.A. 2017. Inferring the thermal resistance and effective thermal mass distribution of a wall from in situ measurements to characterise heat transfer at both the interior and exterior surfaces. Energy and Buildings. DOI: 10.1016/j.enbuild.2016.10.043.

2 In the following the average temperature difference between the inside and external surfaces of the wall is referred to as "average temperature difference" for conciseness.

ber was lower than current best-practice guidelines for *in-situ* measurements[3] (Siviour and McIntyre, 1982; Energy Saving Trust, 2005; Baker and van Dijk, 2008; Desogus et al., 2011), for completeness each *in-situ* wall was also tested on a time series with average temperature difference of at least 10 °C as recommended by best-practice (indicated as "higher temperature difference" case in the following). The following chapters (Chapter 6 and Chapter 7) will extend this analysis to warmer seasons and differently oriented walls.

5.1 LITERATURE THERMOPHYSICAL PROPERTIES

The U-value and the effective thermal mass were calculated from tabulated thermophysical properties for the building materials constituting the case studies. Specifically, the literature total R-value[4] (and U-value) was computed according to the method for the calculation of the R-value of a multi-layer element (described in Section 2.1), while the effective thermal mass contributing to the internal and external thermal zones was obtained using the effective thickness method (introduced in Section 4.2.2.2).

The total R-value (and U-value) was computed by adding constant internal (R_{si}, 0.13 m^2KW^{-1}) and external (R_{se}, 0.04 m^2KW^{-1}) air film resistances to the sum of the R-values of each layer (as discussed in Section 2.1). Plausible ranges of U-values were defined in the cases where specific information about the properties of visually inspected materials were not available.

5.1.1 *Solid wall in a thermal chamber (TCWall)*

According to the thermal conductivity stated by the manufacturer (Table 5.1 on page 147) for the materials constituting the TCWall (described in Section 4.1.2.1), the calculated R-value of the wall (determined according to Equation 2.10) was 2.72 m^2KW^{-1}. It resulted in an U-value of 0.35 $Wm^{-2}K^{-1}$ after considering the thermal resistance of the internal and external air film.

The effective thermal mass of the wall was calculated according to the effective thickness method, described in the EN ISO 13786 (2008, Appendix A) Standard and reported in Section 4.2.2.2. Imposing the criteria for the determination of the effective thickness

3 Due to the refurbishment of the building housing the thermal chamber, this thesis took advantage of a previous experimental research to test the method under controlled environmental conditions although the temperature difference was lower than best-practice recommendations.

4 The use of R-value and total R-value in Chapter 5, Chapter 6 and Chapter 7 reflects the definitions in the BS ISO 9869-1 (2014) Standard, as introduced in Section 2.1.

Material	d [mm]	λ [mKW^{-1}]
Gypsum fiberboard	12.5	0.32
Woodfibre insulation	100	0.043
Lime plaster	5	0.70
Gypsum plaster	10	0.20
Aerated clay blocks	175	0.58

Table 5.1: Tabulated thermal conductivity (λ) of the materials constituting the TCWall according to the manufacturer's specifications, and thickness (d) of each layers.

Material	ρ [kgm^{-3}]	c [Jkg^{-1}K^{-1}]
Gypsum fiberboard	1150	1100
Woodfibre insulation	175	2100
Aerated clay blocks	1400	850

Table 5.2: Tabulated density (ρ) and specific heat capacity (c) of the materials contributing to the internal and external effective thermal mass of the TCWall. The thermophysical properties of the building materials were taken from the manufacturer's specifications.

(summarised in Section 4.2.2.2), 100 mm was required both on the internal and external sides of the TCWall[5]. Consequently, the gypsum fiberboard (12.5 mm) and part of the woodfibre insulation (87.5 mm) contributed to the internal effective thermal mass, while the aerated clay blocks layer (100 mm) contributed to the external one. Although the criteria to calculate the effective thickness of the element would impose to include only the materials up to the first insulation layer (*i.e.* the thin gypsum fiberboard in this case), part of the woodfibre insulation was also accounted for, since this material is usually denser than common insulating materials and therefore is more likely to contribute to the thermal mass of the wall. The density and specific heat capacity stated by the manufacturer are summarised in Table 5.2 on page 147. The internal and external effective thermal mass were respectively of 48000 Jm^{-2}K^{-1} and 119000 Jm^{-2}K^{-1}.

5.1.2 *Solid wall in an office building (OWall)*

The ranges for the thermal conductivity of each layer constituting the OWall (described in Section 4.1.2.2) were taken from the widely used Chartered Institute of Building Services Engineers (CIBSE) Environmental Design - Guide A (CIBSE, 2007), and are summarised in Table 5.3 on page 148. Mortar joints between bricks were not accounted for separately in the calculation (*i.e.* the brick layer was considered a homogeneous layer)

5 The effective thermal masses both at the internal and external sides of the element were calculated to compare with the estimates of the two effective thermal masses estimated by the 2TM model.

Material	d [mm]	λ_{min} [mKW^{-1}]	λ_{max} [mKW^{-1}]
Lime plaster	20	0.70	0.80
Solid brick	350	0.50	1.31

Table 5.3: Minimum and maximum tabulated thermal conductivity ($\lambda_{min}, \lambda_{max}$) for the materials (CIBSE, 2007) expected to constitute the OWall, and thickness (d) of each layer.

Material	ρ_{min} [kgm^{-3}]	ρ_{max} [kgm^{-3}]	c_{min} [Jkg^{-1}K^{-1}]	c_{max} [Jkg^{-1}K^{-1}]
Lime plaster	1600	1600	840	840
Solid brick	1200	2080	800	1000

Table 5.4: Minimum and maximum tabulated density (ρ_{min}, ρ_{max}) and specific heat capacity (c_{min}, c_{max}) of the materials (CIBSE, 2007) contributing to the internal and external effective thermal mass of the OWall.

as the thermal conductivity of mortar was within the thermal conductivity range for solid brick. Substituting the values in Table 5.3 on page 148 into the equation for the calculation of the R-value of multi-layer structures, yielded the range $[0.29, 0.73]\,m^2KW^{-1}$. Adding the thermal resistance of the air film, the U-value of the OWall was expected to be in the range $[1.11, 2.16]\,Wm^{-2}K^{-1}$.

The internal and external effective thermal mass ranges were calculated from the ranges of density and specific heat capacity (CIBSE, 2007) of the materials constituting the effective thickness (Table 5.4 on page 148), which was 100 mm on both sides according to the criteria summarised in Section 4.2.2.2. Specifically, lime plaster (20 mm) and part of the solid brick (80 mm) layer contributed to the effective thermal mass on the internal side, while 100 mm of solid brick contributed to the external one. Consequently, the two effective thermal masses were respectively in the range of $[107500, 180100]\,Jm^{-2}K^{-1}$ and $[100800, 191600]\,Jm^{-2}K^{-1}$.

5.1.3 *Cavity wall in an occupied house (CLWall)*

The ranges of tabulated thermal conductivity for the materials constituting the CLWall (described in Section 4.1.2.3) are summarised in Table 5.5 on page 149. The thermophysical properties of the urea formaldehyde foam were taken from Kalthod and Knickle (1982), while the CIBSE (2007) guide was used for all other materials. Assuming that the cavity is fully filled, the calculated U-value is expected to be in the range $[0.32, 0.40]\,Wm^{-2}K^{-1}$. The observed shrinkage of the insulation layer and the consequent potential air movement within the resulting air gaps (Section 4.1.2.3) are likely to increase the U-value range. However, it was not possible to quantify this contribution

Material	d [mm]	λ_{min} [mKW^{-1}]	λ_{max} [mKW^{-1}]
Plaster	10	0.22	0.81
Aerated concrete block	100	0.15	0.24
Urea formaldehyde foam	65	0.031	0.035
Outer leaf brick work	100	0.50	1.31

Table 5.5: Minimum and maximum tabulated thermal conductivity ($\lambda_{min}, \lambda_{max}$) for the materials (Kalthod and Knickle, 1982; CIBSE, 2007) constituting the OWall, and the thickness (d) of each layer.

Material	ρ_{min} [kgm^{-3}]	ρ_{max} [kgm^{-3}]	c_{min} [$Jkg^{-1}K^{-1}$]	c_{max} [$Jkg^{-1}K^{-1}$]
Plaster	720	1680	840	1340
Aerated concrete block	500	750	1000	1000
Outer leaf brick work	1200	2080	800	1000

Table 5.6: Minimum and maximum tabulated density (ρ_{min}, ρ_{max}) and specific heat capacity (c_{min}, c_{max}) values (Kalthod and Knickle, 1982; CIBSE, 2007) for the materials contributing to the internal and external effective thermal mass of the CLWall.

due to the lack of information, for example on the uniformity of the shrinkage of the material within the whole cavity, the size and the potential interconnection of the air pockets, and the air speed within them.

The internal and external effective thermal mass were calculated using an effective thickness of 100 mm for both sides (Section 4.2.2.2). Specifically, the plaster (10 mm) and part of the aerated concrete blocks (90 mm) contributed to the internal effective thermal mass, while the outer leaf brick work (100 mm) contributed to the external one. The ranges of density and specific heat capacity of these materials are summarised in Table 5.6 on page 149. The calculated internal effective thermal mass ranged in $[51048, 90012]\,Jm^{-2}K^{-1}$ and the external one in $[96000, 208000]\,Jm^{-2}K^{-1}$.

5.1.4 *Cavity wall in an unoccupied house (HSWall)*

The calculated U-value of the north-facing wall in the unoccupied house (HSWall_N) was the same as that of the CLWall ($[0.32, 0.40]\,Wm^{-2}K^{-1}$), as the two constructions were assumed to be identical from visual inspection (Section 4.1.2.4). Since the thickness of the cavity on the east-facing wall (HSWall_E) is slightly thicker, the U-value on this side is expected to be in $[0.29, 0.36]\,Wm^{-2}K^{-1}$. The internal and external effective thermal masses are also expected to coincide with those of the CLWall for both walls (respectively, $[51048, 90012]\,Jm^{-2}K^{-1}$ and $[96000, 208000]\,Jm^{-2}K^{-1}$) as the characteristics of the most internal and most external layers contributing to the effective thickness and

their proportions have been assumed to be identical, based on physical inspection and construction type.

5.2 TESTING THE MODELS FOR LOWER AVERAGE TEMPERATURE DIFFERENCE

This section investigates the performance of the dynamic grey-box method proposed on four case studies, one solid wall housed in a thermal chamber and three north-facing *in-situ* walls (one solid and two cavity). The case studies were selected ensuring a comparable average temperature difference to the thermal chamber settings (*i.e.* 4.8 °C). The length of the time series analysed was determined according to the first scenario described in Section 4.4. Specifically, the criteria in the BS ISO 9869-1 (2014) Standard were imposed to determine the number of full days required by the AM to stabilise[6] and the time series obtained were also used to evaluate the thermophysical properties of the walls by means of the proposed dynamic method.

The estimates obtained from the average and dynamic method were compared to the thermophysical properties calculated from look up tables (Section 5.1). The dynamic method was tested using both the single thermal mass (1TM) (with either the internal (1 HF) or both (2 HF) heat flux measurements) and the two thermal mass (2TM) models (Section 3.3). Both the MAP and the MCMC approaches (Section 3.4.3 and Section 4.3.1) were used to estimate the parameters of the models and the associated statistical and systematic errors (Section 4.5). The performance of the proposed models is compared and validated in Section 5.4, followed by a general discussion of the results.

For the dynamic and average method the total R-value (and U-value) was computed by adding the constant indoor and external air film resistances (Section 5.1, BS EN ISO 6946 (2007)) to the R-value estimates from the measurements (for the dynamic method, the R-value is the the sum of the lumped R-values estimates) and removing the thermal resistance(s) of the HFP(s). Since the absolute statistical errors on the U-value were of the order of 10^{-2} at maximum (compared to typical absolute systematic errors one order of magnitude bigger), the total error was dominated by the systematic error. Consequently the statistical error is generally omitted when reporting the results, unless stated otherwise.

6 As defined in Section 4.4, the concept of "stabilisation" is used to indicate the condition where after a minimum number of observations the addition of new data does not enhance the prediction of the parameters anymore and the values stabilise around a final value.

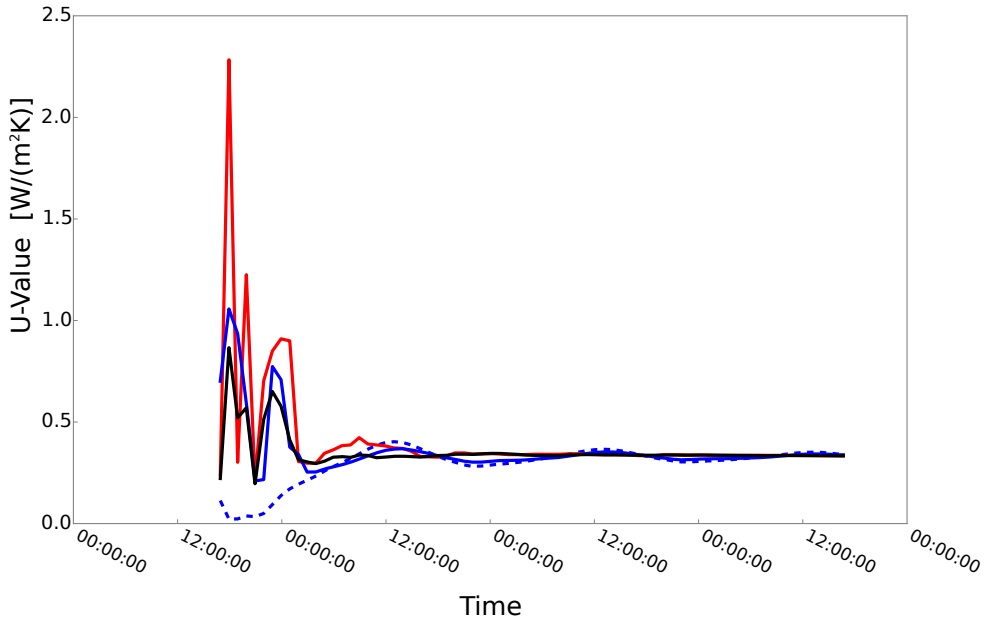

Figure 5.1: Evolution of the U-value for the TCWall for the three-day period required by the BS ISO 9869-1 (2014) Standard to stabilise. The AM (dashed blue line), the 1TM (1 HF) model (solid red line), the 1TM (2 HF) model (solid blue line) and the 2TM model (black solid line) are shown. The MAP approach and uniform priors were used for the dynamic method.

5.2.1 *Solid wall in the thermal chamber (TCWall)*

For the TCWall case study (described in Section 4.1.2.1), the AM stabilised within the criteria listed in the BS ISO 9869-1 (2014) standard (Section 2.3.1) in three full-days of data (dataset available online (Marincioni and Altamirano, 2016)). The U-value estimated using the AM was $(0.34 \pm 0.05)\,\mathrm{Wm^{-2}K^{-1}}$. As illustrated in the next sections, this value was in close agreement with literature calculation and the estimates from the dynamic method.

5.2.1.1 *Maximum a posteriori estimates using uniform priors on the parameters of the models*

The evolution of the U-value over the monitoring period (Figure 5.1 on page 151), estimated using the MAP approach and uniform priors on the parameters of the models, shows that the time series selected was also sufficient for the dynamic method to stabilise. Specifically, the evolution of the U-value obtained using the 1TM (1 HF) and the 2TM models were in close agreement and asymptotically stabilised to the same value after one day of observations. The 1TM (2 HF) presented daily oscillations similar to those of the AM method, although attenuated. All four approaches were in close agreement at the end of the three-day period.

Parameters	Literature	AM	1TM (1 HF)	1TM (2 HF)	2TM	Units
R_1			0.268±0.003	2.555±0.012	0.308±0.004	m^2KW^{-1}
R_2			2.563±0.016	0.254±0.001	2.276±0.018	m^2KW^{-1}
R_3					0.248±0.001	m^2KW^{-1}
C_1	$4.8{\cdot}10^4$		$(7.31{\pm}0.09){\cdot}10^4$	$(13.76{\pm}0.30){\cdot}10^4$	$(4.79{\pm}0.06){\cdot}10^4$	$Jm^{-2}K^{-1}$
C_2	$11.9{\cdot}10^4$				$(11.63{\pm}0.09){\cdot}10^4$	$Jm^{-2}K^{-1}$
$T^0_{C_1}$			18.86±0.02	14.92±0.03	18.86±0.02	°C
$T^0_{C_2}$					14.97±0.03	°C
R-value	2.72	2.79	2.832±0.015	2.809±0.012	2.832±0.016	m^2KW^{-1}
U-value	0.35	0.34	0.333±0.002	0.337± 0.002	0.335±0.002	$Wm^{-2}K^{-1}$

Table 5.7: Thermophysical properties of the TCWall, calculated from the literature and estimated from *in-situ* measurements (both using the AM and the dynamic method). The dynamic estimates for the 1TM (1 HF), 1TM (2 HF) and 2TM models were obtained using the MAP approach and uniform priors on the parameters of the model. Only the statistical error is shown, and the number of significant figures was chosen to illustrate the level of the error.

A summary of the thermophysical estimates of the wall and their associated statistical error is reported in Table 5.7 on page 152[7], while Figure 5.2 on page 153 summarises the same information providing a visualisation of the thermal structure of the wall under study. The U-values calculated from the manufacturer's specifications and the estimates returned by the AM and dynamic method were all in close agreement and within the margin of error (Table 5.7 on page 152). Specifically, the U-value and the associated systematic error was (0.34 ± 0.05) $Wm^{-2}K^{-1}$ for the AM, (0.33 ± 0.04) $Wm^{-2}K^{-1}$ for the 1TM (1 HF) model, and (0.34 ± 0.03) $Wm^{-2}K^{-1}$ for the 1TM (2 HF) and the 2TM model. The internal and external effective thermal mass calculated from tabulated values ($C_{in} = 4.8 \cdot 10^4\,Jm^{-2}K^{-1}$; $C_{ext} = 11.9 \cdot 10^4\,Jm^{-2}K^{-1}$) and the those estimated by the 2TM model ($C_1 = (4.79 \pm 0.06) \cdot 10^4\,Jm^{-2}K^{-1}$; $C_2 = (11.63 \pm 0.09) \cdot 10^4\,Jm^{-2}K^{-1}$) were also in close agreement (Table 5.7 on page 152). As noted previously (Biddulph et al., 2014; Naveros et al., 2014; Deconinck and Roels, 2017), the effective thermal mass estimates of the lumped-thermal-mass models do not capture the total thermal mass of the wall but rather the apparent thermal mass coupled with the ambient or the thermal zone where the measurements are located (as also suggested by the EN ISO 13786 (2008) standard). This is shown in Figure 5.2 on page 153, where the location (in thermal resistance space) of the effective thermal mass(es) varies with the location of the heat flux measurement. Specifically, the 1TM (2 HF) and 2TM models identified the dominant thermal mass to be a relatively small thermal resistance from the external surface, while the 1TM (1 HF) model positioned the effective thermal mass close to the interior

7 When showing literature values in tables, the C_1 entry is used to report the effective thermal mass associated to the interior ambient and C_2 for the exterior one.

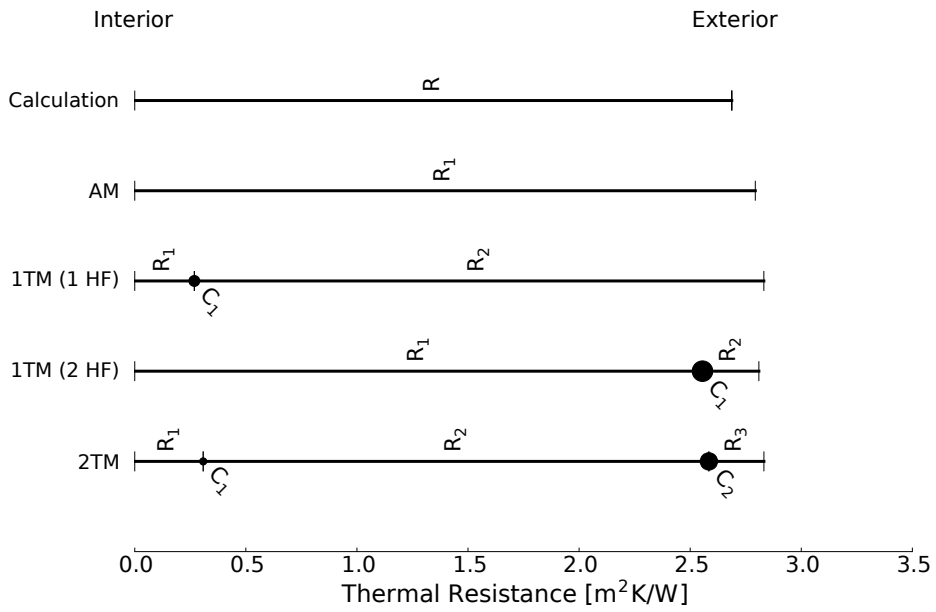

Figure 5.2: Summary of the R-value and size of the effective thermal mass(es) for the TCWall, as calculated from tabulated values and estimated form *in-situ* measurements (using the AM and the 1TM (1 HF), 1TM (2 HF) and 2TM models). The dynamic estimates were obtained using the MAP approach and uniform priors on the parameters of the model. The thermal resistance(s) are proportional to the length of the segments, while the magnitude of the thermal mass(es) is proportional to the radius of the solid circles.

surface. The 2TM model showed a small effective thermal mass close to the interior surface (in thermal resistance space), separated from the other effective thermal mass by a large thermal resistance. This reflects the known structure of the wall (Section 4.1.2.1), where 100 mm of woodfibre insulation (lower thermal mass than the other materials) was placed between the aerated clay blocks and the gypsum fibreboard (thin layer of high specific thermal mass material) (Gori et al., 2017). Interestingly, the 2TM model located the internal and external effective thermal masses almost in the same position (in thermal resistance space) of the effective thermal mass respectively estimated by the 1TM (1 HF) model (where only the internal heat flux measurement was used) and that estimated by the 1TM (2 HF) model (where both internal and external heat flux measurements were used).

Figure 5.3 on page 154 shows the measured and estimated heat flux data streams using the family of dynamic models devised, as recommended in Madsen et al. (2016) (Section 3.5). When only the internal heat flux measurements were used to fit the 1TM model (top panel in the figure), a reasonable match was observed between the predicted and measured interior heat flux but a poor fit was shown when predicting the heat transferring through the exterior surface of the wall. The prediction of the external heat flux is improved when fitting the 1TM model using both heat flux data streams

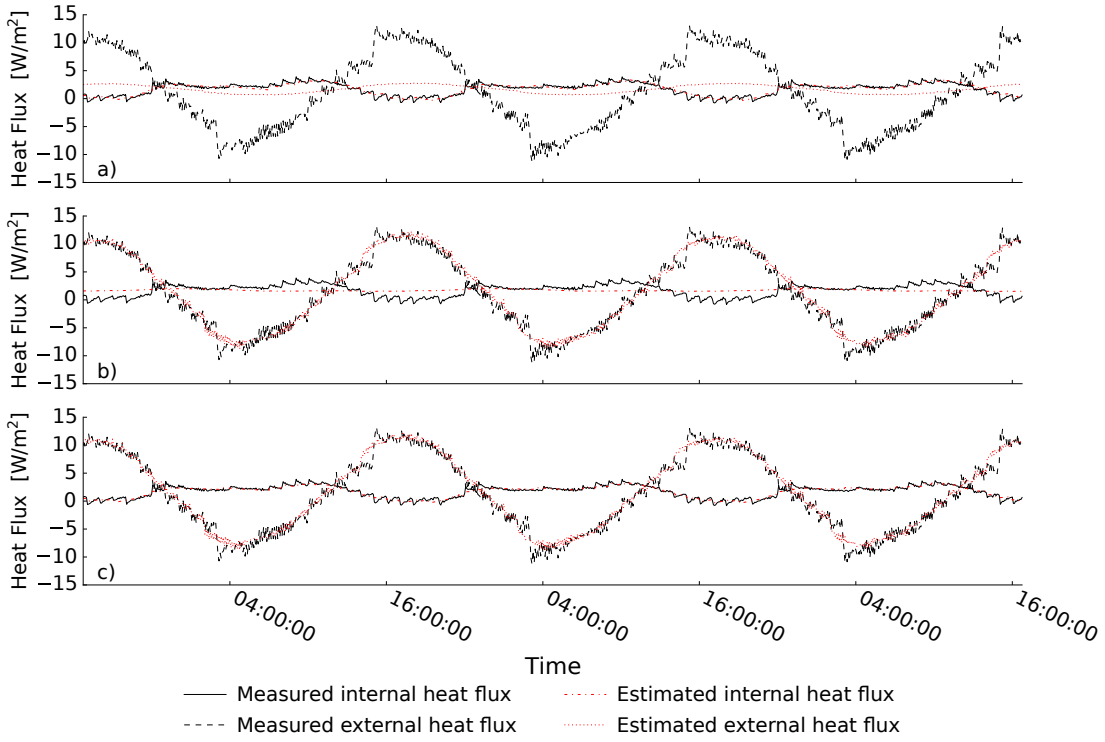

Figure 5.3: Measured and estimated heat flows through the TCWall by: (a) the 1TM (1 HF) model, (b) the 1TM (2 HF) model, and (c) the 2TM model.

(middle panel), to the detriment of the fit to the internal heat flux. Conversely, the use of the internal and external heat flux observations in combination with the 2TM model (bottom panel) showed a very good match of the measured and estimated heat fluxes at both surfaces of the wall, suggesting that the 2TM model may be best at describing the underlying physical process both at the internal and external surfaces. Model selection and validation is further investigated in Section 5.4.

5.2.1.2 *Markov Chain Monte Carlo estimates using uniform priors on the parameters of the models*

The MCMC approach using uniform priors on the parameters of the model was performed to compare the performance of the dynamic method with different optimisers and to investigate the possibility of gaining useful information from the distribution of the thermophysical parameters of the model. A summary of the thermophysical estimates[8] obtained is shown in Table 5.8 on page 155. For each lumped-thermal-mass model, the thermophysical parameters and the associated uncertainties (Table 5.8 on page 155) were almost identical to those estimated by the MAP approach (Table 5.7 on page 152), showing that the same parameter estimates (within the statistical error) were obtained regardless of the optimisation approach. Similarly, the U-values were

8 As introduced in Section 4.3.1.2, the thermophysical estimates shown for comparison with the MAP approach were calculated as the mean of the distributions obtained using the MCMC approach.

Parameters	1TM (1 HF)	1TM (2 HF)	2TM	Units
R_1	0.268±0.004	2.559±0.017	0.307±0.005	m^2KW^{-1}
R_2	2.567±0.018	0.255±0.002	2.290±0.025	m^2KW^{-1}
R_3			0.248±0.001	m^2KW^{-1}
C_1	$(7.31\pm0.09)\cdot10^4$	$(1.38\pm0.03)\cdot10^5$	$(4.78\pm0.07)\cdot10^4$	$Jm^{-2}K^{-1}$
C_2			$(11.64\pm0.10)\cdot10^4$	$Jm^{-2}K^{-1}$
$T^0_{C_1}$	18.85±0.02	14.93±0.04	18.86±0.02	°C
$T^0_{C_2}$			14.97±0.03	°C
U-value	0.333±0.002	0.336±0.002	0.333±0.003	$Wm^{-2}K^{-1}$

Table 5.8: Thermophysical properties of the TCWall for the dynamic method (1TM (1 HF), 1TM (2 HF) and 2TM models) using the MCMC approach and uniform priors on the parameters of the model. Only the statistical error is shown, and the number of significant figures was chosen to illustrate the level of the error.

also within the systematic error of the MAP estimates. Specifically, the U-values estimated by the MCMC approach were (0.33 ± 0.04) $Wm^{-2}K^{-1}$ for the 1TM (1 HF) model, (0.34 ± 0.04) $Wm^{-2}K^{-1}$ for the 1TM (2 HF) model, and (0.33 ± 0.03) $Wm^{-2}K^{-1}$ for the 2TM model.

The distribution of the parameters of the model is shown in the corner plots in Figure 5.4 on page 156. The graphs do not present strong correlation among the lumped thermal resistances. The result seems to support the insights gained from Figure 5.2 on page 153, showing that the effective thermal masses appeared to be associated with the materials with higher thermal capacity and providing useful information about the thermal structure of the wall.

5.2.2 *Solid wall in an office building (OWall)*

For the OWall case study (described in Section 4.1.2.2), the AM stabilised within the criteria listed in the BS ISO 9869-1 (2014) Standard (Section 2.3.1) in three full-days of data (between the 5th and the 8th of October 2014, starting at 16:30; dataset available online (Gori and Elwell, 2016)). The average of the temperature differences at each time interval was 5.1 °C and the heat was consistently leaving the indoor space (*i.e.* the indoor ambient was always warmer than the exterior over the monitored period). Uniform and log-normal priors (both on the parameters of the model and the U-value) were adopted to estimate the thermophysical properties of the OWall using both the MAP and the MCMC approaches.

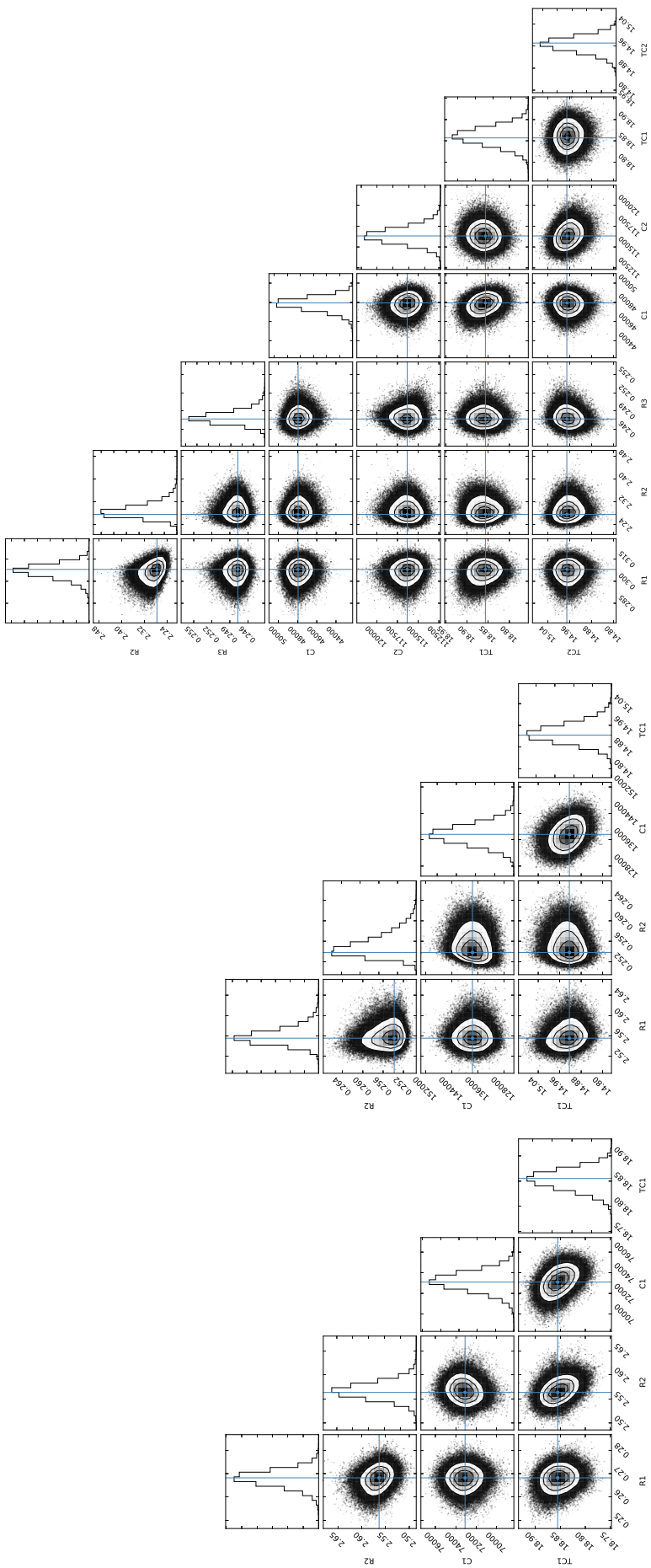

Figure 5.4: Distribution of the thermophysical properties of the TCWall estimated using the MCMC approach and uniform priors on the parameters of the model. The turquoise crossed lines indicate the MAP estimation used as starting point for the MCMC walk. From the left, the corner plots show the parameter distribution estimated using the 1TM (1 HF), the 1TM (2 HF) and the 2TM models.

The U-value calculated with the AM was $1.89 \pm 0.36\,\mathrm{Wm^{-2}K^{-1}}$. As shown in the next sections, this value is in line with literature calculation (detailed in Section 5.1.2) and within the margin of error of the estimates obtained from the dynamic method.

5.2.2.1 *Maximum a posteriori estimates*

UNIFORM PRIOR DISTRIBUTIONS ON THE PARAMETERS OF THE MODELS Similarly to the TCWall case study (Section 5.2.1.1), the evolution of the U-value for the OWall was estimated using the AM and the MAP approach with uniform priors on the parameters of the model (Figure 5.5 on page 158). The 1TM (1 HF) and the 2TM models had similar behaviour and stabilised within the final value in one and a half days, and their U-value estimates coincided at the end of the monitoring period. Conversely, the final U-value for the AM and 1TM (2 HF) model was slightly higher but still within the margin of the systematic error of the estimates obtained with the other two models.

While the estimates obtained with the 1TM (1 HF) and 2TM models stabilised after the first 36 hours, those of the AM and the 1TM (2 HF) model still presented some residual fluctuations. The sinusoidal behaviour shown in the AM is due to the diurnal patterns in the environmental conditions the element is exposed to, and the fact that the method is not able to model them. Specifically, periods shorter than 24 hours violate the assumption of comparable heat storage at the beginning and the end of the monitoring period, as they do not account for the full daily cycle. To avoid this effect the BS ISO 9869-1 (2014) Standard recommends analysing an integer number of days.

The MAP U-value estimates obtained using uniform priors were $(1.72 \pm 0.27)\,\mathrm{Wm^{-2}K^{-1}}$ for the 1TM (1 HF), $(1.82 \pm 0.29)\,\mathrm{Wm^{-2}K^{-1}}$ for the 1TM (2 HF), and $(1.72 \pm 0.26)\,\mathrm{Wm^{-2}K^{-1}}$ for the 2TM model (Table 5.9 on page 158). A summary of the thermophysical parameters and their statistical error is reported in Table 5.9 on page 158. The R-values and U-value estimates from the dynamic and the average method fall within the ranges calculated from the literature, while the internal and external effective thermal mass estimates obtained from the 2TM model were comparable with those obtained from look up tables (Table 5.9 on page 158).

The thermal structure of the wall is visualised in Figure 5.6 on page 159. The position and magnitude of the effective thermal mass(es) varied depending on the model used. The 1TM (1 HF) and 1TM (2 HF) models estimated an effective thermal mass of similar magnitude (unlike the TCWall) but located at a different position in thermal resistance space depending on the data stream used for the fitting, as also observed in Gori et al. (2017). However, unlike the TCWall case study (Figure 5.2 on page 153), the position (in thermal resistance space) of the internal and external effective thermal masses estimated

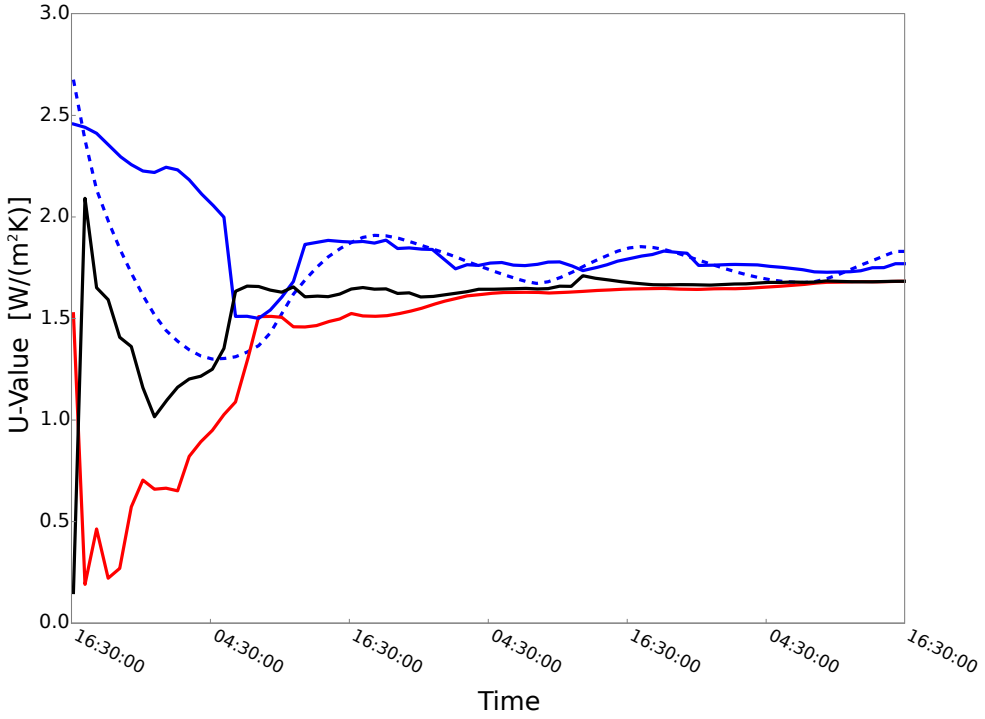

Figure 5.5: Evolution of the U-value for the OWall for the three-day period required by the BS ISO 9869-1 (2014) Standard to stabilise. The AM (dashed blue line), the 1TM (1 HF) model (solid red line), the 1TM (2 HF) model (solid blue line) and the 2TM model (black solid line) are shown. The MAP approach and uniform priors were used for the dynamic method.

Parameters	Literature	AM	1TM (1 HF)	1TM (2 HF)	2TM	Units
R_1			0.068±0.001	0.267±0.003	0.075±0.001	m^2KW^{-1}
R_2			0.356±0.002	0.125±0.001	0.285±0.003	m^2KW^{-1}
R_3					0.065±0.002	m^2KW^{-1}
C_1	$[1.08, 1.80]\cdot10^5$		$(2.24\pm0.02)\cdot10^5$	$(2.50\pm0.06)\cdot10^5$	$(2.17\pm0.02)\cdot10^5$	$Jm^{-2}K^{-1}$
C_2	$[1.01, 1.92]\cdot10^5$				$(0.98\pm0.02)\cdot10^5$	$Jm^{-2}K^{-1}$
$T^0_{C_1}$			16.20±0.03	15.22±0.06	16.07±0.03	°C
$T^0_{C_2}$					15.18±0.05	°C
R-value	[0.29, 0.73]	0.37	0.423±0.002	0.392±0.003	0.424±0.002	m^2KW^{-1}
U-value	[1.11, 2.16]	1.89	1.721±0.009	1.821±0.018	1.720±0.012	$Wm^{-2}K^{-1}$

Table 5.9: Thermophysical properties of the OWall calculated from the literature and estimated from *in-situ* measurements (both using the AM and dynamic method). The dynamic estimates for the 1TM (1 HF), 1TM (2 HF) and 2TM models were obtained using the MAP approach and uniform priors on the parameters of the model. Only the statistical error is shown, and the number of significant figures was chosen to illustrate the level of the error.

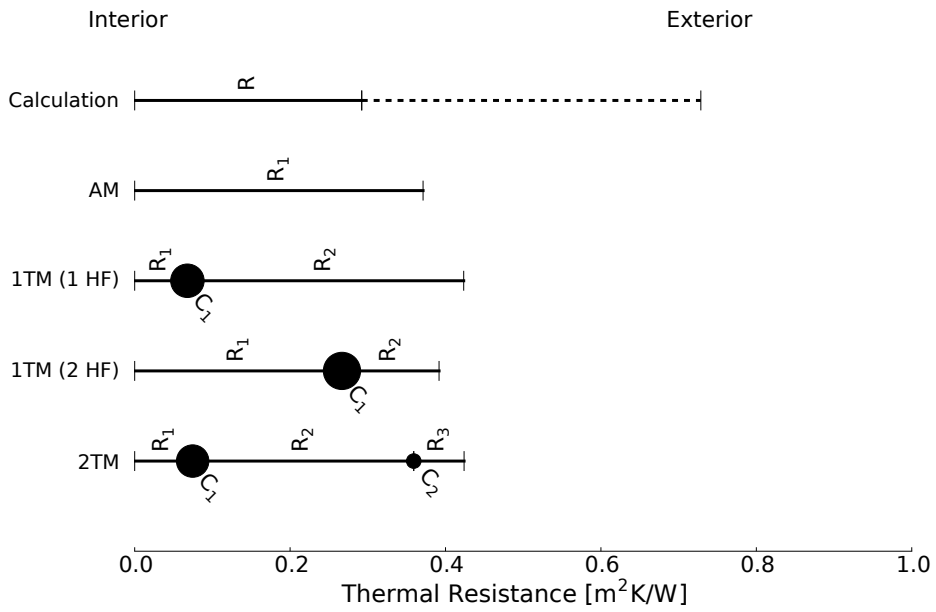

Figure 5.6: Summary of the R-value and size of the effective thermal mass(es) for the OWall, as calculated from tabulated values and estimated form *in-situ* measurements (using the AM and the 1TM (1 HF), 1TM (2 HF) and 2TM models). The dynamic estimates were obtained using the MAP approach and uniform priors on the parameters of the model. The thermal resistance(s) are proportional to the length of the segments, while the magnitude of the thermal mass(es) is proportional to the radius of the solid circles. The dashed line indicates the range of R-values calculated from the literature.

by the 2TM model did not mirror the positions that each thermal mass had when using the 1TM models. Specifically, for the 2TM model one effective thermal mass was located closer to the external surface than for the 1TM (2 HF) model, whilst the dominant effective thermal mass was the internal one. This behaviour may be explained by the structure of the wall. Unlike the TCWall, where the layers constituting the wall had distinct thermophysical properties (Section 5.1.1), the materials constituting the OWall (*i.e.* brick and plaster) have similar properties (Section 5.1.2) and therefore the position of the effective thermal mass may not be well defined due to the weak physical constraints. Similarly to the TCWall case study, additional insights into the thermal structure of the wall can be gained from the MCMC analysis as discussed below.

Figure 5.7 on page 160 shows the measured and estimated heat flux time series. Similarly to the TCWall case study, the estimates by 1TM (1 HF) model (top panel) reasonably matched the interior observations but not the exterior ones while the 1TM (2 HF) improved the exterior estimates to the detriment of the internal ones (middle panel). The use of both internal and external heat flux observations and a 2TM model showed a good match between the measured and estimated heat fluxes at both surfaces of the wall. This result suggests a satisfactory performance of the dynamic method and spe-

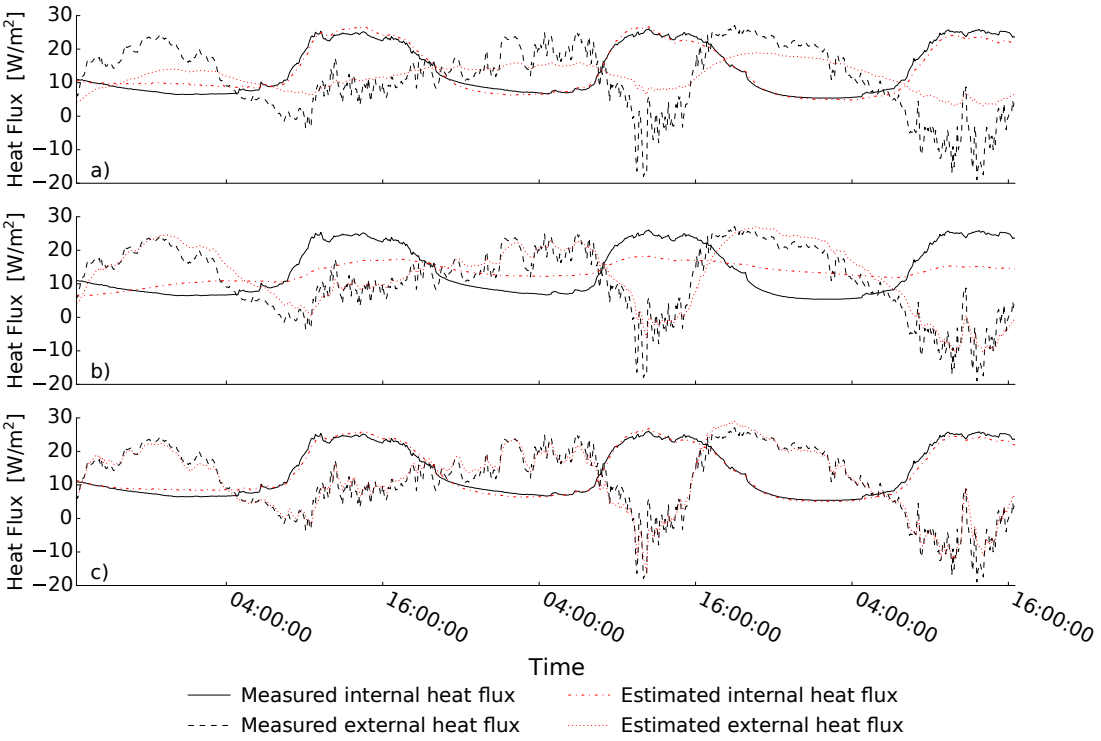

Figure 5.7: Measured and estimated heat flows through the OWall by: (a) the 1TM (1 HF) model, (b) the 1TM (2 HF) model, and (c) the 2TM model.

cifically of the 2TM model with *in-situ* observations, which is further investigated using model selection and cross-validation techniques (Section 5.4).

LOG-NORMAL PRIORS Given the information available about the thermophysical properties of the materials constituting the OWall (Section 4.2.2.2), log-normal distributions on the parameters of the models and on the U-value (described in Section 4.2.2) were used as an alternative to uniform priors to test their impact on the performance of the models. A comparison of the evolution of the U-value for the different models and type of priors is shown in Figure 5.8 on page 161, Table 5.9 on page 162, and Table 5.10 on page 162. For the 1TM (1 HF) and the 2TM models, the introduction of non-uniform priors on the parameters of the model improved the estimations during the initial phase of the analysis, where few observations were available. Subsequently, the estimates stabilised to the same value and the U-value estimates coincided at the end of the monitoring period. Conversely, no major improvement was observed for the 1TM (2 HF) model. It is worth noticing that, as introduced in Section 4.2.2.3, the prior available may have been defined from data collected on walls thinner than the OWall, limiting its expected accuracy. However, the graphs show that the data were sufficient to cope with the potential inaccuracy of the prior, leading to estimates comparable with those obtained from uniform and log-normal priors on the parameters of the model and

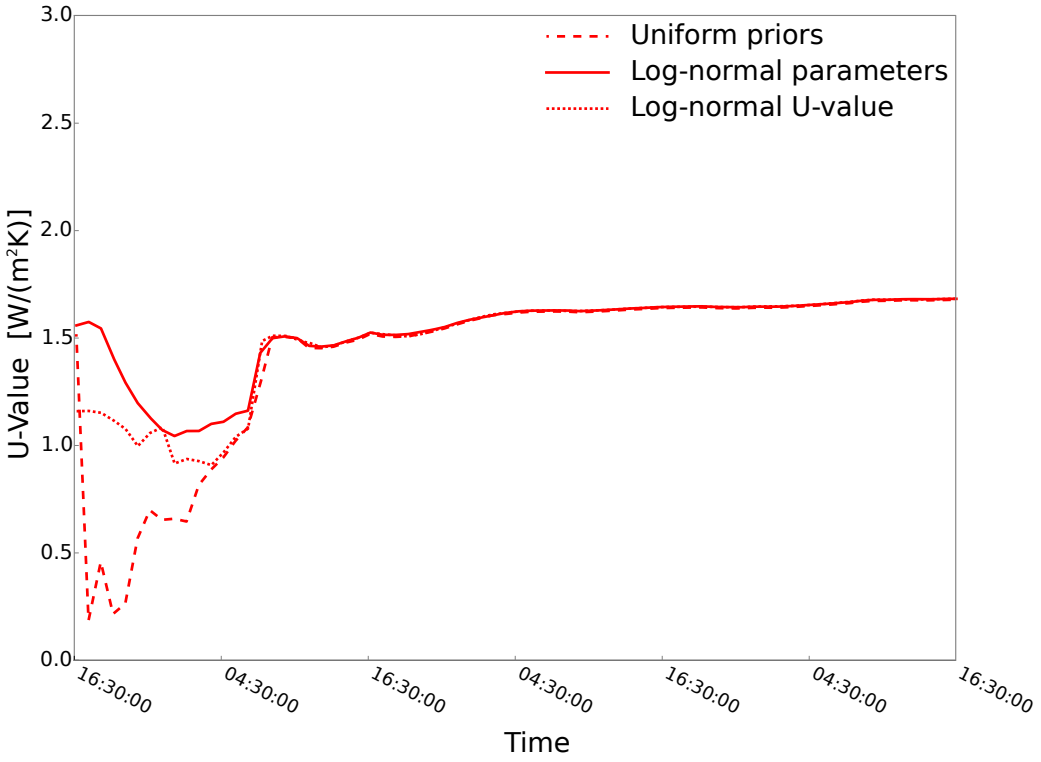

Figure 5.8: Comparison of the evolution of the U-value for the OWall using the 1TM (1 HF) model. Uniform (dashed line) and log-normal priors on the parameters of the model (solid line), and log-normal priors on the U-value (dotted line) were used with the MAP approach.

indicating that the method is robust to such issues. The thermal structure of the wall and the estimation of the heat flux over the monitoring period are not reported in the interest of conciseness as these presented the same behaviour shown in Figure 5.6 on page 159 and Figure 5.7 on page 160 using uniform priors.

At the end of the monitoring period, the U-value was $(1.72 \pm 0.27)\,\mathrm{Wm^{-2}K^{-1}}$ for the 1TM (1 HF), $(1.82 \pm 0.29)\,\mathrm{Wm^{-2}K^{-1}}$ for the 1TM (2 HF), and $(1.72 \pm 0.24)\,\mathrm{Wm^{-2}K^{-1}}$ for the 2TM model. The values obtained also coincided with those estimated using uniform priors (Section 5.2.2.1, Table 5.9 on page 158), and were consequently within the margin of the systematic error of the AM and the range of calculated values from the literature. The estimates of the thermophysical parameters of the models are summarised in Table 5.10 on page 163.

5.2.2.2 *Markov Chain Monte Carlo estimates*

Similarly to the TCWall case study, the analysis performed using the MAP approach was repeated with the MCMC framework. As observed previously, the U-value estimates obtained using the MCMC approach with all types of prior distributions (*i.e.* uniform and log-normal on the parameters of the model, and log-normal on the U-value) were

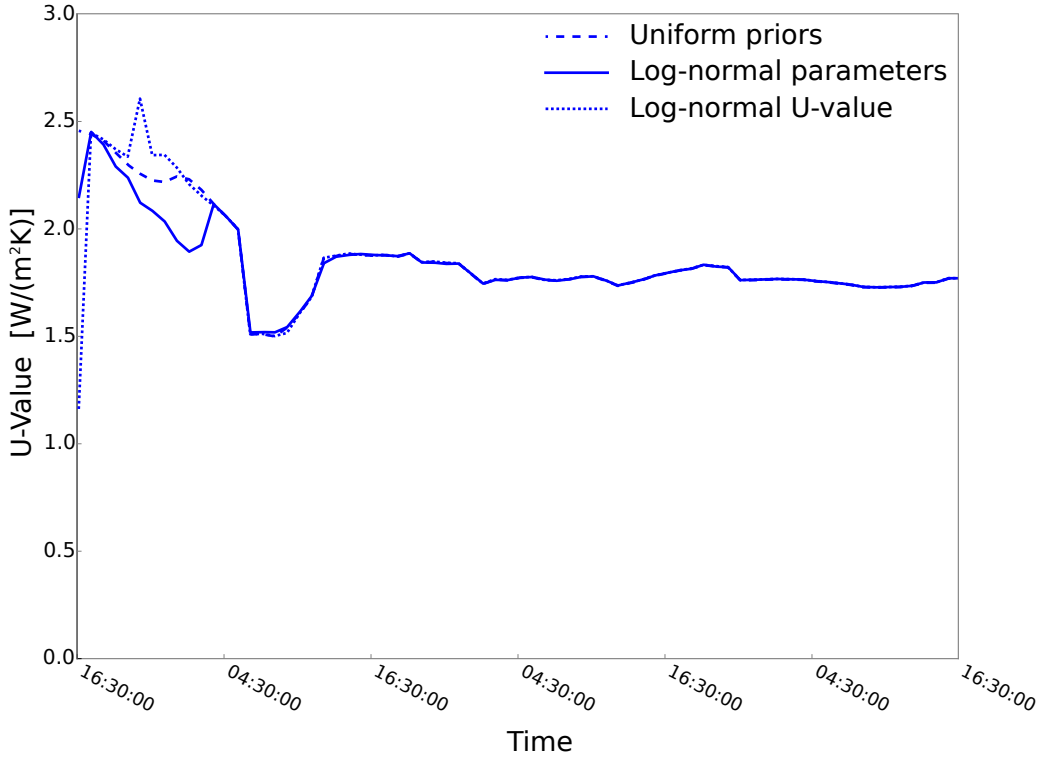

Figure 5.9: Comparison of the evolution of the U-value for the OWall using the 1TM (2 HF) model. Uniform (dashed line) and log-normal priors on the parameters of the model (solid line), and log-normal priors on the U-value (dotted line) were used with the MAP approach.

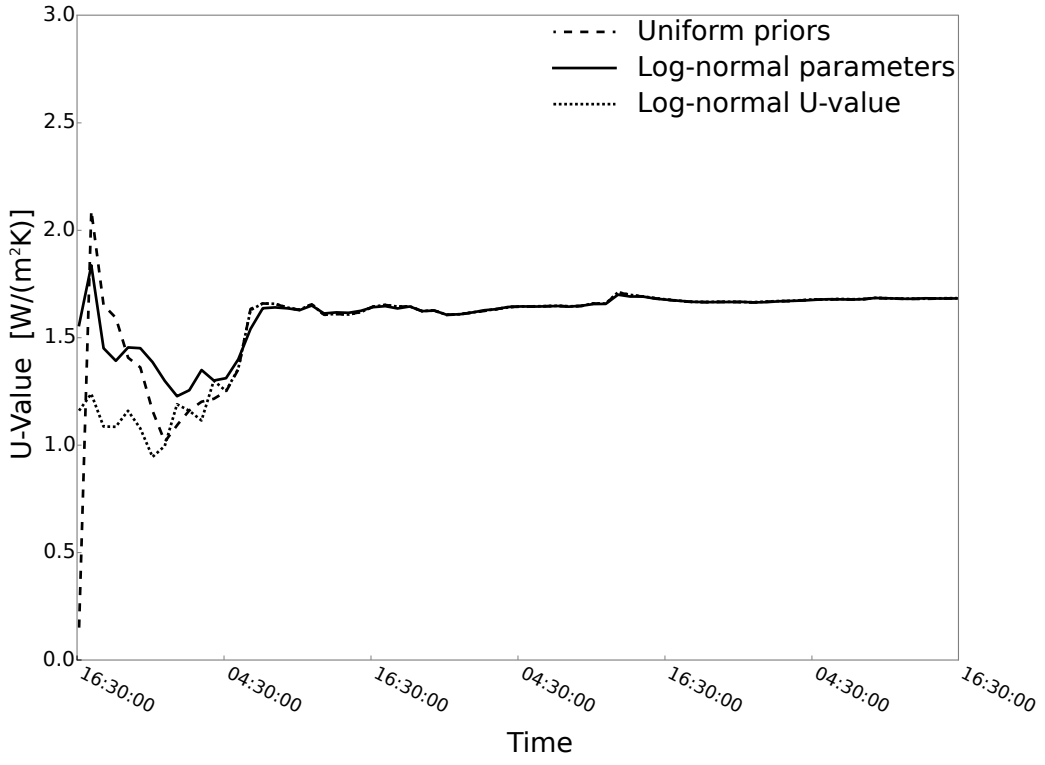

Figure 5.10: Comparison of the evolution of the U-value for the OWall using the 2TM model. Uniform (dashed line) and log-normal priors on the parameters of the model (solid line), and log-normal priors on the U-value (dotted line) were used with the MAP approach.

Parameters	1TM (1 HF) LN P	1TM (1 HF) LN U	1TM (2 HF) LN P	1TM (2 HF) LN U	2TM LN P	2TM LN U	Units
R_1	0.068±0.001	0.068±0.001	0.267±0.003	0.267±0.003	0.075±0.001	0.075±0.001	m^2KW^{-1}
R_2	0.356±0.002	0.356±0.002	0.125±0.001	0.125±0.001	0.284±0.003	0.285±0.003	m^2KW^{-1}
R_3					0.066±0.002	0.065±0.002	m^2KW^{-1}
C_1	$(2.24\pm0.02)\cdot10^5$	$(2.24\pm0.02)\cdot10^5$	$(2.48\pm0.06)\cdot10^5$	$(2.50\pm0.06)\cdot10^5$	$(2.17\pm0.02)\cdot10^5$	$(2.17\pm0.02)\cdot10^5$	$Jm^{-2}K^{-1}$
C_2					$(0.99\pm0.02)\cdot10^5$	$(0.98\pm0.02)\cdot10^5$	$Jm^{-2}K^{-1}$
$T^0_{C_1}$	16.19±0.03	16.19±0.03	15.20±0.06	15.22±0.06	16.07±0.03	16.07±0.03	°C
$T^0_{C_2}$					15.17±0.05	15.18±0.05	°C
U-value	1.721±0.009	1.721±0.009	1.820±0.017	1.821±0.017	1.719±0.012	1.720±0.012	$Wm^{-2}K^{-1}$

Table 5.10: Thermophysical properties of the OWall for the dynamic method (1TM (1 HF), 1TM (2 HF) and 2TM models) using the MAP approach and log-normal priors, both on the parameters of the model (LN P) and the U-value (LN U). Only the statistical error is shown, and the number of significant figures was chosen to illustrate the level of the error.

within the margin of the systematic error of each other and of the corresponding cases using the MAP framework (Section 5.2.2.1). Specifically, the MCMC U-value estimates at the end of the monitoring period were $(1.72 \pm 0.27)\,\mathrm{Wm^{-2}K^{-1}}$ for the 1TM (1 HF), $(1.82 \pm 0.29)\,\mathrm{Wm^{-2}K^{-1}}$ for the 1TM (2 HF), and $(1.72 \pm 0.26)\,\mathrm{Wm^{-2}K^{-1}}$ for the 2TM model regardless of the prior used. Similarly, for each model the MCMC estimates of the thermophysical parameters obtained using log-normal prior distributions on the parameters of the model and the U-value were all within the margin of the statistical error of each other and of the corresponding MAP estimates (Table 5.10 on page 163).

Since the parameter estimates obtained with the different priors coincided at the end of the monitoring period, as expected their posterior distribution did not show significant differences. Consequently, only the corner plots for the uniform prior case is shown (Figure 5.11 on page 165) in the following for conciseness (the parameters' distribution would have shown differences if shorter monitoring periods were analysed, although this is outside the scope of this chapter). As observed previously, the corner plots provide valuable insights into the thermal structure of the element investigated. All models showed a negative relationship among the thermal resistance estimates, as the contours of the posterior probability distribution was rotated in respect to the Cartesian axes (Figure 5.11 on page 165). This behaviour suggests that the total R-value of the wall (and consequently its U-value) was constant but the relative magnitude of the estimates of the individual lumped thermal resistances may vary (*e.g.*, an increase in R_1 tended to be compensated by a decrease in R_2). The result seems to support the findings of Figure 5.6 on page 159 and to reflect the known structure of the OWall, where the similar thermophysical properties of its materials provide weak constraints to model for the positioning of the effective thermal masses in thermal resistance space.

5.2.3 *Cavity wall in an occupied house (CLWall)*

For the CLWall case study (described in Section 4.1.2.3), the AM stabilised within the criteria listed in the BS ISO 9869-1 (2014) Standard (Section 2.3.1) in eleven full-days of data (between the 24$^{\text{th}}$ of May and the 4$^{\text{th}}$ of June 2016, starting at 00:00). During this period, the temperature difference between the inside and outside ambient was 4.7 °C. This was the closest temperature difference to the TCWall case study that could also ensure almost no reversion of the heat flux direction over the monitoring period (the external temperature was higher than the internal one only for few hours in the afternoon on three consecutive days). The U-value estimated by the AM was $(0.55 \pm 0.10)\,\mathrm{Wm^{-2}K^{-1}}$. As discussed below, this value was within the margin of error of the estimates obtained

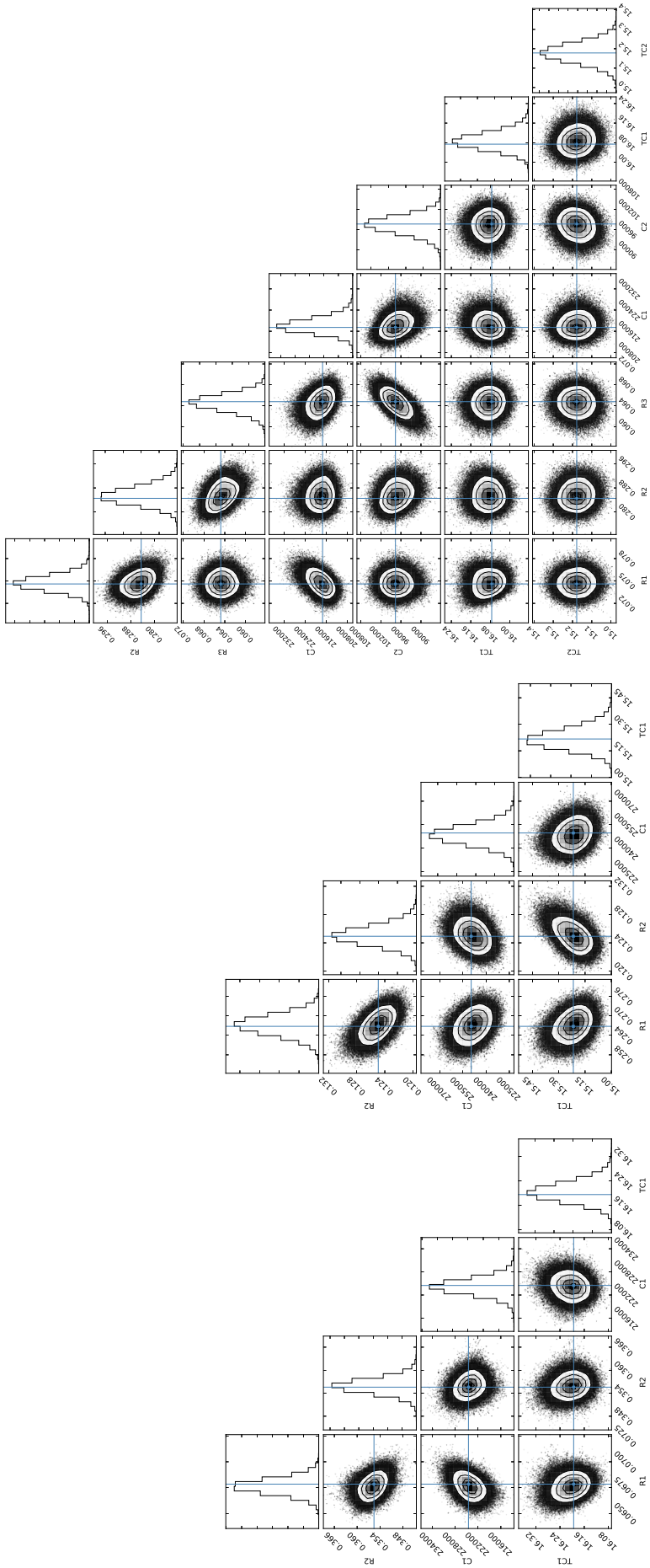

Figure 5.11: Distribution of the thermophysical properties of the OWall estimated using the MCMC approach and uniform priors on the parameters of the model. The turquoise crossed lines indicate the MAP estimation used as starting point for the MCMC walk. From the left, the corner plots show the parameter distribution estimated using the 1TM (1 HF), the 1TM (2 HF) and the 2TM models.

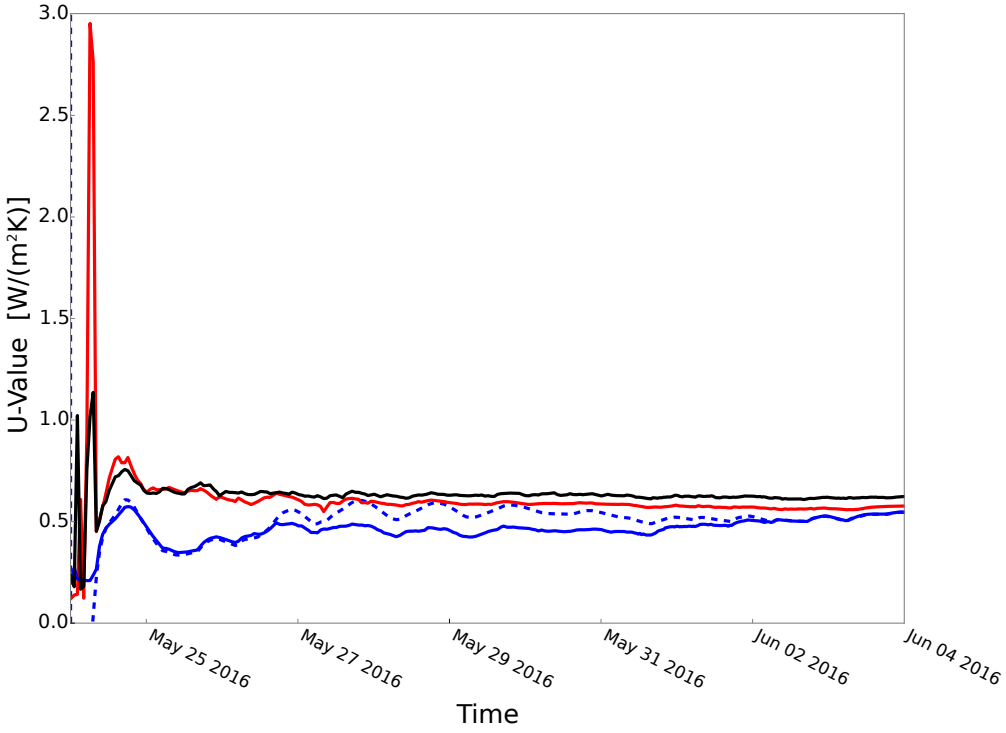

Figure 5.12: Evolution of the U-value for the CLWall for the eleven-day period analysed required by the BS ISO 9869-1 (2014) Standard to stabilise. The AM (dashed blue line), the 1TM (1 HF) model (solid red line), the 1TM (2 HF) model (solid blue line) and the 2TM model (black solid line) are shown. The MAP approach and uniform priors were used for the dynamic method.

from the dynamic method, but higher than the literature calculation (detailed in Section 5.1.3).

5.2.3.1 *Maximum a posteriori estimates using uniform priors on the parameters of the models*

Similarly to the previous case studies, the evolution of the U-value (Figure 5.12 on page 166) was estimated for the CLWall using the AM and the MAP approach with uniform priors on the parameters of the models. Figure 5.12 on page 166 shows that the estimates of the 2TM model had stabilised after approximately four days of data. Additionally, the evolution of the U-value estimated with the 1TM (1 HF) behaved similarly to that estimated by the 2TM model, while the estimates by the 1TM (2 HF) model followed the behaviour of the AM and the two traces overlapped at the end of the monitoring period. The 1TM (1 HF) and 2TM models stabilised to a slightly higher U-value. All estimates were within the margin of systematic error at the end of the monitoring period.

The MAP U-value estimates were $(0.58 \pm 0.08)\,\mathrm{Wm^{-2}K^{-1}}$ for the 1TM (1 HF) model, $(0.55 \pm 0.07)\,\mathrm{Wm^{-2}K^{-1}}$ for the 1TM (2 HF), and $(0.63 \pm 0.07)\,\mathrm{Wm^{-2}K^{-1}}$ for the 2TM (Table 5.11 on page 167). The estimated thermophysical properties, their statistical errors,

Parameters	Literature	AM	1TM (1 HF)	1TM (2 HF)	2TM	Units
R_1			0.078±0.001	1.590±0.005	0.081±0.001	m^2KW^{-1}
R_2			1.487±0.006	0.0716±0.0004	1.289±0.010	m^2KW^{-1}
R_3					0.0663±0.0004	m^2KW^{-1}
C_1	$[5.10, 9.00]\cdot10^4$		$(10.65\pm0.11)\cdot10^4$	$(10.51\pm0.04)\cdot10^4$	$(10.03\pm0.07)\cdot10^4$	$Jm^{-2}K^{-1}$
C_2	$[9.60, 20.8]\cdot10^4$				$(10.26\pm0.05)\cdot10^4$	$Jm^{-2}K^{-1}$
$T^0_{C_1}$			18.82±0.03	13.04±0.04	18.82±0.03	°C
$T^0_{C_2}$					12.79±0.04	°C
R-value	[2.36, 3.01]	1.67	1.565±0.005	1.661±0.005	1.436±0.009	m^2KW^{-1}
U-value	[0.32, 0.40]	0.55	0.578±0.002	0.550±0.002	0.628±0.005	$Wm^{-2}K^{-1}$

Table 5.11: Thermophysical properties of the CLWall calculated from the literature and estimated from *in-situ* measurements (both using the AM and dynamic method). The dynamic estimates for the 1TM (1 HF), 1TM (2 HF) and 2TM models were obtained using the MAP approach and uniform priors on the parameters of the model. Only the statistical error is shown, and the number of significant figures was chosen to illustrate the level of the error.

and the calculated values from the literature are summarised in Table 5.11 on page 167, and visualised in Figure 5.13 on page 168.

In all cases, the U-value estimates from *in-situ* measurements were higher than the range calculated from the literature. This is not an unexpected result given the observed shrinkage of the insulation layer (Section 4.1.2.3), which may have affected the thermal performance of the wall (*e.g.*, allowing air movement within the cavity). The internal and external effective thermal mass estimated with the 2TM model were in good agreement with the values calculated from look up tables. Specifically, the external effective thermal mass was within the literature range, while the internal one was slightly higher.

Figure 5.13 on page 168 provides a visualisation of the thermal structure of the CLWall. Similarly to the TCWall (and unlike the OWall), the position of the thermal mass in thermal resistance space was located close to the wall surface and it was consistent across the different models. Specifically, the distance in thermal resistance space of the internal and external thermal masses estimated by the 2TM model were respectively comparable to the effective thermal mass estimates obtained with the 1TM (1 HF) and the 1TM (2 HF) models. The magnitude of the thermal masses was also comparable in all cases. The visual description in Figure 5.13 on page 168 seems to reflect the known thermal structure of the wall, where two masonry layers (one internal and one external) of similar thermal properties (*i.e.* low thermal resistance and high thermal capacitance) were separated by an insulation layer of high thermal resistance.

The measured and estimated heat flux time series are shown in Figure 5.14 on page 169 to check the ability of the different models to predict the observations. Similarly to the previous case studies, the 2TM model was able to provide a good description of the

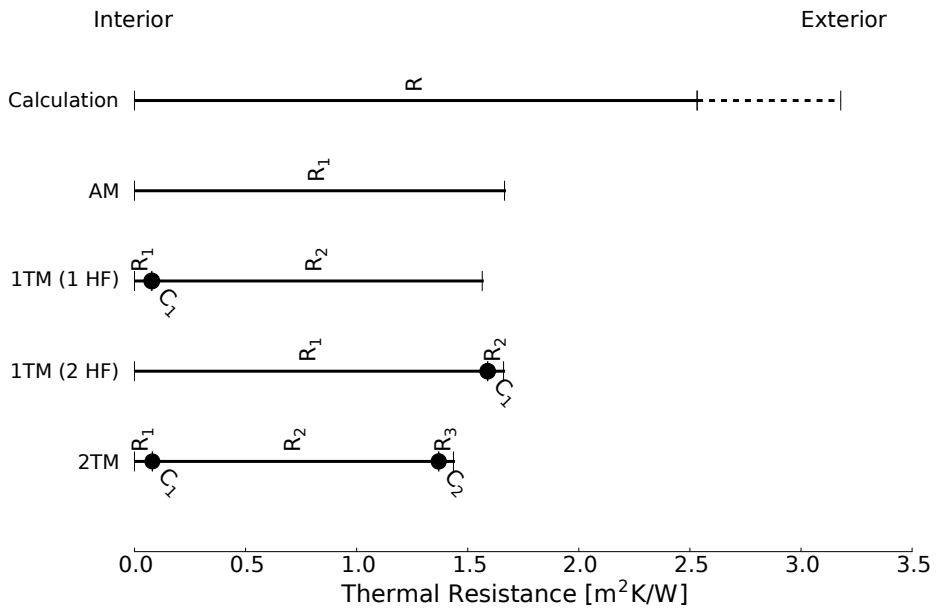

Figure 5.13: Summary of the R-value and size of the effective thermal mass(es) for the CLWall, as calculated from tabulated values and estimated form *in-situ* measurements (using the AM and the 1TM (1 HF), 1TM (2 HF) and 2TM models). The dynamic estimates were obtained using the MAP approach and uniform priors on the parameters of the model. The thermal resistance(s) are proportional to the length of the segments, while the magnitude of the thermal mass(es) is proportional to the radius of the solid circles. The dashed line indicates the range of R-values calculated from the literature.

heat flow both at the interior and exterior surfaces of the wall, while the 1TM models could only provide an accurate description of one of the two time series (*i.e.* the heat flux measured on the internal surface of the wall for the 1TM (1 HF) model and the external heat flux for the 1TM (2 HF) one). This results seems to suggest that the performance of the dynamic method is satisfactory for *in-situ* measurements regardless of the wall structure (further discussion on the validation of the method is provided in Section 5.4).

5.2.3.2 *Markov Chain Monte Carlo estimates using uniform prior distributions*

In line with the results for the TCWall and OWall, the MCMC estimates of the thermophysical parameters (Table 5.12 on page 169) of the CLWall were all within the margin of statistical error with the MAP values (Table 5.11 on page 167). The U-value was $(0.58 \pm 0.08)\,\mathrm{Wm^{-2}K^{-1}}$ for the 1TM (1 HF), $(0.55 \pm 0.07)\,\mathrm{Wm^{-2}K^{-1}}$for the 1TM (2 HF) and $(0.63 \pm 0.07)\,\mathrm{Wm^{-2}K^{-1}}$ for the 2TM model, and coincided with the MAP estimates reported in Section 5.2.3.1.

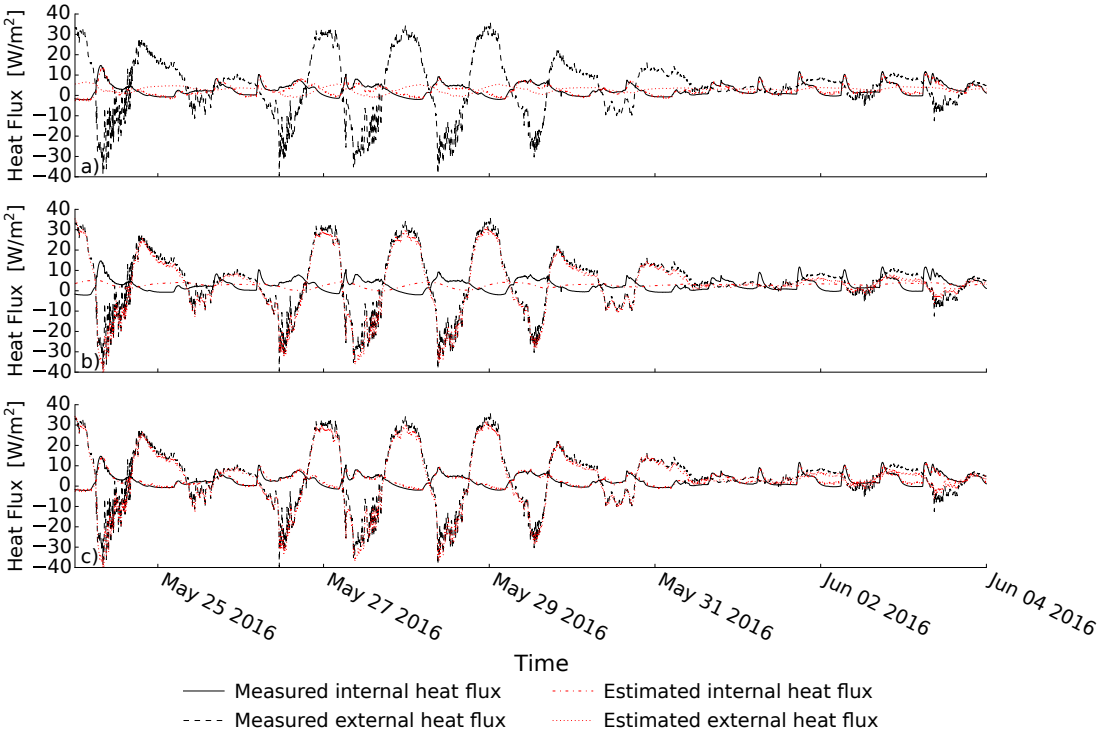

Figure 5.14: Measured and estimated heat flows through the CLWall by: (a) the 1TM (1 HF) model, (b) the 1TM (2 HF) model, and (c) the 2TM model.

Parameters	1TM (1 HF)	1TM (2 HF)	2TM	Units
R_1	0.078±0.001	1.589±0.006	0.081±0.001	m^2KW^{-1}
R_2	1.492±0.009	0.0715±0.0004	1.289±0.010	m^2KW^{-1}
R_3			0.0663±0.0004	m^2KW^{-1}
C_1	(10.62±0.11)·10^4	(10.52±0.05)·10^4	(10.03±0.07)·10^4	$Jm^{-2}K^{-1}$
C_2			(10.24±0.05)·10^4	$Jm^{-2}K^{-1}$
$T^0_{C_1}$	18.83±0.03	13.04±0.04	18.82±0.03	°C
$T^0_{C_2}$			12.78±0.04	°C
U-value	0.578±0.003	0.550±0.002	0.628±0.005	$Wm^{-2}K^{-1}$

Table 5.12: Thermophysical properties of the CLWall for the dynamic method (1TM (1 HF), 1TM (2 HF) and 2TM models) using the MCMC approach and uniform priors on the U-value. The number of significant figures was chosen to illustrate the level of statistical error.

The shape of the posterior distribution of the parameters in the corner plots (Figure 5.15 on page 171) showed no correlation between the individual R-values[9], similarly to the TCWall case study and unlike the OWall. Otherwise stated, the model found the thermal resistances to be independent of each other and so the position of the thermal mass in thermal resistance space. This result can be interpreted in the light of the known physical structure of the wall. Specifically, the distinct thermophysical properties of the materials constituting the cavity wall (*i.e.* a layer of aerated solid brick and a layer of aerated blocks separated by a layer of insulation) helped the model specifying the configuration of the wall in thermal resistance space. This result supports the findings of Figure 5.13 on page 168, where the position of the effective thermal mass(es) in thermal resistance space was observed to be consistent across different models and at comparable distance from the surfaces of the wall.

5.2.4 *North-facing wall in an unoccupied house (HSWall_N)*

For the HSWall_N case study, the AM stabilised within the criteria listed in the BS ISO 9869-1 (2014) Standard (Section 2.3.1) in three full-days of data (between the 7th of May and the 10th of May 2015, starting at 14:00). The average temperature difference between the inside and outside ambient was 5.5 C, which was the closest temperature difference to the TCWall settings also ensuring no heat flux reversion during the monitoring period. The U-value estimated by the AM was $(0.72 \pm 0.11)\,\mathrm{Wm^{-2}K^{-1}}$. Similarly to the CLWall case study, the U-value was within the margin of error of the estimates obtained from the dynamic method, but higher than the literature range.

5.2.4.1 *Maximum a posteriori estimates using uniform prior distributions*

Similarly to the other case studies, the evolution of the U-value (Figure 5.16 on page 172) estimated by the 1TM (1 HF) and the 2TM model quickly stabilised to an asymptotic value (in just above one day), while the 1TM (2 HF) model presented similar sinusoidal behaviour to the AM. The 1TM (1 HF) and 1TM (2 HF) model stabilised almost to the same value at the end of the monitoring period, while the 2TM model and the AM returned slightly higher estimates, although all were within the margin of the systematic error.

9 Correlation between other parameters of the models (*e.g.*, thermal resistances and thermal masses) may be observed. This is not unexpected as the product of two quantities determines the time constant of the element.

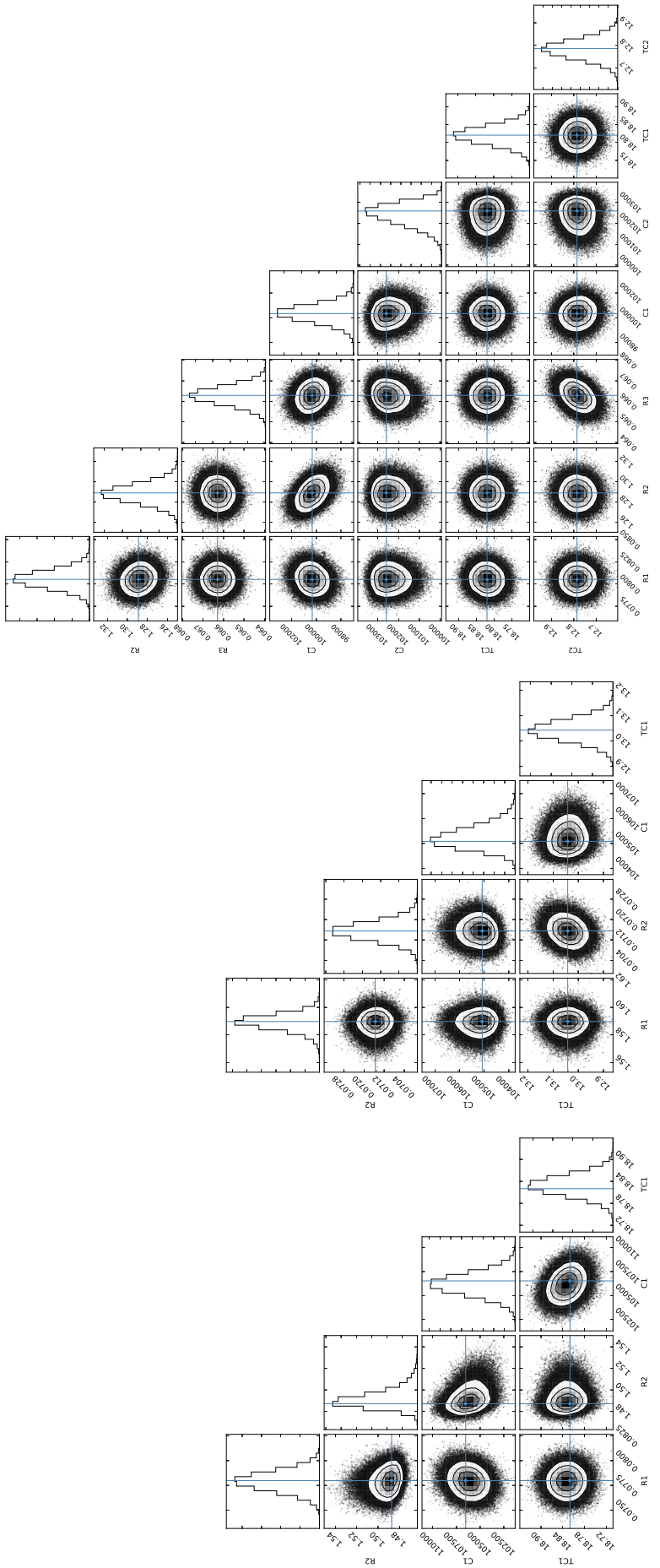

Figure 5.15: Distribution of the thermophysical properties of the CLWall estimated using the MCMC approach and uniform priors on the parameters of the model. The turquoise crossed lines indicate the MAP estimation used as starting point for the MCMC walk. From the left, the corner plots show the parameter distribution estimated using the 1TM (1 HF), the 1TM (2 HF) and the 2TM models.

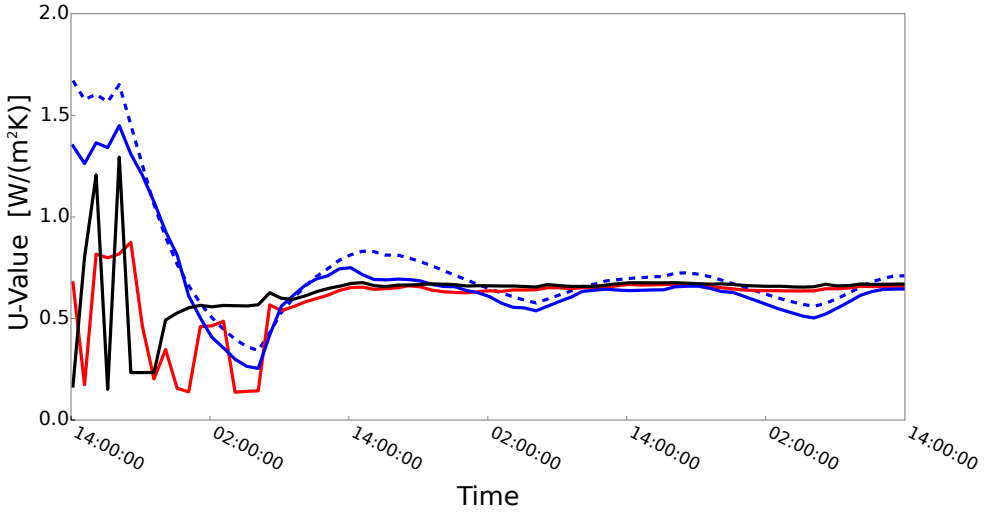

Figure 5.16: Evolution of the U-value for the HSWall_N for the three-day period analysed required by the BS ISO 9869-1 (2014) Standard to stabilise. The AM (dashed blue line), the 1TM (1 HF) model (solid red line), the 1TM (2 HF) model (solid blue line) and the 2TM model (black solid line) are shown. The MAP approach and uniform priors were used for the dynamic method.

The U-value obtained using the MAP approach and uniform prior probabilities was $(0.67 \pm 0.08)\,\mathrm{Wm^{-2}K^{-1}}$ for the 1TM (1 HF), $(0.66 \pm 0.06)\,\mathrm{Wm^{-2}K^{-1}}$ for the 1TM (2 HF), and $(0.68 \pm 0.08)\ \mathrm{Wm^{-2}K^{-1}}$ for the 2TM model. The thermophysical properties of the wall are shown in Table 5.13 on page 173 and summarised in Figure 5.17 on page 173. Similarly to the CLWall, the position of the thermal masses in thermal resistance space is at a comparable distance from the surface of the wall across all models. The total R-values and U-values estimated from *in-situ* measurements are higher than the range calculated from tabulated thermophysical properties of the building material, suggesting that the visual inspection of the wall may have lead to potential performance gap issues when choosing the thermophysical properties of the materials from look up tables, and/or that the monitored portion of the wall may be of different construction compared to the visual inspection (*e.g.*, in terms of materials or type of structure). Additionally, a potential source for a performance gap is the observed shrinkage of the insulation layer, possibly leaving uneven air gaps. This highlights the usefulness of *in-situ* measurements for the characterisation of the thermal performance of the building envelope, since it would not have been possible to identify this reduced thermal performance only from visual inspection.

Figure 5.18 on page 174 shows the measured and estimated heat flux time series. The traces confirm the findings of the previous case studies presented. Specifically, the 1TM models were able to provide satisfactory estimations of either the internal (1TM (1 HF) model) or the external (1TM (2 HF) model) heat flux but not both simultaneously. The

Parameters	Literature	AM	1TM (1 HF)	1TM (2 HF)	2TM	Units
R_1			0.061±0.001	1.297±0.021	0.061±0.001	m^2KW^{-1}
R_2			1.277±0.009	0.069±0.001	1.198±0.009	m^2KW^{-1}
R_3					0.060±0.001	m^2KW^{-1}
C_1	$[0.51, 0.90]\cdot10^5$		$(1.28\pm0.02)\cdot10^5$	$(1.02\pm0.01)\cdot10^5$	$(1.13\pm0.02)\cdot10^5$	$Jm^{-2}K^{-1}$
C_2	$[0.96, 2.08]\cdot10^5$				$(0.938\pm0.006)\cdot10^5$	$Jm^{-2}K^{-1}$
$T^0_{C_1}$			18.17±0.03	14.65±0.08	18.19±0.03	°C
$T^0_{C_2}$					14.93±0.07	°C
R-value	[2.36, 3.01]	1.219	1.338±0.009	1.336±0.021	1.319±0.009	m^2KW^{-1}
U-value	[0.32, 0.40]	0.723	0.666±0.005	0.656±0.011	0.677±0.005	$Wm^{-2}K^{-1}$

Table 5.13: Thermophysical properties of the HSWall_N calculated from the literature and estimated from *in-situ* measurements (both using the AM and dynamic method). The dynamic estimates for the 1TM (1 HF), 1TM (2 HF) and 2TM models were obtained using the MAP approach and uniform priors on the parameters of the model. Only the statistical error is shown, and the number of significant figures was chosen to illustrate the level of the error.

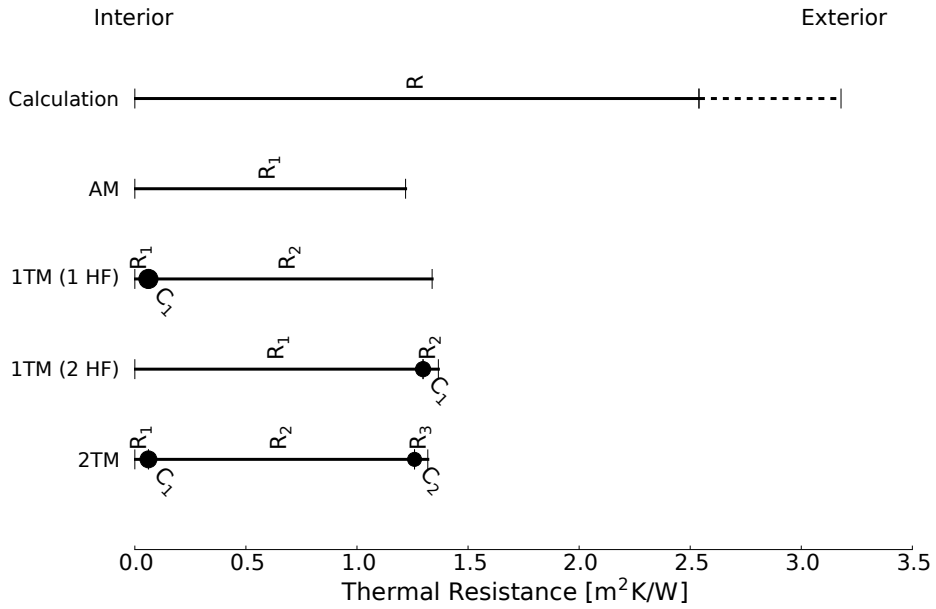

Figure 5.17: Summary of the R-value and size of the effective thermal mass(es) for the HSWall_N, as calculated from tabulated values and estimated form *in-situ* measurements (using the AM and the 1TM (1 HF), 1TM (2 HF) and 2TM models). The dynamic estimates were obtained using the MAP approach and uniform priors on the parameters of the model. The thermal resistance(s) are proportional to the length of the segments, while the magnitude of the thermal mass(es) is proportional to the radius of the solid circles. The dashed line indicates the range of R-values calculated from the literature.

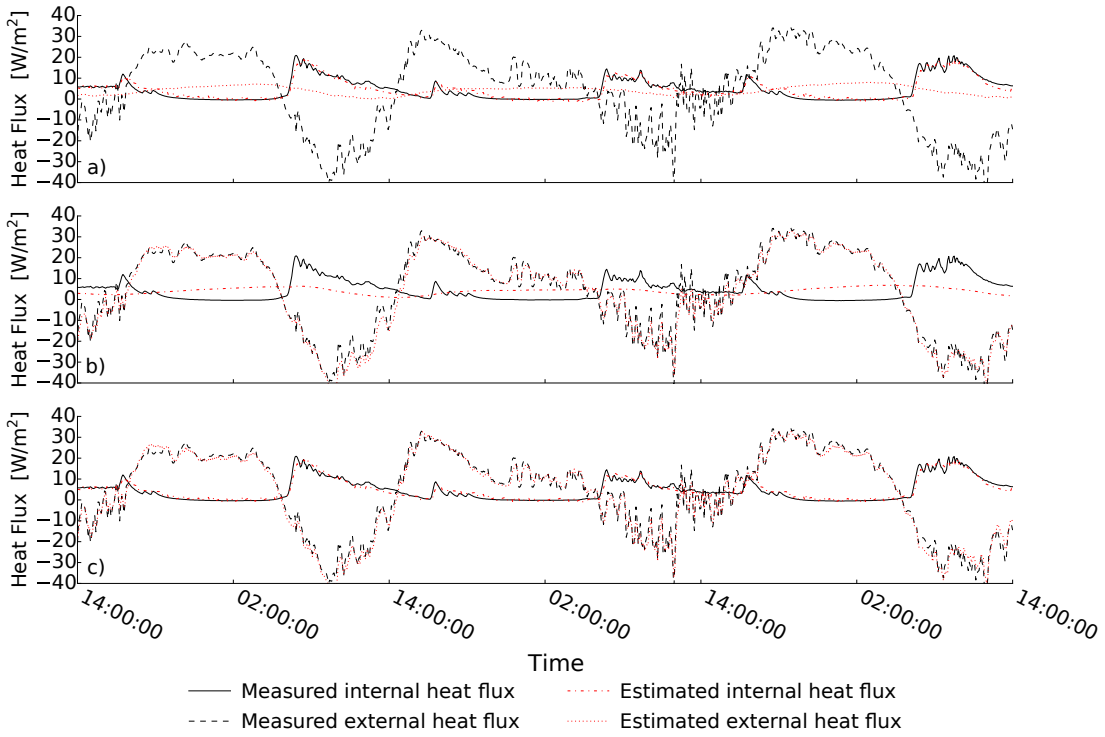

Figure 5.18: Measured and estimated heat flows through the HSWall_N by: (a) the 1TM (1 HF) model, (b) the 1TM (2 HF) model, and (c) the 2TM model.

introduction of an additional thermal mass (2TM) enabled the location of one thermal mass near each surface of the wall, better characterising the heat flux at both sides.

5.2.4.2 *Markov Chain Monte Carlo estimates using uniform priors*

As observed for the previous case studies presented, the MCMC estimates of the U-value and the thermophysical parameters (Table 5.14 on page 176) were within the margin of error of the MAP values. Specifically, the U-value was $(0.66 \pm 0.08)\,\mathrm{Wm^{-2}K^{-1}}$ for the 1TM (1 HF), $(0.65 \pm 0.06)\,\mathrm{Wm^{-2}K^{-1}}$ for the 1TM (2 HF), and $(0.68 \pm 0.07)\,\mathrm{Wm^{-2}K^{-1}}$. Similarly to the TCWall and the CLWall, the posterior distribution of the R-values (Figure 5.19 on page 175) was not correlated, seeming to support the findings of the MAP approach (Figure 5.17 on page 173) and those for the CLWall (Section 5.2.3). Also in this case, the corner plots seem to confirm that the distinct properties of the materials constituting the cavity walls caused the model to position the lumped parameters within the masonry layers.

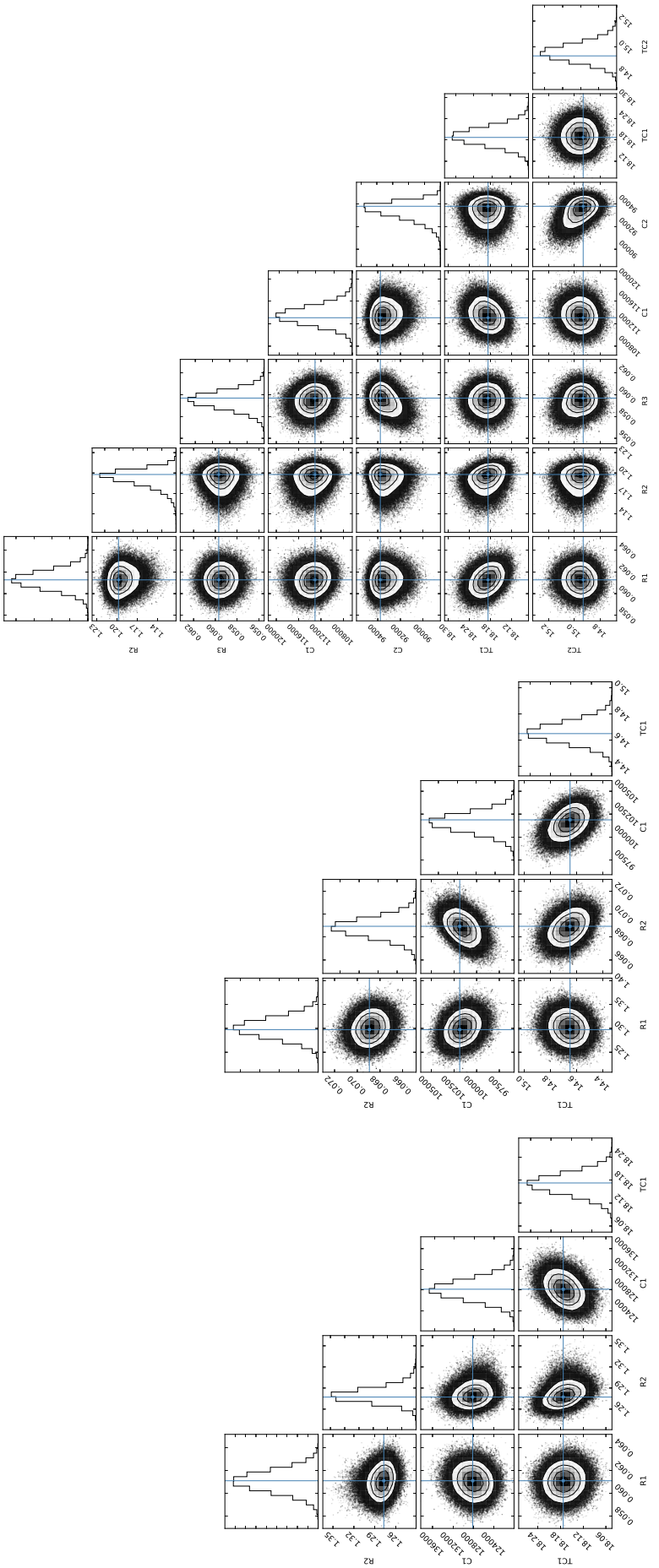

Figure 5.19: Distribution of the thermophysical properties of the HSWall_N estimated using the MCMC approach and uniform priors on the parameters of the model. The turquoise crossed lines indicate the MAP estimation used as starting point for the MCMC walk. From the left, the corner plots show the parameter distribution estimated using the 1TM (1 HF), the 1TM (2 HF) and the 2TM models.

Parameters	1TM (1 HF)	1TM (2 HF)	2TM	Units
R_1	0.0610±0.0009	1.301±0.021	0.061±0.01	m^2KW^{-1}
R_2	1.281±0.011	0.069±0.001	1.192±0.013	m^2KW^{-1}
R_3			0.0595±0.0008	m^2KW^{-1}
C_1	$(1.28\pm0.02)\cdot10^5$	$(1.02\pm0.01)\cdot10^5$	$(1.13\pm0.02)\cdot10^5$	$Jm^{-2}K^{-1}$
C_2			$(0.93\pm0.08)\cdot10^5$	$Jm^{-2}K^{-1}$
$T^0_{C_1}$	18.17±0.03	14.66±0.08	18.19±0.03	°C
$T^0_{C_2}$			14.96±0.07	°C
U-value	0.664±0.006	0.655±0.011	0.680±0.007	$Wm^{-2}K^{-1}$

Table 5.14: Thermophysical properties of the HSWall_N for the dynamic method (1TM (1 HF), 1TM (2 HF) and 2TM models) using the MCMC approach and uniform priors on the U-value. The number of significant figures was chosen to illustrate the level of statistical error.

5.3 TESTING THE MODELS WITH A HIGHER AVERAGE TEMPERATURE DIFFERENCE

Since the temperature difference set up in the thermal chamber was lower than best-practice recommendations for *in-situ* monitoring campaigns (as previously introduced in Chapter 5), the performance of the dynamic method was tested for completeness on three additional time series (one for each *in-situ* case study) meeting the average temperature difference of 10 °C suggested by best-practice guidelines (Energy Saving Trust, 2005). The same approach described in Section 5.2 was adopted for the selection of the time series to analyse. The average temperature difference was 9.6 °C for the OWall (monitoring period between the 29th of November and the 4th of December 2014, starting at 16:30), 10.0 °C for the HSWall_N (monitoring period between the 12th and the 19th of March 2015, starting at 14:00), and 10.5 °C for the CLWall (monitoring period between the 9th and the 17th of February 2016, starting at 00:00).

The U-value estimates obtained using the MAP approach and uniform priors were summarised in Table 5.15 on page 176, while the thermophysical parameter estimates are shown in Table 5.17 on page 178, Table 5.18 on page 179, and Table 5.16 on page 177. For each case study, the U-values were all within the margin of systematic error of the AM. Additionally, for each case study and model, the U-values were all within

	AM	1TM (1 HF)	1TM (2 HF)	2TM	Units
OWall	1.69±0.25	1.75±0.18	1.72±0.16	1.70±0.16	$Wm^{-2}K^{-1}$
CLWall	0.58±0.08	0.59±0.05	0.57±0.04	0.58±0.04	$Wm^{-2}K^{-1}$
HSWall_N	0.61±0.08	0.63±0.05	0.61±0.04	0.63±0.05	$Wm^{-2}K^{-1}$

Table 5.15: U-value estimates (and systematic error) for the *in-situ* case studies exposed to a temperature difference around 10 °C. The estimates were obtained using the MAP approach and uniform priors.

Parameters	Literature	AM	1TM (1 HF)	1TM (2 HF)	2TM	Units
R_1			0.071±0.001	0.074±0.001	0.075±0.001	m^2KW^{-1}
R_2			0.344±0.002	0.350±0.003	0.318±0.003	m^2KW^{-1}
R_3					0.040±0.002	m^2KW^{-1}
C_1	$[1.08, 1.80]\cdot10^5$		$(2.26\pm0.04)\cdot10^5$	$(2.31\pm0.05)\cdot10^5$	$(2.26\pm0.04)\cdot10^5$	$Jm^{-2}K^{-1}$
C_2	$[1.01, 1.92]\cdot10^5$				$(0.48\pm0.02)\cdot10^5$	$Jm^{-2}K^{-1}$
$T^0_{C_1}$			18.25±0.05	18.26±0.06	18.24±0.06	°C
$T^0_{C_2}$					12.56±0.06	°C
R-value	[0.29, 0.73]	0.42	0.415±0.001	0.425±0.002	0.432±0.002	m^2KW^{-1}
U-value	[1.11, 2.16]	1.69	1.748±0.006	1.718±0.011	1.696±0.0112	$Wm^{-2}K^{-1}$

Table 5.16: Thermophysical properties of the OWall calculated from the literature and estimated from *in-situ* measurements (both using the AM and dynamic method). The dynamic estimates for the 1TM (1 HF), 1TM (2 HF) and 2TM models were obtained using the MAP approach and uniform priors on the parameters of the model. Only the statistical error is shown, and the number of significant figures was chosen to illustrate the level of the error.

the margin of the systematic error of those obtained for the lower average temperature difference case. Similarly to Section 5.2:

- the use of non-uniform priors (both on the parameters of the model and the U-value) for the OWall case study did not lead to a significant influence on the thermophysical estimates at the end of the monitoring period (*i.e.* the parameters' estimates were all within the margin of the statistical error);
- the mean estimates from the MCMC approach were all within the margin of the statistical error of the MAP estimates obtained for the same model and case study.

Consequently, for conciseness, only the MAP estimates with uniform priors will be presented below.

The R-value and U-value of the OWall showed good agreement with the literature values and the AM estimates (Table 5.16 on page 177), as well as the estimations obtained for the lower temperature difference (Section 5.2.2). The only exception was represented by the lumped thermal resistances for the 1TM (2 HF) model, where the magnitude of R_1 increased to the detriment of R_2 compared to the smaller temperature difference case. The internal effective thermal mass (Table 5.16 on page 177) was within the margin of error of the values obtained in Section 5.2.2 for all models, and the estimate for the 2TM model was also comparable to that calculated according to the effective thickness method. Conversely, the estimated external effective thermal mass is smaller than the literature value and the estimates obtained for the lower average temperature difference (Section 5.2.2).

Parameters	Literature	AM	1TM (1 HF)	1TM (2 HF)	2TM	Units
R_1			0.075±0.001	1.528±0.014	0.0749±0.0006	m^2KW^{-1}
R_2			1.457±0.012	0.0664±0.0007	1.417±0.011	m^2KW^{-1}
R_3					0.0663±0.0006	m^2KW^{-1}
C_1	$[5.10, 9.00]\cdot10^4$		$(6.44\pm0.10)\cdot10^4$	$(10.10\pm0.05)\cdot10^4$	$(6.48\pm0.07)\cdot10^4$	$Jm^{-2}K^{-1}$
C_2	$[9.60, 20.8]\cdot10^4$				$(10.12\pm0.04)\cdot10^4$	$Jm^{-2}K^{-1}$
$T^0_{C_1}$			15.38±0.04	7.48±0.05	15.38±0.04	°C
$T^0_{C_2}$					7.44±0.05	°C
R-value	[2.36, 3.01]	1.56	1.533±0.012	1.594±0.014	1.558±0.011	m^2KW^{-1}
U-value	[0.32, 0.40]	0.57	0.587±0.005	0.571±0.005	0.583±0.005	$Wm^{-2}K^{-1}$

Table 5.17: Thermophysical properties of the CLWall calculated from the literature and estimated from *in-situ* measurements (both using the AM and dynamic method). The dynamic estimates for the 1TM (1 HF), 1TM (2 HF) and 2TM models were obtained using the MAP approach and uniform priors on the parameters of the model. Only the statistical error is shown, and the number of significant figures was chosen to illustrate the level of the error.

For the CLWall case study, the thermophysical properties estimated using the proposed dynamic method (Table 5.17 on page 178) supported the findings obtained for the lower average temperature difference case. Specifically, the R-value and U-value were confirmed to be higher than the expected values from the literature, and within the margin of the statistical error of the smaller temperature difference case. Similarly, both effective thermal masses for the 2TM model were within the literature ranges. Analogously to the CLWall case study, the thermophysical estimates for the HSWall_N (Table 5.18 on page 179) also supported the findings obtained for the lower average temperature difference case. The dynamic estimates were comparable in the two cases and in agreement with the AM, although the *in-situ* estimates were higher than literature values as previously observed. Similarly, the effective internal and external thermal mass estimates for the 2TM model were within the literature ranges.

For each case study, the distribution of the thermophysical parameters of the different models obtained with the MCMC approach had comparable behaviour to the lower temperature difference case. Specifically, the thermal resistances of the OWall showed a negative relationship, meaning that several similarly probable combinations for the locations of the effective lumped thermal masses may be possible and consequently the estimate of the thermal resistances may vary depending on the position of the effective thermal mass, although their total R-value is constant. As already introduced above, this behaviour may be explained by the weak physical constraints offered by the comparable thermophysical properties of the materials constituting a traditional solid wall, like the OWall. Conversely, the thermal resistances of the two CLWall and HSWall_N were not correlated as their posterior probability distributions. The distinct thermophysical

Parameters	Literature	AM	1TM (1 HF)	1TM (2 HF)	2TM	Units
R_1			0.0663±0.0006	1.412±0.004	0.067±0.001	m^2KW^{-1}
R_2			1.358±0.005	0.062±0.001	1.294±0.005	m^2KW^{-1}
R_3					0.061±0.001	m^2KW^{-1}
C_1	$[0.51, 0.90]\cdot10^5$		$(0.82\pm0.01)\cdot10^5$	$(0.94\pm0.01)\cdot10^5$	$(0.80\pm0.01)\cdot10^5$	$Jm^{-2}K^{-1}$
C_2	$[0.96, 2.08]\cdot10^5$				$(0.93\pm0.09)\cdot10^5$	$Jm^{-2}K^{-1}$
$T^0_{C_1}$			17.56±0.03	11.39±0.05	17.51±0.03	°C
$T^0_{C_2}$					11.40±0.05	°C
R-value	[2.36, 3.01]	1.476	1.425±0.005	1.473±0.004	1.422±0.005	m^2KW^{-1}
U-value	[0.32, 0.40]	0.607	0.630±0.002	0.613±0.002	0.633±0.003	$Wm^{-2}K^{-1}$

Table 5.18: Thermophysical properties of the HSWall_N calculated from the literature and estimated from *in-situ* measurements (both using the AM and dynamic method). The dynamic estimates for the 1TM (1 HF), 1TM (2 HF) and 2TM models were obtained using the MAP approach and uniform priors on the parameters of the model. Only the statistical error is shown, and the number of significant figures was chosen to illustrate the level of the error.

properties of the materials constituting the two cavity walls strongly constrained the locations of the thermal mass(es) and consequently the magnitude of the lumped thermal resistances.

5.4 MODEL SELECTION AND VALIDATION

Model selection and validation were undertaken for all case studies and temperature difference configurations, to identify the model that is both more likely to describe the underlying physical process and to ensure that the best model is also robust, generalisable, and replicable (Section 3.5) .

5.4.1 *Model selection*

Model selection was performed according to the odds ratio method, which represents a measure of the relative plausibility of two models fitted to their most probable parameters (Section 3.5.1). The performance of the 2TM model in respect to the 1TM (2 HF)[10] was compared to check whether the additional complexity of the former model was justified, leading to a significant improvement in the fit. Given the close agreement between results obtained with uniform and non-uniform prior distributions reported above, it is expected that their impact on the odds ratio is also small. Table 5.19 on page 180 and

10 The odds ratios reported in Table 5.19 on page 180 and Table 5.20 on page 180 were calculated as the difference between the natural logarithm of the evidence for the 2TM and that for the 1TM (1 HF) model. Consequently, positive values indicate the 2TM model as the best to describe the observed data.

	TCWall Un	OWall Un	OWall LN P	OWall LN U	CLWall Un	HSWall Un
MAP	1439	1961	1972	1981	8255	3847
MCMC	1436	1958	1968	1978	8251	3842

Table 5.19: Natural logarithm of the odds ratio comparing the 1TM (2 HF) and 2TM model for all case studies exposed to the lower (~5 °C) average temperature difference. The odds ratio was calculated both from the MAP and MCMC approaches using uniform (Un) and log-normal (LN P) priors on the parameters of the model, and a log-normal prior on the U-value (LN U).

	OWall Un	OWall LN P	OWall LN U	CLWall Un	HSWall Un
MAP	835	814	854	6312	7699
MCMC	832	851	851	6310	7694

Table 5.20: Natural logarithm of the odds ratio comparing the 1TM (2 HF) and 2TM model for the *in-situ* case studies exposed to the higher (~10 °C) average temperature difference. The odds ratio was calculated both from the MAP and MCMC approaches using uniform (Un) and log-normal (LN P) priors on the parameters of the model, and a log-normal prior on the U-value (LN U).

Table 5.20 on page 180 show the odds ratio (both from the MAP and MCMC approaches) for all case studies respectively exposed to the lower and higher average temperature differences.

In all cases the odds ratio strongly supported the 2TM model as the one providing a substantially better representation of the observations. The result suggests that the inclusion of an additional effective thermal mass improved the physical representation of both solid and cavity walls. As previously observed, the 2TM model enables the simultaneous characterisation of the heat flow into and out of the walls at each surface, which can be valuable for practical applications as discussed in Section 5.5.

5.4.2 *Cross-validation*

Cross-validation analysis was performed as a model-checking technique to investigate the ability of the best model selected to generalise to new observations (Section 3.5.2). It was undertaken on all case studies presented, both on the lower and higher temperature difference configurations. Uniform and log-normal priors were also tested for the OWall. However, as expected from the close performance of the 2TM model with different priors in the model selection (Table 5.19 on page 180 and Table 5.20 on page 180), the use of different types of prior did not show considerable differences in the cross-validated time series. Consequently, only the case for uniform priors is shown below.

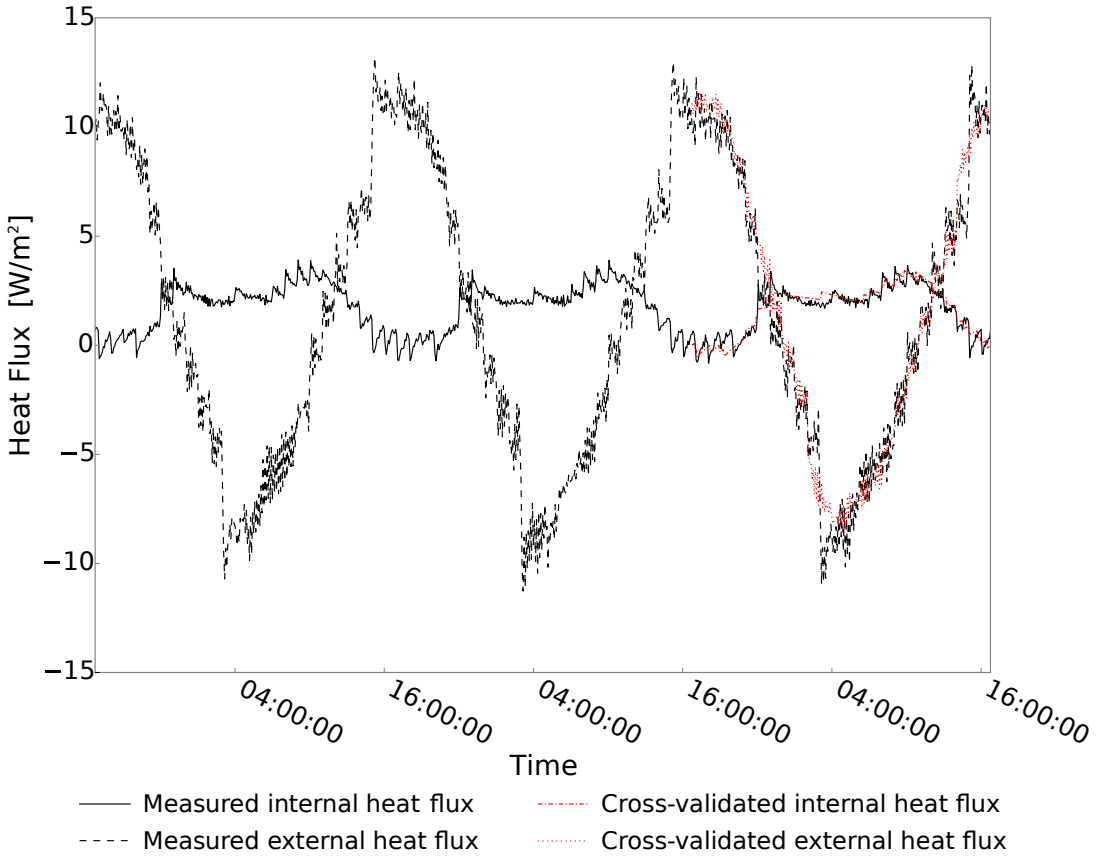

Figure 5.20: Cross-validation of the heat flux time series for the TCWall using the 2TM model.

The 2TM model was able to generalise to new observations and ensure a good match between the measured and cross-validated time series in all cases, including three-day-long series (Figure 5.20 on page 181, Figure 5.23 on page 184, Figure 5.22 on page 183, and Figure 5.21 on page 182). Notably, this result shows that the model was able to accurately estimate the heat flux on out-of sample data using only one full day of training data (Section 3.5.2).

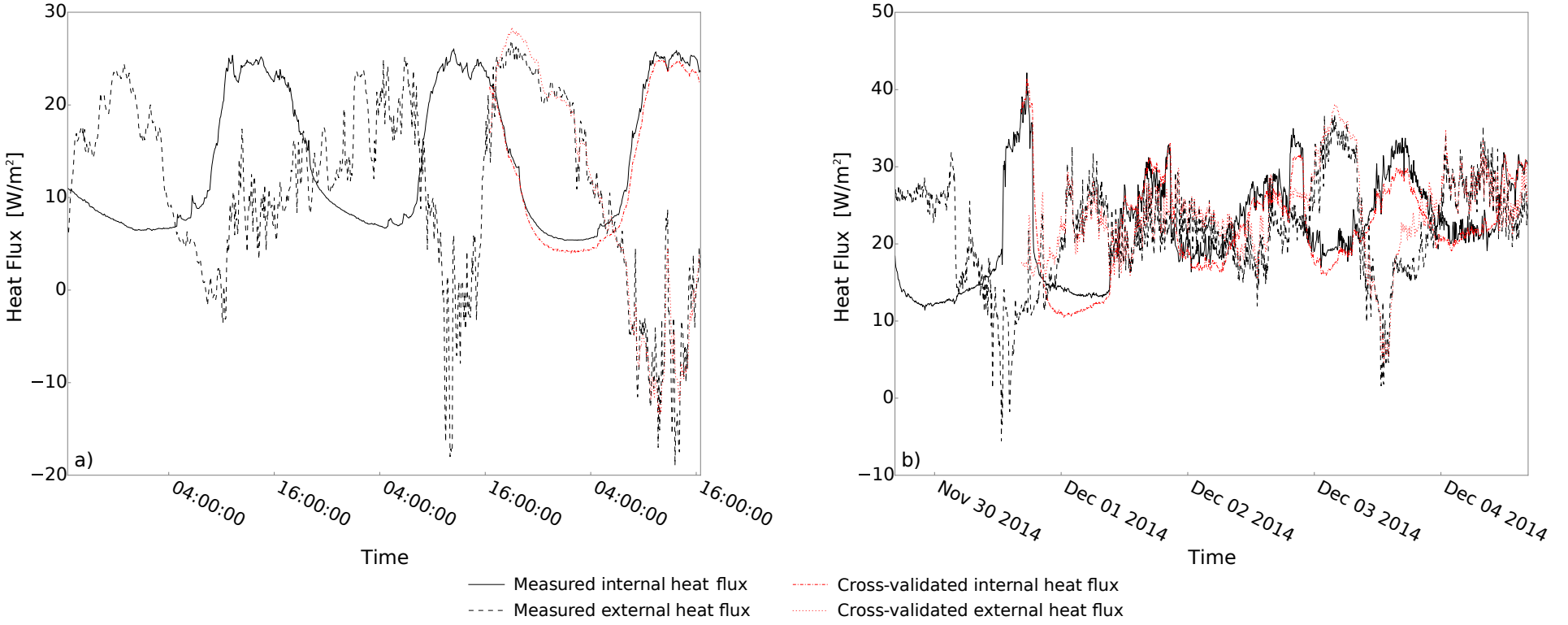

Figure 5.21: Cross-validation of the heat flux estimations for the OWall_N using the 2TM model to analyse: (a) the lower and (b) the higher average temperature difference cases.

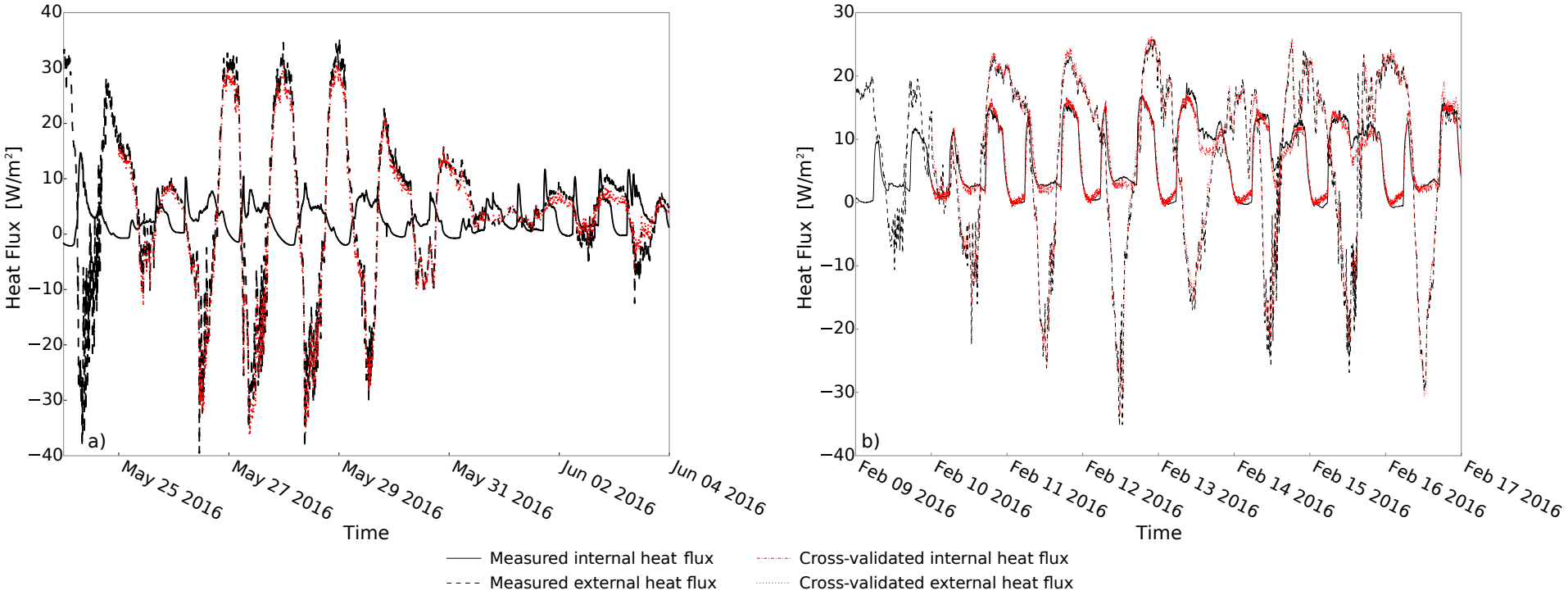

Figure 5.22: Cross-validation of the heat flux estimations for the CLWall using the 2TM model to analyse: (a) the lower and (b) the higher average temperature difference cases.

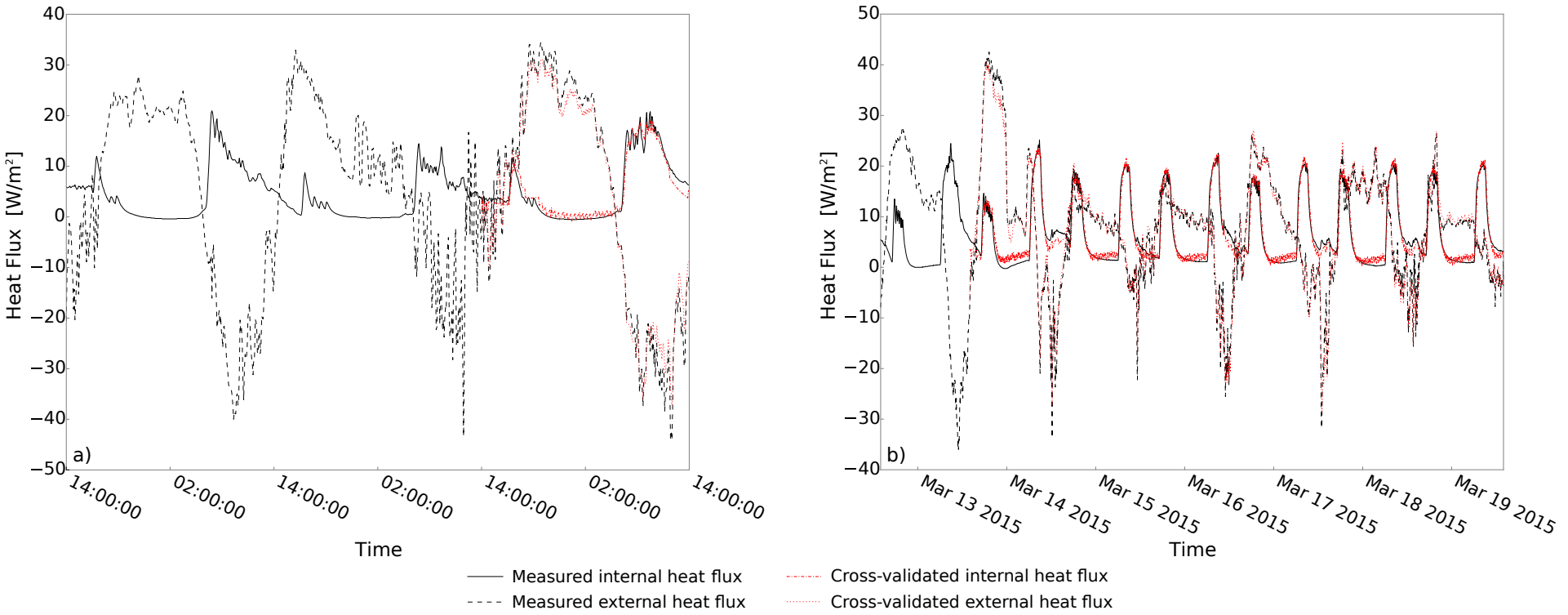

Figure 5.23: Cross-validation of the heat flux estimations for the HSWall_N using the 2TM model to analyse: (a) the lower and (b) the higher average temperature difference cases.

5.5 DISCUSSION AND SUMMARY

In this chapter the proposed dynamic method was tested on four walls, one housed in a thermal chamber and three *in-situ*, under two temperature scenarios. The first one consisted of testing the proposed method on each case study for a period where the average temperature difference between the indoor and outside ambient was comparable with the thermal chamber settings (referred to as "lower average temperature difference" case), while the second one tested the dynamic method on each *in-situ* case studies for a period where the average temperature difference was around 10 °C as suggested by common-practice guidelines for *in-situ* monitoring. The criteria listed in the ISO 9869-1 (2014) Standard (and reported in Section 2.3.1) were imposed to check the duration of the time series to be analysed. Specifically, the criteria were used to determine the number of full days required by the AM to stabilise and the period selected was also used to evaluate the thermophysical properties of the walls by means of the proposed dynamic method. Both the MAP and MCMC approaches were tested for all the lumped thermal mass models adopted (1TM (1 HF), 1TM (2 HF) and 2TM). Additionally, uniform and log-normal prior probability distributions on the parameters of the model as well as log-normal priors on the U-value were also tested for the OWall case study, which was the only one where suitable information for the calculation of priors was available (Section 4.2.2).

The evolution of the U-value showed that the period selected according to the AM was also sufficient for the dynamic estimates to stabilise. Specifically, the dynamic method was usually quicker to stabilise and in principle its formulation does not require the analysis of an integer number of days. In particular the 2TM was the quickest among the models devised, taking between 24 to 36 hours on average. The use of non-uniform priors (*i.e.* log-normal in this case) improved the U-value estimates during the initial phases of the analysis, where few observation were available. However, the evolution of the U-value stabilised to comparable estimates at the end of the monitoring period identified for the analysis. This result suggests that the dynamic method was able to meet the objective of reducing the length of the monitoring period compared to standard method, while ensuring robust estimates of the thermophysical performance of the wall. An additional advantage of non-uniform prior compared to uniform ones is related to the fact that the former are more robust than the latter in case of a poor choice of the prior as they allow the assignment of low probabilities to unlikely but possible events. Future work will aim to define new criteria for the identification of the minimum length

	AM	1TM (1 HF)	1TM (2 HF)	2TM
TCWall (Un)	14.5%	10.6%	10.3%	10.4%
OWall (Un)	19.3%	15.7%	16.1%	15.2%
OWall (LN P)	-	15.7%	16.1%	15.0%
OWall (LN U)	-	15.7%	16.1%	15.2%
CLWall (Un)	17.6%	14.1%	13.6%	10.8%
HSWall_N (Un)	15.1%	11.7%	9.4%	11.3%

Table 5.21: Relative systematic error on the U-value for the lower average temperature difference case. Estimates for each case study are shown for the AM and the dynamic method, using the 1TM (1 HF), 1TM (2 HF) and 2TM models and the MAP approach with uniform (Un) and log-normal priors on the parameters of the model (LN P) and log-normal priors on the U-value (LN U).

	AM	1TM (1 HF)	1TM (2 HF)	2TM
OWall (Un)	14.8%	10.4%	9.4%	9.5%
OWall (LN P)	-	10.4%	9.4%	9.6%
OWall (LN U)	-	9.6%	9.4%	9.5%
CLWall (Un)	13.3%	8.9%	6.5%	6.7%
HSWall_N (Un)	13.4%	8.7%	6.7%	8.4%

Table 5.22: Relative systematic error on the U-value for the higher average temperature difference case. Estimates for each case study are shown for the AM and the dynamic method, using the 1TM (1 HF), 1TM (2 HF) and 2TM models and the MAP approach with uniform (Un) and log-normal priors on the parameters of the model (LN P) and log-normal priors on the U-value (LN U).

of the time series to be analysed with dynamic methods, working towards addressing the current lack of standardised stabilisation criteria for dynamic approaches.

For each case study and lumped thermal mass model the analysis using the MAP and MCMC approaches returned parameter estimates within the margin of the statistical error, both for the lower (Section 5.2) and higher (Section 5.3) average temperature difference scenarios. The comparable performance of the two approaches showed that the two optimisers were robust for these case studies. The U-value estimates at the end of the monitoring period were within the systematic error of the AM. However the magnitude of the associated systematic error varied depending on the method used for the data analysis, reflecting the different mathematical modelling of the dynamic and average methods (Section 4.5).

Table 5.21 on page 186 and Table 5.22 on page 186 compare the relative systematic error on the U-value[11] obtained for the two average temperature difference configurations (as mentioned above, given the close agreement observed only the errors for the MAP approach were shown for conciseness). As expected, the higher average temper-

11 The relative systematic error on the U-value represents the additive systematic uncertainties on the U-value expressed as a percentage of its value.

ature difference decreased the relative systematic error for all methods (Desogus et al., 2011). Similarly, for each case study the systematic error was smaller for the dynamic method compared to the AM, and the use of more than one data stream (*i.e.* 1TM (2 HF) and 2TM) further reduced it (Section 4.5). These results showed the robustness of the dynamic method in returning estimates within acceptable error ranges even in cases where the average temperature difference is smaller than current best-practice recommendations.

The *in-situ* estimates were generally in agreement with the literature values. For the CLWall and HSWall_N the *in-situ* U-values were higher than those calculated from look-up tables. However, this result was not unexpected since visual inspection showed a shrinkage of the insulation layer in the CLWall, and a similar behaviour may be expected for the HSWall_N given the observed similarity in the stratigraphy and year of construction of the two case studies. The results highlights the importance of monitoring campaigns to characterise the *in-situ* performance of building elements since it would not be possible to characterise and quantify the potential impact the ageing process of the building materials or imperfections in the layout only from visual inspection.

The distribution of the thermophysical parameters of the model obtained with the MCMC approach provided useful insights into the thermal structure of the walls investigated that can be interpreted in the light of the known physical structure of the element. Specifically, the TCWall, the CLWall and the HSWall_N, which were characterised by distinct thermophysical properties of the constituent materials (*i.e.* a high thermal resistance and low thermal mass material interposed between two layers of lower thermal resistance), did not show correlations between the lumped thermal resistances of the model. The strong physical constraints seemed to impose a unique solution to the values of the constituent effective thermal masses of the model and consequently the magnitude of the lumped R-values was also fixed. Conversely, a negative relationship was observed for the OWall, where the weak physical constraints characterising the traditional solid wall allowed several similarly probable combinations for the locations of the effective lumped thermal masses. Therefore, the size of the constituent thermal resistances varied depending on the effective thermal mass position, although their total R-value was constant (Section 6.4 further extends this analysis to long-term monitoring).

Model comparison and validation confirmed that the 2TM model was the best at describing the observed heat transfer across all case studies compared to the 1TM (2 HF) model, showing that the extra complexity introduced by a second thermal mass was justified. The result is not unexpected as the performance of the model was shown to be limited in a number of occasions, possibly due to the fact that a model with

only one thermal mass is not sufficient to simultaneously account for two heat flux inputs. Cross-validation analysis supported the insights gained with model comparison, showing that the 2TM model was also able to generalise to new observations. Notably, the model was able to accurately estimate the heat flux on out-of sample data using as little as one full day of training data. The ability of the 2TM model to simultaneously model and account for both the heat flow into and out of a building element and the insights gained from the probability distributions produced by the MCMC approach open up a number of practical applications for the method proposed. These include the possibility of extending the seasons in which monitoring campaigns may be undertaken and the development of tailored retrofitting solutions aiming at improving the indoor thermal comfort and closing the performance gap by minimising the energy use through insulation, heating and cooling strategies (Chapter 6 and Chapter 7 further discuss these aspects).

Given the encouraging results obtained in this chapter for *in-situ* elements exposed to an average temperature difference lower than best-practice recommendations, Chapter 6 and Chapter 7 extend this analysis to measurements taken at all times of the year and on differently oriented walls. The analyses test the robustness of the proposed dynamic method outside the conventional monitoring conditions of the winter season and north-oriented walls to investigate the ability of the dynamic method to extend the monitoring period and shorten the length of the monitoring campaigns compared to current methods.

6

PERFORMANCE OF THE DYNAMIC GREY-BOX METHOD OF CHARACTERISING THE THERMAL PROPERTIES OF WALLS AT ALL TIMES OF YEAR

Chapter 5 tested the performance of the proposed grey-box dynamic method on a wall housed in a thermal chamber and three north-facing *in-situ* walls of different construction. Firstly, the time series analysed were selected to ensure that the average temperature difference for the *in-situ* walls was comparable to that used during the thermal chamber experiments. This configuration allowed the investigation of the performance of the dynamic method on structures exposed to a similar temperature differences (~5 °C) between the internal and external surfaces of the wall[1], but different boundary conditions (*i.e.* a controlled environment in the thermal chamber and real non-stationary excitations *in-situ*). However, since the average temperature difference the walls were exposed to was lower than current recommendations for *in-situ* measurements, for completeness the dynamic method was also tested on time series meeting best-practice requirements of 10 °C or more (Siviour and McIntyre, 1982; Energy Saving Trust, 2005; Baker and van Dijk, 2008; Desogus et al., 2011).

The evolution of the U-value showed the potential for the dynamic method to shorten the length of the monitoring period compared to the average method, while the estimates with the two approaches were within the margin of errors and generally in line with literature values. Specifically, the systematic error estimates by the dynamic method were smaller than the AM and acceptable also for the smaller average temperature difference configuration. The thermophysical parameters estimated by the maximum a posteriori and the Markov Chain Monte Carlo approaches were comparable (within the margin of the statistical error), indicating that the two optimisers are robust. Additionally, the estimates provided useful insights into the thermal structure of the walls that can be interpreted in the light of the known physical structure of the element. Model

1 In the following the average temperature difference between the inside and external surfaces of the wall is referred to as "average temperature difference" for conciseness.

comparison selected the 2TM model as best at describing the measured data and cross validation confirmed that the best-model was also able to generalise to out-of-sample observations.

Given the encouraging results achieved in Chapter 5, the present chapter extends the analysis on the same case studies (OWall, CLWall and HSWall_N) to long-term monitoring campaigns (between four-months and one-year long, detailed in Section 6.1) spanning different seasons, variable environmental factors (*e.g.*, air movement, moisture migration; Section 2.2), and average temperature differences (outside best-practice recommendations). The analysis aimed to explore the potential to expand the seasons over which the method may be applied with confidence (both in terms of estimates and associated errors), as well as its ability to reduce the length of the monitoring period without sacrificing accuracy. Two analysis schemes using the hypothetical monitoring campaign approach described in Section 4.4 were conceived in this chapter to test the aforementioned aspects of the dynamic method.

Firstly, Section 6.2 compares the performance of the lumped thermal mass models adopted in Chapter 5 (*i.e.* 1TM (1 HF), 1TM (2 HF), 2TM) and the AM at estimating the U-values and the associated relative systematic error (defined in Section 4.5.2 and Section 4.5.3) using data collected at all times of the year. It used hypothetical monitoring campaigns whose minimum length were defined according to the AM (*i.e.* "first scenario" described in Section 4.4). Since the 1TM (2 HF) and the 2TM models were tested on time series of equal length, Bayesian model comparison was performed to identify the best model at describing the observations over the changing seasons.

The second analysis scheme (Section 6.3) investigated the ability of the best model selected to reduce the stabilisation time[2] at all times of the year while ensuring robust thermophysical estimates. This analysis was undertaken by using hypothetical monitoring campaigns whose minimum length was independently defined according to the different analysis methods adopted (*i.e.* "second scenario" in Section 4.4). The probability distribution of the estimates of the thermophysical parameters obtained in Section 6.3 using the MCMC approach are analysed in Section 6.4 to further investigate whether these can provide useful insights into the thermal structure of walls, as suggested by the analysis undertaken in Chapter 5.

A general discussion on the performance of the dynamic method at all times of the year is presented in Section 6.5. The analysis is further extended in Chapter 7 to investigate the potential influence of wind and solar radiation on the thermophysical estimates

2 As defined in Section 4.4, the concept "stabilisation" is used to indicate the condition where after a minimum number of observations the addition of new data does not significantly enhance the prediction of the parameters anymore and the values stabilise around a final value.

of the dynamic method, and consequently explore the ability of the dynamic grey-box method to expand the monitoring to elements with different orientation.

6.1 DATA SELECTION

Prior to starting the data analysis, the raw time series were checked and cross-referenced with the metadata to identify obvious problems in the data collection or repeated missing data. In the cases where issues were identified, the corresponding data were excluded from the analysis. Table 6.1 on page 192 shows for each case study the periods covered by the long-term time series investigated in this chapter and the subsets discarded (if applicable). Starting from the "start date" (Table 6.1 on page 192), hypothetical monitoring campaigns starting one-week apart over the monitoring period were defined according to the description in Section 4.4. Hypothetical monitoring campaigns that:

- were to start during a period of missing data;
- had not met the stabilisation criteria (as defined in Section 2.3.1) before a period of missing data;
- had not met the stabilisation criteria within 30 days;

were excluded from the analysis. The 30-day threshold on the length of the hypothetical monitoring campaigns was introduced for the following reasons. During long monitoring campaigns, the risk of considerable changes in the environmental conditions the building element is exposed to increases, for example due to wind patterns, moisture content within centimetres from the external wall surface due to wind-driven rain and subsequent solar-driven evaporation. Consequently, the assumption of constant model's parameters to explain the observations may not hold anymore (as introduced in Section 4.4). A limit of thirty days also reflects commercial pressures in the light of expanding the use of *in-situ* surveys in the building sector (*e.g.*, for benchmark characterisation of a building prior to retrofitting interventions or quality insurance of new built properties).

Case study	Start date	End date	Excluded periods
OWall	2/11/2013 00:00	29/11/2014 00:00	16/5/2014 00:00 to 30/5/2014 23:55
CLWall	9/2/2016 00:00	28/8/2016 00:00	30/3/2016 00:00 to 11/4/2016 23:55
HSWall_N	12/3/2015 14:00	31/8/2015 14:00	-

Table 6.1: Monitoring period surveyed for each case study and periods excluded from the analysis due to faults during the data collection only. The excluded periods in the table do not cover the hypothetical monitoring campaigns not complying the criteria listed above.

6.2 IMPACT OF THE INDOOR TO EXTERIOR TEMPERATURE GRADIENT ON U-VALUE ESTIMATES AND SYSTEMATIC ERRORS

The U-value and its associated systematic errors estimated with the 1TM (1 HF), 1TM (2 HF) and 2TM models were investigated in this section and compared to the AM estimates. The analysis was performed adopting the hypothetical monitoring campaign approach whose length was determined according to the minimum number of observations necessary for the AM to stabilise ("first scenario" in Section 4.4), and the time series so obtained were also used with the dynamic method. Three north-facing *in-situ* walls (*i.e.* OWall, CLWall, HSWall_N) were used as case studies to extend the analysis in Chapter 5 to all times of the year. The use of equally long time series for each hypothetical monitoring campaign enabled a relative comparison of the U-value estimates and the associated systematic errors using the average and dynamic method with different lumped thermal mass models, while minimising the influence of the uncertainties introduced by variations of the environmental conditions during the survey. It also enabled the Bayesian model comparison between the 1TM (2 HF) and the 2TM models, as it requires that the models are compared on the same information in terms of monitoring period, number of data streams used to fit the models, and observations (Section 3.5.1).

The outcomes of the analysis on a solid (OWall) and cavity (CLWall and HSWall_N) walls are discussed below. Only the MAP estimates are presented, as Chapter 5 showed that these did not significantly differ from the mean of the MCMC parameter distributions (the values were always within the margin of the statistical error). Both uniform and log-normal priors (as defined in Section 4.2.2) on the parameters of the models were adopted for the analysis of the OWall. The analysis using the log-normal prior on the U-value was not undertaken in this chapter as the distribution available for the calculation of its location and dispersion was potentially unrepresentative of the OWall (as discussed in Section 4.2.2.3). It is also notable that the choice is anyway conservative as

Chapter 5 showed that the evolution of the U-value obtained with the log-normal prior on the U-value had intermediate behaviour between the uniform and log-normal priors on the parameters (Figure 5.8 on page 161, Table 5.9 on page 162, Table 5.10 on page 162), and the final estimates (*i.e.* the estimates at the end of the period analysed) were within the margin of error of the other cases.

6.2.1 *Solid wall in an office building (OWall)*

6.2.1.1 *Uniform priors on the parameters of the lumped thermal mass models*

From the time series collected on the OWall (Table 6.1 on page 192), fifty-two hypothetical monitoring campaigns were analysed after removing those that failed to meet the acceptance criteria described in Section 6.1. The length of each hypothetical monitoring campaign ranged between three and thirty days; a smaller number of days was needed in the autumn and winter period (up to ten days) and gradually increased over the rest of the year.

The U-value estimates from the AM and the dynamic method using the 1TM (1 HF), 1TM (2 HF) and the 2TM models were within the margin of the systematic error for all hypothetical monitoring campaigns. The minimum, maximum, mean and standard deviation of the U-value estimates are summarised in Table 6.2 on page 194. The range of values obtained was within that expected from the literature (calculated in Section 5.1.2). The mean U-value for the AM, 1TM (1 HF) and the 2TM models virtually coincided, while it was slightly higher (about 4%) for the 1TM (2 HF) model (although within the standard deviation of the other cases). The 2TM model had the smallest standard deviation (*i.e.* the spread of the U-value estimates from the mean value over the fifty-two periods), while the AM had the largest. The standard deviation of the 2TM model was half that of the AM.

The ranges of relative systematic error on the U-values calculated with the different methods and models over the fifty-two hypothetical monitoring campaigns are summarised in Table 6.2 on page 194. The AM presented the highest minimum and maximum values, while the dynamic method was generally characterised by smaller ranges. In particular, the 2TM model had the smallest range of relative systematic error throughout the year, between 9% and 27%. The relative systematic error was investigated as a function of the average temperature difference observed during the hypothetical monitoring campaign to test the robustness of the different methods and models to small temperature differences. Figure 6.1 on page 195 shows the relative systematic error on

		Min	Max	Mean	St Dev	Units
U-value	AM	1.28	1.92	1.71	0.14	$Wm^{-2}K^{-1}$
	1TM (1 HF)	1.34	1.88	1.71	0.13	$Wm^{-2}K^{-1}$
	1TM (2 HF)	1.61	2.00	1.77	0.11	$Wm^{-2}K^{-1}$
	2TM	1.60	1.85	1.72	0.07	$Wm^{-2}K^{-1}$
Rel sys err	AM	14%	50%	22%	8%	-
	1TM (1 HF)	10%	31%	17%	6%	-
	1TM (2 HF)	9%	51%	17%	8%	-
	2TM	9%	27%	16%	5%	-

Table 6.2: Minimum, maximum, mean and standard deviation of the U-value estimates and the associated relative systematic error for the OWall. The values were estimated using the average and the dynamic method with the 1TM (1 HF), 1TM (2 HF), 2TM models. The dynamic method used the MAP approach and uniform priors on the parameters of the model.

the U-value estimated with the AM as a function of the average temperature difference. As expected from its mathematical formulation (Section 4.5.3), the relative systematic error increased as the average temperature difference decreased and reached a maximum of 50% error for the smallest average temperature difference observed (*i.e.* 1.6 °C). This result shows that for low average temperature differences, even when the stability criteria are met (BS ISO 9869-1, 2014) and the estimates look plausible (Table 6.2 on page 194) compared to literature values (Section 5.1.2), the associated rise in systematic error limits the insight that may be derived from such *in-situ* measurements.

Figure 6.2 on page 196 shows the relative systematic error on the U-value as a function of the average temperature difference for the dynamic method. Similarly to the case for the AM method, the magnitude of the errors increased as the temperature difference decreased although the range was smaller (generally up to 30%). This result can be ascribed to the different mathematical modelling of the dynamic method, where the temperature difference is calculated at each observation instead of averaged (as discussed in Section 4.5). A comparison of the relative systematic error on the U-value for the dynamic method (Figure 6.3 on page 197) showed that, as expected from the assumption of uncorrelated uncertainties on the heat flux measurements, the errors estimated from lumped thermal mass models optimising two heat flux data streams (1TM (2 HF) and 2TM models) were smaller than those obtained from the optimisation of only one heat flux time series (1TM (1 HF) model). Additionally, the relative systematic errors for the 2TM model were generally smaller than those for the 1TM (2 HF) model.

The use of the Bayesian approach and the investigation of equal-length hypothetical monitoring campaign to test the performance of the dynamic method enabled an objective comparison of the 1TM (2 HF) and the 2TM model to identify the best one at

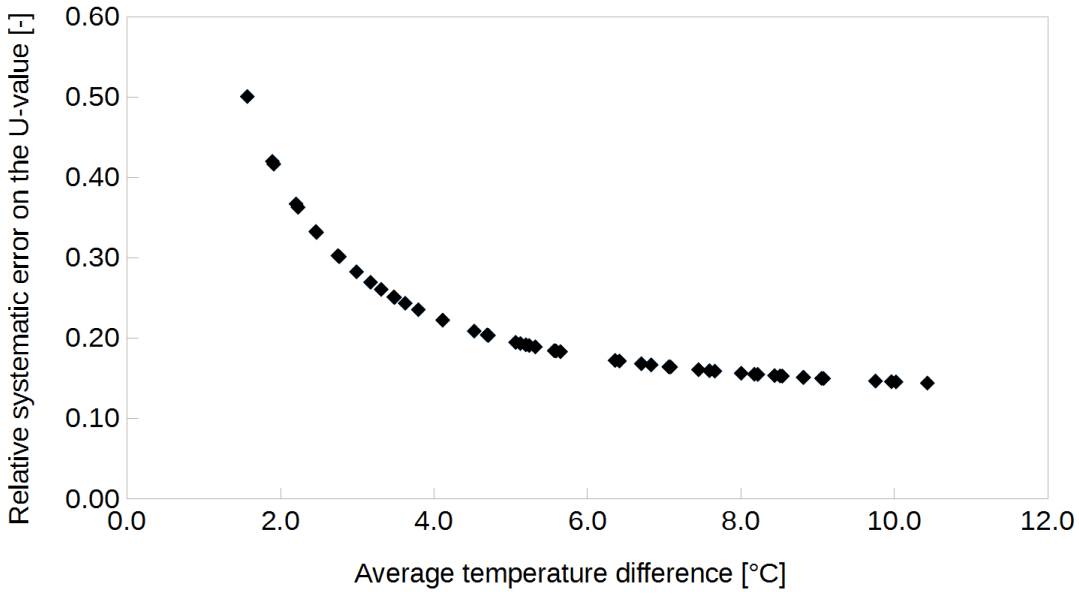

Figure 6.1: Relative systematic error on the U-values of the OWall as a function of the average temperature difference using the AM.

describing the observations. The odds' ratio strongly supported the 2TM model for all fifty-two hypothetical monitoring campaigns. This result confirms and extends the finding of Chapter 5, where the 2TM model was selected for all case studies and data analysis scenarios (*i.e.* higher and lower average temperature difference).

6.2.1.2 *Log-normal priors on the parameters of the lumped thermal mass model*

The analysis undertaken above was repeated adopting log-normal priors on the parameters of the lumped thermal mass models. For each hypothetical monitoring campaign the time series analysed coincided with those investigated in the previous section as their minimum length was defined according to the number of days needed for the AM to stabilise. Table 6.3 on page 197 reports the minimum, maximum, mean and standard deviation of the U-values obtained using the MAP approach and log-normal priors on the parameters of the lumped thermal mass models. The use of log-normal priors showed negligible effect on the U-value estimated at the end of the monitoring period compared to those obtained with uniform priors (Table 6.2 on page 194). The result supports the findings in Section 5.2.2.1 where the log-normal priors improved the evolution of the U-value at the initial stage of the analysis, when few observations were available, while stabilising to the same value as the uniform prior at the end of the monitoring period (Figure 5.8 on page 161 to Table 5.10 on page 162). For each model, the scatter plots of the U-value estimates as a function of the average temperature difference showed a similar trend to those shown for uniform priors; consequently they are not presented for

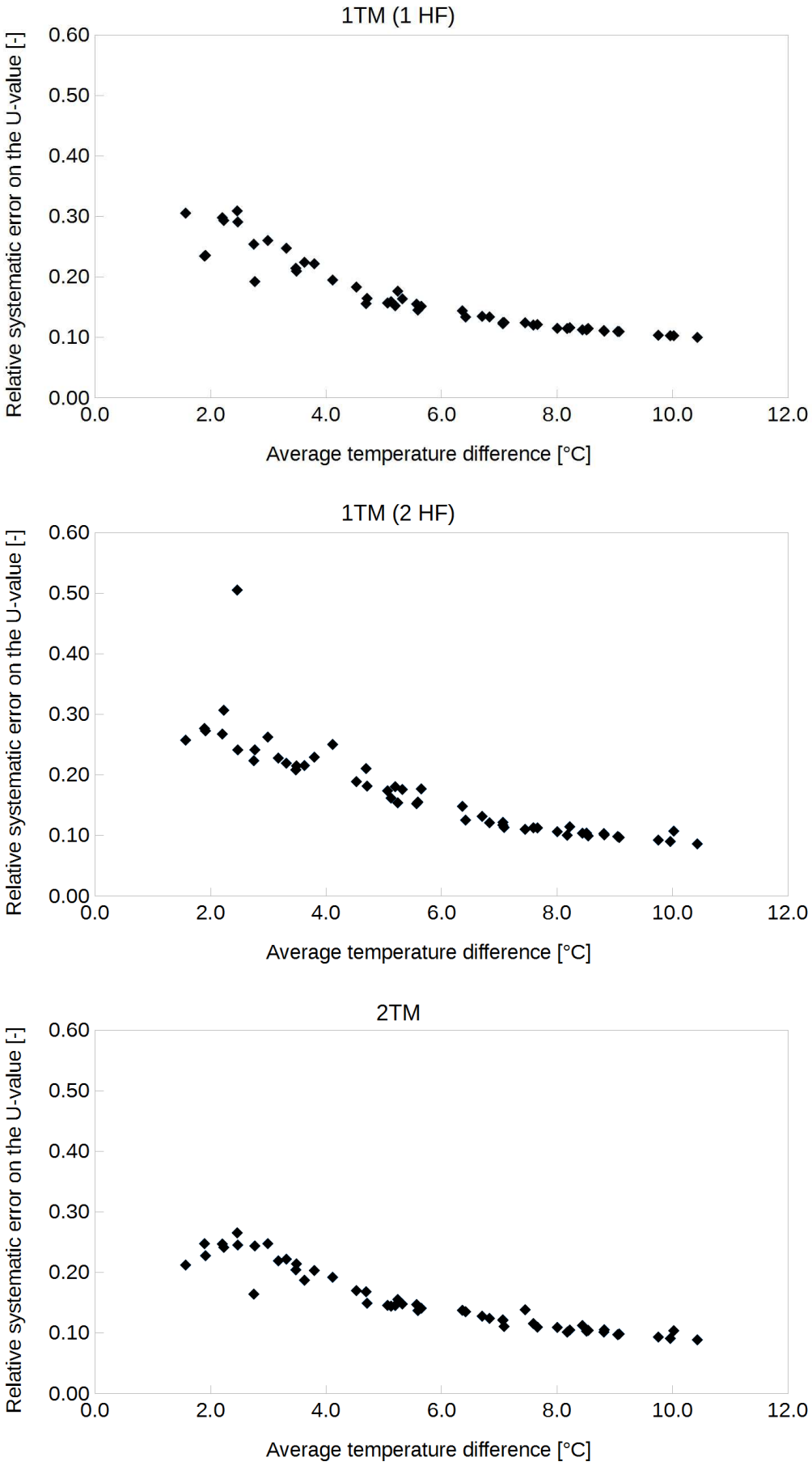

Figure 6.2: Relative systematic error on the U-values of the OWall as a function of the average temperature difference using the lumped-thermal-mass models.

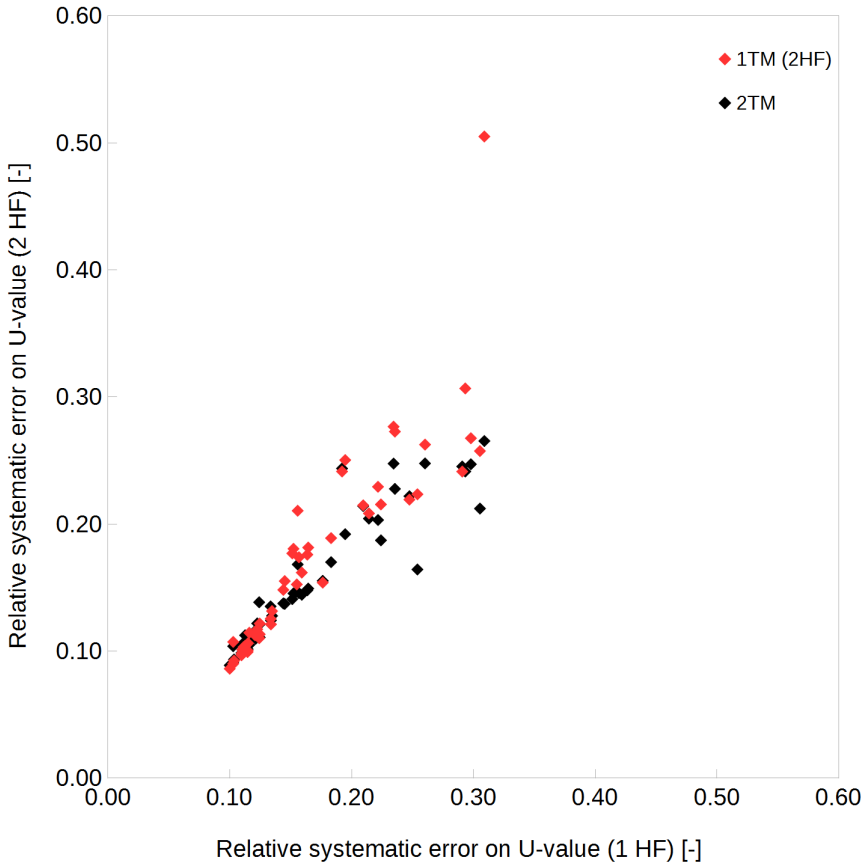

Figure 6.3: Comparison of the relative systematic error on the U-value estimated by the dynamic method optimising one (1TM (1 HF)) and two (1TM (2 HF) and 2TM model) heat flux data streams for the OWall.

		Min	Max	Mean	St Dev	Units
U-value	1TM (1 HF)	1.47	1.99	1.74	0.09	$Wm^{-2}K^{-1}$
	1TM (2 HF)	1.61	2.00	1.77	0.11	$Wm^{-2}K^{-1}$
	2TM	1.60	1.85	1.72	0.07	$Wm^{-2}K^{-1}$
Rel sys err	1TM (1 HF)	10%	38%	17%	7%	-
	1TM (2 HF)	8%	47%	17%	7%	-
	2TM	9%	26%	15%	5%	-

Table 6.3: Minimum, maximum, mean and standard deviation of the U-value estimates for the OWall using fixed-length hypothetical monitoring campaigns.

CLWall	Min	Max	Mean	St Dev	Units
AM	0.52	0.73	0.59	0.04	$Wm^{-2}K^{-1}$
1TM (1 HF)	0.45	0.76	0.57	0.06	$Wm^{-2}K^{-1}$
1TM (2 HF)	0.35	0.65	0.52	0.09	$Wm^{-2}K^{-1}$
2TM	0.58	0.69	0.62	0.03	$Wm^{-2}K^{-1}$

HSWall_N	Min	Max	Mean	St Dev	Units
AM	0.59	1.00	0.71	0.08	$Wm^{-2}K^{-1}$
1TM (1 HF)	0.63	0.79	0.69	0.04	$Wm^{-2}K^{-1}$
1TM (2 HF)	0.47	0.72	0.59	0.08	$Wm^{-2}K^{-1}$
2TM	0.63	0.82	0.70	0.05	$Wm^{-2}K^{-1}$

Table 6.4: Minimum, maximum, mean and standard deviation of the U-value estimates for the CLWall (top) and HSWall_N (bottom), using the average and the dynamic method with the 1TM (1 HF), 1TM (2 HF), 2TM models. The dynamic method used the MAP approach and uniform priors on the parameters of the model.

conciseness. Similarly, the relative systematic error on the U-value estimates using the log-normal priors (Table 6.3 on page 197) were comparable to those obtained above with uniform priors (Table 6.2 on page 194), and their scatter plots as a function of the average temperature difference also presented a similar trend. Model selection confirmed the 2TM model to be the best (compared to the 1TM (2 HF) model) at describing the observed heat transfer across the wall for all hypothetical monitoring campaigns.

6.2.2 *Cavity walls in an occupied and an unoccupied house (CLWall, HSWall_N)*

A similar analysis to that presented for the OWall was repeated for the CLWall and HSWall_N to test the performance of the dynamic method on walls of different construction. Twenty-two hypothetical monitoring campaigns were analysed for the CLWall and twenty-four for the HSWall. The length of each hypothetical monitoring campaign (determined according to the minimum number of days the AM took to stabilise) ranged between three and twenty-two full days for the former case study and between three and twenty-eight days for the latter.

A summary of the minimum, maximum, mean and standard deviation of the U-values for the two cavity walls estimated with the average and dynamic method (using the 1TM (1 HF), 1TM (2 HF) and 2TM models) is presented in Table 6.4 on page 198. Similarly to the results in Chapter 5, the U-values obtained for both case studies were higher than the range ($[0.32, 0.40]$ $Wm^{-2}K^{-1}$) calculated from the literature (Section 5.1.3 and Section 5.1.4). Additionally, the 1TM (2 HF) model had a lower mean than the other methods and models and a large standard deviation.

CLWall	Min	Max	Mean	St Dev
AM	13%	30%	19%	5%
1TM (1 HF)	8%	25%	15%	6%
1TM (2 HF)	6%	24%	13%	5%
2TM	7%	19%	12%	4%

HSWall_N	Min	Max	Mean	St Dev
AM	13%	21%	16%	3%
1TM (1 HF)	8%	18%	12%	3%
1TM (2 HF)	7%	14%	10%	2%
2TM	6%	16%	11%	2%

Table 6.5: Minimum, maximum, mean and standard deviation of the relative systematic error on the U-value for the CLWall and HSWall_N, using the average and the dynamic method with the 1TM (1 HF), 1TM (2 HF), 2TM models.

The ranges of relative systematic error on the U-value for the different approaches and case studies is shown in Table 6.5 on page 199. As previously observed for the OWall, the AM presented the highest minimum and maximum value for the relative systematic error on the U-value in both cases. However, the error ranges were generally smaller for the CLWall and HSWall_N compared to the OWall. The reduction of the systematic error may be ascribed to the use of higher accuracy temperature sensors (Section 4.1.2 and Table 4.1 on page 114) in the former two case studies. Specifically, the thermistors used on the CLWall and HSWall_N had an accuracy of 0.1 °C while the type-T thermocouples installed on the OWall had an accuracy of 0.5 °C.

The relative systematic error on the U-value as a function of the average temperature difference for the AM (Figure 6.4 on page 200) and dynamic method (Figure 6.5 on page 201 and Figure 6.6 on page 202) had comparable behaviour to the OWall, although the error ranges were generally smaller. As previously observed, the relative systematic errors on the U-values tended to increase when the walls were exposed to smaller average temperature difference. This behaviour was observed both for the average (Figure 6.4 on page 200) and dynamic method (Figure 6.5 on page 201 and 6.6). The latter (and the 2TM model in particular) tended to decrease the magnitude of the error.

Model comparison strongly supported the 2TM model both for the CLWall and the HSWall_N case studies, also confirming the findings in Chapter 5 for the two case studies and the results for the OWall. Consequently, the lumped thermal mass model consisting of two thermal masses and three thermal resistances was shown to provide a good description of data collected at all times of the year for all the north-facing case studies, which included building elements of different construction (*i.e.* solid and cavity walls).

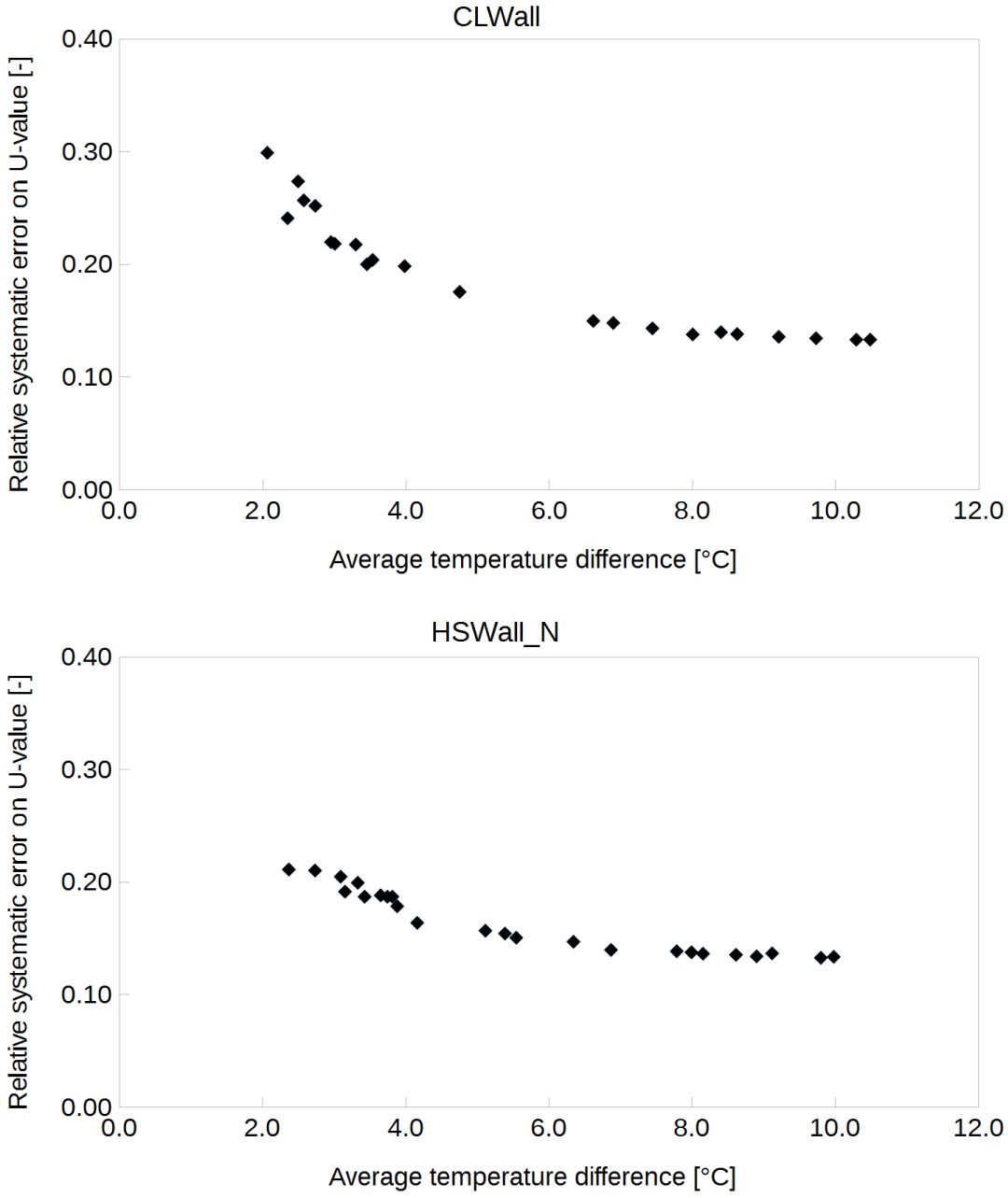

Figure 6.4: Relative systematic error on the U-value (estimated with the AM) as a function of the average temperature difference for the CLWall and HSWall_N. The length of each hypothetical monitoring campaign was based on the number of days needed for the AM to stabilise.

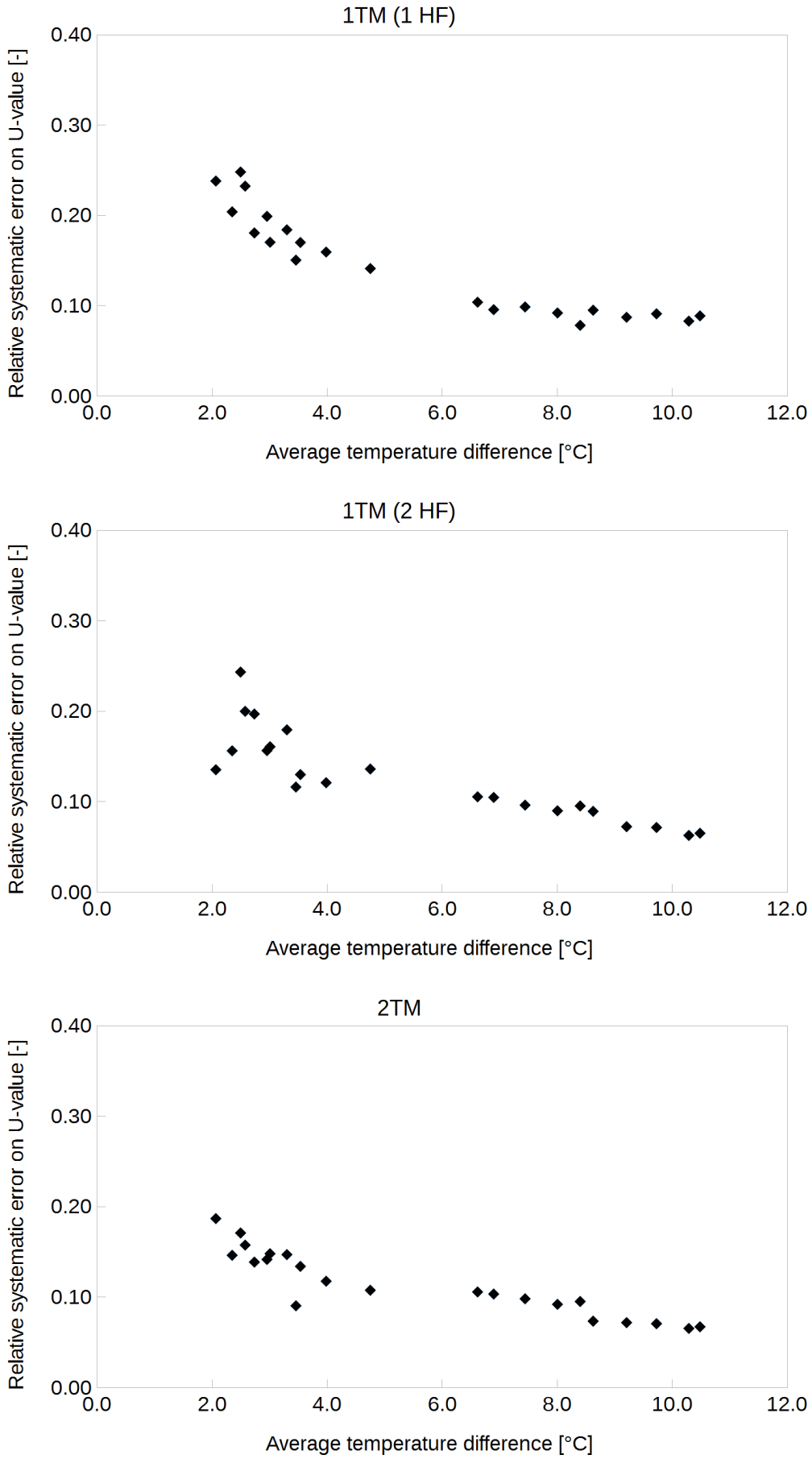

Figure 6.5: Relative systematic error on the U-values of the CLWall as a function of the average temperature difference using the lumped-thermal-mass models. The U-values were estimated using the MAP approach and uniform priors on the parameters of the models.

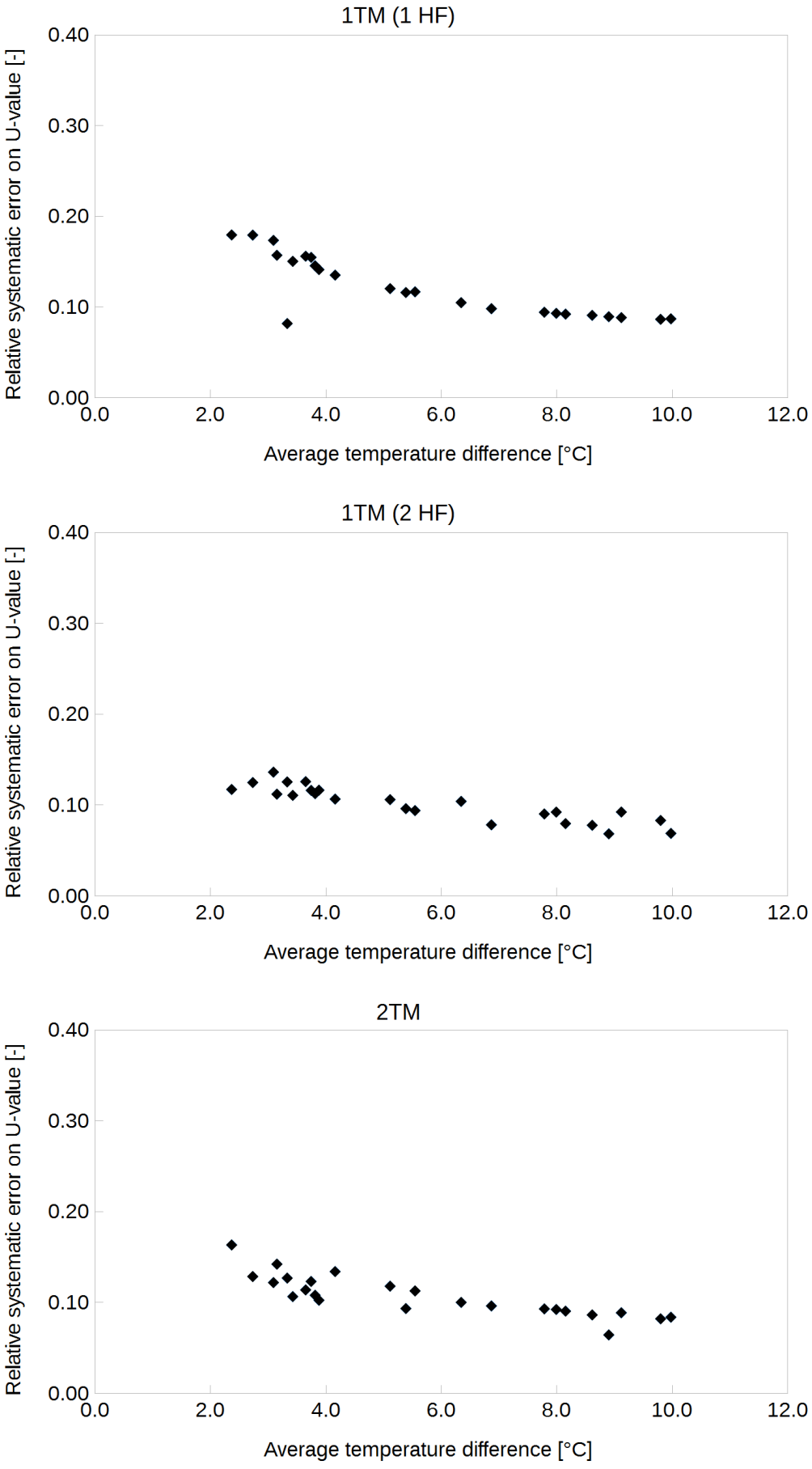

Figure 6.6: Relative systematic error on the U-values of the HSWall_N as a function of the average temperature difference using the lumped-thermal-mass models. The U-values were estimated using the MAP approach and uniform priors on the parameters of the models.

6.3 IMPACT OF THE INTERIOR TO EXTERIOR TEMPERATURE GRADIENT ON THE LENGTH OF MONITORING CAMPAIGNS

The previous section tested the ability of the dynamic method to produce reliable U-value estimates at all times of the year while reducing the associated systematic error compared to the AM. The 2TM model was selected as the best one among the lumped thermal mass models investigated at describing the monitored data.

This section discusses the ability of the dynamic method to shorten the monitoring period throughout the year while returning robust U-values. The 2TM model was used following the work presented in (Chapter 5 and Section 6.2) indicating that this model best describes the available data. Analogously to Section 6.2, the analysis was performed adopting the hypothetical monitoring campaign approach but, rather than using the stabilisation time of the AM for all methods, the length of each time series was independently determined according to the minimum number of observations necessary for each method to stabilise ("second scenario" in Section 4.4) according to the criteria listed in the BS ISO 9869-1 (2014) Standard (listed in Section 2.3.1). For the AM this length has already been determined in Section 6.2 while for the 2TM model the MAP approach was adopted to analyse the data (summarised in Section 6.1). The outcomes for the OWall, CLWall and HSWall_N case studies are presented in the following sections.

6.3.1 *Solid wall in an office building (OWall)*

From the time series collected on the OWall (Table 6.1 on page 192), of the fifty-five potential hypothetical monitoring campaigns, all met the acceptance criteria described in Section 6.1 for the dynamic method (both using uniform and log-normal priors on the model's parameters) while fifty-two did so for the AM. The length of the time series so obtained spanned between three and thirty days for the AM and between three and twenty days for the 2TM model. Note that a minimum length of three days was required by the BS ISO 9869-1 (2014) Standard (Section 2.3.1), although this may be potentially overestimating the minimum number of observations needed for the dynamic method to stabilise (as discussed in Section 4.4 and Section 5.2.2). However, due to the lack of a standardised method for the determination of the minimum number of observations to be analysed with the dynamic method, this work applied the same stabilisation criteria prescribed for the AM to the dynamic analysis as a conservative approach (as discussed in Section 4.4).

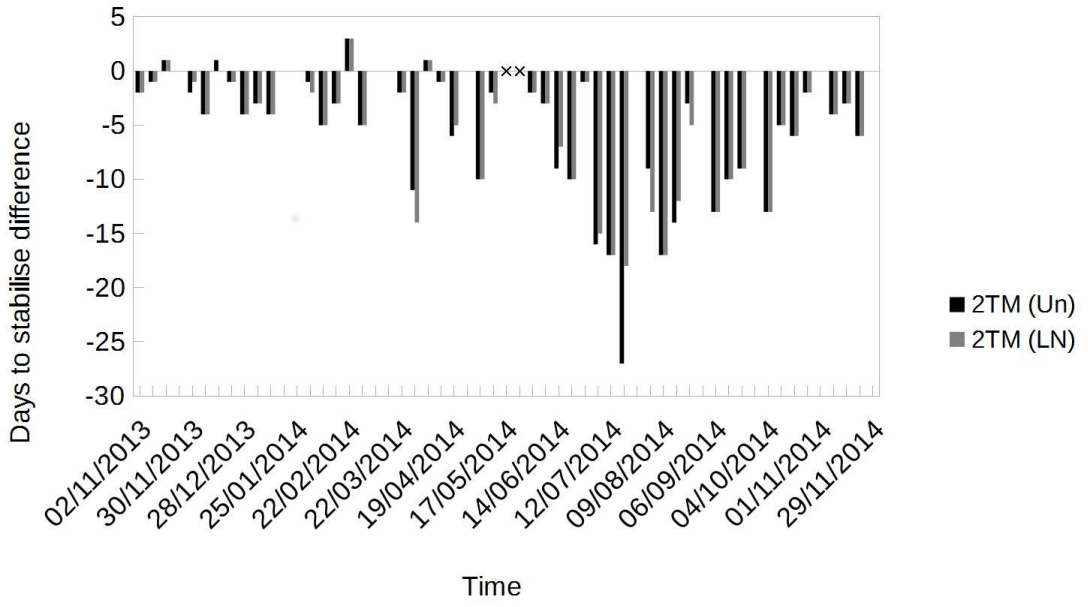

Figure 6.7: Difference between the length of the hypothetical monitoring campaign (in days) required by the 2TM model and the AM model to stabilise for the OWall. Negative values indicate that the 2TM model was quicker to stabilise than the AM, while the crosses mark a period of missing data. The dynamic analysis used the MAP approach and both uniform (Un) and log-normal (LN) priors on the parameters of the model.

LENGTH OF HYPOTHETICAL MONITORING CAMPAIGNS OVER THE MONITORED PERIOD

Figure 6.7 on page 204 presents a comparison of the length of each monitoring campaign for the dynamic (both using uniform and log-normal priors on the parameters of the 2TM model) and average method, which clearly shows that the former generally reduced the stabilisation period throughout the year. For the three hypothetical monitoring campaigns where the AM did not meet the acceptance criteria described in Section 6.1 (but the 2TM model did), either the maximum number of days before missing data or thirty days were considered to produce Figure 6.7 on page 204.

Given the seasonal pattern observed in Figure 6.7 on page 204, the length of the hypothetical monitoring campaigns for both the AM and the 2TM model was analysed as a function of the average temperature difference observed during each monitoring period to investigate whether seasonality and temperature differences may have affected the stabilisation of the estimates. Figure 6.8 on page 206 (top graph) shows that the minimum length of the hypothetical monitoring campaigns for the AM was always below ten days when the average temperature difference was above 6 °C, while a broader range was observed for smaller average temperature differences. Additionally, below 5 °C temperature difference the hypothetical monitoring campaigns never stabilised within three days. Conversely, the 2TM always stabilised within one week of data when the average temperature difference was above 4 °C (Figure 6.8 on page 206, bottom graph). Fur-

thermore, unlike the AM, three full days of data were sufficient for the 2TM model to stabilise also with small temperature differences.

Although the average temperature difference is a metric commonly used in the context of *in-situ* measurements, it does not describe the variability of the temperature (and consequently the rate of change of the boundary conditions) during that period, as it might be appropriate for a dynamic method. For example, the length of the survey may not only be influenced by small temperature differences but also by the extent of the temperature variation in relation to the average temperature difference observed during the survey, which may imply that the heat flux direction has reverted. To account for the variability of the observations, the coefficient of variation (CoV) of the temperature differences[3] is used in this thesis as a metric to investigate the minimum number of observations for each hypothetical monitoring campaign. The CoV (also known as "relative standard deviation") is defined as:

$$\mathrm{CoV} = \frac{\sigma_{\Delta T}}{\overline{x}_{\Delta T}} \tag{6.1}$$

where $\sigma_{\Delta T}$ is the standard deviation of the time series of temperature differences during the monitoring period analysed; $\overline{x}_{\Delta T}$ is the sample mean of the same time series. Consequently, a large CoV indicates that the variation of the temperature differences over time (*e.g.*, due to diurnal oscillations) were large compared to the average temperature difference over the monitoring period. The scatter plot of the length of the hypothetical monitoring campaigns as a function of the coefficient of variation (Figure 6.9 on page 207) for the AM shows that the length of the survey was always below ten days when the coefficient of variation of the temperature differences was smaller than 0.3, meaning that the average temperature difference was larger than daily oscillation. Additionally, the minimum stabilisation period of three days was never achieved when the coefficient of variation was higher than 0.5. A similar graph plotting the minimum number of days to stabilise as a function of the coefficient of variation for the 2TM model (Figure 6.10 on page 208) shows that the dynamic approach is more robust to temperature changes over the monitoring period. Specifically, the length of the monitoring period was generally below seven days when the coefficient of variation was below 1 (within this range, thirteen days were required only on one occasion).

EVOLUTION OF U-VALUE AND SYSTEMATIC ERROR OVER THE MONITORED PERIOD

A summary of the U-value estimates obtained with the AM and 2TM model is shown

3 In the following the "coefficient of variation of the temperature differences" is also referred to as "coefficient of variation" for conciseness.

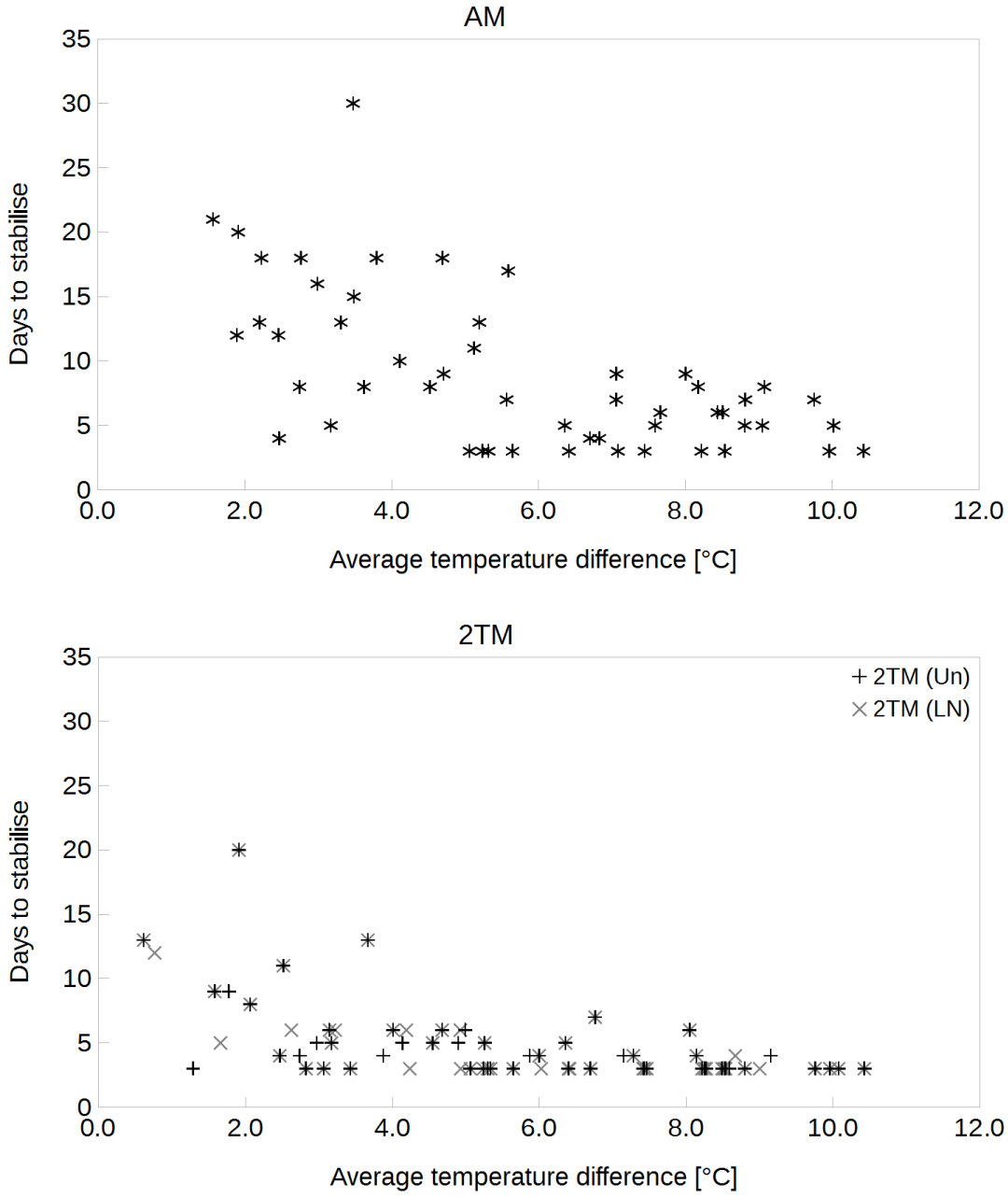

Figure 6.8: Length of the hypothetical monitoring campaign (according to the AM and 2TM model) as a function of the average temperature difference for the OWall. The dynamic method used the MAP approach and uniform (Un) or log-normal (LN) priors on the parameters of the model.

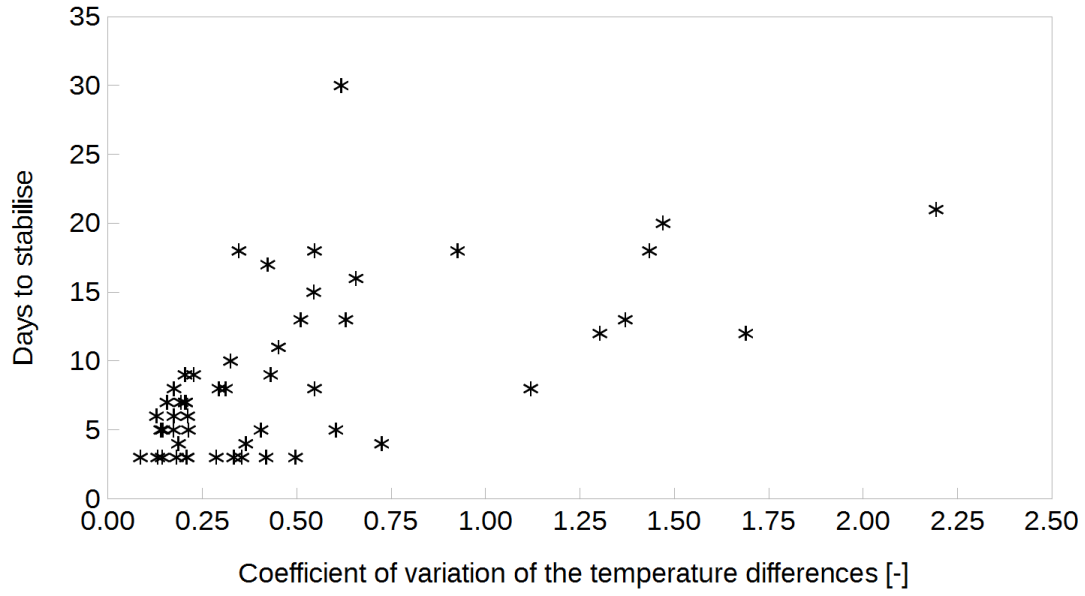

Figure 6.9: Length of the hypothetical monitoring campaign according to the AM as a function of the coefficient of variations of the temperature differences for the OWall.

in Table 6.6 on page 209 (note that for the AM the U-values presented are the same as those shown in Table 6.2 on page 194). Further insights into the thermophysical parameter estimates using the 2TM model (using the MCMC approach) are presented in Section 6.4. The mean U-value (Table 6.6 on page 209) estimated by the 2TM (either with uniform or log-normal priors on the parameters) using the shortened hypothetical monitoring campaigns defined according to the second scenario (Section 4.4) do not differ significantly from the mean U-value (Table 6.2 on page 194 and Table 6.3 on page 197) estimated by the same model on the longer hypothetical monitoring campaigns determined according to number of days required by the AM to stabilise ("first scenario" in Section 4.4). All U-values were within the margin of the systematic error, and the 2TM model (with both type of priors) reduced the mean relative systematic error by 47% compared to the AM (Table 6.6 on page 209). The use of the 2TM model reduced the variability of the estimates compared to the AM and in particular the use of log-normal priors showed the smallest standard deviation of the U-value. The U-value estimated with the AM (Figure 6.11 on page 210, top graph) and the 2TM model (Figure 6.11 on page 210, bottom graph) showed a similar trend as a function of the average temperature difference. Conversely, in both cases the U-value estimates presented a higher dispersion around its mean value as the coefficient of variation increases (Figure 6.12 on page 211, Figure 6.13 on page 212), suggesting that the coefficient of variation is a better indicator of difficulty faced by the data analysis methods. In fact, a higher coefficient of variation

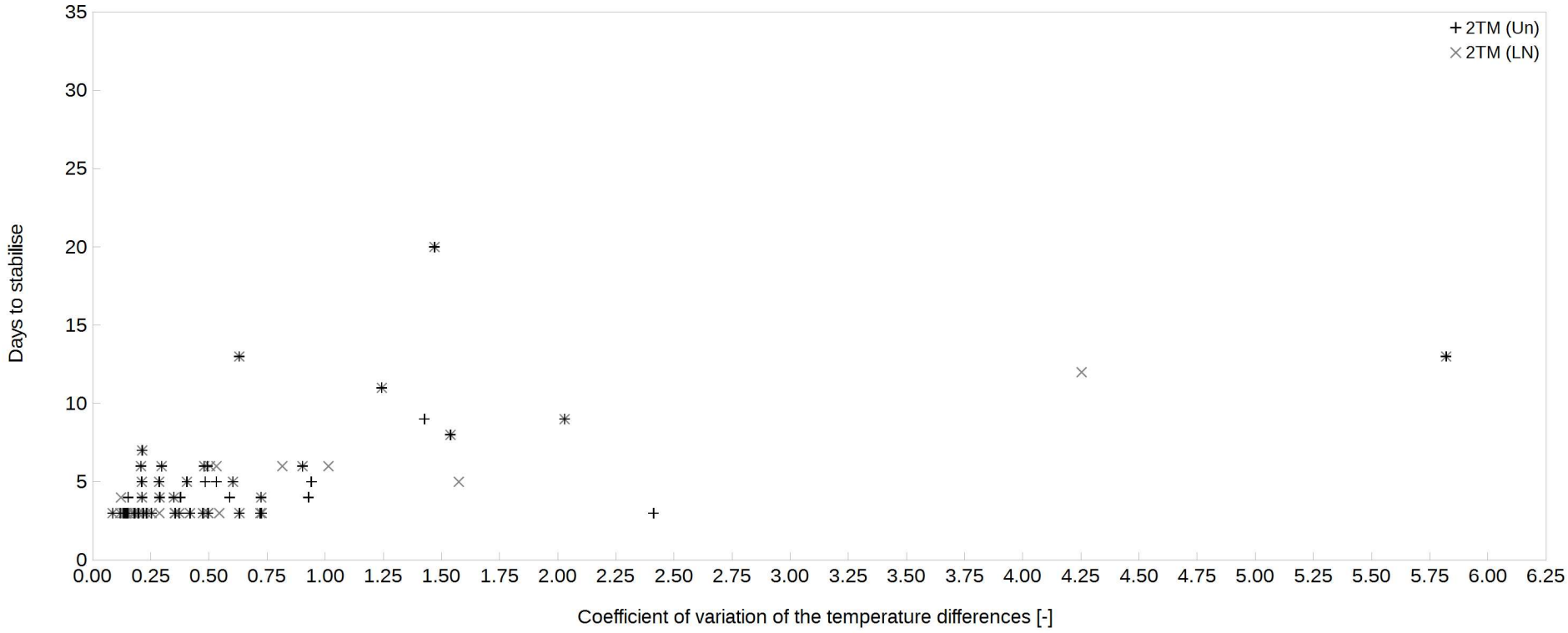

Figure 6.10: Length of the hypothetical monitoring campaign according to the 2TM model as a function of the coefficient of variation of the temperature differences for the OWall. The number of days to stabilise was determined using the MAP approach and the 2TM model with uniform (Un) and log-normal (LN) priors on its parameters.

		Min	Max	Mean	St Dev	Units
U-value	AM	1.28	1.92	1.71	0.14	$Wm^{-2}K^{-1}$
	2TM (Un)	1.35	1.90	1.73	0.10	$Wm^{-2}K^{-1}$
	2TM (LN)	1.43	1.87	1.72	0.08	$Wm^{-2}K^{-1}$
Rel sys err	AM	14%	50%	22%	8%	-
	2TM (Un)	8%	31%	15%	6%	-
	2TM (LN)	8%	32%	15%	6%	-

Table 6.6: Minimum, maximum, mean and standard deviation of U-value and relative systematic error estimates for the OWall using the average and the dynamic method with the 2TM model. The dynamic method used the MAP approach and both uniform (Un) and log-normal (LN) priors on the parameters of the model.

is often associated with large daily swings and an average temperature difference close to zero.

A further analysis was undertaken to compare the U-values estimated in this section by the 2TM (either with uniform or log-normal priors on the parameters) using the shortened hypothetical monitoring campaigns defined according to the second scenario (Section 4.4) and those estimated by the same model on the longer hypothetical monitoring campaigns determined according to number of days required by the AM to stabilise ("first scenario" in Section 4.4). The comparison (Figure 6.14 on page 213) showed that although a considerable reduction in the length of the hypothetical monitoring campaigns was observed, especially during the spring and summer periods, the reduced number of observations analysed did not considerably affect the U-value estimated using the 2TM model (with either uniform and log-normal prior on the parameters). Specifically, Figure 6.14 on page 213 shows the probability density of the relative discrepancy between the U-value estimated by the 2TM model on the shorter hypothetical monitoring campaigns compared to that estimated on longer ones (as in Section 6.2.1). The graphs showed that the U-value discrepancies were generally smaller than 5% both using uniform and log-normal priors on the parameters of the model.

6.3.2 *Cavity walls in an occupied and an unoccupied house (CLWall, HSWall_N)*

From the time series collected on the HSWall_N (Table 6.1 on page 192) twenty-four hypothetical monitoring campaigns were possible, and all met the acceptance criteria described in Section 6.1 both for the AM and the 2TM model. Similarly, twenty-five hypothetical monitoring campaigns were possible for the CLWall, of which twenty-four met the acceptance criteria in Section 6.1 for the dynamic and twenty for the average method. Note that the only hypothetical monitoring campaign that did not meet the

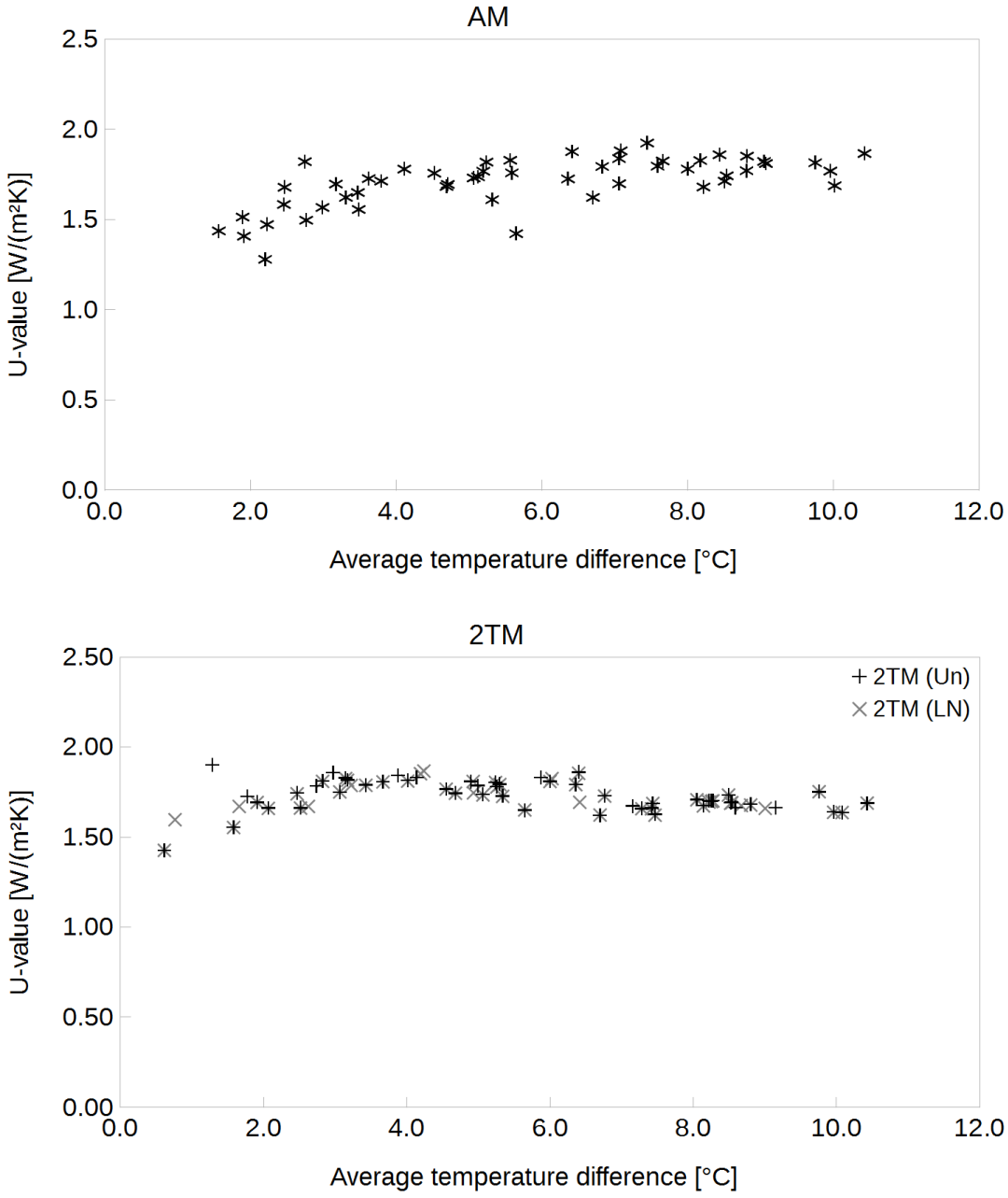

Figure 6.11: U-value estimates as a function of the average temperature difference for the AM and the 2TM model for the OWall. The dynamic analysis used the MAP approach and the 2TM model with uniform (Un) and log-normal (LN) priors on its parameters.

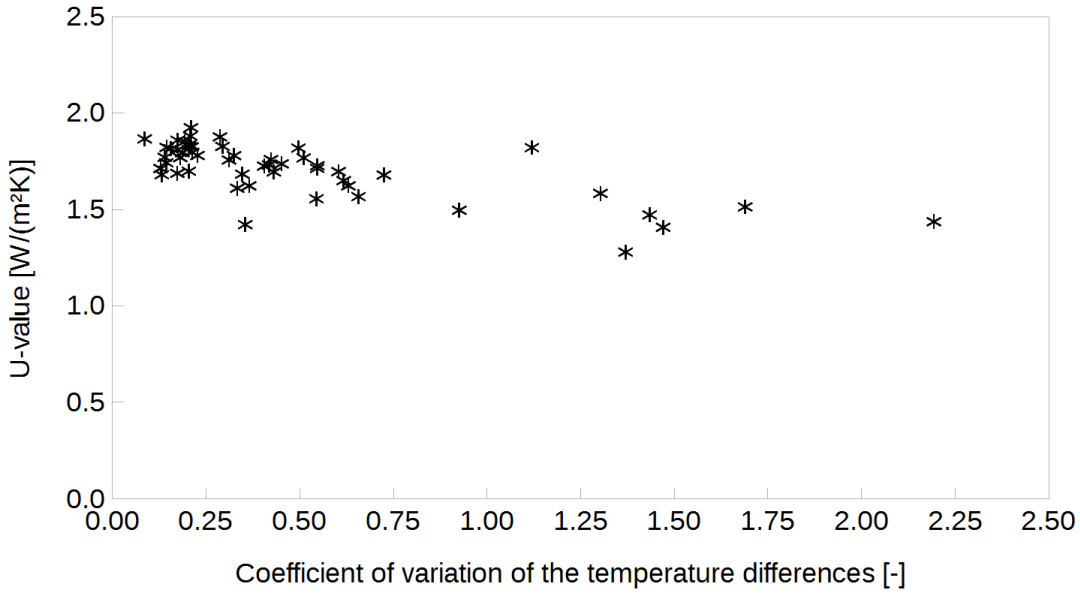

Figure 6.12: U-value estimates as a function of the coefficient of variation of the temperature differences for the AM for the OWall.

criteria for the 2TM model corresponded to one of those that were excluded from the AM as well.

LENGTH OF HYPOTHETICAL MONITORING CAMPAIGNS OVER THE MONITORED PERIOD

The reduction in the length of each monitoring campaign using the 2TM model compared to the AM is shown in Figure 6.15 on page 214, for both case studies. In all cases the 2TM model was quicker to stabilise than the AM throughout the monitoring period, supporting the results obtained for the OWall (Figure 6.15 on page 214). Similarly to the OWall, for the four hypothetical monitoring campaigns of the CLWall where the AM did not meet the acceptance criteria described in Section 6.1 (but the 2TM model did) a limit of thirty days was applied to produce the plots. Since the difference in the number of days taken to stabilise seemed to increase towards the warm period (similarly to the outcomes from the OWall) for both case studies, the length of the hypothetical monitoring campaigns was investigated as a function of the average temperature difference and the coefficient of variation of the temperature differences observed during the monitoring period. Figure 6.16 on page 215 shows that for the AM (top graph) the CLWall stabilised within three days of data only for high average temperature difference (above 8 °C); this was not the case for the HSWall, where the AM stabilised within three and nine days when the average temperature difference was above 4 °C. Conversely, with the 2TM model (Figure 6.16 on page 215, bottom graph) both case studies stabilised within three days for average temperature differences just above 2 °C for the CLWall and above

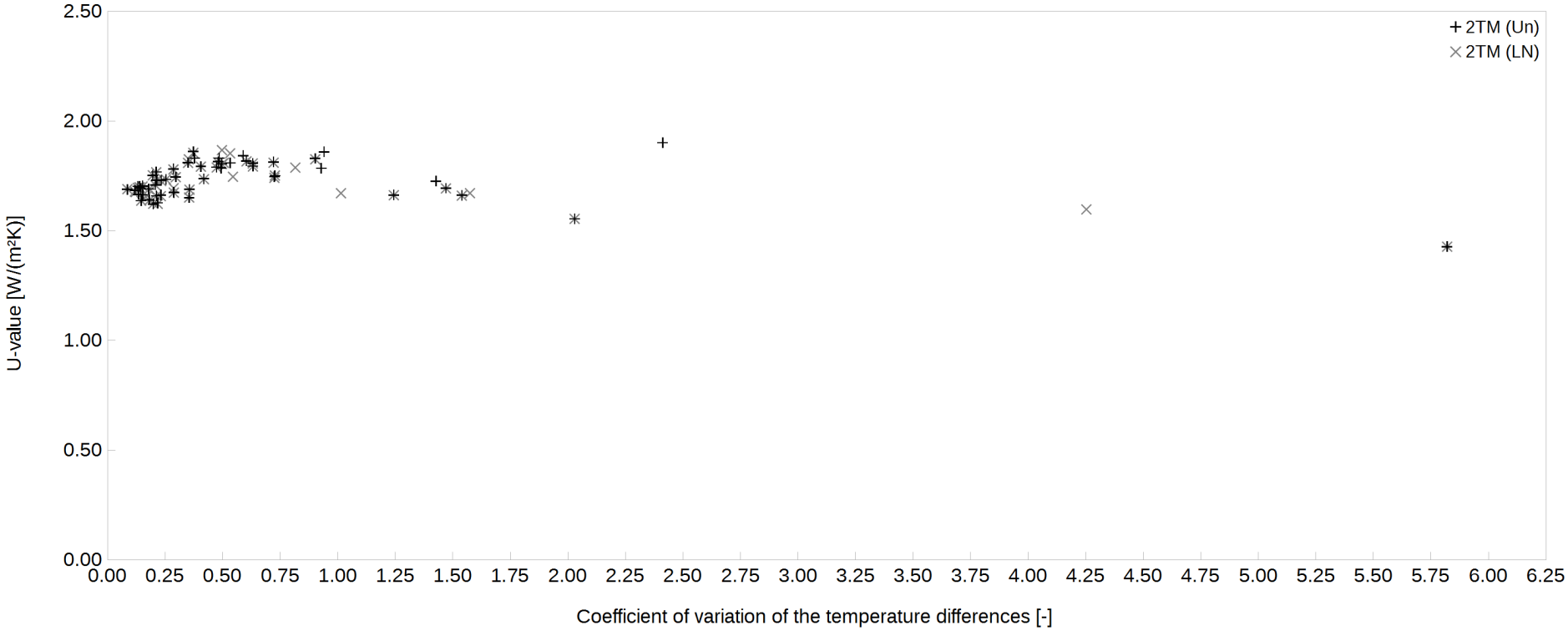

Figure 6.13: U-value estimates as a function of the coefficient of variation of the temperature differences for the 2TM model for the OWall.

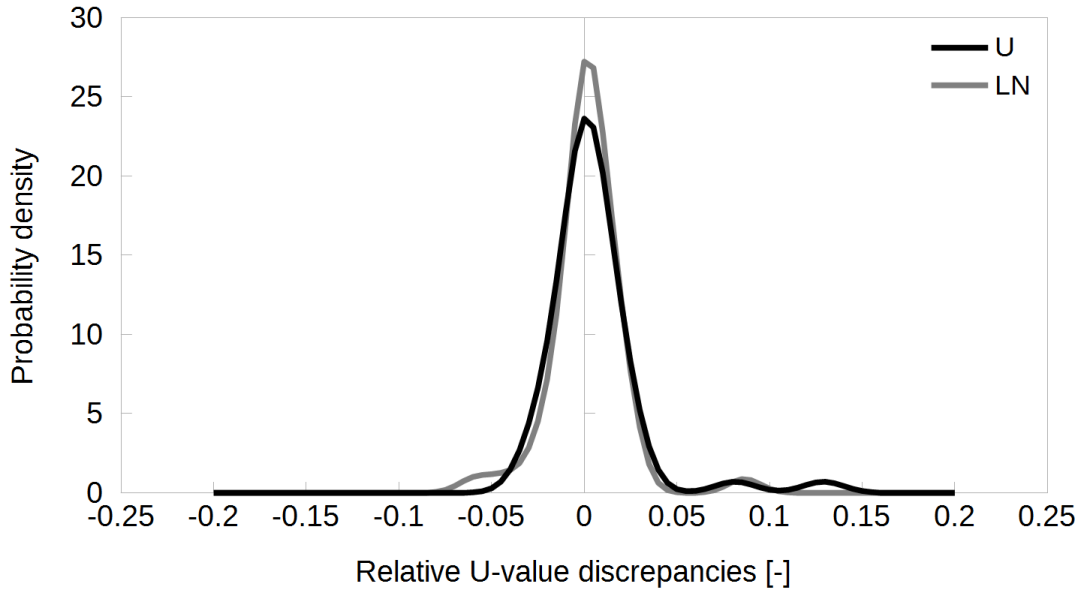

Figure 6.14: Probability density of the relative discrepancies between the U-values estimated by the 2TM model using hypothetical monitoring campaigns determined according to the minimum number of observations required according to the 2TM and the AM to stabilise. The plot shows the OWall case study. The U-values were estimated with the MAP approach with uniform (Un) and log-normal (LN) priors on the parameters of the 2TM model. The probability density function was estimated using kernel density estimation with bandwidth determined according to Silverman's rule of thumb (Silverman, 1986).

3 °C for the HSWall. Additionally, in both case studies the length of the hypothetical monitoring campaigns was always below five days for the 2TM model for average temperature differences as low as 4 °C, while below this threshold the maximum number of days taken to stabilise was eight at most.

An analysis of the length of the hypothetical monitoring campaign as a function of the coefficient of variation (Figure 6.16 on page 215) showed that, unlike the AM, the 2TM model stabilised within three days for coefficients of variation up to 1.25 for both case studies. This result suggests that the dynamic method is able to model periods where the observations are very variable during the monitoring survey. Additionally, the number of days to stabilise were always below four for coefficients of variations below 0.50.

EVOLUTION OF U-VALUE AND SYSTEMATIC ERROR OVER THE MONITORED PERIOD

A summary of the statistics for the U-values and relative systematic errors estimated by AM and the 2TM model is shown in Table 6.7 on page 216 (note that for the AM the U-values are the same as those shown in Table 6.2 on page 194). Further insights into the thermophysical parameter estimates using the 2TM model is presented in Section 6.4. For the HSWall, the mean U-value for the AM and 2TM model was in close agreement

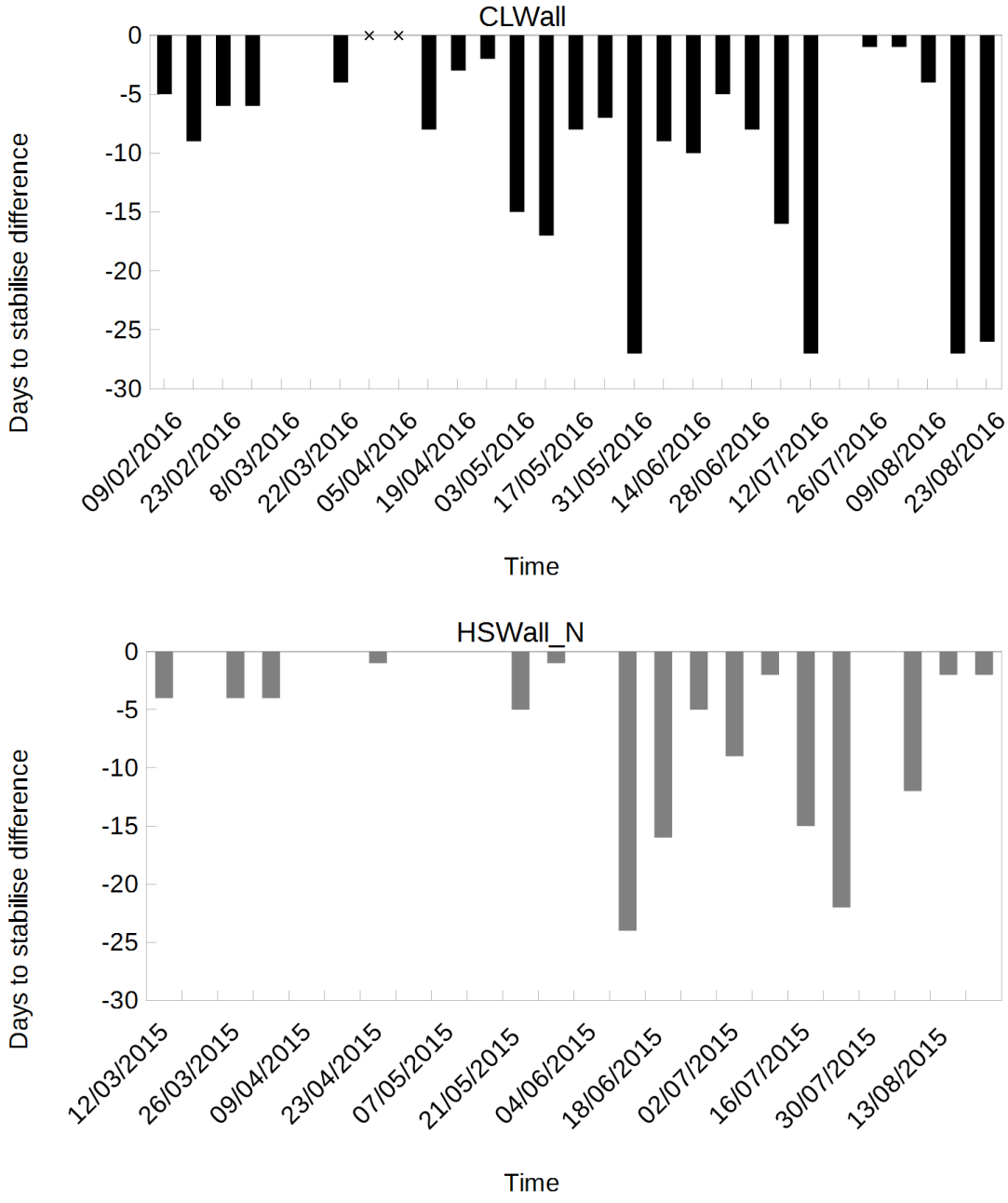

Figure 6.15: Difference between the length of the hypothetical monitoring campaign (in days) required by the 2TM model and by the AM model to stabilise for the CLWall and the HSWall_N. Negative values indicate that the 2TM model was quicker to stabilise than the AM, while the crosses mark a period of missing data. The dynamic analysis used the MAP approach and both uniform priors on the parameters of the model.

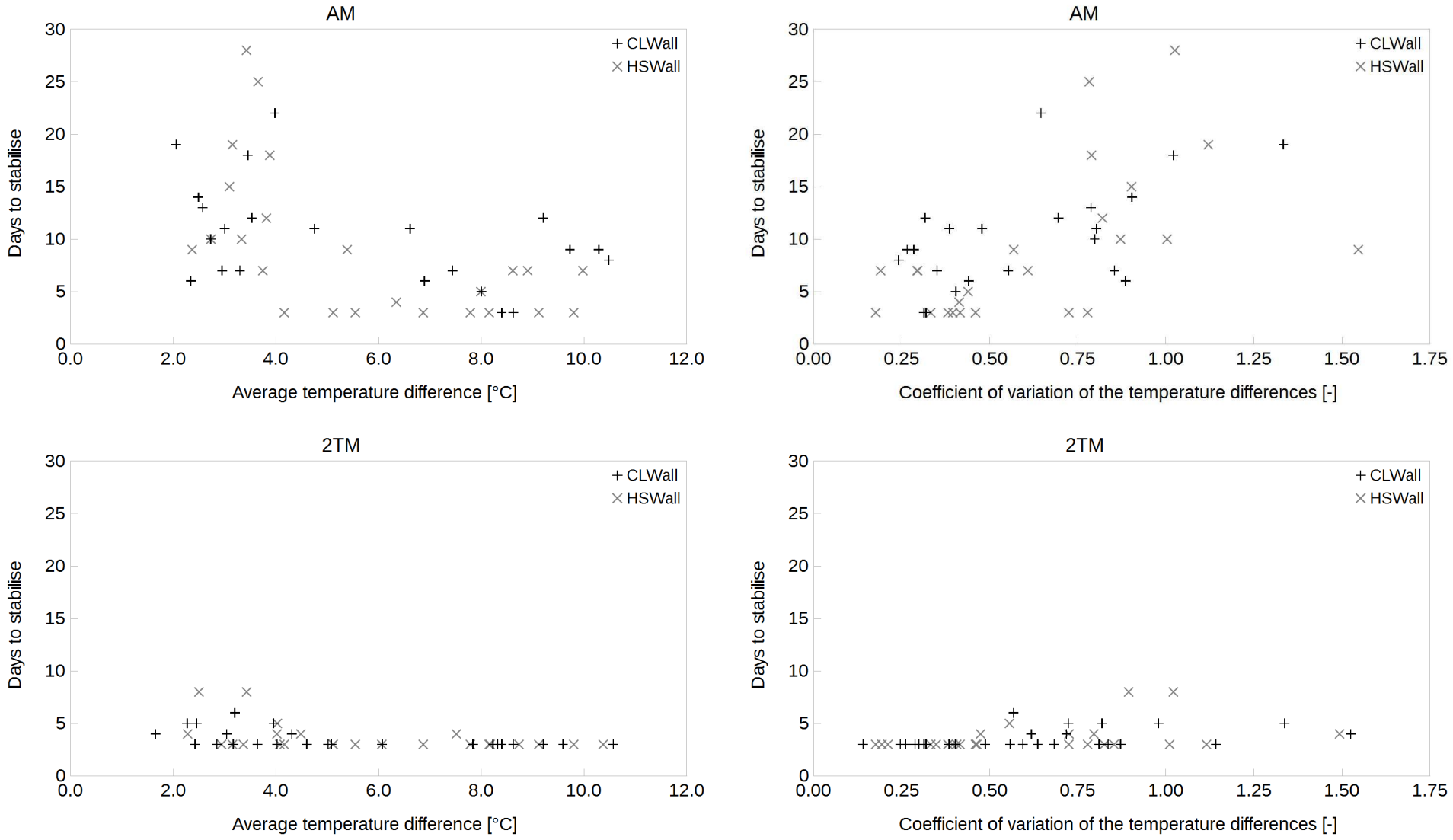

Figure 6.16: Length of the hypothetical monitoring campaign according to the AM and the 2TM model for the CLWall and HSWall_N. The minimum number of days to stabilise is shown as a function of the average temperature difference and the coefficient of variation of the temperature differences.

	CLWall	Min	Max	Mean	St Dev	Units
U-value	AM	0.52	0.73	0.59	0.04	$Wm^{-2}K^{-1}$
	2TM	0.56	0.70	0.63	0.05	$Wm^{-2}K^{-1}$
Rel sys err	AM	13%	30%	19%	5%	-
	2TM	7%	31%	13%	5%	-

	HSWall_N	Min	Max	Mean	St Dev	Units
U-value	AM	0.59	1.00	0.71	0.08	$Wm^{-2}K^{-1}$
	2TM	0.64	0.82	0.70	0.05	$Wm^{-2}K^{-1}$
Rel sys err	AM	13%	21%	16%	3%	-
	2TM	7%	14%	10%	2%	-

Table 6.7: Minimum, maximum, mean and standard deviation of U-value and relative systematic error estimates for the CLWall (top table) and HSWall_N (bottom table) using the average and the dynamic method with the 2TM model. The dynamic method used the MAP approach and uniform priors on the parameters of the model.

although, as previously observed for the OWall, the dynamic method helped reduce the variability of the estimates. Conversely, the U-value estimates for the CLWall had comparable variability but the mean U-values presented a discrepancy of about 7%. For each case study, the mean U-value was comparable with the estimate obtained for longer hypothetical monitoring campaigns (Table 6.2 on page 194), and all U-value estimates were within the margin of the systematic error. The 2TM model decreased the mean relative systematic error by 46% for the CLWall and 60% for the HSWall_N compared to the AM, while the standard deviation of the error estimates was comparable between the two methods (Table 6.2 on page 194).

An analysis of the U-values as a function of the average temperature difference and the coefficient of variation for both case studies is shown in Figure 6.17 on page 217. The graphs show that for each case study the estimates were almost constant throughout the monitoring period, both in respect to the average temperature difference and the coefficient of variation.

Similarly to the OWall case study, Figure 6.18 on page 219 investigates the impact of the reduction of the length of the monitoring period on the U-value estimates using the 2TM model. Specifically, the graph compares the 2TM U-values estimated using the shortened hypothetical monitoring campaigns defined according to the second scenario (Section 4.4) and those estimated by the same model on the longer hypothetical monitoring campaigns determined according to number of days required by the AM to stabilise ("first scenario" in Section 4.4). The plots show that the reduction of the monitoring length generally had a small impact on the U-value estimates. The discrepancies were

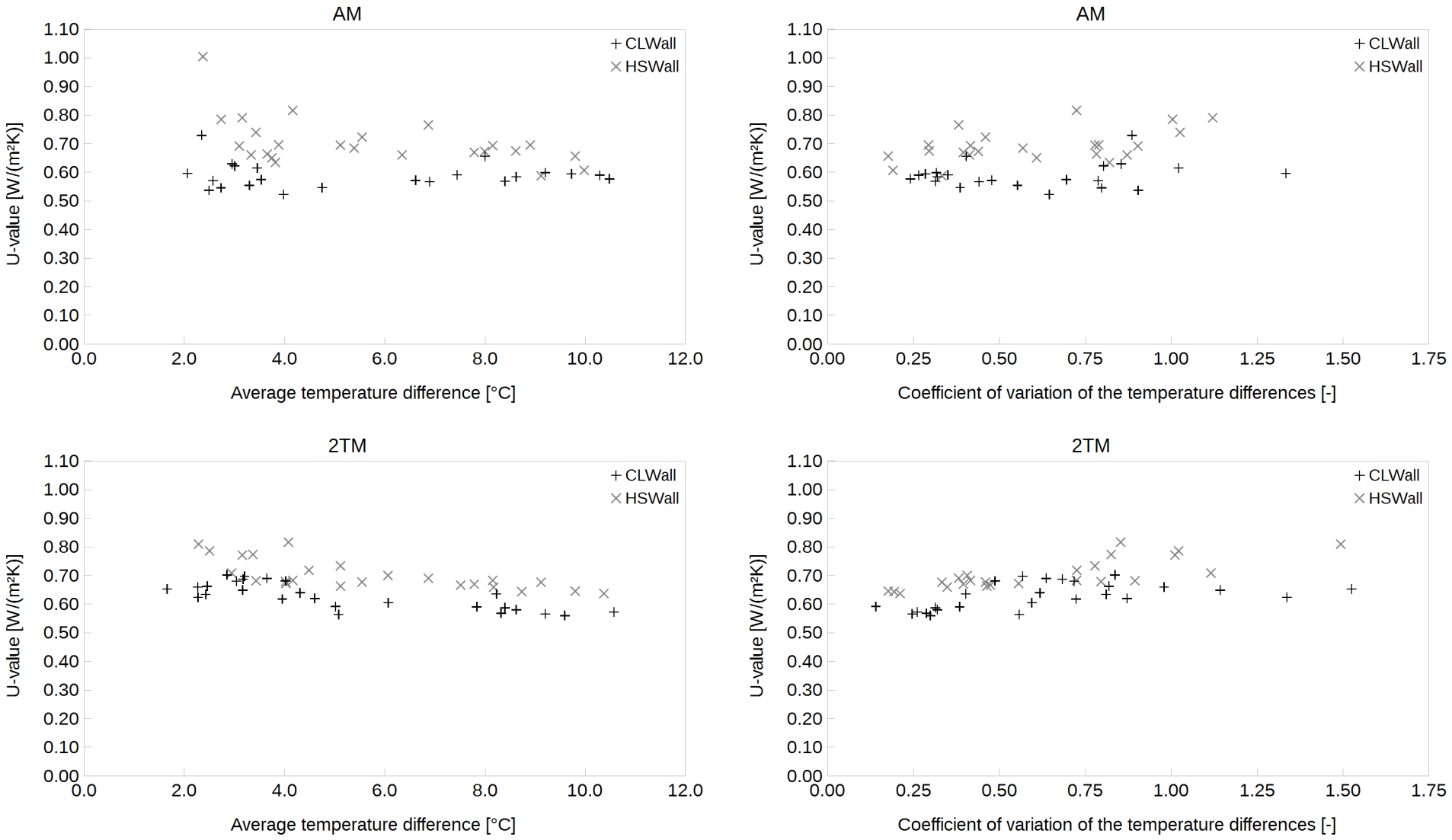

Figure 6.17: U-value estimates from the AM and the 2TM model for the CLWall and HSWall_N. The U-values are shown as a function of the average temperature difference and the coefficient of variation of the temperature differences.

more probable between -5% and 10% for the CLWall and less than ±5% on the HSWall_N.

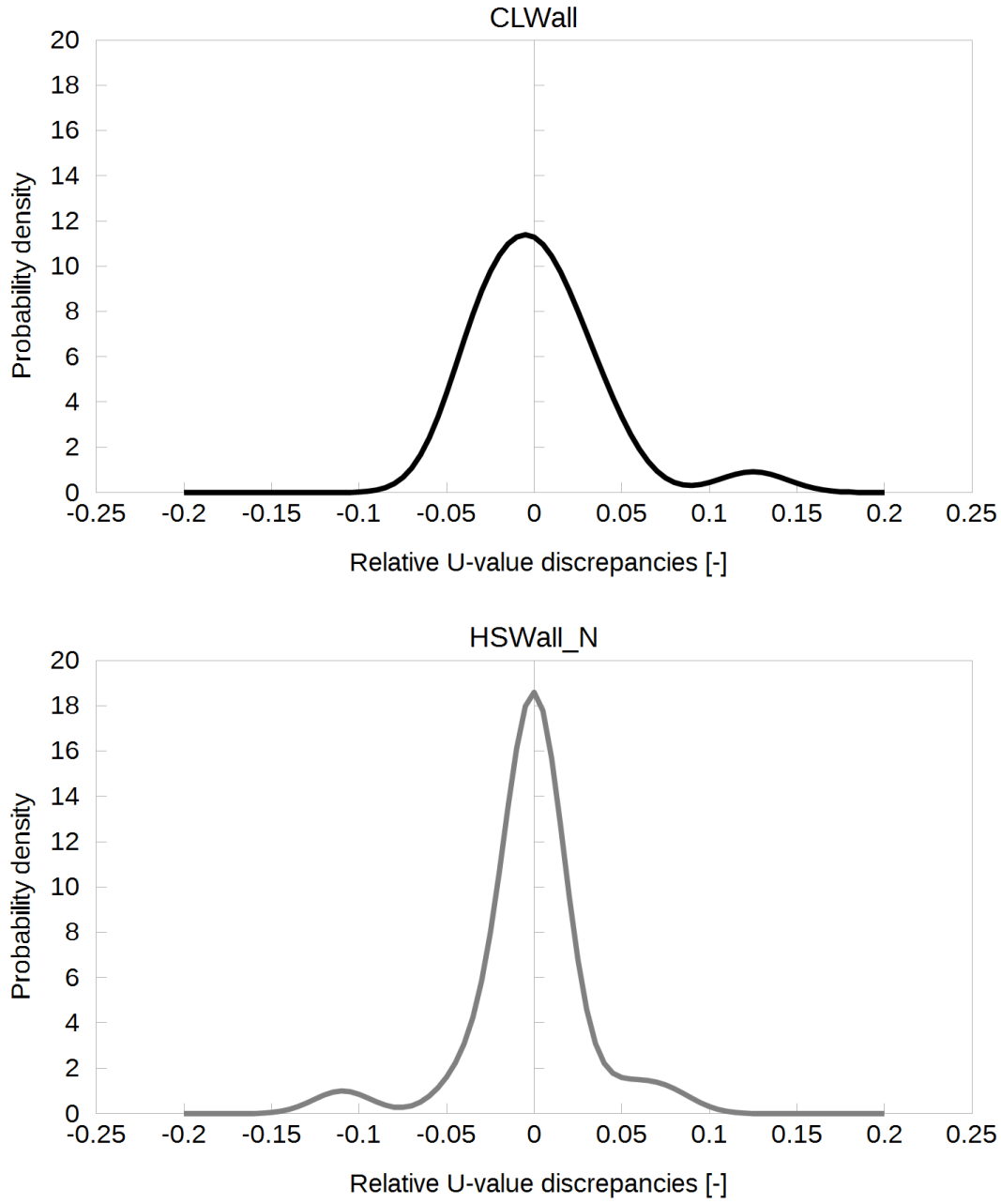

Figure 6.18: Probability density of the relative discrepancies between the U-values estimated by the 2TM using hypothetical monitoring campaigns determined according to the minimum number of observations required by the 2TM model and the AM to stabilise. The plots show the CLWall and HSWall case studies. The U-values were estimated with the MAP approach with uniform priors on the parameters of the model. The probability density function was estimated using kernel density estimation with bandwidth determined according to Silverman's rule of thumb (Silverman, 1986).

6.4 BAYESIAN CHARACTERISATION OF THE THERMAL STRUCTURE OF WALLS AT ALL TIMES OF THE YEAR

Section 6.3 investigated the ability of the 2TM model to shorten the length of *in-situ* monitoring campaigns undertaken at all times of the year, while robustly characterising the thermophysical properties of the elements investigated. For a comparison of the performance of the average and dynamic methods, the U-values for each hypothetical monitoring campaign were presented. All estimates were within the margin of the systematic error throughout the year, and the dynamic method with the 2TM model showed a reduction of the systematic error between 46% and 60% depending on the case study.

Since the dynamic method does not only characterise the total R- or U-value but also the lumped thermophysical properties of the model, the evolution of these parameters was investigated over the monitored period[4]. Figure 6.19 on page 221 shows the values of the three lumped thermal resistances and the R-value (*i.e.* the sum of the three resistances) of the OWall for each hypothetical monitoring campaign presented in Section 6.3.1. The graphs show that during the winter the R-value was generally stable, while the lumped thermal resistances (R_1 and R_2 in particular) were variable from one hypothetical monitoring campaign to the next one. The observed behaviour may be indicating either a short-term physical phenomenon affecting the thermal characteristics of the building element or some artefact in the estimation process affecting the individual parameters but not the total value. The MCMC approach was used to further investigate this aspect, given its ability to estimate the full probability distribution of the parameters of the models (as discussed in Section 3.4.3.2) and characterise the thermal structure of building elements (as shown in Chapter 5). The corner plots obtained during the winter period (Figure 6.20 on page 222 presents a representative example) showed a negative correlation among the lumped thermal resistance estimates (*i.e.* the axis of the posterior probability distributions of the lumped R_s were not aligned with the Cartesian axis), indicating that the model could identify several similarly probable combinations for the the magnitude of the estimates of individual R_s leading to the same R-value (*e.g.*, as observed, a decrease in R_1 tended to be compensated by an increase in R_2). The result, supporting the findings in Chapter 5, can be interpreted in the light of the known physical structure as previously discussed. Specifically, given the similar thermophysical properties of the materials constituting the solid wall, the

4 This Section expands the results shown in Gori, V., Elwell, C. Characterisation of the thermal structure of different building constructions using in-situ measurements and a Bayesian analysis. Paper accepted at the Northern Symposium on Building Physics (NSB2017) conference.

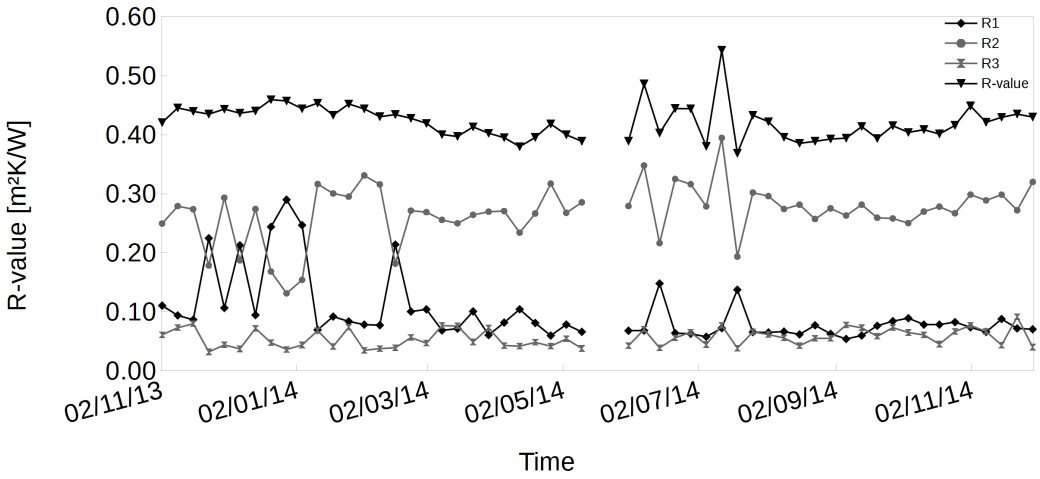

Figure 6.19: Lumped thermal resistances and R-value of the OWall for each hypothetical monitoring campaign presented in Section 6.3.1.

algorithm struggles to identify a unique solution for the lumped thermal resistances but can find the total thermal resistance to which they contribute.

Given the potential relationship of the observed behaviour with the physical structure of the wall (as also discussed in Chapter 5), the analysis was repeated for the CLWall and HSWall_N since their structure presents distinct thermophysical properties (*i.e.* a layer of high thermal resistance and low thermal mass between two layers with lower thermal resistance). Figure 6.21 on page 222 shows the lumped thermal resistances and R-value of the CLWall (the HSWall_N was not shown as it presented similar behaviour). Unlike the OWall, the lumped thermal resistances showed a consistent behaviour. The corner plots (Figure 6.22 on page 223 shows a representative example) showed no correlation between the thermal resistances of the CLWall and HSWall (*i.e.* the axis of the posterior probability distributions of the estimates of the lumped R_s were aligned with the Cartesian axis). The result, supporting the findings in Chapter 5, suggests that the model found the lumped R-values to be independent of each other, possibly due to the strong physical constraints of the wall seemed to help the model to identify a unique solution for the values of the constituent effective thermal masses and consequently the magnitude of the lumped R-values.

Whilst the topic of future work, the relation between the physical structure of the building element and the model results, through the MCMC probability distributions, open up the possibility for practical applications of this approach (*i.e.* non destructive *in-situ* monitoring campaigns and MCMC analysis) as a tool to support and inform the design and decision-making process. For example, it may be possible to use this method to identify the most probable materials and structure constituting a building element and to evaluate whether a building structure is likely to be insulated prior

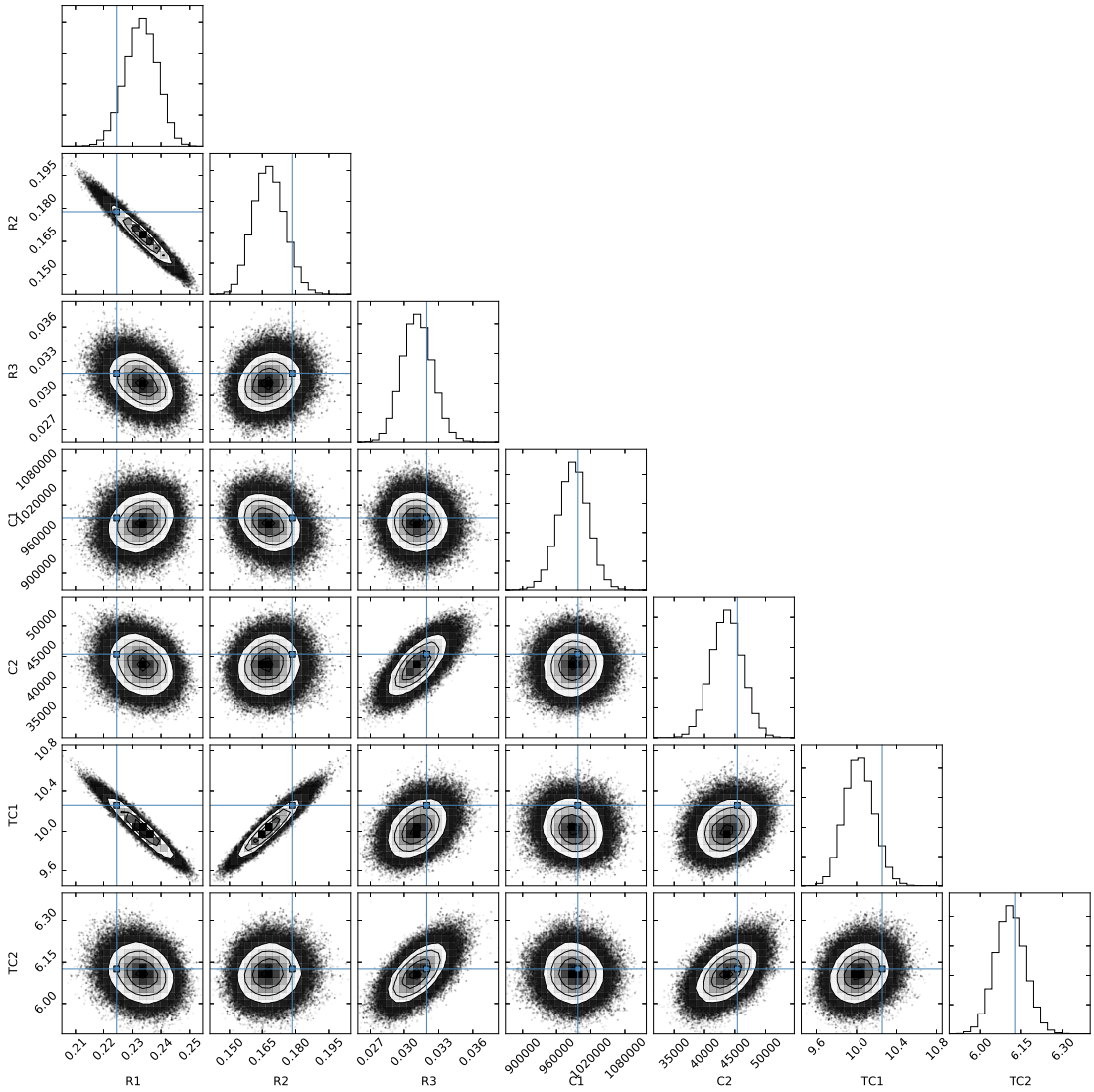

Figure 6.20: Corner plot showing the estimates of the thermophysical parameters from the fourth hypothetical monitoring campaign for the OWall.

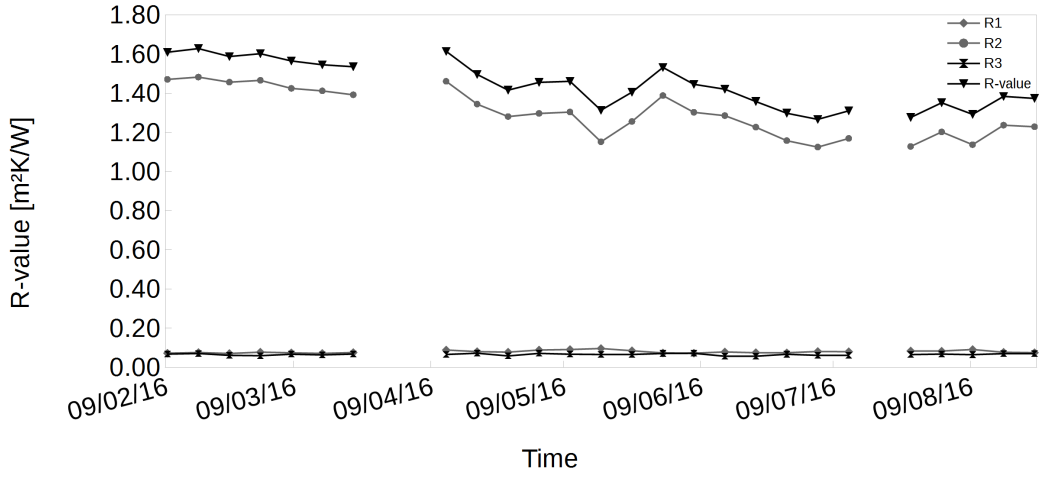

Figure 6.21: Lumped thermal resistances and R-value of the CLWall for each hypothetical monitoring campaign presented in Section 6.3.2.

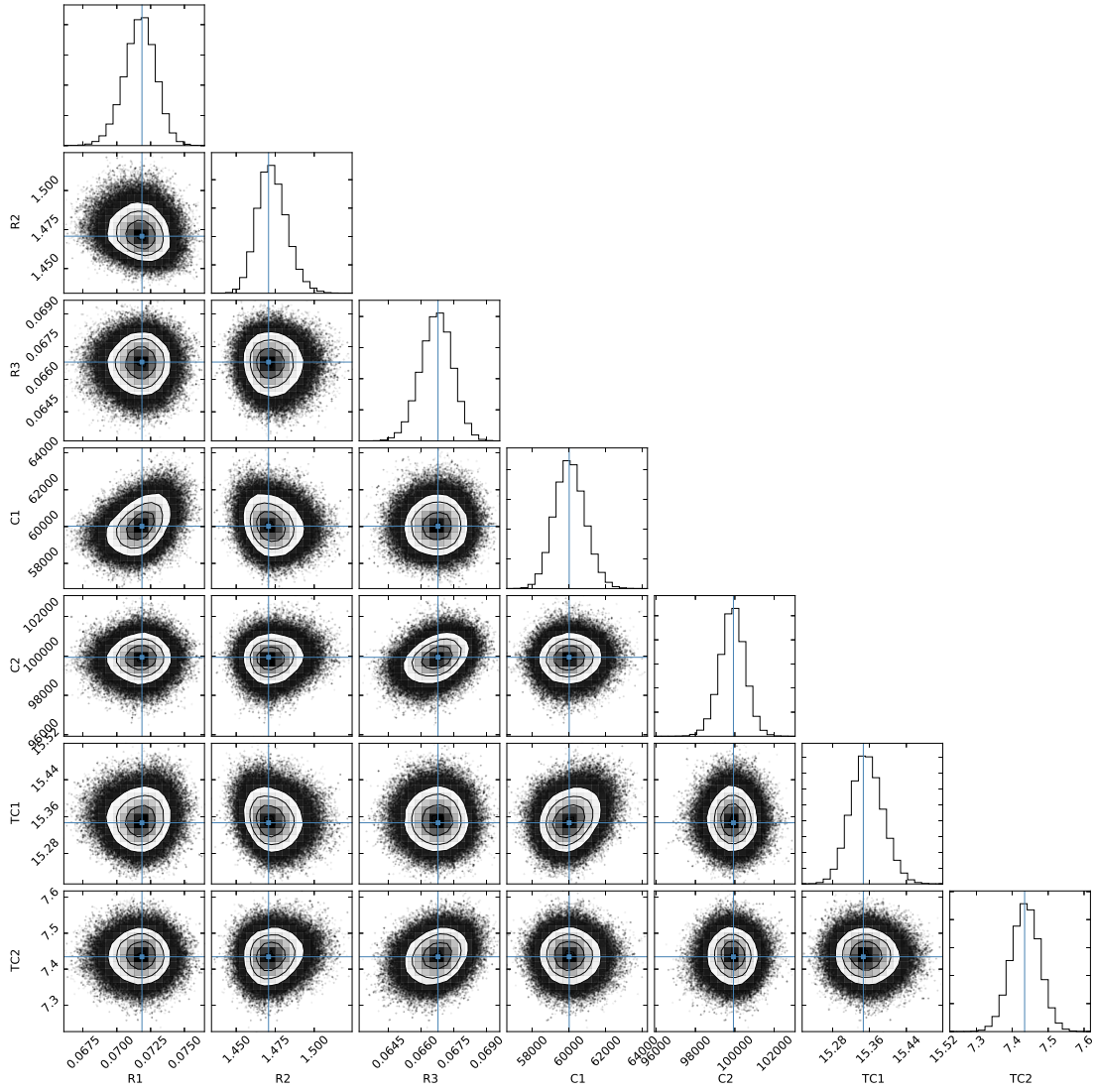

Figure 6.22: Corner plot showing the estimates of the thermophysical parameters from the first hypothetical monitoring campaign for the CLWall.

to retrofitting interventions; and to propose tailored retrofitting strategies aiming to maximise the thermal comfort within the indoor ambient and the thermal performance of the building, while minimising the overall energy consumption.

6.5 DISCUSSION AND SUMMARY

This chapter investigated the ability of the grey-box dynamic method developed in this research to provide robust estimates of the thermophysical properties of *in-situ* walls at all times of the year, while reducing the length of the monitoring period. Data analysis was undertaking using hypothetical monitoring campaigns (described in Section 4.4) selected the 2TM model as the one providing the best representation of the observed data compared to the 1TM (2 HF) model, confirming the results obtained in Chapter 5. Although the latter model is useful for model comparison, the use of only one effective thermal mass to simultaneously describe the heat flux measurements from the two heat flux data streams is not sufficient for the model to produce accurate estimates. As shown in Chapter 5 the 1TM (2 HF) (*i.e.* the 1TM model fitting both to the internal and external heat flux measurements) was able to estimate well the external heat flux but not the internal one.

The 2TM model considerably reduced the minimum number of days required on average for the analysis to ensure stable estimates (up to twenty-seven less) compared to the AM, regardless of the type of structure surveyed and the time of the year the monitoring was undertaken. Short monitoring campaigns (*i.e.* three full days long) were often sufficient for the analysis to stabilise even when the average temperature difference was low (down to 2 °C) and the environmental conditions very variable (*i.e.* high coefficient of variation of the temperature differences) over the monitoring period. Of note, three full days of data is the minimum number of observation required by the criteria in the BS ISO 9869-1 (2014) Standard.

This research has revealed that the dynamic method (and the 2TM in particular) may be capable to generally stabilise to the final value in less than three days (as for example illustrated in Chapter 5), although the aforementioned criteria may be too conservative for the dynamic method. The definition of new stabilisation criteria for dynamic methods, for example based on cross-validation, is the topic of future research.

The reduction of the length of the monitoring campaigns from those set by the AM did not cause any significant decrease in the accuracy of the U-value estimated by the dynamic method and the associated systematic error at all times of the year. The mean U-value estimates obtained from the 2TM model on short hypothetical monitoring cam-

paigns was close to that obtained from the same method on longer monitoring campaigns (discrepancies generally smaller than 5%) and the AM, although the standard deviation was smaller for the 2TM model. Similarly, the 2TM model was able to reduce the relative systematic error on the U-value compared to the AM. While with the latter method the relative systematic error was as higher as 50% for small temperature differences, effectively limiting the applicability of the AM even in cases when the stabilisation criteria were met and the estimates looked plausible, the systematic error with the 2TM model was around 30% at maximum (and generally much lower).

An analysis of the thermophysical estimates of the 2TM model with the MCMC approach showed that insights into the thermal structure of building elements of different construction may be gained from the full probability distribution of the parameters. The analysis undertaken on both solid and cavity walls showed that the lumped R-values estimates were anticorrelated for the former type of wall while these were independent for the latter. The results may be interpreted in the light of the different physical structure of the two constructions. In fact, the distinct thermophysical properties of filled cavity wall may define well the position of the effective thermal masses within the masonry layers and consequently impose a unique solution to the estimates of the model. Conversely, the comparable thermophysical properties of the material constituting a traditional solid wall, impose weaker physical constraints allowing several similarly probable combinations for the locations of the effective lumped thermal masses. Consequently, the size of the R estimates varies depending on the position of the effective thermal mass, but their total R-value is constant. Future research is required to further investigate the practical applications for a tool based on non-destructive *in-situ* measurements and MCMC analysis to inform the design and the decision making process, for example at retrofitting stage.

The outcomes of this chapter showed that the novel grey-box dynamic method developed met the objectives of extending the data collection to all times of the year and shortening the length of monitoring campaigns compared to current methods for the estimation of the thermophysical properties of building elements. The next chapter will explore the robustness of the novel dynamic method on differently oriented building elements. It expands the analysis presented in this chapter to data collected on an east-facing wall over four months (form the spring to the summer period). The analysis aims to test the performance of the dynamic method on a building element exposed to high levels of incoming solar radiation, variable environmental conditions and small average temperature differences. The chapter will also investigate the air movement close to the external surface of the structure, which affects the heat transfer at the interface between

the building element and the external air influencing the thermal resistance of the air film.

7

ESTIMATION OF THE THERMOPHYSICAL PROPERTIES OF WALLS ACCOUNTING FOR WIND AND DIRECT SOLAR RADIATION

The previous chapter tested the performance of the dynamic method at estimating the thermophysical properties of north-facing walls using data collected at all times of the year. The orientation of the walls was chosen according to current best-practice guidelines for *in-situ* monitoring campaigns (Energy Saving Trust, 2005), as it allowed the minimisation of the effects of direct solar radiation on the measurements. The dynamic method, and specifically the 2TM model, was able to return robust estimates of the U-value of the walls surveyed while reducing both the length of the monitoring period and the magnitude of the associated systematic error compared to the AM.

The present chapter further expands the encouraging results obtained in Chapter 6 by analysing an east-facing cavity wall (HSWall_E) surveyed over four months during the spring and summer season (Section 7.2). Additionally, the potential effects of wind and air movement on the thermal resistance of the external air film (Section 7.1) are investigated. Environmental factors (*e.g.*, solar radiation and air movement, such as wind and convective flows) may introduce errors in the estimation of the thermophysical properties of the building element and, as a consequence, simulations using those estimates may not be representative of the average behaviour of the element. Accounting for these environmental factors in the estimations is even more important for short monitoring campaigns where the effects of atypical weather conditions are less likely to be averaged out during the monitoring period. This chapter explores the performance of the grey-box dynamic model to best account for environmental factors, aiming at extending the use of *in-situ* measurements to differently oriented building elements.

7.1 THE IMPACT OF WIND ON ESTIMATES OF THE THERMOPHYSICAL PROPERTIES OF WALLS

As introduced in Section 2.2, wind speed and air movement adjacent to the surface of building elements affect the heat transfer at the interface between the structure and the surrounding air, which is reflected in the thermal resistance of the air film and consequently on the U-value (Section 2.1, BS EN ISO 6946 (2007)). When estimating the thermophysical properties from *in-situ* measurements, it is common practice to measure surface temperatures to estimate the R-value of the element and add constant air film resistances tabulated in the literature: $U = (R_{si} + \sum_i R_i + R_{se})^{-1}$. For walls, the conventional values suggested by the BS EN ISO 6946 (2007, Table 1) Standard are $0.13\,m^2KW^{-1}$ for the thermal resistance of the internal air film (R_{si}) and $0.04\,m^2KW^{-1}$ for the external one (R_{se}), which are calculated from empirical relationships (described in Section 2.1) assuming typical values of hemispherical emissivity, mean thermodynamic temperature, and wind speed adjacent to the surface. While wind on the wall surface should have minimal effect on the estimates of the R-value[1] computed from surface-temperature measurements of the element, it can considerably affect the U-value through R_{se} when the thermal resistance of the air film deviates from constant conventional values. The investigation of this aspect in the focus of the remaining of this section.

An exploratory analysis was performed to provide an indicative quantification of the magnitude of the error potentially introduced in the U-value when the air film resistance deviates from the conventional values. Figure 7.1 on page 229 shows the relative error on the U-value if a minimum wind speed of $1\,ms^{-1}$ (corresponding to an R_{se} of $0.08\,m^2KW^{-1}$) or a maximum wind speed of $10\,ms^{-1}$ (corresponding to an R_{se} of $0.02\,m^2KW^{-1}$) were observed, compared to the conventional value of thermal resistance of the air film of $0.04\,m^2KW^{-1}$ (corresponding to a wind speed of $4\,ms^{-1}$). Note, the minimum and maximum wind speeds were chosen according to the values reported in Table A2 of the BS EN ISO 6946 (2007) Standard. The graph shows that the effects introduced by the use of an unrepresentative air film resistance vary depending on the relative magnitude of the thermal resistance of the air film compared to the R-value of the wall. As expected, the lower the R-value of the wall, the greater the potential impact of the thermal resistance of the air film. For example, for a solid wall similar to the OWall (whose literature R-value ranged in $[0.29, 0.73]\,m^2KW^{-1}$, Section 5.1.2) the error on the U-value would approximately be between -12% and 8%, while for a cavity wall

1 Although wind, air movement, and pressure differences may affect heat and mass transfer within cavities and building materials, the investigation of these effects is beyond the scope of the present work.

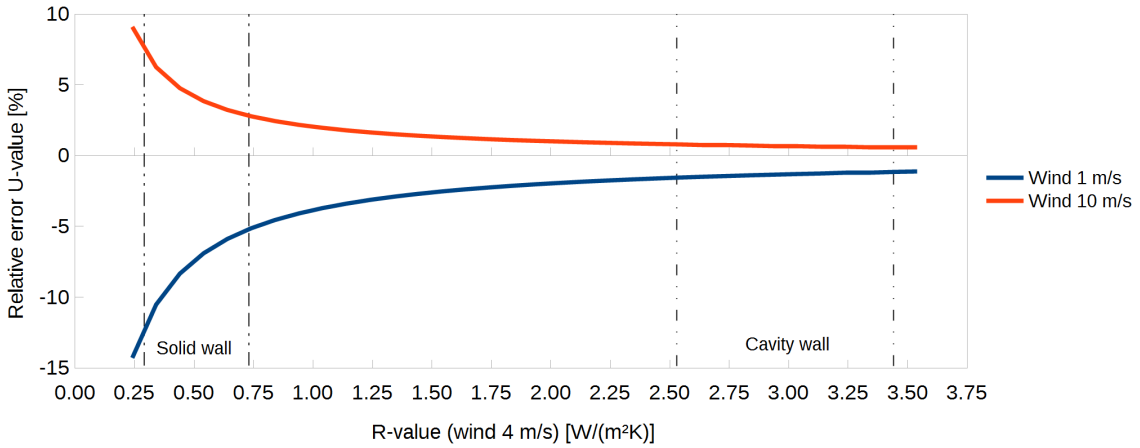

Figure 7.1: Relative error on the U-value when the thermal resistance of the external air film deviates from the conventional value of 0.04 m^2KW^{-1} (corresponding to a wind speed of 4 ms^{-1}) due to variations of wind speed. Specifically, the graph shows the case for an external air film resistance of 0.02 m^2KW^{-1}, corresponding to a wind speed of 10 ms^{-1}, and 0.08 m^2KW^{-1}, corresponding to a wind speed of 1 ms^{-1} (BS EN ISO 6946, 2007, Table A2). The range of literature R-values for a solid wall and a cavity wall similar to those monitored in this study are indicated for comparative purposes.

like those surveyed in this work (whose literature R-value ranged in [2.53, 3.44] m^2KW^{-1}, Section 5.1.4) the error would be between -2% and 1% (Figure 7.1 on page 229).

7.1.1 *Measured thermal resistance of the external air film for the CLWall*

As introduced in Section 4.1.2.3, the configuration of the CLWall enabled the installation of two air velocity sensors (one measuring the vertical and one the horizontal air flow) in the proximity of the external surface of the wall (Figure 7.2 on page 230) to investigate the potential deviation of the thermal resistance of the air film observed *in-situ* from the conventional assumption of 0.04 m^2KW^{-1} (BS EN ISO 6946, 2007). The thermal resistance of the external air film was calculated for each hypothetical monitoring campaign presented in Section 6.3.2, whose length was independently determined according to the minimum number of observations required by the AM and 2TM model to stabilise. The analysis covered the period starting on the 12th of April[2] to the end of August 2016. Specifically, for each hypothetical monitoring campaign the thermal resistance of the air film was calculated at each observation and used to calculate the distribution and the mean R_{se} value during the period investigated (separate values were calculated from the horizontal and vertical air flow measurements).

The thermal resistance of the air film was calculated according to Equation (2.11) (and following), making the following assumptions. The hemispherical emissivity of the wall

2 The hypothetical monitoring campaign starting on the 12th of April 2016 was the first after the installation of the air velocity sensors.

Figure 7.2: Air velocity sensors installed close to the surface of the CLWall. Note, although still present in the picture, the loose end of the cable ties were cut prior to the start of the monitoring to minimise the disruption to the air flow.

was assumed to be 0.9 as this value is deemed appropriate for both internal and external surfaces by the Standard (BS EN ISO 6946, 2007), and no information was available to account for any effects of deterioration and dust accumulation with time as required by the standard when a different value of emissivity is used. The mean thermodynamic temperature of the surface and of its surroundings in the calculation of the radiation heat transfer was approximated with the surface temperature of the wall (as in Hens (2012)).

Similar estimates of the thermal resistance of the air film were obtained for each hypothetical monitoring campaign using both the vertical and horizontal air velocity[3]. Similar values of R_{se} were also obtained for time series whose length was determined according to the minimum number of days required by either the AM or 2TM model to stabilise, throughout the period surveyed (a summary of the results is shown in Table 7.1 on page 231). In both cases, the average thermal resistance of the air film estimated from the measurements was $0.10\,m^2KW^{-1}$, 150% higher than the conventional value of $0.04\,m^2KW^{-1}$. The R_{se} values obtained for each hypothetical monitoring campaign were used to replace the constant value used in Section 6.3.2 and recalculate the U-values

3 Although the vertical and horizontal components could be combined to obtain a vector velocity, the two were studied separately for the following reasons: a) whilst close, the sensors were not colocated and the turbulent nature of the wind would lead to potentially misleading results; b) the two components are different in nature since the horizontal one is mainly wind-driven while the vertical one is also affected by buoyancy effects.

AM	Min	Max	Mean	St Dev	Units
Horizontal air flow	0.095	0.104	0.099	0.02	m^2KW^{-1}
Vertical air flow	0.097	0.104	0.101	0.02	m^2KW^{-1}

2TM	Min	Max	Mean	St Dev	Units
Horizontal air flow	0.087	0.105	0.099	0.004	m^2KW^{-1}
Vertical air flow	0.094	0.105	0.101	0.003	m^2KW^{-1}

Table 7.1: Minimum, maximum, mean and standard deviation of the thermal resistance of the external air film estimated from *in-situ* measurements of air velocity and surface temperatures for the CLWall. The estimates were calculated for the hypothetical monitoring campaigns presented in Section 6.3.2, both for the AM (top table) and 2TM model (bottom table).

(Figure 7.3 on page 232). As expected from Figure 7.1 on page 229, the U-values obtained using the thermal resistance of the air film estimated from the data were comparable to those in Section 6.3.2 since the magnitude of R_{se} is relatively small compared to the R-value of the wall. The recalculated U-values showed an average improvement of about 4% both for the AM and 2TM model.

As suggested by Figure 7.1 on page 229, the impact of air movement on the estimated U-value is likely to have been greater for the OWall due to its lower thermal resistance. The potential impact on the U-value of the OWall of a thermal resistance of the air film similar to those summarised in Table 7.1 on page 231 was investigated and compared to the estimates obtained using the conventional value. The calculation was undertaken only selecting the R-value estimates for the period comprised between April and August (*i.e.* the same months of wind speed data for the CLWall case study). The estimated R-value of the wall with the AM ranged between [0.39, 0.62] m^2KW^{-1}, leading to a range of U-values in [1.17, 1.61] $Wm^{-2}K^{-1}$ using an external air film of 0.10 m^2KW^{-1} compared to a range of [1.26, 1.78] $Wm^{-2}K^{-1}$ using the conventional value. Similarly, the R-value ranged in [0.37, 0.54] m^2KW^{-1} with the 2TM model, leading to U-values in [1.29, 1.67] $Wm^{-2}K^{-1}$ with the thermal resistance of the air film estimated from the data compared to U-values of [1.40, 1.86] $Wm^{-2}K^{-1}$ with the conventional value. The use of a thermal resistance of the air film estimated from the data would have improved the U-value by about 7% to 10% for the AM and between 8% and 10% for the 2TM model. These discrepancies would potentially have introduced non-negligible effects if the U-value estimates would be used for example for the evaluation of the energy consumption of a dwelling or the characterisation of the *in-situ* thermophysical behaviour of the building element.

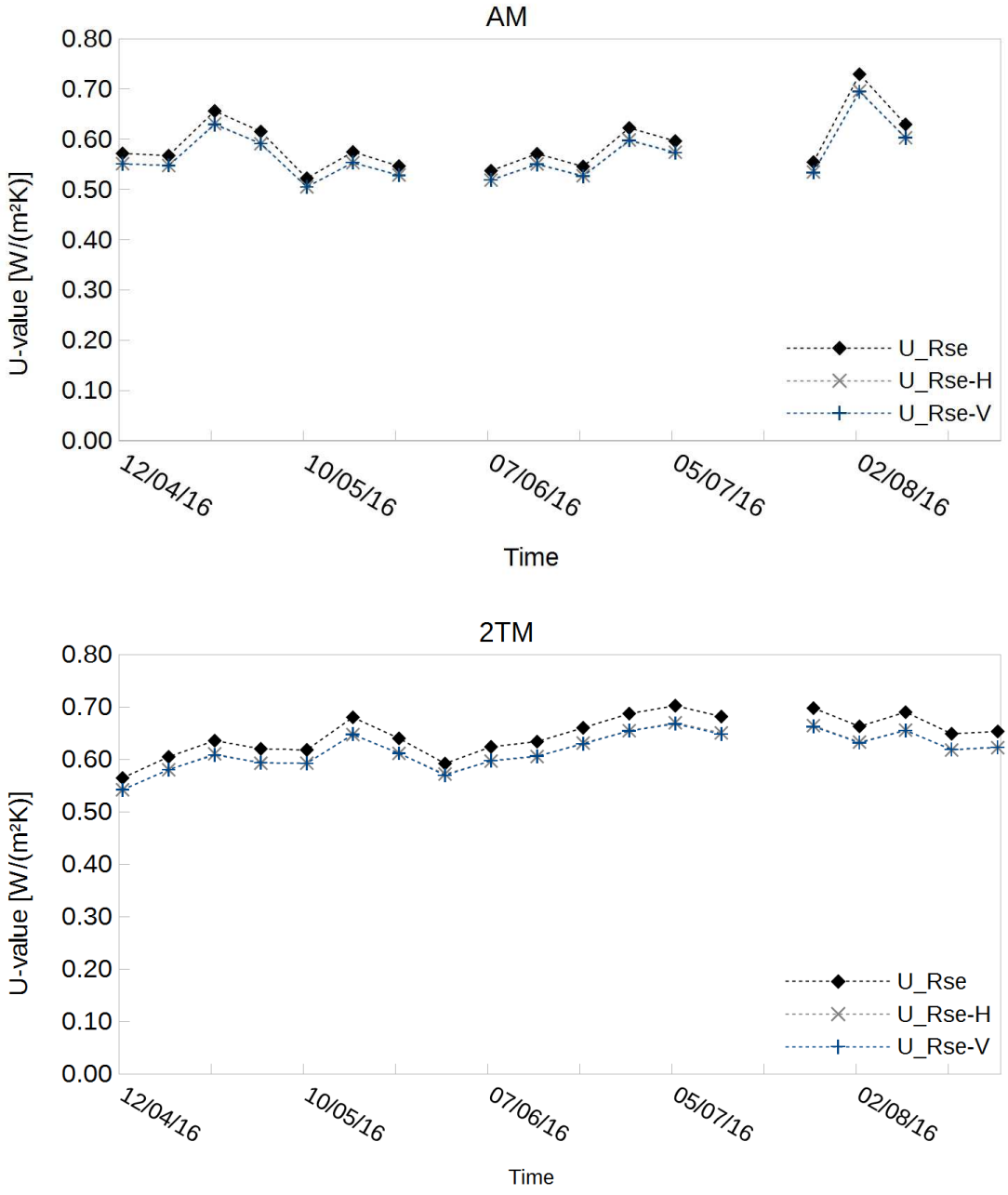

Figure 7.3: Comparison of the U-values obtained using the conventional air film resistance of 0.04 m^2KW^{-1}(U_Rse) and that estimated from *in-situ* measurements of surface temperature and air velocity in proximity of the external wall. The U-value estimates using the horizontal (U_Rse-H) and vertical (U_Rse-V) air flows are shown for the AM and 2TM model.

7.2 THE IMPACT OF DIRECT SOLAR RADIATION ON ESTIMATES OF THE THERMOPHYSICAL PROPERTIES OF WALLS

This section expands the analysis undertaken in Chapter 5 and Section 6.3 to an east-facing cavity wall (HSWall_E) monitored between April and August 2015 to test the ability of the dynamic method to robustly estimate the thermophysical properties of building elements exposed to direct solar radiation, effectively investigating whether the method may be applied to data collected on differently oriented building elements at different times of the year.

Initially, both the 2TM model with and without solar radiation input (described in Section 3.3.2) were applied to the data using hypothetical monitoring campaigns of same length ("first scenario" in Section 4.4). For each campaign, the AM using surface-to-surface measurements was used to determine the minimum number of days to analyse. The performance of the two 2TM models was compared using the odds ratio (Section 3.5.1). Subsequently, the 2TM model that best described the observed data was used to determine the length of the hypothetical monitoring campaigns (according to the "second scenario" in Section 4.4) over the four months surveyed and to investigate the performance of the model in relation to the incoming solar radiation impacting to the HSWall_E. The MAP approach and uniform priors on the parameters of the models were adopted in all cases.

7.2.1 *Data selection*

Prior the start of the data analysis, the raw time series were checked and cross-referenced with the metadata to identify obvious issues with the data collection or repeated missing data. Similarly to Section 6.1, hypothetical monitoring campaigns whose estimates had not stabilised within a thirty-day period or before a period of missing data were excluded from the analysis. The data investigated covered the period between April and August 2015 (Table 7.2 on page 234).

7.2.2 *Comparison of the 2TM models with and without solar radiation input for an east-facing wall*

The performance of the dynamic method on the east-facing wall (HSWall_E) was investigated comparing the performance of the 2TM model with and without solar radiation

Case study	Analysis	Start date	End date	Excluded periods
HSWall_E	Surface temperature	16/4/2015 14:00	31/8/2015 14:00	-
HSWall_E	Air temperature & solar radiation	16/4/2015 14:00	31/8/2015 14:00	30/4/2015 14:00 to 21/5/15 13:55

Table 7.2: Monitoring period surveyed for the HSWall_E and periods excluded from the analysis due to issues during the data collection only. The excluded periods in the table do not cover the hypothetical monitoring campaigns not complying the criteria listed above.

input (*i.e.* using either surface temperatures, or air temperatures and incoming solar radiation as separate source of information). The analysis was undertaken on the four-month period shown in Table 7.2 on page 234 using hypothetical monitoring campaigns whose length was determined according to the minimum number of observations required by the AM to stabilise (*i.e.* "first scenario" in Section 4.4). Of the nineteen possible hypothetical monitoring campaigns (Table 7.2 on page 234) only ten were analysed as the AM did not stabilise within a thirty-day period on six occasions and a further three were affected by missing data. For the hypothetical monitoring campaigns analysed, the average diurnal solar radiation[4] ranged between 129 Wm^{-2} and 189 Wm^{-2}, while the average temperature difference ranged between 0.8 °C and 5.2 °C for the surface-to-surface case and between 3.7 °C and 9.3 °C for air-to-air measurements.

In general, the use of a more complex model both improves the model fit and enlarges the prior probability space of the parameters. The Bayesian framework accounts for both these effects by using the evidence as a criterion for model comparison, effectively penalising unnecessarily more complicated models (Section 3.5.1). Figure 7.4 on page 235 shows the natural logarithm of the odds ratio of the 2TM model using surface temperatures compared to the one using air temperatures and solar radiation input as separate information. For all hypothetical monitoring campaigns, the model selection supported the former lumped thermal mass model. The result indicates that the extra-complexity of the 2TM model incorporating solar radiation separately is not justified by a sufficient improvement of the data fit.

For illustrative purpose, the first hypothetical monitoring campaign was selected to show the ability of the two 2TM models to estimate the measured heat flux both at the interior and exterior surfaces. This time series, spanning between the 16th and the 28th of April 2015 (starting at 14:00), has the highest average diurnal solar radiation of all hypothetical monitoring campaigns (189 Wm^{-2}), while the average temperature

4 The average diurnal solar radiation was calculated using a 5 Wm^{-2} threshold. This value corresponds to the pyranometer's "zero offset", *i.e.* the amplitude of spurious readings observable even in the absence of solar radiation caused by temperature changes (Table 4.1 on page 114).

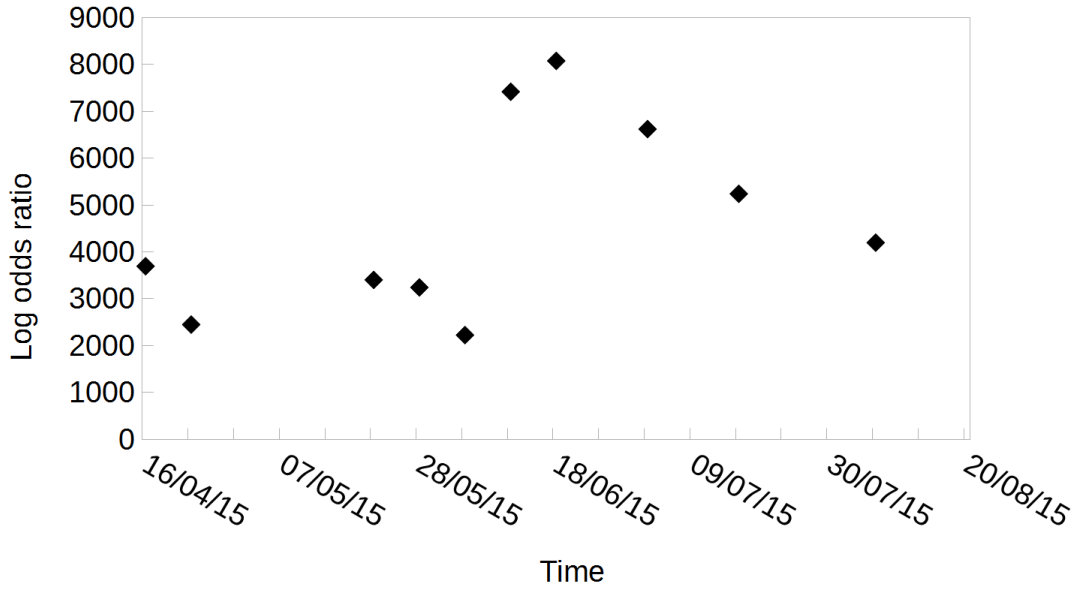

Figure 7.4: Natural logarithm of the odds ratio, comparing the 2TM model using surface temperatures to the 2TM model using air temperatures and incoming solar radiation as an additional heat source.

difference was 5.2 °C for the surface-to-surface case and 9.2 °C for the air-to-air. The raw time series for the measured solar radiation is presented in Figure 7.5 on page 236. Figure 7.6 on page 237 illustrates the measured and estimated heat flux both at the interior and exterior surface of the wall, using the 2TM models with and without solar radiation input. Both graphs show a good match between the measurements and the estimations, and no significant differences can be observed qualitatively in the two cases. This result supports the outcomes of the model comparison where the increased complexity of the 2TM model was not found to improve the data fit. Similarly to the heat flux estimations, the cross-validated time series both at the interior and external surface had a comparable behaviour qualitatively and showed a good match between the measurements and the estimates (Figure 7.7 on page 238). Thus, the two models were also able to generalise to out-of-sample data.

7.2.3 *Performance of the 2TM model without solar radiation input on an east-facing wall*

The 2TM model using surface temperatures was selected as the model best able to describe the recorded data, compared to the one using air temperature and solar radiation as additional heat source. Therefore, this model was used on the HSWall_E to test its performance in terms of monitoring length, U-value estimation and the associated systematic error for building element with different orientations and surveyed during the warmer months of the year. For this purpose, the monitoring period between the 16th

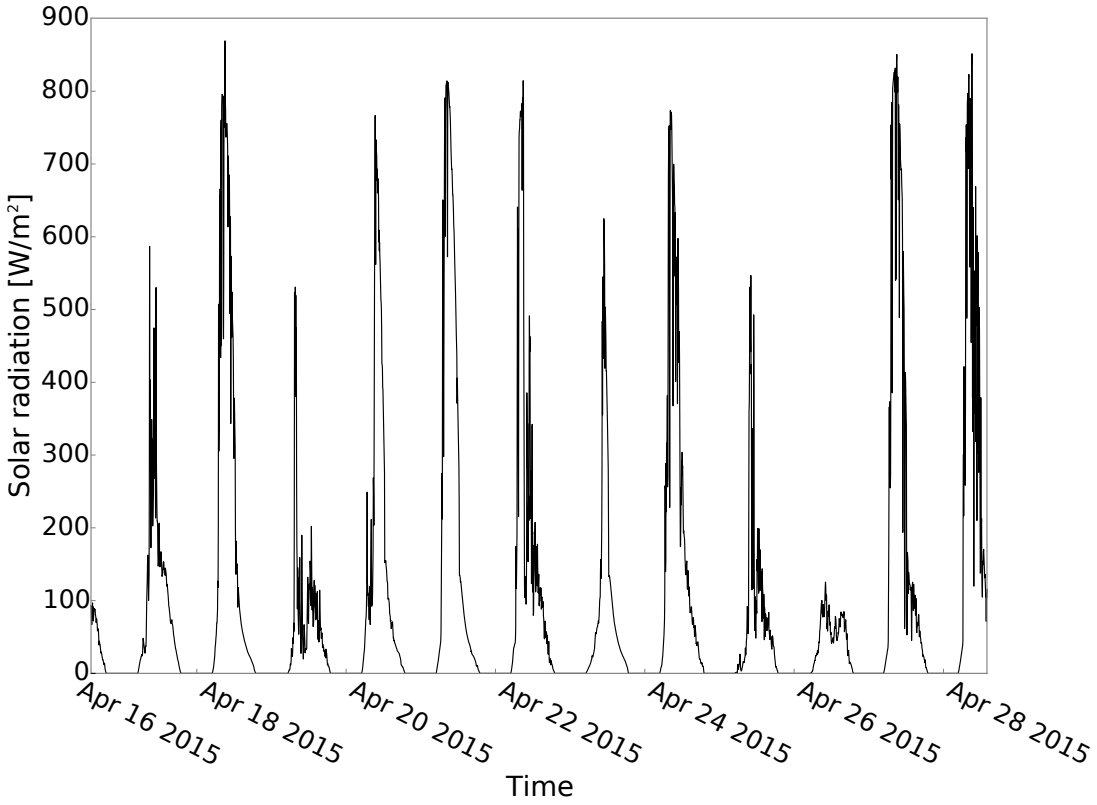

Figure 7.5: Measured solar radiation for the hypothetical monitoring campaign starting on the 16th of April 2015.

of April and the 31st of August 2015 was analysed using the hypothetical monitoring campaign approach, whose length was determined according to the minimum number of observations required by the 2TM model to stabilise according to the criteria in the BS ISO 9869-1 (2014) Standard (*i.e.* "second scenario" in Section 4.4). Out of the nineteen possible hypothetical monitoring campaigns, seventeen were accepted. The average diurnal solar radiation ranged between 80 Wm^{-2} and 191 Wm^{-2}, while the average temperature difference between the indoor and external surfaces spanned between 0.6 °C and 5.8 °C.

The monitoring length ranged between three and twenty-two days. The length of the monitoring period was analysed as a function of the average diurnal solar radiation and the its coefficient of variation (*i.e.* the ratio of the standard deviation of the solar radiation observations over their mean) to investigate the potential influence of this environmental factor on the minimum number of days required to stabilise (Figure 7.8 on page 239). No obvious correlation was observed between average solar radiation and the number of days required by the 2TM model to stabilise (top graph), while an increase in the length of the monitoring period may be possibly related to the variability of solar radiation during the survey (bottom graph).

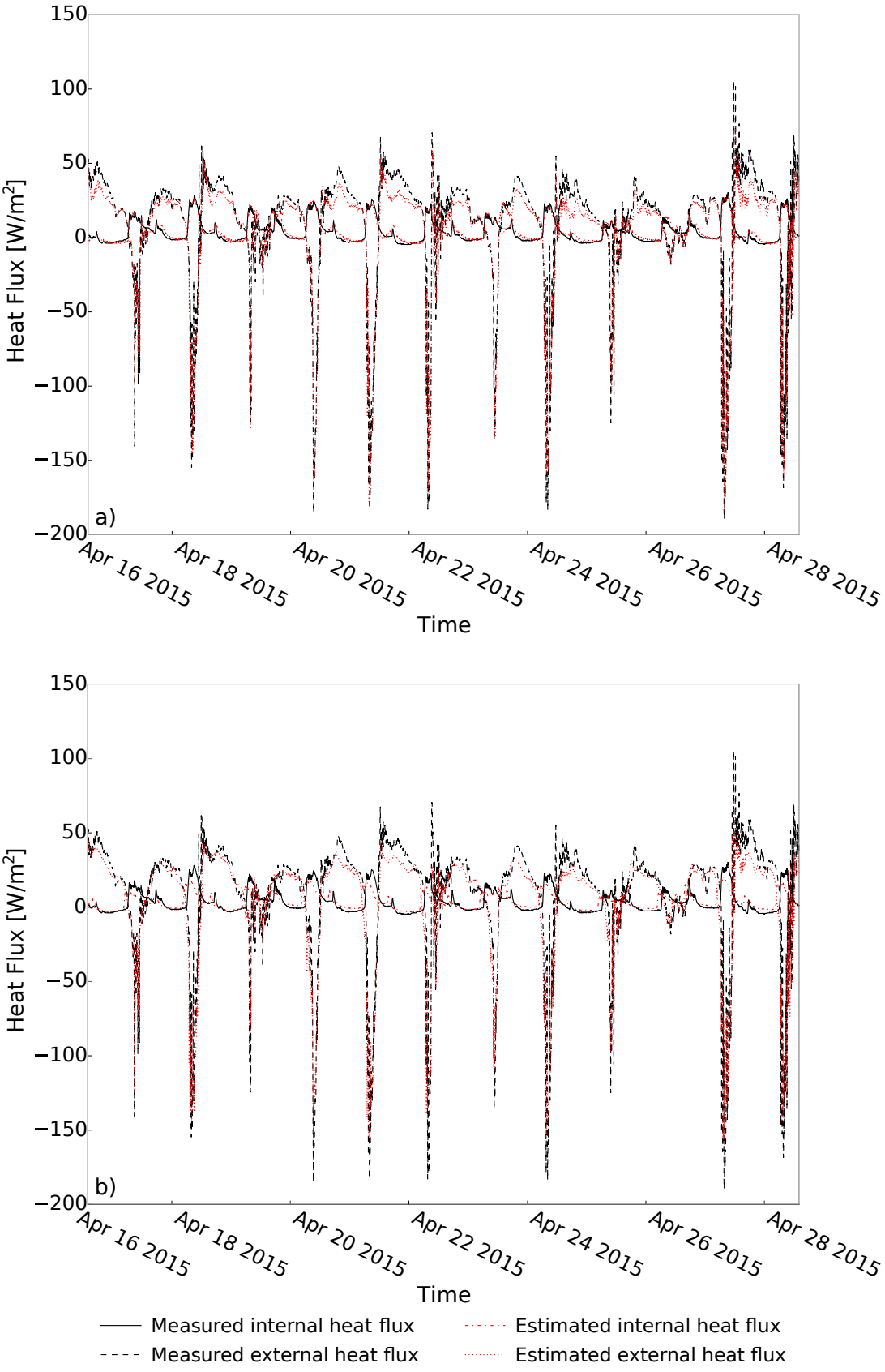

Figure 7.6: Measured and estimated heat flux through the HSWall_E using the 2TM model with: (a) surface temperatures, and (b) air temperatures and solar radiation.

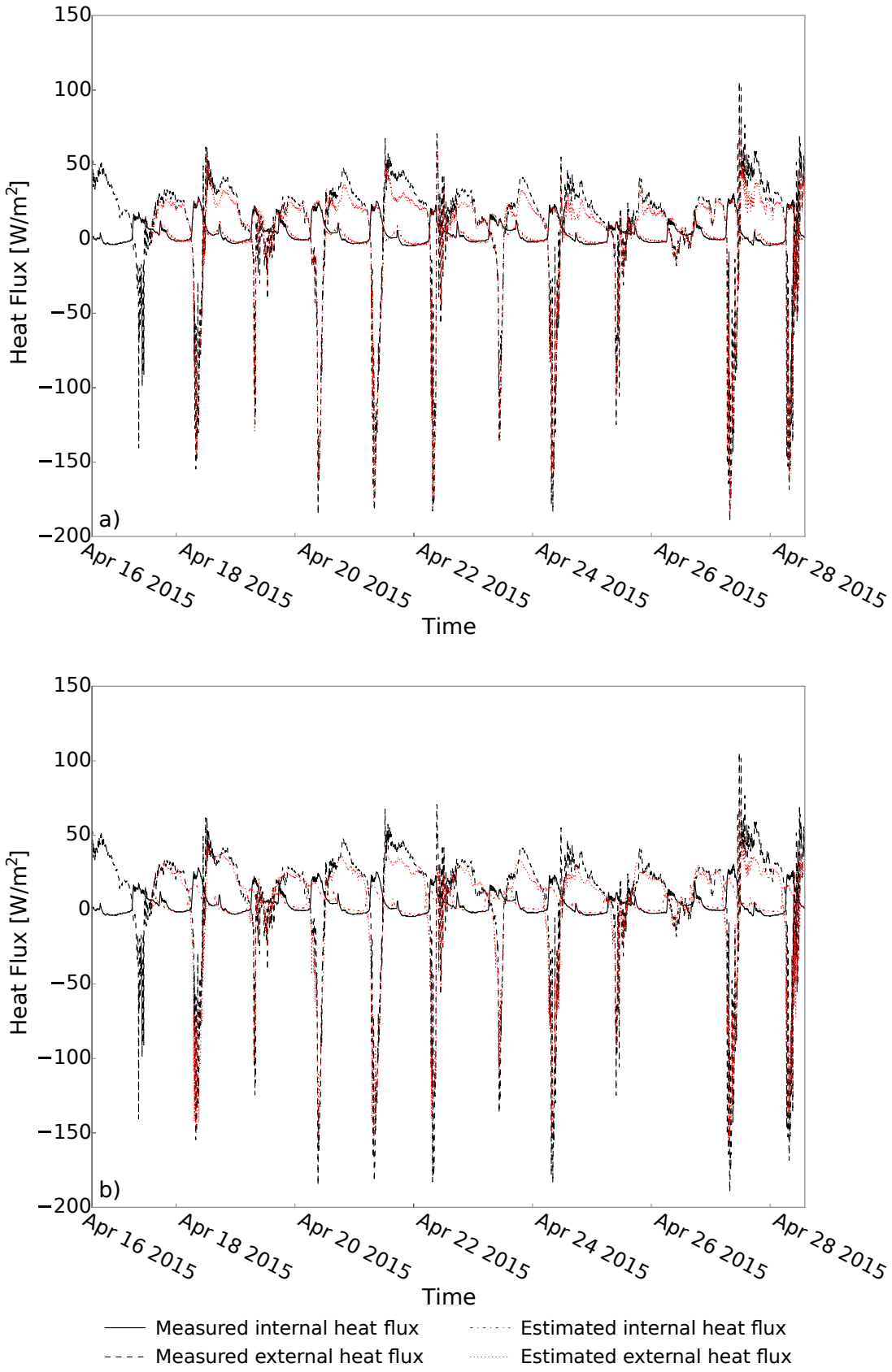

Figure 7.7: Cross-validation of the heat flux estimations for the HSWall_E using the 2TM model with: (a) surface temperatures, and (b) air temperatures and solar radiation.

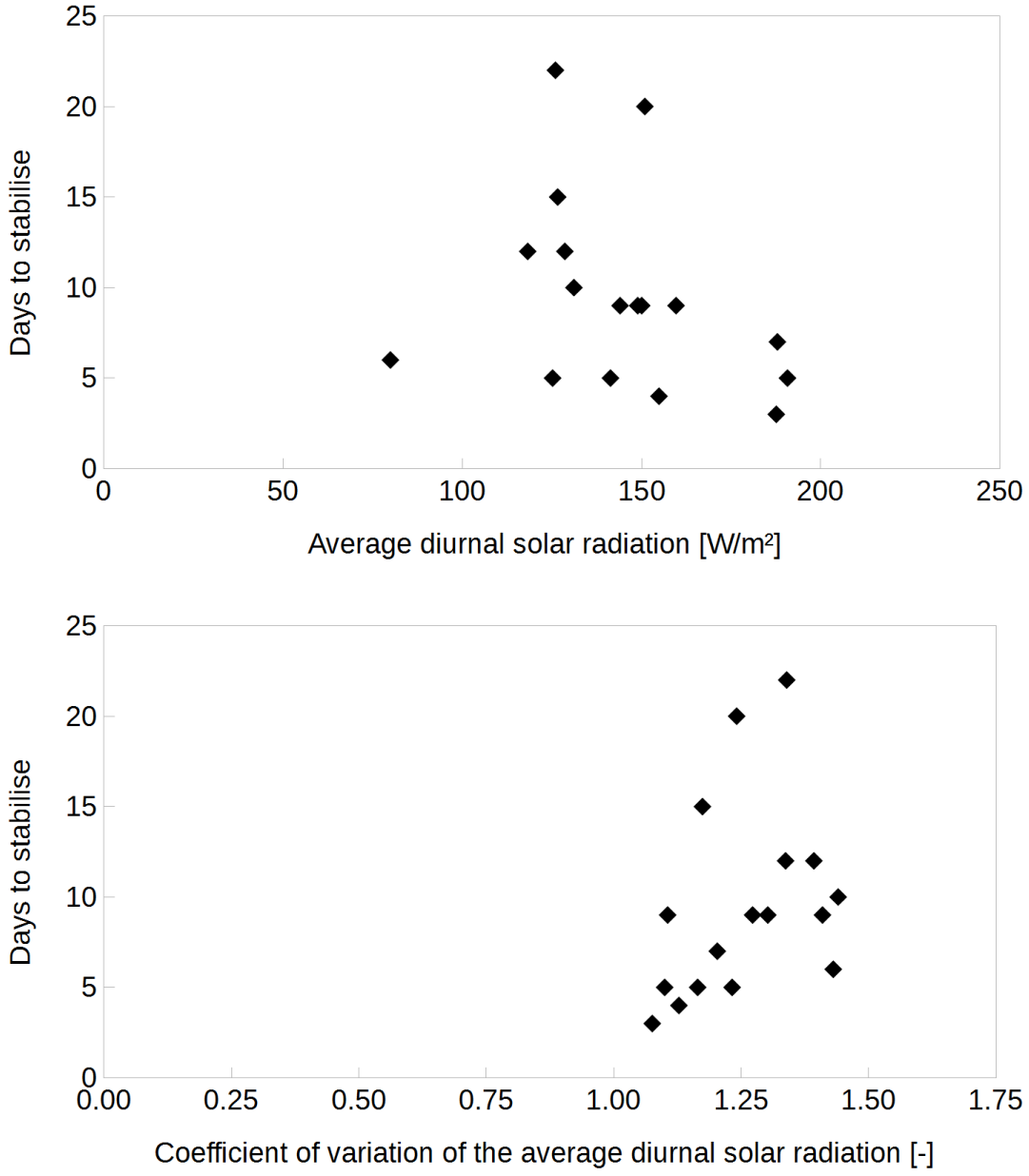

Figure 7.8: Length of the hypothetical monitoring campaign as a function of the average diurnal solar radiation (top graph) and the coefficient of variation of the average diurnal solar radiation (bottom graph) for the HSWall_E.

	Min	Max	Mean	St Dev	Units
U-value	0.68	0.92	0.77	0.05	$Wm^{-2}K^{-1}$
Rel sys err	0.05	0.37	0.16	0.09	-

Table 7.3: Minimum, maximum, mean and standard deviation of U-value and relative systematic error estimates for the HSWall_E using the 2TM model without solar radiation input (*i.e.* surface-to-surface temperatures).

A summary of the U-value estimates and the associated systematic error is shown in Table 7.3 on page 240. Similarly to the length of the monitoring period, the average solar radiation and its coefficient of variation does not exhibit a clear correlation with the U-value estimates (Figure 7.9 on page 241) and the relative systematic error on it (Figure 7.10 on page 242). These results suggest that the 2TM model was robust both at different levels of direct solar radiation impacting on the wall during the monitoring period and its variability. The length of the hypothetical monitoring campaigns for HSWall_E using the AM (between eight and twenty-nine) was always longer than using the 2TM model and the relative systematic error on the U-value was significantly higher (between 43% and 294%). These results are in line with the outcomes observed in Chapter 6 for north-facing walls during the warmer months of the year. The range of U-values obtained from the 2TM model for the HSWall_E (Table 7.3 on page 240) were comparable to those estimated for a north-facing wall (HSWall_N) of the same property during the same monitoring period (ranging between [0.66, 0.82] $Wm^{-2}K^{-1}$, with mean of 0.72 $Wm^{-2}K^{-1}$ and standard deviation of 0.05 $Wm^{-2}K^{-1}$), although the average U-value was slightly higher for the HSWall_E (the standard deviation coincided in the two cases). Figure 7.11 on page 243 shows that all U-value estimates were within the margin of error for the two case studies.

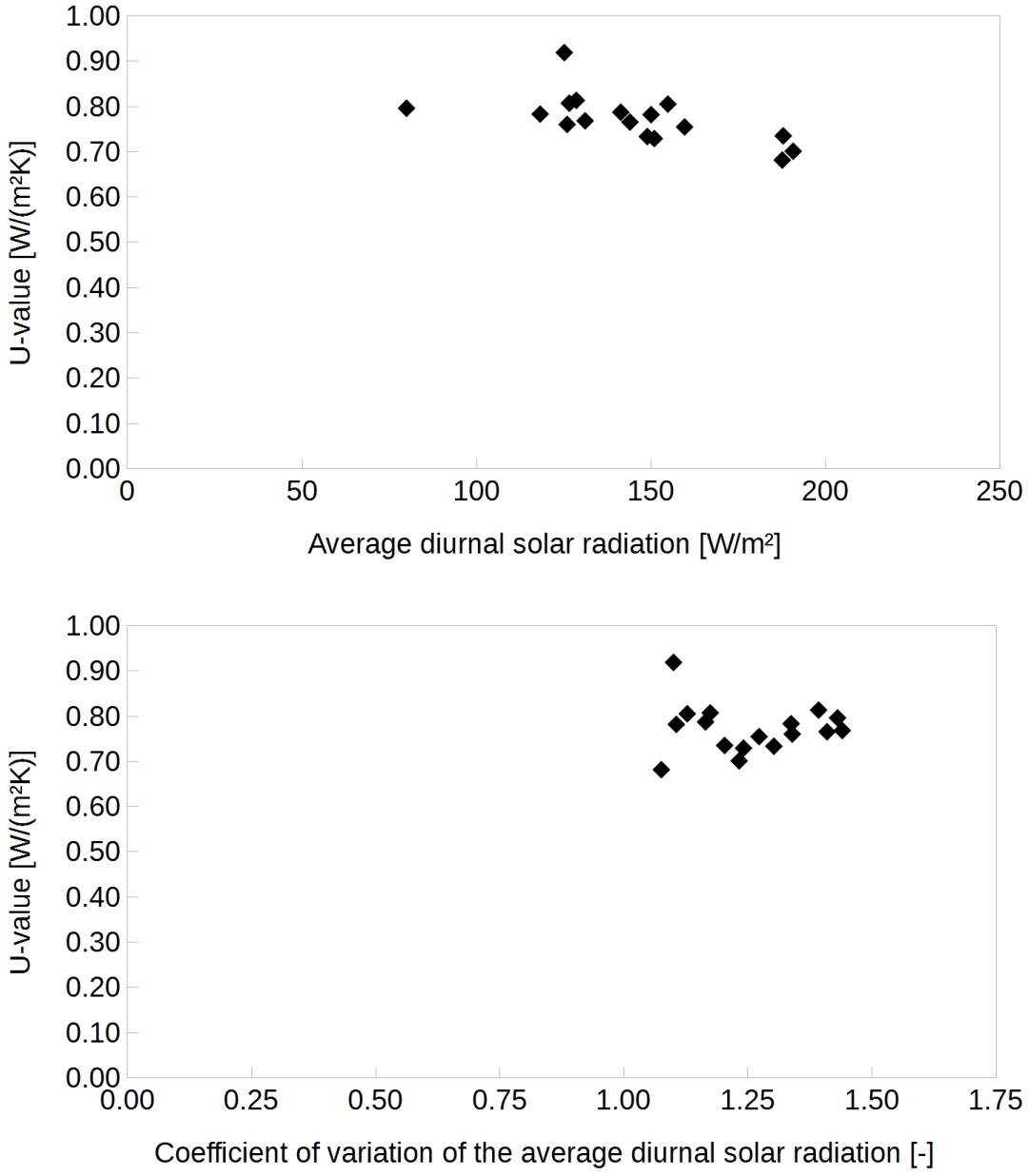

Figure 7.9: U-value estimates as function of the average diurnal solar radiation (top graph) and its coefficient of variation (bottom graph).

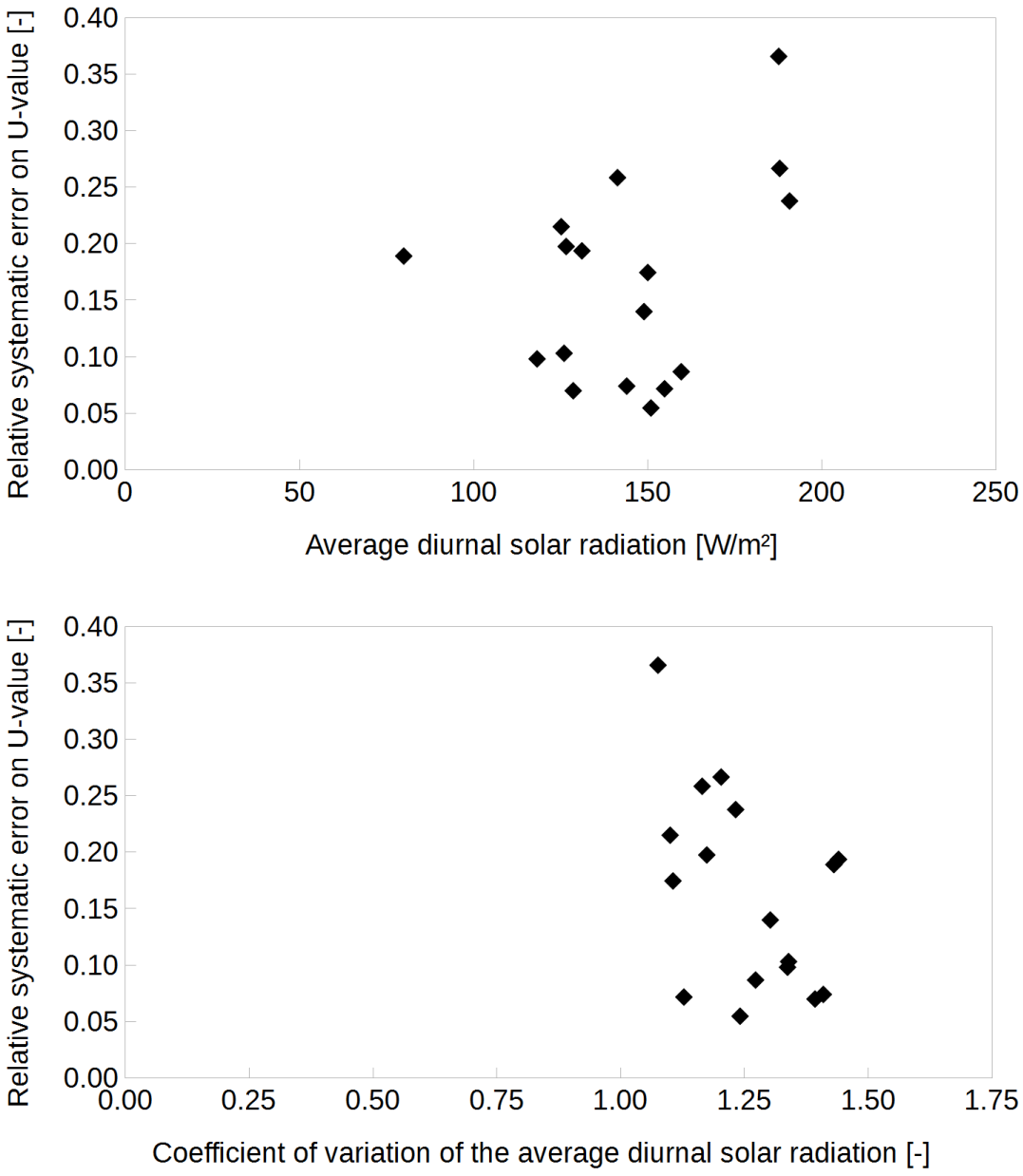

Figure 7.10: Relative systematic error on the U-value estimates as function of the average diurnal solar radiation (top graph) and its coefficient of variation (bottom graph).

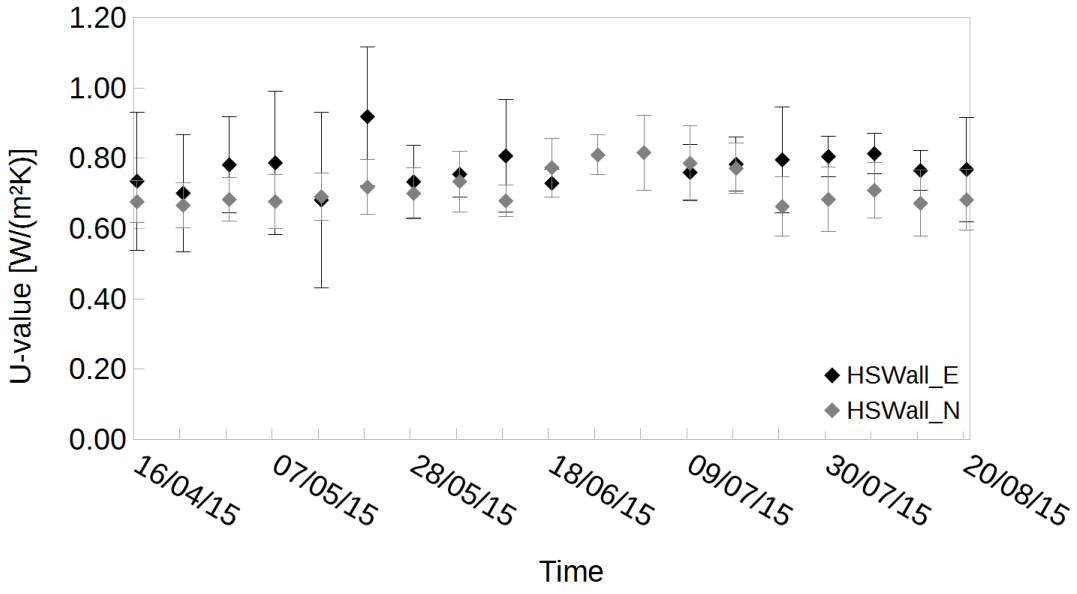

Figure 7.11: U-value estimates and systematic error for the HSWall_E and HSWall_N using the 2TM model with surface temperatures. The length of the hypothetical monitoring campaigns in each case study was independently determined according to the minimum number of days required by the model to stabilise.

7.3 CONCLUSIONS

This chapter investigated the potential effects of wind and direct solar radiation on the estimates of the thermophysical properties of walls, as these environmental factors may introduce uncertainties in the estimates. The impact of air movement on the heat transfer at the external surface of the wall was tested by comparing the thermal resistance of the air film calculated from surface temperature and air speed measurements (BS EN ISO 6946, 2007, Annex A) to the conventional value of the thermal resistance of the air film of 0.04 m^2KW^{-1} (corresponding to a wind speed of 4 ms^{-1}) (BS EN ISO 6946, 2007, Table 1). The analysis, undertaken for the CLWall, showed that the thermal resistance of the air film during the hypothetical monitoring campaigns investigated was was 0.10 m^2KW^{-1}, 150% higher than the conventional value. However, the effects of using an inaccurate value led to a small overestimation of the U-value, as the magnitude of R_{se} was relatively small compared to the R-value of the CLWall. Conversely, the impact of variations in wind speed on U-value estimates increases as the thermal resistance of the building element drop to values close to the resistance of the air film (*e.g.*, for solid walls). This was illustrated by a simple calculation of the potential impact of the measured wind speed at the CLWall site on the results from the OWall case study. The use of an R_{se} value estimated from the data would have improved the OWall U-value up to a 10%. In the future it would be interesting to extend the analysis undertaken on the CLWall

over a longer time period to cover different seasons and investigate the average thermal resistance of the air film over the full year. Additionally, repeating a similar monitoring on lower thermal resistance constructions, such as solid walls, would enable further investigation of the potential importance of this effect.

The performance of the 2TM model for a wall exposed to direct solar radiation was investigated using the data collected on the HSWall_E for the period between April and August 2015. This analysis aimed to investigate the applicability of the dynamic grey-box method across a wider range of environmental conditions, in order to investigate the feasibility of obtaining robust U-value estimates from the monitoring of walls of all orientations. The 2TM model with and without solar radiation input were compared using the odds ratio criterion to identify the best of the two models at describing the monitored data. The Bayesian model comparison selected the 2TM model without solar radiation input, showing that the extra complexity of the model with solar radiation as a separate source of heat was not justified, possibly because the use of surface temperature already accounted for the combined effect of ambient temperature and solar radiation. The ability to characterise the thermal performance of building elements exposed to direct solar radiation with the use of surface temperatures and heat flux plates at both sides of the element investigated has practical monitoring implications. Specifically, it avoids the necessity to install an expensive and fragile pyranometer, and the challenges of its correct and representative placement on the wall surface.

A further analysis of the 2TM model without solar radiation input was undertaken to investigate the length of the monitoring periods required by this method to stabilise and its robustness at charactering the thermophysical properties of non-north-facing elements during the warmest months of the year. This analysis showed that the monitoring length ranged between three and twenty-two days, a commonly accepted duration of winter-time monitoring campaigns using steady-state approaches on north-facing walls. The monitoring campaigns required for the 2TM model were shorter than those required for the AM during the same period, and the relative systematic error on the U-value was significantly lower for the 2TM model. The U-value estimates obtained on the HSWall_E were comparable and within the margin of errors of the estimates on the north-facing wall (HSWall_N). Specifically, the standard deviation of the U-value estimates coincided for the two walls, although the average U-value for the HSWall_E was slightly higher than that for the HSWall_N. The results obtained showed that the 2TM model using temperatures and heat flux measurements recorded at both surfaces of the wall during the spring and summer periods was able to characterise the thermophysical properties

of the HSWall_E. Additional long-term monitoring campaigns on different types of wall and orientations (*e.g.*, south-facing) will be monitored to further test the method.

The outcomes from this investigation suggest that *in-situ* measurements may be analysed with the dynamic grey-box method to provide insights into the thermal structure of buildings during winter, summer and transition months, potentially extending the monitoring to differently oriented elements. The method requires relatively simple equipment (*i.e.* thermistors, HFPs and data logger(s)), avoiding the need for pyranometers and containing the associated costs and limitations. The performance of the dynamic grey-box method observed in this chapter on the HSWall_E might be underestimated as the building was unoccupied and free running. An improved performance may in principle be observed for case studies where the internal ambient would be conditioned, effectively increasing the average temperature difference between the indoor and the outside at each observation. The ability of the 2TM model to both characterise the thermophysical performance of the building fabric and its thermal structure (as shown in Chapter 6) also for elements exposed to direct solar radiation provide insights into the impact of different retrofitting, heating, and cooling strategies that may be required to maintain thermal comfort in warm and cool periods.

8

CONCLUSIONS

The research undertaken towards this thesis developed a novel grey-box dynamic method for the estimation of the thermophysical properties of building elements from data monitored *in-situ*. The method, building on and significantly expanding the work by Biddulph et al. (2014), shortened the length of the monitoring period to be analysed (compared to the average method) to obtain robust estimates of the thermophysical properties of the elements with generally moderate systematic error at all times of the year, also using data collected on elements exposed to direct solar radiation. The method met the aims and objectives of characterising the thermal performance of *in-situ* building elements while extending the monitoring period to all times of the year, ensuring robust estimates, and providing useful physical insights into their thermal structure.

The dynamic grey-box method implemented is characterised by two distinct phases: model fitting and model validation. In the model-fitting phase, a family of plausible and physically informed lumped thermal mass models was devised to simulate the heat transfer through the building element and estimate the set of parameters that best reproduces the measurements. The optimal parameters were identified by analysing the posterior probability distribution of the parameters given the data and the model investigated, both using MAP estimates and MCMC sampling approaches. The posterior was calculated using a likelihood function that accounts for the potential autocorrelation of the residuals by means of a discrete cosine transform prior on their covariance matrix (obviating the commonly used, strong assumption of iid residuals), and uniform or log-normal priors on the parameters (or estimates, for example the U-value) of the model. Once the best set of parameters of the models devised was estimated, model selection and cross-validation were undertaken to identify the one that best describes the observations available and test its ability to generalise to an out-of-sample data set. Model selection was performed using the odds ratio, *i.e.* the ratio of the posterior probability distribution of the two models tested given the observations.

The choice of a dynamic grey-box method within a Bayesian framework was selected as it presented a number of advantages. The grey-box method enabled the combination of the advantages of extracting information from the data available and accounting for previous knowledge about the underlying physical process(es) investigated, while characterising both the heat transfer and storage of the building element. The use of Bayesian statistics provided estimates of the parameters of the model and their distribution (through the MCMC sampling), estimated the statistical error on the parameters accounting for their correlation, allowed the inclusion of prior knowledge about the parameters (if available), and offered an objective technique (based on statistical evidence) to compare and select the model that is more likely to describe the measurements observed *in-situ*. Although Bayesian-based methods have been successfully used for the solution of inverse heat transfer problems, their use in building physics applications is only recent and their application is still limited in the field.

The basic analysis framework and some functionalities of the method were developed prior to this work (Biddulph et al., 2014). During this research the existing models and software were substantially revised, refactored and improved, in addition to be tested on the data gathered during the study. More importantly, several new theoretical models and methods (Chapter 3, Chapter 4) were developed during this doctoral research and subsequently implemented in the software. Briefly:

- Lumped-thermal-mass models with solar radiation input (1TM to 4TM models) were devised as well as more complex lumped-thermal-mass models of building elements (3TM and 4TM models).
- The method for the approximation of linear differential equations with finite difference equations was improved using the bilinear transform.
- Non-uniform prior probability distributions (*i.e.* log-normal) both on the parameters or the estimates (e.g., U-value) of the models were implemented as an alternative to uniform priors, to account for the availability of relevant information about the distribution of the thermophysical properties for the materials constituting the element under study.
- A likelihood function with a discrete cosine transform prior distribution on the residuals to account for their potential autocorrelation was implemented to obviate the strong iid assumption. Consequently, the autocorrelation function and cumulated periodogram do not have to be checked in this framework.
- A method for the propagation of the systematic error on the U-value obtained from the dynamic analysis was devised to reflect its different mathematical modelling compared to the AM. The mathematical formulation of the dynamic method does not

present the fundamental limits of the AM (where the temperature differences are the denominator of the formula to calculate the U-value), effectively extending its applicability to periods with small temperature differences between the indoor and outside ambient.

• An MCMC-based approach was introduced for parameter estimation as it provides useful information on the full distribution of the posterior probability and the parameters of the model, which are not available from MAP estimates.

• A method for cross-validation was presented to test the ability of the model to generalise to new observations. The need for an altered cross-validation method arose from the fact that the initial temperature of the thermal mass is one of the parameters of the model, and that the requirement of independence for the test and training sets is usually difficult to achieve in time series analysis.

8.1 SUMMARY OF FINDINGS

The performance and robustness of the novel dynamic method in relation to the aims of this research was tested on five walls of different construction and orientation. Specifically, two solid walls (one housed in a thermal chamber and one *in-situ*, north-west-facing) and three cavity walls (all *in-situ*, two north- and one east-facing) were monitored and analysed. Long-term measurements (*i.e.* between four months and one year of data) were undertaken on the *in-situ* case studies .

Initially, the dynamic method (*i.e.* 1TM (1 HF), 1TM (2 HF) and 2TM models) was tested on the wall in the thermal chamber and the three north-facing ones (Chapter 5). The thermodynamic estimates obtained (both using the MAP and MCMC approaches) were compared to those obtained from the AM and the values calculated from tabulated properties of the materials constituting the elements under study. The periods analysed were selected such that the average temperature difference was comparable with that (~5 °C) in the thermal chamber. An additional period was analysed for completeness for the *in-situ* case studies ensuring that the average temperature difference observed met best-practice guidelines (~10 °C or more). The criteria listed in the BS ISO 9869-1 (2014) Standard were used to determine the minimum length of the time series to be analysed for each case study. The period selected was determined according to the minimum number of days required by the AM to stabilise and the same data were used also for the dynamic method with all lumped-thermal-mass models to ensure a fair comparison. The evolution of the U-value showed that the periods selected were also sufficient for the estimates from the dynamic method to stabilise. Specifically, the dynamic method

was generally quicker to stabilise than the AM and the 2TM model was the quickest of the three lumped-thermal-mass models devised, often taking between 24 and 36 hours.

Uniform priors were used for all case studies, while log-normal priors both on the parameters of the models and the U-value were also used on the OWall (as it was the only case study that had the relevant information available). The use of non-uniform priors showed an improvement of the U-value estimate during the initial phase of its evolution (where few observations were available), while the estimates stabilised to comparable values to the other models and methods at the end of the monitoring period. The result suggests that the use of non-uniform priors may be helpful in cases when small datasets are available. Non-uniform priors may also mitigate the effects of the placement of equipment on major unexpected construction defects, whose properties may not be representative of the expected performance of the wall as a whole.

For each case study all U-value estimates at the end of the selected monitoring period (both with the dynamic and average method) were within the systematic error. Additionally, for each lumped-thermal-mass model the parameter estimates with the MAP and MCMC approaches were within the margin of the statistical error, showing that the two optimisers were robust. As expected, the magnitude of the systematic error varied depending on the method (*i.e.* average or dynamic method) and model (*i.e.* optimising one or two heat flux data streams) used, reflecting their different mathematical formulation. Specifically, the 2TM model generally presented the smallest systematic error while the AM the largest. Furthermore, the systematic error for the models optimising two data streams was usually smaller than the error obtained from the model using only one data stream. The U-value estimates were in agreement with the literature values, except for the cavity walls where the *in-situ* estimates were higher than tabulated values. This outcome, however, was not unexpected following visual inspection as the insulation layer for the CLWall had significantly shrunk within the cavity and similar behaviour may be expected for the HSWalls. This result showed the value of using *in-situ* measurements for the characterisation of the thermophysical performance of real building elements as the quantification of the effects of the ageing process of the insulation material would have not been possible otherwise. The probability distribution of the parameters of the model estimated through the MCMC sampler provided insightful information on the thermophysical characteristics of the element, which can be interpreted in the light of the stratigraphy of the element and may be potentially used for practical applications in the future.

Model comparison and validation supported the 2TM model since the odds ratio selected this model as the best at describing the heat transfer across the wall compared

to the 1TM (2 HF) model. Cross-validation showed that the model selected was also able to generalise to out-of sample data. Notably, as little as one full day of unobserved data was sufficient for the 2TM model to estimate the heat transfer through the walls.

Given the promising results obtained from the initial investigation described above, the analysis on the three north-facing walls was extended to data collected at all times of the year (Chapter 6). The analysis aimed to test whether the dynamic method was also able to provide robust estimates outside best-practice conditions for *in-situ* measurements (*i.e.* winter periods with average temperature differences ideally of 10 °C or above), while shortening the length of the monitoring campaigns. For this purpose, the data were analysed such to replicate the case where hypothetical monitoring campaigns were started one week apart and lasted until the stabilisation criteria listed in the BS ISO 9869-1 (2014) Standard were fulfilled. The criteria were used to determine the minimum monitoring length with both the average and dynamic methods as no standardised criteria are available (to the candidate's knowledge) for the latter ones.

The analysis showed that the 2TM model was generally able to considerably reduce the minimum length of the monitoring period (up to twenty-seven days less) compared to the AM without compromising the quality of the estimates, regardless of the type of wall and period of the year. In some cases, three full days of data were sufficient for the 2TM model to stabilise, also when the temperature differences were as low as 2 °C and the environmental conditions very variable over the period monitored. Notably, a minimum period of three full days of data is imposed by the criteria in the BS ISO 9869-1 (2014) Standard, although the evolution of the U-value showed that the estimates may have stabilised within a shorter timespan (as observed from the evolution of the U-value).

Model comparison confirmed the 2TM model as the best for all case studies throughout the year. The reduction of the monitoring length however did not affect the robustness of the U-values obtained with the 2TM model, which were generally within the 5% of the estimates obtained in the same period using longer time series (*i.e.* according to the AM). Similarly, the relative systematic error on the U-value was significantly smaller compared to the AM (specifically, it was never above 30%).

The outcomes of this analysis showed that the aim of extending the monitoring period to all times of the year and reducing the length of the monitoring period was achieved for north-facing walls with the novel grey-box dynamic method devised. A further study to account for wind and direct solar radiation in the thermophysical estimates was undertaken (Chapter 7). The influence of air movement on the heat transfer at the external surface of the structure was investigated by calculating the thermal resistance of

the air film from *in-situ* measurements of surface temperatures and wind speed in proximity of the element, according to the method described in the BS EN ISO 6946 (2007, Appendix A) Standard. Specifically, the analysis aimed at investigating the discrepancy between the calculated R_{se} value obtained from the data and the conventional value of 0.04 m^2KW^{-1} usually adopted for U-value calculations when surface temperature are used for the estimations. The analysis was undertaken for the CLWall and the R_{se} values from the data were used to recalculate the U-value previously obtained with the conventional value. The thermal resistance of the air film was found to be 0.10 m^2KW^{-1} on average for all hypothetical monitoring campaigns investigated (period between April and August). Although this value was 150% higher than the value previously used, it only improved the U-value by a 4% since the magnitude of the air film resistance was relatively small compared to the R-value of the wall. It was estimated however that an average R_{se} value like that obtained for the CLWall would have improved up to a 10% the U-value of a solid wall like the OWall. The greater improvement for a solid wall is due to the fact that the magnitude of the air film resistance would be closer to the R-value of the wall.

The aim of extending the monitoring period to differently oriented building elements exposed to direct solar radiation was tested using data collected on an east-facing wall (HSWall_E) during the spring and summer months. Firstly, the hypothetical monitoring campaign approach was undertaken to compare the performance of the 2TM model with and without solar radiation as additional source of heat on monitoring campaigns of the same length. The odds ratio selected the model without solar input as the best at describing the measurements, showing that the extra complexity of the other model was not justified. This is possibly because surface temperatures are already accounting for the combined effects of ambient temperature and solar radiation.

Subsequently, the hypothetical monitoring campaign approach was used to test the performance of the 2TM model without solar radiation input and investigate the minimum number of days to stabilise. The HSWall_E data showed that the monitoring length ranged between three and twenty-two days, which is comparable to the length of surveys currently required by the AM to stabilise using data collected on north-facing walls during the winter time. Additionally, the U-value estimates were comparable and within the margin of errors of those obtained on a north-facing wall of the same property monitored over the same period.

8.2 RESEARCH LIMITATIONS AND FUTURE WORK

The application of the dynamic grey-box method on the five case studies surveyed allowed testing the performance of the dynamic method under a range of conditions, with encouraging results in respect of the aims and objectives of this research. Further monitoring campaigns and analysis are required to test the dynamic method on walls of different construction and orientation (*e.g.*, south-facing) at all times of the year. The survey of sites allowing the simultaneous measurement of environmental factors such as wind speed and solar radiation may improve the understanding of the impact of these factors on the estimation of the thermophysical properties of real building elements.

Since current criteria for the identification of the minimum length of monitoring campaigns were designed for the AM, they may be too conservative for dynamic approaches. Both theoretical arguments and results obtained in this research suggest that less conservative criteria can be devised for dynamic methods, allowing a further reduction of the length of the time series to be analysed. This will be the topic of future research.

The further investigation of *in-situ* measurements and MCMC sampling for the identification of the thermal structure of building elements would be of value to explore the potential for practical applications of these techniques as a non-destructive diagnostic tool. The survey and data analysis of additional case studies, building types, and longer monitoring periods are required for this purpose.

8.3 IMPLICATIONS FOR POLICY MAKING AND INDUSTRY PRACTICES

The features of the dynamic grey-box method devised and the analysis undertaken showed the potential of this method to widen the use of *in-situ* measurements for a robust characterisation of the thermal performance of building elements in their environment and state of conservation, for example to be used as a benchmark for retrofitting interventions or quality assurance of the building process. A wider use of thermophysical properties estimated from *in-situ* measurements has been identified as key to enhance the current limited understanding of the as-built energy performance across the whole construction sector and reduce the performance gap (International Energy Agency, 2011a; Zero Carbon Hub, 2014). Several studies have shown a mismatch between the thermal performance of buildings (and building elements) measured *in-situ* and that estimated from literature values or software simulations, which can be attributed to a number of uncertainties affecting the thermal performance of buildings. These

include environmental conditions, defects of the structure, inaccuracies in the monitoring and modelling process, uncertainties due to the use of tabulated values selected from visual inspections and quick surveys of the case study.

For its several advantages over current methods, the dynamic grey-box method presented may be relevant to both policy-making and industry. Given its ability to extend the use of monitoring campaigns to intermediate seasons and the summer period and to characterise the *in-situ* performance of building elements also exposed to direct solar radiation, the method can be used at the large scale to analyse the performance of the building stock at national level. In turn, this analysis can be used to inform policies on energy efficiency, devise tailored energy-saving-oriented incentives and evaluate their cost-effectiveness, increasing the efficacy and robustness of policy prioritisation and long-term programmes. Similarly, the method can be used in industry as a non-destructive testing tool used to design tailored retrofitting solutions aiming at improving thermal comfort while minimising the energy demand for space heating and cooling. Specifically, it can help practitioners investigate the most-likely thermal structure of a building element and assess whether this is likely to be insulated or not, evaluate the cost-effectiveness of energy-efficient interventions, meet quality assurance requirement and close the performance gap by feeding back the lessons learned into the building industry.

8.4 FINAL REMARKS

The development of a dynamic grey-box method using a lumped-thermal mass model constituted of two thermal masses and three thermal resistances (2TM model) showed the ability of accounting for both heat flow into and out of a building element, also exposed to direct solar radiation. The use of physically representative models based on the electrical analogy to heat, Bayesian statistics, and *in-situ* measurements supported a greater understanding of the thermal structure and performance of building elements using relatively simple monitoring equipment.

This method supports an extension of both the seasons in which the measurements may be undertaken and the orientation of the elements that can be surveyed, allowing a wider usage of monitored data for the characterisation of the thermophysical performance of the building envelope at all times of the year. It can be used to support improved thermal comfort and energy performance within the indoor ambient, inform tailored retrofitting solutions and space heating and cooling strategies, and help closing the performance gap.

BIBLIOGRAPHY

Ames, W. F., 1992. Numerical Methods for Partial Differential Equations. Academic Press. (Cited on page 65.)

Anderson, B., 1984. Site-Testing Thermal Performance: a CIB survey. Batiment International, Building Research and Practice 12 (3), 147–149. (Cited on pages 41, 51, and 57.)

Anderson, B., 2006. BR 443:2006 - Conventions for U-value calculations.
URL https://www.bre.co.uk/filelibrary/pdf/rpts/BR_443_(2006_Edition).pdf
(Cited on page 52.)

Androutsopoulos, A., Bloem, J., van Dijk, H., Baker, P., Feb. 2008. Comparison of user performance when applying system identification for assessment of the energy performance of building components. Building and Environment 43 (2), 189–196. (Cited on pages 67 and 68.)

Arens, E. A., Williams, P. B., May 1977. The effect of wind on energy consumption in buildings. Energy and Buildings 1 (1), 77–84. (Cited on page 51.)

Baker, P., Feb. 2008. Evaluation of round-robin testing using the PASLINK test facilities. Building and Environment 43 (2), 181–188. (Cited on page 68.)

Baker, P., 2011. Historic Scotland Technical Paper '10 - U-values and traditional buildings. Tech. rep., Historic Scotland Alba Aosmhor.
URL http://www.historic-scotland.gov.uk/index/learning/publications/publicationsresultsdetail.htm?id=50f8ada27 (Cited on pages 40, 45, and 127.)

Baker, P. H., van Dijk, H. A. L., Feb. 2008. PASLINK and dynamic outdoor testing of building components. Building and Environment 43 (2), 143–151. (Cited on pages 41, 42, 45, 57, 67, 146, and 189.)

Balocco, C., Gori, V., Marmonti, E., Citi, L., Jun. 2012. Building–plant system energy sustainability. An approach for transient thermal performance analysis. Energy and Buildings 49, 443–453. (Cited on page 64.)

Bankvall, C., 1978. Forced Convection Practical Thermal Conductivity In An Insulated Structure Under The Influence From Workmanship And Wind. In: ASTM symposium

on Advances in Heat Transmission Measurement on Thermal Insulation Material Systems. Vol. 660. pp. 409–425. (Cited on page 45.)

Bayes, T., Price, R., 1763. An Essay towards solving a Problem in the Doctrine of Chances. Philosophical Transactions, 370–418. (Cited on page 76.)

Berger, J., Orlande, H. R., Mendes, N., Guernouti, S., Sep. 2016. Bayesian inference for estimating thermal properties of a historic building wall. Building and Environment 106, 327–339. (Cited on pages 42 and 68.)

Biddulph, P., Gori, V., Elwell, C. A., Scott, C., Rye, C., Lowe, R., Oreszczyn, T., Aug. 2014. Inferring the thermal resistance and effective thermal mass of a wall using frequent temperature and heat flux measurements. Energy and Buildings 78, 10–16. (Cited on pages 41, 42, 43, 68, 73, 81, 83, 129, 131, 152, 247, and 248.)

Bohm, G., Zech, G., 2010. Introduction to statistics and data analysis for physicists. DESY. (Cited on pages 125, 136, 137, 138, 140, and 141.)

Box, T., 1868. A practical treatise on heat, as applied to the useful arts for the use of engineers, architects, etc. Spon. (Cited on page 56.)

Brisken, W., Reque, S., 1956. Heat load calculations by thermal response. ASHVE Transactions 62 (1), 391–424. (Cited on page 64.)

Bruckmayer, F., 1940. The equivalent brickwall. Gesundheuts- Ingenieur (63), 61–65. (Cited on page 61.)

BS EN ISO 6946, 2007. Building components and building elements - thermal resistance and thermal transmittance - Calculation method. (Cited on pages 24, 48, 49, 50, 51, 150, 228, 229, 230, 243, and 252.)

BS EN ISO 7345, 1996. Thermal insulation - Physical quantities and definitions. (Cited on pages 49, 50, and 125.)

BS ISO 9869-1, 2014. Thermal insulation – Building elements – In-situ measurement of thermal resistance and thermal transmittance. Part 1: Heat flow meter method. (Cited on pages 17, 18, 19, 20, 25, 41, 43, 46, 49, 50, 56, 57, 58, 59, 60, 69, 122, 123, 134, 141, 146, 150, 151, 155, 157, 158, 164, 166, 170, 172, 194, 203, 224, 236, 249, and 251.)

Building Research Establishment, 2011. SAP 2009 The Government's Standard Assessment Procedure for Energy Rating of Dwellings. (Cited on page 52.)

Burnand, G., 1952. The study of the thermal behaviour of structures by electrical analogy. British Journal of Applied Physics 3 (2), 50. (Cited on page 63.)

Byrne, A., Byrne, G., Davies, A., Robinson, A. J., Jun. 2013. Transient and quasi-steady thermal behaviour of a building envelope due to retrofitted cavity wall and ceiling insulation. Energy and Buildings 61, 356–365. (Cited on pages 40, 45, and 52.)

C1155-95, A., 2011. Standard Practice for Determining Thermal Resistance of Building Envelope Components from the In-Situ Data. (Cited on pages 55, 56, and 115.)

Campbell Scientific, 2015. CR1000 Measurement and Control Datalogger. URL https://www.campbellsci.co.uk/cr1000 (Cited on page 114.)

Castillo, L., Enríquez, R., Jiménez, M., Heras, M., Oct. 2014. Dynamic integrated method based on regression and averages, applied to estimate the thermal parameters of a room in an occupied office building in Madrid. Energy and Buildings 81, 337–362. (Cited on pages 40 and 45.)

Cengel, Y., 2002. Heat and mass transfer, 2nd Edition. McGraw-Hill Education. (Cited on pages 46, 47, and 48.)

Cesaratto, P. G., De Carli, M., Apr. 2013. A measuring campaign of thermal conductance in situ and possible impacts on net energy demand in buildings. Energy and Buildings 59, 29–36. (Cited on pages 41, 45, and 55.)

Cesaratto, P. G., De Carli, M., Marinetti, S., Jul. 2011. Effect of different parameters on the in situ thermal conductance evaluation. Energy and Buildings 43 (7), 1792–1801. (Cited on pages 45, 51, 53, and 54.)

Chambers, J., Gori, V., Biddulph, P., Hamilton, I. G., Oreszczyn, T., Elwell, C. A., 2015. How solid is our knowledge of solid walls? - Comparing energy savings through three different methods. In: Proceedings of CISBAT 2015 International Conference on Future Buildings and Districts - Sustainability from Nano to Urban Scale. Vol. 1. Lausanne, Switzerland, pp. 107–112. (Cited on page 45.)

CIBSE, 2007. Environmental Design - Guide A. (Cited on pages 26, 41, 56, 147, 148, and 149.)

Clarke, J., Yaneske, P., Pinney, A., 1990. The Harmonisation of Thermal Properties of Building Materials. Tech. Rep. BRE/169/12/1, BRE. URL https://pdfs.semanticscholar.org/4356/607bd4822d5514d002e5081cc3dcc285afe3.pdf (Cited on page 124.)

Climate Change Act, 2008. C. 27. (Cited on page 40.)

Coakley, D., Raftery, P., Keane, M., Sep. 2014. A review of methods to match building energy simulation models to measured data. Renewable and Sustainable Energy Reviews 37, 123–141. (Cited on pages 66 and 67.)

Congdon, P., 2006. Bayesian statistical modelling, 2nd Edition. Wiley series in probability and statistics. John Wiley & Sons, Chichester, England ; Hoboken, NJ, oCLC: ocm70673258. (Cited on pages 93, 96, 98, 102, 103, 107, and 132.)

Crawley, D. B., Hand, J. W., Kummert, M., Griffith, B. T., Apr. 2008. Contrasting the capabilities of building energy performance simulation programs. Building and Environment 43 (4), 661–673. (Cited on pages 40 and 45.)

Danter, E., 1960. Periodic heat flow characteristics of simple walls and roofs. Journal of the Institution of Heating and Ventilating Engineers 28, 136–146. (Cited on page 64.)

Davies, M. G., Jan. 1984. The heat storage loss ratio for a building and its response time. Applied Energy 18 (3), 179–238. (Cited on page 62.)

Davies, M. G., 2004. Building Heat Transfer. John Wiley & Sons, Ltd. (Cited on page 62.)

de Wit, S., 2004. Uncertainty in building simulation. In: Advanced building simulation. Taylor & Francis, Abingdon (UK). (Cited on pages 40, 41, and 45.)

DECC, 2009. The UK Low Carbon Transition Plan – National strategy for climate and energy. (Cited on page 39.)

Deconinck, A.-H., Roels, S., Oct. 2016. Comparison of characterisation methods determining the thermal resistance of building components from onsite measurements. Energy and Buildings 130, 309–320. (Cited on pages 41, 42, 45, 46, 52, 56, 58, 59, 61, and 68.)

Deconinck, A.-H., Roels, S., Feb. 2017. Is stochastic grey-box modelling suited for physical properties estimation of building components from on-site measurements? Journal of Building Physics, 174425911668838. (Cited on page 152.)

Desogus, G., Mura, S., Ricciu, R., Oct. 2011. Comparing different approaches to in situ measurement of building components thermal resistance. Energy and Buildings 43 (10), 2613–2620. (Cited on pages 57, 146, 187, and 189.)

Diciccio, T. J., Kass, R. E., Raftery, A., Wasserman, L., Sep. 1997. Computing Bayes Factors by Combining Simulation and Asymptotic Approximations. Journal of the American Statistical Association 92 (439), 903–915. (Cited on pages 108 and 109.)

Dubois, S., McGregor, F., Evrard, A., Heath, A., Lebeau, F., Nov. 2014. An inverse modelling approach to estimate the hygric parameters of clay-based masonry during a Moisture Buffer Value test. Building and Environment 81, 192–203. (Cited on pages 42 and 68.)

Eames, M. E., Ramallo-Gonzalez, A. P., Wood, M. J., May 2016. An update of the UK's test reference year: The implications of a revised climate on building design. Building Services Engineering Research and Technology 37 (3), 316–333. (Cited on page 127.)

Eltek, 2015. Squirrel 450/850 Series Data Logger.
URL http://www.eltekdataloggers.co.uk/450_series.html (Cited on page 114.)

EN ISO 13786, 2008. Thermal performance of building components - Dynamic thermal characteristics - Calculation methods. (Cited on pages 64, 126, 146, and 152.)

Energy Saving Trust, 2005. CE128/GIR64: Post-construction testing - a professionals guide to testing housing for energy efficiency. (Cited on pages 41, 46, 55, 57, 115, 146, 176, 189, and 227.)

Esser, W., Krischer, O., 1930. Die Berechnung der Anheizung und Auskuh- lung ebener und zylindrischer Wande. Julius Springer, Berlin. (Cited on pages 61 and 62.)

Euler, L., 1755. Institutiones calculi differentialis. St. Petersburg (RU). (Cited on page 65.)

European Community, 2009. The EU Climate and Energy Package.
URL http://ec.europa.eu/clima/policies/package/index_en.htm (Cited on page 40.)

European Community, 2010. Roadmap for moving to low-carbon economy in 2050.
URL http://ec.europa.eu/clima/policies/roadmap/index_en.htm (Cited on page 40.)

Feuermann, D., Apr. 1989. Measurement of envelope thermal transmittances in multifamily buildings. Energy and Buildings 13 (2), 139–148. (Cited on pages 40, 45, and 55.)

Fienberg, S. E., 2006. When did Bayesian inference become "Bayesian"? Bayesian Analusis 1 (1), 1–40. (Cited on page 76.)

Flanders, S. N., 1980. Time constraints on measuring building R-value. Tech. Rep. 80-15, United States army corps of engineers, cold regions research and engineering laboratory, Hanover, New Hempshire, USA. (Cited on page 55.)

Foreman-Mackey, D., Hogg, D. W., Lang, D., Goodman, J., 2013. emcee: The MCMC hammer. Publications of the Astronomical Society of the Pacific 125 (925), 306. (Cited on page 131.)

Gelman, A., Carlin, J., Stern, H., Dunson, D., Vehtari, A., Rubin, D., 2013. Bayesian Data Analysis, 3rd Edition. CRC press. (Cited on pages 75, 76, 77, and 102.)

Gelman, A., Rubin, D. B., 1992. Inference from iterative simulation using multiple sequences. Statistical science, 457–472. (Cited on page 103.)

Glickman, M. E., Van Dyk, D. A., 2007. Basic bayesian methods. Topics in Biostatistics, 319–338. (Cited on pages 76 and 77.)

Godfrey-Smith, P., 2006. The strategy of model-based science. Biology and Philosophy 21 (5), 725–740. (Cited on page 79.)

Good, I. J., 1968. Corroboration, Explanation, Evolving Probability, Simplicity and a Sharpened Razor. The British Journal for the Philosophy of Science 19 (2), 123–143. (Cited on page 106.)

Goodman, J., Weare, J., 2010. Ensemble samplers with affine invariance. Communications in applied mathematics and computational science 5 (1), 65–80. (Cited on page 131.)

Gori, V., 2013. Can thermodynamic quantities estimated from in-situ measurements be extensively used to characterise building elements during energy simulations? - Errors and uncertainties in in-situ measurements and parameters estimation processes. MRes Dissertation, University College London, London. UK. (Cited on page 50.)

Gori, V., Biddulph, P., Elwell, C. A., Scott, C., Rye, C., Lowe, R., Oreszczyn, T., 2014. Seasonal factors influencing the estimation of the U-value of a wall. In: Proceedings of the 2014 Building Simulation and Optimization Conference. The Bartlett, UCL Faculty of the Built Environment Institute for Environmental Design and Engineering, London. UK. (Cited on page 117.)

Gori, V., Elwell, C., 2016. In-situ measurements of heat flux and temperature on a solid-brick wall in office building.
URL http://discovery.ucl.ac.uk/1526521/ (Cited on page 155.)

Gori, V., Elwell, C., 2017. Characterization of the thermal structure of different building constructions using in-situ measurements and Bayesian analysis. Paper presented at

the Nordic Symposium on Building Physics (NSB2017) and to be published on Energy Procedia. (Cited on pages 73, 91, and 132.)

Gori, V., Marincioni, V., Biddulph, P., Elwell, C., 2017. Inferring the thermal resistance and effective thermal mass distribution of a wall from in situ measurements to characterise heat transfer at both the interior and exterior surfaces. Energy and Buildings. (Cited on pages 42, 73, 83, 88, 117, 153, and 157.)

Gouda, M., Danaher, S., Underwood, C., 2002. Building Thermal Model Reduction Using Nonlinear Constrained Optimization. Building and Environment 37 (12), 1255–1265. (Cited on pages 62, 63, 65, and 66.)

Gough, M., 1982. Modelling heat flow in buildings: an eigenfunction approach. Ph.D. thesis, University of Cambridge, Cambridge (UK). (Cited on page 65.)

Gregory, P., 2005. Bayesian Logical Data Analysis for the Physical Sciences - A comparative approach with mathematica support. Cambridge University Press, New York, USA. (Cited on page 91.)

Guattari, C., Evangelisti, L., Gori, P., Asdrubali, F., Jan. 2017. Influence of internal heat sources on thermal resistance evaluation through the heat flow meter method. Energy and Buildings 135, 187–200. (Cited on page 53.)

Guide, I., Book, A., 1970. The Institution of Heating and Ventilating Engineers, 5. (Cited on page 64.)

Gutschker, O., Feb. 2008a. Parameter identification with the software package LORD. Building and Environment 43 (2), 163–169. (Cited on pages 42 and 63.)

Gutschker, O., Feb. 2008b. Parameter identification with the software package LORD. Building and Environment 43 (2), 163–169. (Cited on page 67.)

Harrje, D., Dutt, G. S., Beyea, J., 1979. Locating and Eliminating Obscure But Major Energy Losses in Residential Housing. ASHRAE Transactions 85 (2), 521–534. (Cited on page 52.)

Hastie, T., Tibshirani, R., Friedman, J., 2008. The Elements of Statistical Learning Data Mining, Inference, and Prediction, 2nd Edition. Elsevier. (Cited on pages 104, 109, and 110.)

Hauser, J. R., 2009. Numerical methods for nonlinear engineering models. Springer, Dordrecht, oCLC: ocn310400762. (Cited on pages 80 and 81.)

Hens, H., 2012. Building Physics - Heat, Air and Moisture: Fundamentals and Engineering Methods with Examples and Exercises. Ernst & Sohn Verlag für Architektur und technische Wissenschaften GmbH & Co. KG, Germany. (Cited on pages 46, 47, 48, 57, and 230.)

Hittle, D. C., Bishop, R., Nov. 1983. An improved root-finding procedure for use in calculating transient heat flow through multilayered slabs. International Journal of Heat and Mass Transfer 26 (11), 1685–1693. (Cited on page 65.)

Hopfe, C. J., Hensen, J. L. M., Oct. 2011. Uncertainty analysis in building performance simulation for design support. Energy and Buildings 43 (10), 2798–2805. (Cited on pages 40 and 45.)

Howard, A., 2010. Elementary linear algebra, 10th Edition. John Wiley & Sons, USA. (Cited on page 88.)

Hughes, M., Palmer, J., Cheng, V., Shipworth, D., Sep. 2015. Global sensitivity analysis of England's housing energy model. Journal of Building Performance Simulation 8 (5), 283–294. (Cited on pages 40 and 45.)

Hukseflux, 2016. User manual HFP01 & HFP03 Heat flux plate / heat flux sensor (v1620).
URL http://www.hukseflux.com/sites/default/files/product_manual/HFP01_HFP03_manual_v1620.pdf (Cited on pages 114 and 118.)

International Energy Agency, 2011a. IEA EBC Annex 58, Reliable building energy performance characterisation based on full scale dynamic measurements.
URL http://www.ecbcs.org/annexes/annex58.htm (Cited on pages 41, 74, and 253.)

International Energy Agency, 2011b. Technology Roadmap Energy-efficient Buildings: Heating and Cooling Equipment. (Cited on page 39.)

International Energy Agency, 2013. Transition to Sustainable Buildings Strategies and Opportunities to 2050. Tech. rep.
URL http://www.iea.org/publications/freepublications/publication/Building2013_free.pdf (Cited on page 39.)

International Energy Agency, 2016a. IEA EBC Annex 70, Building energy epidemiology: analysis of real building energy use at scale. (Cited on page 74.)

International Energy Agency, 2016b. IEA EBC Annex 71, Building energy performance assessment based on in-situ measurements. (Cited on page 74.)

ISO 9869-1, 2014. Thermal insulation – Building elements – In-situ measurement of thermal resistance and thermal transmittance – Part 1: Heat flow meter method. (Cited on page 185.)

James, F., Winkler, M., 2004. MINUIT User's Guide.
URL http://seal.web.cern.ch/seal/documents/minuit/mnusersguide.pdf (Cited on page 131.)

Janssen, H., Blocken, B., Roels, S., Carmeliet, J., 2007. Wind-driven rain as a boundary condition for HAM simulations: analysis of simplified modelling approaches. Building and Environment 42 (4), 1555–1567. (Cited on page 51.)

Janssens, A., 2016. Report of Subtask 1b: Overview of methods to analyse dynamic data. Tech. rep. (Cited on page 68.)

Jaynes, E. T., 1986. Bayesian Methods: General Background - An introductory tutorial. (Cited on page 76.)

Jefferys, W. H., Berger, J. O., Jan. 1992. Ockham's Razor and Bayesian Analysis. American Scientist 80 (1), 64–72. (Cited on page 106.)

Jeffreys, H., 1998. The Theory of Probability. OUP Oxford, google-Books-ID: vh9Act9rtzQC. (Cited on page 106.)

Jiménez, M., Madsen, H., Andersen, K., Feb. 2008. Identification of the main thermal characteristics of building components using MATLAB. Building and Environment 43 (2), 170–180. (Cited on page 67.)

Jiménez, M. J., Madsen, H., Feb. 2008. Models for describing the thermal characteristics of building components. Building and Environment 43 (2), 152–162. (Cited on pages 41, 46, 56, and 68.)

Jiménez, M. J., Porcar, B., Heras, M. R., Feb. 2009. Application of different dynamic analysis approaches to the estimation of the building component U value. Building and Environment 44 (2), 361–367. (Cited on pages 42, 46, 68, 104, 105, 106, and 122.)

Johnston, D., Miles-Shenton, D., Farmer, D., Sep. 2015. Quantifying the domestic building fabric 'performance gap'. Building Services Engineering Research and Technology 36 (5), 614–627. (Cited on pages 40, 41, and 45.)

Kaipio, J. P., Fox, C., 2011. The Bayesian Framework for Inverse Problems in Heat Transfer. Heat Transfer Engineering 32 (9), 718–753. (Cited on page 68.)

Kalthod, V., Knickle, H. N., Jul. 1982. The Effect of Aging of Urea-Formaldehyde Foam On Thermal Conductance. Journal of Building Physics 6 (1), 14–38. (Cited on pages 26, 52, 118, 148, and 149.)

Kipp and Zonen, 2016. CMP3 Pyranometer.
URL http://www.kippzonen.com/Product/11/CMP3-Pyranometer (Cited on page 114.)

Kramer, R., van Schijndel, J., Schellen, H., 2012. Simplified Thermal and Hygric Building Models: A Literature Review. Frontiers of Architctural Research 1 (4), 318–325. (Cited on pages 42, 63, 66, and 67.)

Kristensen, N. R., Madsen, H., Jørgensen, S. B., Feb. 2004. Parameter estimation in stochastic grey-box models. Automatica 40 (2), 225–237. (Cited on pages 42, 63, 66, 67, 68, and 102.)

Labfacility, 2016. Thermocouple reference data.
URL http://www.labfacility.co.uk/pdf/temperature-handbook-9-to-13.pdf (Cited on page 114.)

Laplace, P.-S., 1774. Mémoire sul la Probabilité des Causes par les événements. Mémoires de Mathématique et de Physique Presentés á l'Académie Royale des Science, Par Divers Savants, & Lûs dans ses Assemblées 6, 621–656. (Cited on page 76.)

Lathi, B. P., Green, R. A., Apr. 2014. Essentials of Digital Signal Processing. Cambridge University Press. (Cited on page 80.)

Lecompte, J. G., 1987. Airthightness of masonry walls. Ueberlingen, Federal Republic of Germany. (Cited on page 51.)

Levermore, G. J., Parkinson, J. B., Nov. 2006. Analyses and algorithms for new Test Reference Years and Design Summer Years for the UK. Building Services Engineering Research and Technology 27 (4), 311–325. (Cited on page 116.)

Li, F. G. N., Smith, A., Biddulph, P., Hamilton, I. G., Lowe, R., Mavrogianni, A., Oikonomou, E., Raslan, R., Stamp, S., Stone, A., Summerfield, A., Veitch, D., Gori, V., Oreszczyn, T., Oct. 2014. Solid-wall U-values: heat flux measurements compared with standard assumptions. Building Research & Information 43 (2), 238–252. (Cited on pages 41, 45, and 127.)

Limpert, E., Stahel, W. A., Abbt, M., 2001. Log-normal Distributions across the Sciences: Keys and CluesOn the charms of statistics, and how mechanical models resembling

gambling machines offer a link to a handy way to characterize log-normal distributions, which can provide deeper insight into variability and probability—normal or log-normal: That is the question. BioScience 51 (5), 341–352. (Cited on page 99.)

Lindfors, A., Christoffersson, A., Roberts, R., Anderlind, G., Jan. 1995. Model Based Frequency Domain Estimation of the Thermal Properties of Building Insulation. Journal of Building Physics 18 (3), 229–260. (Cited on pages 55 and 57.)

Lowe, R. J., Wingfield, J., Bell, M., Bell, J. M., May 2007. Evidence for heat losses via party wall cavities in masonry construction. Building Services Engineering Research and Technology 28 (2), 161–181. (Cited on page 52.)

Macdonald, I. A., 2002. Quantifying the effects of uncertainty in building simulation. University of Strathclyde. (Cited on pages 124 and 136.)

MacKay, D. J. C., 2007. Information Theory, Inference and Learning Algorithms, sixth printing 2007 edition Edition. Cambridge University Press. (Cited on pages 63, 77, 94, 99, 100, 101, 104, 105, 106, 107, 108, and 138.)

Mackey, C., Wright, L., 1944. Periodic heat flow - homogeneous walls or roofs. ASHVE Transactions 50, 293–312. (Cited on pages 63 and 64.)

Mackey, C., Wright, L., 1946. Periodic heat flow - composite walls or roofs. ASHVE Transactions 52, 283–296. (Cited on pages 63 and 64.)

Madsen, H., 2007. Time Series Analysis. CRC Press, google-Books-ID: oyFNKoIWdFkC. (Cited on pages 90, 92, 95, 104, and 109.)

Madsen, H., Bacher, P., Bauwens, G., Deconinck, A., Reynders, G., Roels, S., Himpe, E., Lethe, G., 2016. Subtask 3b: Thermal performance characterisation using time series data. Tech. rep. (Cited on pages 104, 105, 106, and 153.)

Madsen, H., Bacher, P., Bauwens, G., Deconinck, A.-H., Reynders, G., Roels, S., Himpe, E., Lethé, G., 2015. Thermal Performance Characterization using Time Series Data - IEA EBC Annex 58 Guidelines. Tech. Rep. DTU Compute-Technical Report-2015; No. 8, Technical University of Denmark (DTU). (Cited on page 53.)

Madsen, H., Holst, J., Mar. 1995. Estimation of continuous-time models for the heat dynamics of a building. Energy and Buildings 22 (1), 67–79. (Cited on pages 42 and 46.)

Marincioni, V., Altamirano, H., 2016. Measurement of heat flux and temperature on a solid wall in an environmental chamber.
URL http://discovery.ucl.ac.uk/1527422/ (Cited on page 151.)

Marincioni, V., Altamirano-Medina, H., May, N., Sanders, C., Sep. 2016. Estimating the impact of reveals on the transmission heat transfer coefficient of internally insulated solid wall dwellings. Energy and Buildings 128, 405–412. (Cited on page 52.)

Marincioni, V., Altamirano-Medina, H., Ridley, I., 2014. Performance of internal wall insulation systems - experimental test for the validation of a hygrothermal simulation tool. In: Proceedings of Nordic Symposium on Building Physics. Lund, Sweden. (Cited on pages 113 and 115.)

McIntyre, D. A., Feb. 1985. In situ measurement of U-values. Building Services Engineering Research and Technology 6 (1), 1–6. (Cited on pages 51 and 52.)

Meng, X., Yan, B., Gao, Y., Wang, J., Zhang, W., Long, E., Jan. 2015. Factors affecting the in situ measurement accuracy of the wall heat transfer coefficient using the heat flow meter method. Energy and Buildings 86, 754–765. (Cited on pages 53 and 54.)

Mitalas, G., Stephenson, D., 1967. Room thermal response factors. ASHRAE Transaction 73 (1), 1–10. (Cited on page 63.)

Mustafaraj, G., Chen, J., Lowry, G., Mar. 2010. Development of room temperature and relative humidity linear parametric models for an open office using BMS data. Energy and Buildings 42 (3), 348–356. (Cited on page 66.)

Naveros, I., Bacher, P., Ruiz, D. P., Jiménez, M. J., Madsen, H., Feb. 2014. Setting up and validating a complex model for a simple homogeneous wall. Energy and Buildings 70, 303–317. (Cited on pages 42, 46, 63, 68, 122, and 152.)

Naveros, I., Ghiaus, C., Ruíz, D. P., Castaño, S., Dec. 2015. Physical parameters identification of walls using ARX models obtained by deduction. Energy and Buildings 108, 317–329. (Cited on page 67.)

Nersessian, N. J., 1998. Model-Based Reasoning in Conceptual Reasoning. In: Model-Based Reasoning in Scientific Discoveries. Kluwer Academic/Plenum Publishers, New York, USA, pp. 5–22. (Cited on page 79.)

Nessi, A., Nissolle, L., 1925. Regimes variables de fonctionnement dans les installations de chauffage central. Dunod, Paris, France. (Cited on page 63.)

Norford, L. K., Socolow, R. H., Hsieh, E. S., Spadaro, G. V., 1994. Two-to-one discrepancy between measured and predicted performance of a 'low-energy' office building: insights from a reconciliation based on the DOE-2 model. Energy and Buildings 21 (2), 121–131. (Cited on page 40.)

Norlén, U., 1990. Estimating thermal parameters of outdoor test cells. Building and Environment 25 (1), 17–24. (Cited on page 67.)

Norlén, U., 1994. Determining the thermal resistance from in-situ measurements. In: Workshop on application of system identification in energy saving in buildings. Luxembourg, pp. 402–429. (Cited on pages 46, 67, and 104.)

Nottage, H., Parmelee, G., 1954. Circuit analysis applied to load estimating (part 1). ASHVE Trans. 60, 59–102. (Cited on page 63.)

Oh, S., 2013. Origins of analysis methods in energy simulation programs used for high performance commercial buildings. Ph.D. thesis, Texas A&M University.
URL http://oaktrust.library.tamu.edu/handle/1969.1/151151 (Cited on page 63.)

Oreszczyn, T., Hong, S. H., Ridley, I., Wilkinson, P., The Warm Front Study Group, 2006. Determinants of winter indoor temperatures in low income households in England. Energy and Buildings 38 (3), 245–252. (Cited on page 116.)

Ouyang, K., Haghighat, F., 1991. A Procedure for Calculating Thermal Response Factors of Multi-layer Walls State Space Method. Building and Environment 26 (2), 173–177. (Cited on page 65.)

Parnis, G., 2012. Building Thermal Modelling Using Electric Circuit Simulation. Ph.D. thesis, University of New South Wales, Sydney, Australia.
URL http://www.unsworks.unsw.edu.au//primo_library/libweb/action/dlDisplay.do?vid=UNSWORKS&docId=unsworks_10641&fromSitemap=1&afterPDS=true (Cited on pages 62 and 63.)

Paschkis, V., Baker, H., 1942. A method for determining unsteady-state heat transfer by means of an electrical analogy. Transaction of the American Society of Mechanical Engineers 64, 105–112. (Cited on pages 42 and 62.)

Paschkis, V., Heisler, M. P., Apr. 1944. The Accuracy of Measurements in Lumped R-C Cable Circuits as Used in the Study of Transient Heat Flow. American Institute of Electrical Engineers, Transactions of the 63 (4), 165–171. (Cited on pages 62 and 63.)

Pérez-Lombard, L., Ortiz, J., Pout, C., 2008. A review on buildings energy consumption information. Energy and Buildings 40 (3), 394–398. (Cited on page 39.)

Powell, M. J. D., Jan. 1964. An efficient method for finding the minimum of a function of several variables without calculating derivatives. The Computer Journal 7 (2), 155–162. (Cited on page 131.)

Python Software Foundation, 2017. Python Language Reference, version 3.0. URL http://www.python.org (Cited on page 129.)

Rabl, A., 1988. Parameter estimation in buildings: methods for dynamic analysis of measured energy. Journal of Solar Energy Engineering 110, 52–66. (Cited on pages 46 and 66.)

Rao, K. R., Yip, P. C., 1990. Discrete cosine transform: algorithms, advantages, applications. Academic Press, Boston. (Cited on pages 95 and 96.)

Rasooli, A., Itard, L., Ferreira, C. I., 2016. A Response Factor-Based Method for the Rapid In-Situ Determination of Wall's Thermal Resistance in Existing Buildings. Energy and Buildings. (Cited on pages 55 and 59.)

Robert, C., Casella, G., Feb. 2011. A Short History of Markov Chain Monte Carlo: Subjective Recollections from Incomplete Data. Statistical Science 26 (1), 102–115. (Cited on page 102.)

Roels, S., Bacher, P., Bauwens, G., Madsen, H., Jiménez, M. J., 2015a. Characterising the Actual Thermal Performance of Buildings: Current Results of Common Exercises Performed in the Framework of the IEA EBC Annex 58-Project. Energy Procedia 78, 3282–3287. (Cited on pages 41 and 45.)

Roels, S., Bacher, P., Bauwens, G., Madsen, H., Jiménez, M. J., 2015b. Characterising the Actual Thermal Performance of Buildings: Current Results of Common Exercises Performed in the Framework of the IEA EBC Annex 58-Project. Energy Procedia 78, 3282–3287. (Cited on page 68.)

Roels, S., Carmeliet, J., Hens, H., Adan, O., Brocken, H., Cerny, R., Pavlik, Z., Hall, C., Kumaran, K., Pel, L., Plagge, R., Apr. 2004. Interlaboratory Comparison of Hygric Properties of Porous Building Materials. Journal of Thermal Envelope and Building Science 27 (4), 307–325. (Cited on page 55.)

Rotronic, 2014. HygroLog-NT Manual. (Cited on page 114.)

Rouchier, S., Busser, T., Pailha, M., Piot, A., Woloszyn, M., 2017. Hygric characterization of wood fiber insulation under uncertainty with dynamic measurements and Markov Chain Monte-Carlo algorithm. Building and Environment 114, 129–139. (Cited on pages 42 and 68.)

Rouchier, S., Woloszyn, M., Kedowide, Y., Béjat, T., Jan. 2016. Identification of the hygrothermal properties of a building envelope material by the covariance matrix adap-

tation evolution strategy. Journal of Building Performance Simulation 9 (1), 101–114. (Cited on page 46.)

Roulet, C., Gass, J., Marcus, I., 1987. In-Situ U-Value Measurement: Reliable Results in Shorter Time by Dynamic Interpretation of Measured Data. Thermal Performance of the Exterior Envelopes of Buildings III, 777=784. (Cited on pages 46, 57, and 122.)

Ruivo, C. R., Vaz, D. C., Oct. 2015. Prediction of the heat gain of external walls: An innovative approach for full-featured excitations based on the simplified method of Mackey-and-Wright. Applied Energy 155, 378–392. (Cited on page 64.)

Rye, C., 2012. The SPAB - U-value report. Tech. Rep. 1.
URL https://www.spab.org.uk/downloads/SPABU-valueReportNov2012.pdf (Cited on pages 41 and 118.)

Saitta, L., Zucker, J.-D., 2013. Abstraction in Different Disciplines. In: Abstraction in Artificial Intelligence and Complex Systems. Springer New York, New York, NY, pp. 11–47, dOI: 10.1007/978-1-4614-7052-6_2. (Cited on page 79.)

Samardzioska, T., Apostolska, R., Oct. 2016. Measurement of Heat-Flux of New Type Façade Walls. Sustainability 8 (10), 1031. (Cited on page 45.)

Sánchez, V., Garcia, P., Peinado, A. M., Segura, J. C., Rubio, A. J., 1995. Diagonalizing properties of the discrete cosine transforms. IEEE transactions on Signal Processing 43 (11), 2631–2641. (Cited on page 95.)

Sanders, C., Phillipson, M., 2006. Review of Differences between Measured and Theoretical Energy Savings for Insulation Measures. Tech. rep., Glasgow Caledonian University (Centre for Research on Indoor Climate and Health) for Energy Saving Trust. (Cited on pages 45 and 50.)

ScyPy community, 2016. SciPy reference guide.
URL https://docs.scipy.org/doc/scipy-0.18.1/reference/generated/scipy.optimize.basinhopping.html (Cited on page 131.)

Siebert, W. M., 1986. Circuits, Signals, and Systems. MIT Press. (Cited on page 80.)

Silverman, B. W., 1986. Density estimation for statistics and data analysis. Vol. 26. CRC press. (Cited on pages 22, 23, 213, and 219.)

Siviour, J., 1974. Effects of weather on house heating requirements. Tech. rep. (Cited on page 51.)

Siviour, J., 1994. Experimental U-values of some house walls. Building Services Engineering Research and Technology 15 (1), 35–36. (Cited on pages 41 and 52.)

Siviour, J., McIntyre, D. A., 1982. U-value meters in theory and practice. Building Services Engineering Research and Technology 3, 61–69. (Cited on pages 51, 54, 57, 146, and 189.)

Smith, G. D., 1985. Numerical Solution of Partial Differential Equations: Finite Difference Methods. Clarendon Press. (Cited on pages 66, 81, and 83.)

Sontay, 2010. Single Point Air Velocity Transmitter (AV-DSP). (Cited on page 114.)

Standaert, P., 1987. Numerical analysis of operational errors with surface-mounted heat flux sensors. Tech. rep., Belgium. (Cited on pages 53 and 54.)

Stein, J. R., Meier, A., Apr. 2000. Accuracy of home energy rating systems. Energy 25 (4), 339–354. (Cited on page 40.)

Stephenson, D., 1962. Methods of determining non-steady-state heat flow through walls and roofs of buildings. Journal of the Institution of Heating and Ventilating Engineers 30, 64–73. (Cited on pages 64 and 65.)

Stephenson, D., Mitalas, G., 1971. Calculation of heat conduction transfer functions for multi-layer slabs. ASHRAE Transaction 77 (II), 117–126. (Cited on page 65.)

Stevens, G., Bradford, J., 2013. Do U-value insulation? England's field trial of solid wall insulation. In: ECEEE Summer Study: Rethink, Renew, Restart. pp. 1269–1280. (Cited on pages 41, 45, and 127.)

Stocker, T., Qin, D., Plattner, G.-K., Tignor, M., Allen, S., Boschung, J., Nauels, A., Xia, Y., Bex, V., Midgley, P., 2013. IPCC, 2013: Climate Change 2013: The Physical Science Basis. Contribution of Working Group I to the Fifth Assessment Report of the Intergovernmental Panel on Climate Change. Tech. rep., Cambridge University Press, Cambridge, United Kingdom and New York, NY, USA. (Cited on page 39.)

Swan, L. G., Ugursal, V. I., Oct. 2009. Modeling of end-use energy consumption in the residential sector: A review of modeling techniques. Renewable and Sustainable Energy Reviews 13 (8), 1819–1835. (Cited on pages 40 and 45.)

Thun, M. J., Lakat, M. F., Altman, R., 1982. Symptom survey of residents of homes insulated with urea-formaldehyde foam. Environmental research 29 (2), 320–334. (Cited on page 118.)

Trethowen, H., 1986. Measurement Errors with Surface-mounted Heat Flux Sensors. Building and Environment 21 (1), 41–56. (Cited on pages 53, 54, and 136.)

Underwood, C., Yik, F., 2004. Modelling Methods for Energy in Buildings. Blackwell Science, Oxford. (Cited on pages 62, 65, and 66.)

United Nations, 2015. Paris agreement.
URL http://unfccc.int/files/meetings/paris_nov_2015/application/pdf/paris_agreement_english_.pdf (Cited on page 39.)

Urbikain, M. K., Davies, M. G., Sep. 2008. One-dimensional solutions to Fourier's equation and measures of heat transmission through walls: The role of wall decay times. Building and Environment 43 (9), 1433–1445. (Cited on pages 56, 61, 63, and 64.)

van Dronkelaar, C., Dowson, M., Spataru, C., Mumovic, D., 2016. A Review of the Regulatory Energy Performance Gap and Its Underlying Causes in Non-domestic Buildings. Indoor Environment 1, 17. (Cited on page 40.)

Wales, D., Doye, J., Dullweber, A., Hodges, M., Naumkin, F., Calvo, F., Hernández-Rojas, J., Middleton, T., 2017. The Cambridge Cluster Database.
URL http://www-wales.ch.cam.ac.uk/CCD.html (Cited on page 131.)

Wales, D. J., Doye, J. P., 1997. Global optimization by basin-hopping and the lowest energy structures of Lennard-Jones clusters containing up to 110 atoms. The Journal of Physical Chemistry A 101 (28), 5111–5116. (Cited on page 131.)

Wang, J., Zabaras, N., Aug. 2004. A Bayesian inference approach to the inverse heat conduction problem. International Journal of Heat and Mass Transfer 47 (17–18), 3927–3941. (Cited on page 68.)

Wang, S., Chen, Y., Jan. 2003. Transient heat flow calculation for multilayer constructions using a frequency-domain regression method. Building and Environment 38 (1), 45–61. (Cited on pages 62, 64, and 65.)

Wang, S., Xu, X., Apr. 2006. Simplified building model for transient thermal performance estimation using GA-based parameter identification. International Journal of Thermal Sciences 45 (4), 419–432. (Cited on page 63.)

Winship, C., Western, B., 2016. Multicollinearity and Model Misspecification. Sociological Science 3, 627–649. (Cited on pages 67 and 136.)

Wouters, P., Vandaele, L., Voit, P., Fisch, N., Apr. 1993. The use of outdoor test cells for thermal and solar building research within the PASSYS project. Building and Environment 28 (2), 107–113. (Cited on pages 41 and 45.)

Wright, R., Kantsios, A., Henley, W., 1983. Effect of Mounting on the Performance of Surface Heat Flow Meters Used to Evaluate Building Heat Losses. In: Thermal Insulation, Materials, and Systems for Energy Conservation in the '80s. (Cited on pages 53 and 54.)

Zero Carbon Hub, 2014. Closing the gap between design & as-built performance (end of term report). Tech. rep.
URL http://www.zerocarbonhub.org/sites/default/files/resources/reports/Design_vs_As_Built_Performance_Gap_End_of_Term_Report_0.pdf (Cited on pages 40, 45, 50, 52, 73, 74, and 253.)

Zhao, J., Apr. 2016. Enquiry on stochastic databases for building performance simulation (personal communication). (Cited on page 124.)

Zhao, J., Plagge, R., Ramos, N. M. M., Lurdes Simões, M., Grunewald, J., Jan. 2015. Concept for development of stochastic databases for building performance simulation – A material database pilot project. Building and Environment 84, 189–203. (Cited on pages 52, 124, and 136.)